

# Highly Accurate Quantum Chemistry: Spin-Orbit Splittings via Multireference Coupled-Cluster Methods and Applications in Heavy-Atom Main-Group Chemistry

## Dissertation

zur Erlangung des Grades  
„Doktor der Naturwissenschaften“  
im Promotionsfach Chemie

am Fachbereich Chemie, Pharmazie und Geowissenschaften  
der Johannes Gutenberg-Universität in Mainz

von Leonie Anna Mück  
geboren in Frankfurt a. M.

Mainz, 2012

Tag der mündlichen Prüfung: 27. Februar 2013

# Contents

|  |           |
|--|-----------|
| <b>I. Prologue</b>   | <b>1</b>  |
| <b>1. Introduction</b>   | <b>3</b>  |
| 1.1. Theory's role in chemical sciences . . . . .  | 3         |
| 1.2. The quantitative paradigm: Predictions with high accuracy . . . . .   | 4         |
| 1.3. Coupled-cluster methods: Quantum chemistry with theoretical rigor . . . . .   | 5         |
| 1.4. Molecules with heavy main-group elements: Demonstrating the predictive power of coupled-cluster theory . . . . .                                | 6         |
| 1.5. First-order spin-orbit splittings via multireference coupled-cluster theory: Improving the predictive power of coupled-cluster theory . . . . . | 7         |
| <b>2. Theoretical background</b>   | <b>9</b>  |
| 2.1. The time-independent electronic Schrödinger equation . . . . .  | 9         |
| 2.2. Electron correlation . . . . .  | 9         |
| 2.3. Size consistency and size extensivity . . . . .   | 10        |
| 2.4. Coupled-cluster theory . . . . .  | 10        |
| 2.5. Coupled-cluster extrapolation and additivity schemes . . . . .  | 12        |
| 2.6. The multireference problem . . . . .  | 13        |
| 2.7. Multireference coupled-cluster wave function <i>ansätze</i> . . . . .   | 14        |
| 2.8. Jeziorski-Monkhorst based MRCC methods . . . . .  | 15        |
| 2.8.1. State-universal multireference coupled-cluster theory . . . . .   | 15        |
| 2.8.2. State-specific multireference coupled-cluster theory . . . . .  | 16        |
| 2.9. Comparison of Jeziorski-Monkhorst based MRCC methods . . . . .  | 18        |
| 2.10. Relativistic quantum chemistry . . . . .   | 19        |
| <b>II. Demonstrating the predictive power of quantum chemistry: Heavy-atom main-group molecules</b>  | <b>23</b> |
| <b>3. Introduction: Predicting properties of heavy-atom main-group molecules</b>   | <b>25</b> |
| 3.1. Heavy-atom main-group chemistry . . . . .   | 25        |
| 3.2. Quantum chemistry and rotational spectroscopy . . . . .   | 27        |
| 3.3. Methods for bonding analysis . . . . .  | 28        |
| 3.3.1. Natural bond-orbital analysis . . . . .   | 29        |
| 3.3.2. "Atoms in Molecules" analysis . . . . .   | 29        |
| <b>4. Results: Structures and spectroscopic parameters of small molecules with heavy elements</b>  | <b>31</b> |
| 4.1. HPSi and OSiS - <i>a posteriori</i> explanation of structure and bonding . . . . .  | 31        |
| 4.1.1. Bridged HPSi . . . . .  | 31        |

|  |   |           |
|--|---|-----------|
| 4.1.2.   | Linear OSiS . . . . .   | 33        |
| 4.2.   | Cyclic SiS <sub>2</sub> – a new role of theory in chemistry . . . . .   | 35        |
| 4.2.1.   | A new perspective on the Walsh rules – predicting the accessibility of a cyclic SiS <sub>2</sub> isomer . . . . .                       | 36        |
| 4.2.2.   | Guidance of experiments by calculation of spectroscopic parameters . . . . .  | 37        |
| 4.2.3.   | <i>A posteriori explanation</i> – why is cyclic SiS <sub>2</sub> energetically accessible? . . . . .                                    | 38        |
| 4.2.4.   | Cyclic SiS <sub>2</sub> and the predictive power of quantum chemistry . . . . .   | 40        |
| 4.3.   | Beyond cyclic SiS <sub>2</sub> – cyclic OSiS, OGeS, and GeS <sub>2</sub> , H <sub>2</sub> SiS <sub>2</sub> , HPS <sub>2</sub> . . . . . | 42        |
| 4.3.1.   | Cyclic OSiS . . . . .   | 42        |
| 4.3.2.   | Cyclic OGeS . . . . .   | 45        |
| 4.3.3.   | Cyclic GeS <sub>2</sub> . . . . .   | 47        |
| 4.3.4.   | H <sub>2</sub> SiS <sub>2</sub> . . . . .   | 49        |
| 4.3.5.   | HPS <sub>2</sub> . . . . .  | 53        |
| 4.4.   | Isomerization of SiS <sub>2</sub> – the need for multireference schemes . . . . .   | 56        |
| 4.4.1.   | Barrier height of SiS <sub>2</sub> isomerization . . . . .  | 57        |
| 4.4.2.   | Excited states of SiS <sub>2</sub> – is a photoisomerization of SiS <sub>2</sub> possible? . . . . .                                    | 59        |
| 4.4.3.   | Possible shortcomings of MRCI and alternative methods . . . . .   | 63        |
| <b>III. Improving the predictive power of quantum chemistry: Spin-orbit splittings via multireference coupled-cluster theory</b> |   | <b>65</b> |
| <b>5.</b>  | <b>Introduction: How to calculate spin-orbit splittings with MRCC wave functions</b>  | <b>67</b> |
| 5.1.   | Relativistic effects cause multireference character . . . . .   | 67        |
| 5.2.   | Spin-orbit splittings in <sup>2</sup> Π states . . . . .  | 68        |
| 5.3.   | Calculating spin-orbit splittings in <sup>2</sup> Π states with MRCC theory . . . . .   | 69        |
| 5.4.   | Spin-orbit splittings: A measure for the coupling contribution? . . . . .   | 70        |
| <b>6.</b>  | <b>Theoretical groundwork: From MRCC gradient theory to the spin-free Dirac-Coulomb approach</b>  | <b>73</b> |
| 6.1.   | Mukherjee’s multireference coupled-cluster gradient theory . . . . .  | 73        |
| 6.2.   | The Breit-Pauli spin-orbit operator . . . . .   | 76        |
| 6.3.   | Spin-orbit mean-field approximation for the Breit-Pauli spin-orbit operator . . . . .   | 78        |
| 6.4.   | Exact separation of spin-free and spin-orbit terms in the Dirac-Coulomb Hamiltonian . . . . .   | 80        |
| 6.4.1.   | Spin-separated one-electron terms . . . . .   | 81        |
| 6.4.2.   | Two-electron terms . . . . .  | 81        |
| <b>7.</b>  | <b>Theory: Derivation of working equations for the calculation of spin-orbit splittings via (Mk-)MRCC theory</b>                        | <b>85</b> |
| 7.1.   | Expression for spin-orbit splittings via state-specific MRCC theory . . . . .   | 85        |
| 7.1.1.   | Mukherjee’s multireference coupled-cluster theory . . . . .   | 87        |
| 7.1.2.   | State-universal multireference coupled-cluster theory . . . . .   | 89        |
| 7.1.3.   | Brillouin-Wigner multireference coupled-cluster theory . . . . .  | 91        |
| 7.2.   | Spin-orbit splittings – a measure for the coupling contribution . . . . .   | 92        |
| 7.3.   | Density-matrix formulation of spin-orbit splittings with Mk-MRCC . . . . .  | 94        |
| 7.3.1.   | One-electron treatment of spin-orbit splittings . . . . .   | 94        |
| 7.3.2.   | Effective one-electron treatment via spin-orbit mean-field approximation . . . . .  | 97        |

---

|  |            |
|--|------------|
| 7.3.3. Two-electron treatment . . . . .  | 97         |
| 7.4. Combination with scalar-relativistic effects . . . . .  | 104        |
| 7.4.1. One-electron treatment . . . . .  | 104        |
| 7.4.2. Effective one-electron treatment via a spin-orbit mean-field approach . . . . .   | 105        |
| <b>8. Implementation</b>   | <b>109</b> |
| 8.1. General implementation scheme . . . . .   | 109        |
| 8.2. Reference function: Averaged UHF . . . . .  | 111        |
| 8.3. Generation of two determinants in an SRCC framework . . . . .   | 111        |
| 8.4. Verification . . . . .  | 112        |
| <b>9. Applications: Spin-orbit splitting in di- and triatomic molecules</b>  | <b>115</b> |
| 9.1. One-electron and effective one-electron treatment of spin-orbit interaction . . . . .   | 115        |
| 9.2. Spin-orbit splittings as a quality measure for the coupling contribution . . . . .  | 116        |
| 9.3. Comprehensive one- and two-electron treatment of spin-orbit splittings . . . . .  | 118        |
| 9.4. Scalar-relativistic contribution to the spin-orbit splittings . . . . .   | 120        |
| 9.5. Accuracy in calculations of spin-orbit splittings with Mk-MRCC . . . . .  | 124        |
| <b>IV. Epilogue</b>  | <b>127</b> |
| <b>10. Conclusion</b>  | <b>129</b> |
| 10.1. The endeavor for predictive power via coupled-cluster theory . . . . .   | 129        |
| 10.2. Demonstration of coupled-cluster theory's predictive power: New heavy-atom main group molecules . . . . .  | 129        |
| 10.3. Improvement of coupled-cluster theory's predictive power: Spin-orbit splittings in $^2\Pi$ states with multireference coupled-cluster wave functions . . . . . | 130        |
| 10.4. Outlook . . . . .  | 132        |
| <b>Bibliography</b>  | <b>133</b> |
| <b>Appendix</b>  | <b>143</b> |
| Experimental methods used for rotational-spectroscopy measurements . . . . .   | 143        |
| Spectroscopic parameters of S-SiH-SH, HS-PS, and HP-SS . . . . .   | 144        |
| S-SiH-SH . . . . .   | 144        |
| HS-PS and HP-SS . . . . .  | 146        |
| Calculation of "best-estimate" spin-orbit splittings . . . . .   | 148        |
| List of publications . . . . .   | 149        |



**Part I.**  
**Prologue**



# 1. Introduction

*You have three levels of theory: First-rate theory predicts, second-rate theory forbids, third-rate theory explains after the event.*  
– Alexander Kitaigorodsky

According to Alexander Kitaigorodsky, a Russian physicist, who made important contributions to the theoretical foundation of x-ray crystallography, scientific theories distinguish themselves as “first-rate theories”, if – and only if – they are capable of making good predictions.<sup>1</sup> This dissertation is located in the field of theoretical chemistry, to be more specific in quantum chemistry. For the most part it deals with a very successful quantum-chemical theory, namely coupled-cluster theory. Does coupled-cluster theory possess the crucial feature – predictive power – which makes it a “first-rate theory”? Using examples from heavy-atom main-group chemistry, this dissertation will demonstrate that coupled-cluster theory indeed fulfills this criterion. Highly accurate predictions are achieved and confirmed by experiment. Additionally, an improvement of coupled-cluster theory’s predictive power is accomplished via the development of an accurate method to calculate first-order spin-orbit splittings.

The following introduction outlines the role of theory in chemistry, the concept of predictive power in quantum chemistry, and accuracy in quantum-chemical calculations. It furthermore discusses the virtues of coupled-cluster theory and acquaints the reader with how the demonstration and improvement of coupled-cluster theory’s predictive power are accomplished in this dissertation.

## 1.1. Theory’s role in chemical sciences

Traditionally, chemistry is an experimental science. For a long time this was a necessity. Chemical problems are very complex when it comes to their description by physically sound laws and before the formulation of quantum mechanics<sup>2</sup> the corresponding equations were not even known. This prompted the development of simple, heuristic rules: When investigating new chemical phenomena, chemists relied on experience-based problem-solving<sup>3</sup> rather than theoretically rigorous equations from physics.

Turning the necessity into a virtue, chemists were enormously successful in deriving such rules from experimental results. To this day, successful chemists are thus said to have good “chemical intuition”. Tongue-in-cheek one could say that they have perfected the capacity to solve complicated many-body problems by simply counting electrons. The most prominent example for such a heuristic counting rule is probably Lewis’s model of the shared electron-pair bond.<sup>4</sup> It is most remarkable that Lewis developed this theory in 1916, more than 10 years before Heitler and London solved the Schrödinger equation for the hydrogen molecule.<sup>5</sup>

Nevertheless, the birth of quantum mechanics caused a revolution in theoretical chemistry regardless of the fact that the equations were (and are still to this day) much too complex to be solved for many-body problems. But on their basis a vast number of qualitative theories were developed. Qualitative theories based on sound physics have immense advantages over mere

heuristics: Despite the inherent simplifications they do not only predict what will probably happen, they also explain *why* this phenomenon occurs. One example for such a qualitative set of laws discussed in this dissertation are the Walsh rules.<sup>6</sup> These predict the structure of triatomic molecules based on the number of their valence electrons and can be derived using molecular-orbital theory, which is a qualitative interpretation of the wave function in the Schrödinger equation.<sup>7</sup>

Triggered by the leap in computer performance<sup>8</sup> and by methodological developments,<sup>9</sup> quantum-chemical methods have left the realm of qualitative theories. They can nowadays (approximately) solve the Schrödinger equation for many-electron systems to a good accuracy. In fact, the accuracy is often high enough to obtain results that are reliable in a quantitative sense.

A troika of objectives can be identified that inspires quantum chemistry today:

1. Prediction of new chemical phenomena.
2. Guidance and interpretation of experiments.
3. Explanation of experimental results.

The most important of these objectives is the first one. Predictive power is the acme of theoretical chemistry in general and, referring to Alexander Kitaigorodsky,<sup>1</sup> it is the crucial criterion that distinguishes a “first-rate chemical theory”. Furthermore, it is the only criterion that can consolidate the role of theoretical chemistry as a fundamental chemical discipline – much like theoretical physics is absolutely fundamental to physics as a whole.

Predictive power can be achieved in various ways and is not necessarily based on highly accurate quantum-chemical calculations. A lot of the success stories in modern quantum chemistry involved methods that certainly do not give quantitatively reliable results. For example, Frenking *et al.* predicted the existence of carbodicarbenes and their ability to act as  $\sigma$ -donating ligands based on considerations of the bonding situation. These considerations were first confirmed numerically by relatively low-accuracy calculations (BP86/def-SVP) and then experimentally in a wet-chemical synthesis.<sup>10–12</sup> One might argue that this strategy adheres to the qualitative paradigm<sup>13</sup> of theory described above.

This dissertation is committed to a quantitative paradigm. It strives to make useful and quantitatively reliable predictions – even where qualitative concepts fail. This means that instead of relying on trends and qualitative arguments, the calculations should *numerically* match high-level chemical and physical experiments. To clarify why this is important and how this is reflected in the calculations and methodological developments, it is necessary to give a general discussion of accuracy in quantum chemistry.

### 1.2. The quantitative paradigm: Predictions with high accuracy

When examining the accuracy of a calculation, quantum chemistry cannot avoid the comparison with experiment – “accuracy” can simply not be defined by exclusively considering calculations. If it passes the test, however, theory is indeed capable of making fruitful predictions. However, the required accuracy strongly depends on the type of experiment used for confirmation.

In the panorama of accuracy, a manifest landmark is  $1 \text{ kcal}\cdot\text{mol}^{-1}$ , which suffices to make a realistic prediction for thermochemistry and thus for very important chemical parameters like reaction energies. This landmark is so important that it is referred to as *chemical*

*accuracy*. Reaching an accuracy of  $1 \text{ kcal}\cdot\text{mol}^{-1}$  in quantum chemistry is like climbing up Jacob’s ladder to touch heaven.<sup>14</sup> But even better predictions are desired in many cases. Today, measurements of atomization energies and heats of formation achieve “sub-chemical accuracy” of  $1 \text{ kJ}\cdot\text{mol}^{-1}$ .<sup>15</sup> Additionally, quantum chemists are trying to master fields like atmospheric<sup>16</sup> or interstellar chemistry,<sup>17</sup> where an even higher accuracy is required in order to calculate sensible reaction constants.

Besides thermochemical or kinetic applications, quantum chemistry can predict various spectroscopic parameters, e.g., electronic excitation energies or rotational constants and vibrational frequencies. A lot of spectroscopic methods reach an extremely high accuracy. For example, methods in rotational spectroscopy like Lamb-dip or Fourier transform techniques can usually achieve a resolution of better than 20 kHz. If the quantitative paradigm is taken seriously, quantum-chemical calculations should attempt to be equally accurate. In other words, they should aim at *spectroscopic accuracy*. This also ensures that in difficult cases the predictions are valuable for the interpretation and guidance of experiments. Reaching spectroscopic accuracy is a very hard task, but it will be shown how quantum chemistry can systematically converge to it.

### 1.3. Coupled-cluster methods: Quantum chemistry with theoretical rigor

In the endeavor for quantitatively reliable predictions via quantum chemistry, we are devoted to a certain methodological philosophy. Some quantum chemists argue that the following three principles almost automatically give more and more accurate results:

1. Theories used should be strictly based on first principles. This implies that no empirical parameters are used in any step of derivation or calculation and that all used equations are based on a theoretically rigorous physical description of the system.
2. The possibility for systematic improvement of all used approximation is required.
3. The errors made during the calculation must be controllable, which means that it should be possible to roughly quantify them.

Not all quantum-chemical methods are governed by these three principles. Most density-functional theory methods, for example, use a number of empirical parameters in the design of functionals.<sup>9</sup> A method that does not use any empirical parameters is Hartree-Fock self-consistent-field (HF-SCF) theory.<sup>18</sup> Historically, the HF-SCF method is one of the oldest proposed schemes to approximately solve the many-body Schrödinger equation. Its importance today mainly stems from the fact that it is well known how to systematically improve its solution based on first principles, which leads to the so-called post-Hartree-Fock methods. The HF-SCF method does not describe the electron-electron interaction correctly and therefore misses a portion of the energy, namely the electron-correlation energy.<sup>18,19,a</sup> This is the method’s major limitation, which post-Hartree Fock methods strive to overcome by accounting for a larger portion of the electron-correlation energy.

---

<sup>a</sup>Throughout this work, electron correlation  $E_{\text{corr}}$  is defined as  $E_{\text{corr}} = E(\text{exact}) - E(\text{HF})^\infty$ , with  $E(\text{exact})$  as the exact non-relativistic ground state energy of a system within the Born-Oppenheimer approximation and  $E(\text{HF})^\infty$  as the Hartree-Fock energy in the complete basis-set limit.

One family of post-Hartree-Fock methods, which complies with the methodological philosophy above *and* has the capacity to achieve high accuracy is coupled-cluster theory.<sup>20</sup> Not only does coupled-cluster theory provide a good description of electron correlation, this description can also be systematically improved. Furthermore, the coupled-cluster methods form a rigorous hierarchy regarding their accuracy. It is therefore possible to estimate the error in a certain calculation with the help of a hierarchically superior method.<sup>21</sup> On top of that coupled-cluster theory is size extensive. Size extensivity ensures a physically sensible scaling of the energy with the system size and is important, e. g., when reaction energies are to be calculated. For a lot of molecular properties like gradients, NMR shifts, electronic excitation energies etc. coupled-cluster treatments are nowadays available and provide very accurate results.<sup>21–24</sup>

Coupled-cluster theory in its single-reference formulation is highly elegant. Its major flaw is that it does not perform well for multireference cases.<sup>b</sup> Multireference cases occur when several electronic configurations in a system are energetically degenerate or quasi-degenerate. A lot of interesting and important problems in chemistry like transition-metal compounds or bond-breaking situations require a multireference treatment. However, unlike for other post-Hartree-Fock methods, it is not at all straightforward to find the multireference analogue for coupled-cluster theory. The search for a good multireference coupled-cluster (MRCC) method has been going on for decades – which is why many scientists consider the multireference coupled-cluster problem the “holy grail” of quantum chemistry. No formulation of MRCC theory is known that is of same rigor and elegance as single-reference coupled-cluster methods and the existing methods often do not provide quantitatively satisfactory results at a reasonable computational cost. A number of MRCC methods do not even possess the property of size extensivity.<sup>25</sup>

Therefore the formulation of a satisfactory MRCC theory would contribute immensely to the predictive power of coupled-cluster theory.

#### **1.4. Molecules with heavy main-group elements: Demonstrating the predictive power of coupled-cluster theory**

In Part II we aim at the first goal of this dissertation – the demonstration of the predictive power of coupled-cluster theory – via the prediction of hitherto unknown molecules containing heavy main-group elements. This is achieved in collaboration with the rotational spectroscopists Valerio Lattanzi, Michael C. McCarthy (both from Harvard University, Cambridge, USA), and Sven Thorwirth (from Universität zu Köln, Germany), who confirm our predictions by experimentally detecting and characterizing the corresponding new molecules.

The experimental characterization via rotational spectroscopy is performed in connection with discharge experiments. In discharge experiments a plethora of species is formed and it is crucial to have accurate predictions at hand in order to verify that a particular signal was actually caused by the species in question. Furthermore, accurate predictions for rotational transitions narrow down the experimentally probed bandwidth significantly. Therefore we aim at calculating rotational constants which deviate no more than 0.1% from highly accurate experiments. Typically this corresponds to an accuracy of 5-10 MHz. Rotational constants depend on the structure of the molecule, thus the accuracy aim can also be formulated in

---

<sup>b</sup>To be more exact, for these cases the hierarchy of coupled-cluster methods does not converge with an acceptable rapidity towards the exact result. Very high levels in the hierarchy can treat multireference cases but they are computationally very demanding.

terms of structural parameters. Here, an accuracy of at least 0.001 Å regarding the bond length is desired.

The required accuracy in the calculation of rotational constants and structural parameters can be reached by exploiting the hierarchy of single-reference coupled-cluster methods. The necessary methodological achievements have been completed in the last decade.<sup>26,27</sup> We take on the challenge of identifying exciting applications for these methods. Heavy-atom main-group chemistry is of special interest because it is often inconsistent with chemical intuition. Not many qualitative rules have been formulated to predict structures and chemical behavior in this field, which implies that the predictive power of quantum chemistry can really make a difference here. In addition to the prediction of chemical phenomena, it is demonstrated how coupled-cluster calculations can guide experiments in rotational spectroscopy. Quantum-chemical tools also provide a rigorous analysis of the bonding situation, which explains the results in terms of qualitative chemical rules – and in this sense unites the qualitative and quantitative paradigm. Part II thus covers the complete troika of objectives in quantum chemistry and demonstrates the achievements of coupled-cluster theory and its significance.

## 1.5. First-order spin-orbit splittings via multireference coupled-cluster theory: Improving the predictive power of quantum chemistry

The improvement of predictive power will be presented in Part III and is achieved by developing a new method for the calculation of first-order spin-orbit splittings in  $^2\Pi$  states.

In computational thermochemistry of open-shell molecules, the consideration of first-order spin-orbit splittings is indispensable if chemical or sub-chemical accuracy is to be achieved. The magnitude of spin-orbit splittings lies in the range of a few hundred to a few thousand wave numbers. The heavier the involved elements the larger are spin-orbit effects – for OH the experimental value is 139.2 cm<sup>-1</sup> while for TeH it amounts to 3840 cm<sup>-1</sup>.<sup>28,29</sup> Converting these numbers, spin-orbit splittings in general can contribute 1 to 50 kJ·mol<sup>-1</sup> to the total energy! This underlines how important it is in computational thermochemistry to calculate spin-orbit splittings with good accuracy, preferably 0.1 kJ·mol<sup>-1</sup> (about 10 cm<sup>-1</sup>) or better. Strictly following the quantitative paradigm, however, it is desirable for quantum-chemical calculations to give similarly accurate results as experimental measurements. Via UV/Vis spectroscopy spin-orbit splittings can be determined with a high reliability – but in some cases the interpretation of spectra has proven to be difficult.<sup>30</sup> If theory is to provide predictions which can act as an aid for this interpretation, a spectroscopic accuracy of 1 cm<sup>-1</sup> or better has to be reached. This is hard to accomplish and can only be considered a long-term objective. The development of a more reliable method for the calculation of spin-orbit splittings can be seen as a first step towards this goal.

In contrast to the closed-shell molecules that are considered in Part II, the calculation of first-order spin-orbit splittings in  $^2\Pi$  states represents a multireference case.<sup>c</sup> Since it is so difficult to formulate a satisfactory MRCC theory, no established coupled-cluster method exists to calculate first-order spin-orbit splittings. Presently, the state-of-the-art method for their treatment is therefore multireference-configuration interaction (MRCI), another post-Hartree-Fock method which incorporates electron correlation but lacks the important

<sup>c</sup>The exact reason will be discussed in Chapter 5.

property of size extensivity. MRCI results for spin-orbit splittings are acceptable but do not achieve an accuracy of better than  $10 \text{ cm}^{-1}$  in many cases.<sup>31,32</sup>

We will contribute to the improvement of coupled-cluster theory's predictive power by developing a method for the calculation of spin-orbit splittings in  $^2\Pi$  states using a multireference coupled-cluster wave function. Among the many variants of MRCC theory we choose Mukherjee's MRCC method as the main focus. In contrast to many other methods, Mukherjee's MRCC is size extensive<sup>33</sup> and has been shown to provide acceptable results for some molecular properties, for example for structural parameters.<sup>34</sup> However, recently concerns have been raised regarding methodological shortcomings of this method.<sup>35-37</sup> Furthermore, it has been shown that it does not perform well for all molecular properties.<sup>38,39</sup> In addition to providing acceptable results for spin-orbit splittings it is therefore our goal to learn more about the shortcomings of Mukherjee's MRCC and related methods via this treatment.

Spin-orbit interaction is a relativistic effect and can only be described in the scope of relativistic quantum chemistry. Special relativity also shows itself in spin-independent effects on atoms and molecules, namely scalar-relativistic effects. The heavier the element the more important the scalar-relativistic contribution becomes. In the calculation of spin-orbit splittings in heavy-atom molecules, the scalar-relativistic contribution can be of a large magnitude and its neglect would limit the accuracy significantly. In these cases, an improvement can be achieved if scalar-relativistic effects are rigorously accounted for during the calculation. Spin-free Dirac-Coulomb theory<sup>40</sup> will be used to cope with these effects in this dissertation.

The ideas that are developed for calculating spin-orbit splittings with Mukherjee's MRCC method are general in the sense that they can be transferred to any other MRCC theory. This means that if a better MRCC method will be proposed in the future, the scheme presented in this dissertation can still be applied.

## 2. Theoretical background

### 2.1. The time-independent electronic Schrödinger equation

The core of non-relativistic quantum-chemical methods is the time-independent Schrödinger equation,

$$\hat{H} |\Psi\rangle = E |\Psi\rangle . \quad (2.1)$$

Quantum-chemical methods strive to solve it as accurately (and at the same time efficiently) as possible. The Hamiltonian  $\hat{H}$  generally includes all types of interactions between electrons and nuclei in a molecular system. However, in most cases the Born-Oppenheimer approximation is used to separate the nuclear from the electronic motion, which simplifies the solution of the Schrödinger equation tremendously.<sup>18</sup> In this approximation the total wave function  $\Psi$  is written as a product of the nuclear wave function  $\Psi_N$  and the electronic wave function  $\Psi_e$ . The latter explicitly depends on the electronic coordinates but only parametrically on the nuclear coordinates. The electronic wave function is then determined by solving the electronic Schrödinger equation

$$\hat{H}_e |\Psi_e\rangle = E_e |\Psi_e\rangle , \quad (2.2)$$

with the Hamiltonian

$$\hat{H}_e = -\frac{1}{2} \sum_i \nabla_i^2 - \sum_{i,A} \frac{Z_A}{\mathbf{R}_{iA}} + \sum_{i<j} \frac{1}{\mathbf{r}_{ij}} . \quad (2.3)$$

$Z_A$  is the nuclear charge of the  $A$ th nucleus, which has the distance  $\mathbf{R}_{iA}$  from the  $i$ th electron (in atomic units). The electrons  $i$  and  $j$  are separated by the distance  $\mathbf{r}_{ij}$ . For convenience, the index  $e$  will be omitted in the following if an expression refers to the electronic Schrödinger equation.

One of the most notable ways of solving this equation is the Hartree-Fock self-consistent-field method (HF-SCF), in which the wave function is represented by a Slater determinant. For more information on the HF-SCF method the reader is referred to Ref. 9 or Ref. 18.

### 2.2. Electron correlation

The HF-SCF solution of the electronic-structure problem usually accounts for about 99% of the total energy.<sup>9,18</sup> At first glance this is not a bad performance but the remaining 1% are crucial for the solution of many chemical problems. The energy portion that is neglected in the HF-SCF method is called *correlation energy* and arises because a single Slater-determinantal

description does not include Coulomb correlation. Consequently, the motion of electrons with opposite spins is not correlated.<sup>18</sup>

A rigorous treatment of electron correlation is essential to secure the predictive power of quantum chemistry. It can be accounted for by systematically improving the HF-SCF solution. Instead of only considering one Slater determinant  $\Phi_0$ , the wave function is augmented by weighted contributions of excited Slater determinants  $\Phi_q$ . All possible Slater determinants form a complete set within the  $N$ -electron Hilbert space and the exact wave function of a system can be represented as

$$|\Psi_{\text{exact}}\rangle = |\Phi_0\rangle + \sum_{Q \in \text{all}} c_q |\Phi_q\rangle . \quad (2.4)$$

$c_q$  in the above equation are appropriate weighting coefficients. The eigenvalues of the Hamiltonian matrix  $\langle \Phi_i | \hat{H} | \Phi_j \rangle$  then yield the exact energies of ground and excited states and the corresponding method is called *full configuration-interaction* (full CI) method. Within a given basis set, the full CI method leads to the numerically exact solution of the time-independent electronic Schrödinger equation. Unfortunately, the solution of the full CI problem is not often computationally feasible. The expansion of the wave function is usually cut off at a certain level of excitation, which leads to truncated CI methods.

### 2.3. Size consistency and size extensivity

The main problem with truncated CI *ansätze* for the wave function is that the corresponding methods are neither size consistent nor size extensive. A lack of size consistency implies that the energy of two non-interacting subsystems  $A$  and  $B$ ,  $E_{AB}$ , does not equal the sum of the individual energies  $E_A + E_B$ . For example, the calculation of two non-interacting  $\text{H}_2$  molecules at infinite distance does not give exactly twice the energy of one  $\text{H}_2$  molecule. In truncated CI methods the energy of the two  $\text{H}_2$  molecules is not additively separable and the wave function is not multiplicatively separable.<sup>21,41</sup>

Size extensivity is closely related to the concept of size consistency. If a method is size extensive the (correlation) energy scales linearly with the system size in the limit of an infinitely large system.<sup>41</sup> An associated term is “connectedness”, which is often used in reference to the diagrammatic representation of quantum-chemical equations: If a method exclusively contains connected diagrams in the diagrammatic expansion of the energy, it is size extensive.

Especially in case of size consistency, it is trivial to see that the lack thereof is highly problematic when reaction energies are to be calculated. Therefore, the development of size consistent methods that account for the correlation energy is highly desirable.

### 2.4. Coupled-cluster theory

One solution to the lack of size extensivity and size consistency is coupled-cluster theory. Here, excited determinants are generated via an exponential *ansatz* for the wave function, which guarantees the multiplicative separability of the coupled-cluster wave function  $\Psi_{CC}$ ,<sup>20,21,42,43</sup>

$$|\Psi_{CC}\rangle = e^{\hat{T}} |\Phi_0\rangle . \quad (2.5)$$

$\Phi_0$  is the reference determinant. The cluster operator  $\hat{T}$  is given by

$$\begin{aligned}\hat{T} &= \hat{T}_1 + \hat{T}_2 + \dots \\ \hat{T}_1 &= \sum_{ia} t_i^a a_a^\dagger a_i \\ \hat{T}_2 &= \frac{1}{4} \sum_{ij,ab} t_{ij}^{ab} a_a^\dagger a_i a_b^\dagger a_j \text{ etc. ,}\end{aligned}\tag{2.6}$$

with  $a_a^\dagger$  as a creation operator causing the creation of an electron in the virtual orbital  $a$  and  $a_i$  as an annihilation operator causing the annihilation of an electron in the occupied orbital  $i$ . The coupled-cluster energy can be determined by insertion of the coupled-cluster (CC) wave function into the Schrödinger equation,

$$\hat{H} e^{\hat{T}} |\Phi_0\rangle = E_{CC} e^{\hat{T}} |\Phi_0\rangle .\tag{2.7}$$

Premultiplication with  $e^{-\hat{T}}$  and projection on the reference determinant  $\Phi_0$  yields the expression for the coupled-cluster energy

$$E_{CC} = \langle \Phi_0 | e^{-\hat{T}} \hat{H} e^{\hat{T}} | \Phi_0 \rangle .\tag{2.8}$$

The amplitudes  $t_{ij,\dots}^{ab,\dots}$  can be obtained by projection on excited determinants and solution of the corresponding system of non-linear equations

$$\begin{aligned}\text{Singles} & \quad 0 = \langle \Phi_i^a | e^{-\hat{T}} \hat{H} e^{\hat{T}} | \Phi_0 \rangle \\ \text{Doubles} & \quad 0 = \langle \Phi_{ij}^{ab} | e^{-\hat{T}} \hat{H} e^{\hat{T}} | \Phi_0 \rangle \\ \text{etc.} & \quad\end{aligned}\tag{2.9}$$

If all possible excited determinants are considered, the coupled-cluster wave function is equivalent to a full CI wave function. To decrease the computational cost the expansion of the wave function is usually truncated. Even truncated CC methods possess the property of size extensivity, though. Often only the single- and double-excitation operators  $\hat{T}_1$  and  $\hat{T}_2$  are taken into account, which leads to the CCSD method. However, the triples contributions have been shown to be important for the accurate calculation of many molecular properties.<sup>21,44</sup> Since it is computationally demanding to calculate the full triples contribution, approximate schemes have been developed. The most popular among them is the CCSD(T) truncation scheme.<sup>45-47</sup> Single and double excitations are augmented with those contributions from triple excitations that are required to obtain the energy up to fourth order in Møller-Plesset perturbation theory. These triples are not determined iteratively, but constructed using converged  $\hat{T}_2$  amplitudes. Furthermore, the energy is augmented with a fifth-order contribution constructed with singles amplitudes. Nowadays, CCSD(T) is considered a “gold standard” in electronic-structure theory because it provides accurate results at a reasonable computational cost.

In general, coupled-cluster theory has been extremely successful in giving highly accurate solutions to the electronic-structure problem. We will show in this thesis that coupled-cluster theory has a vast predictive power when it comes to chemical problems.

## 2.5. Coupled-cluster extrapolation and additivity schemes

The predictive power of quantum chemistry hinges on the quantitative comparability with experiment. However, the assumption that the non-relativistic Schrödinger equation within the Born-Oppenheimer approximation provides an accurate description of an experimental situation is not necessarily true. Scalar-relativistic (ScR) and first-order spin-orbit (SO) effects, non-Born-Oppenheimer contributions (BOC), zero-point vibrational effects (ZPE) and many other effects might constitute important corrections to the energy. The best-estimate energy that reproduces the actual situation in experiment can be written as a sum of all those contributions

$$E_{\text{best estimate}} = E_{\text{HF-SCF}} + \Delta E_{\text{correlation}} + \Delta E_{\text{ScR}} + \Delta E_{\text{SO}} + \Delta E_{\text{BOC}} + \Delta E_{\text{ZPE}} + \dots \quad (2.10)$$

In highly accurate extrapolation and additivity schemes, all contributions to the energy are calculated as accurately as possible, preferably via coupled-cluster methods. The methods described in the following were developed for the HEAT (“High accuracy extrapolation *ab initio* thermochemistry”) protocol,<sup>26</sup> which attempts to calculate thermochemical data for small molecules with the highest achievable accuracy.

During the calculation of the Hartree-Fock energy, a severe limit of accuracy is the basis-set approximation. The use of an infinitely large basis set is computationally not feasible. Using the correlation-consistent basis sets of the cc-pVXZ family,<sup>48</sup> for example, one can extrapolate to the basis-set limit  $E(\text{HF})^\infty$ . The extrapolation is achieved using the formula<sup>49</sup>

$$E(\text{HF})^\infty = E(\text{HF}/\text{cc-pVXZ}) + a \cdot e^{-bX}, \quad (2.11)$$

with  $X$  as the cardinal number of the basis set (for example,  $X=3$  for cc-pVTZ,  $X=4$  for cc-pVQZ etc.). The cc-pVXZ basis-set family are designed to form a hierarchy, which implies a systematic convergence towards the basis-set limit with growing cardinal number.<sup>9</sup> In principle the use of any hierarchically designed basis-set family is permitted. In the above formula the parameters  $a$  and  $b$  as well as the Hartree-Fock energy in the complete basis-set limit can be determined from three Hartree-Fock calculations with three subsequent basis sets.

If the correlation energy  $\Delta E_{\text{corr}}$  is to be determined via a coupled-cluster method, the calculation is limited by two approximations: The basis-set approximation and the truncation of the cluster operator. For the extrapolation of coupled-cluster correlation energies to the complete basis-set limit, the following formula has proven to be accurate:<sup>50</sup>

$$E(\text{CC})^\infty = \Delta E(\text{CC}/\text{cc-pVXZ}) - \frac{c}{X^3}. \quad (2.12)$$

This means that only two coupled-cluster calculations are necessary to determine the parameter  $c$  and the coupled-cluster energy in the complete basis-set limit.

These extrapolations are combined with additivity schemes to approach the full CI limit. The correlation energy is then given by

$$\Delta E_{\text{corr}} = \Delta E_{\text{CCSD(T)}} + \Delta E_{\text{CCSDT}} + \Delta E_{\text{CCSDTQ}} + \dots + \Delta E_{\text{core}} \quad (2.13)$$

$\Delta E_{\text{core}}$  is the core-correlation contribution and can be evaluated as the difference between an all-electron calculation and a frozen-core calculation. The contributions involving full triple, quadruple, ..., excitations are usually evaluated with a small basis set to make their calculation computationally practicable.

An example for the short notation of the level of theory used in a specific calculation with extrapolation and additivity schemes is fc-CCSD(T)/cc-pV $\infty$ Z+ $\Delta$ T/cc-pVTZ + $\Delta$ Q/cc-pVDZ + $\Delta$ core/cc-pCV5Z. This means that in this calculation a frozen-core CCSD(T)-calculation was extrapolated to the basis-set limit. The resulting energy was augmented with effects from the corresponding higher excitations calculated with the corresponding basis sets. Core-correlation effects were also taken into account and evaluated on CCSD(T) level using a cc-pCV5Z basis set.

For the relativistic, zero-point vibrational, and Born-Oppenheimer corrections to the energy various methods are in principle imaginable, with the one restriction that they should be evaluated using a coupled-cluster wave function. This requirement is fulfilled for all named effects except for the first-order spin-orbit correction, which is only available at multireference configuration-interaction level. It is one goal of this dissertation to rectify this shortcoming. The described extrapolation and additivity schemes are not only useful when calculating energies, via gradient theory geometry optimizations can be performed as well. Bond lengths and bond angles are then determined to a particularly high accuracy. The bond lengths obtained from the level used for the short notation example is assumed to have an intrinsic accuracy of better than 0.001 Å.<sup>27,51–53</sup>

## 2.6. The multireference problem

A major drawback of truncated CC (and truncated CI) methods is that they give inadequate results for so-called multireference cases. Multireference cases arise when in Eq. 2.4 some of the weights  $c_q$  are very large. In that case, an appropriate zeroth-order wave function must include all determinants with a large weight for the solution to give even a qualitatively correct picture. The zeroth-order wave function  $\Psi_0$  must then be expressed in the following way

$$|\Psi_0\rangle = \sum_{\mu} c_{\mu} |\Phi_{\mu}\rangle, \quad (2.14)$$

with  $\Phi_{\mu}$  representing a determinant with a large weight. All determinants  $\Phi_{\mu}$  are then called reference determinants and span the so-called model space. The reference determinants are often chosen based on the distribution of a certain number of *active electrons* in selected *active orbitals*. If all possible distributions are considered, the resulting active space is called complete active space (CAS). The corresponding determinants  $\Phi_{\mu}$  are then said to span a complete model space.

Examples for multireference cases are molecules with degeneracies or near-degeneracies like transition-metal compounds and biradicals. Furthermore, molecules almost always show multireference character in bond-breaking situations.

It is straightforward to extend the CI method to multireference cases. Instead of Eq. 2.4, we now write for the multireference CI (MRCI) wave function<sup>54</sup>

$$|\Psi_{\text{MRCI}}\rangle = \sum_{\mu} c_{\mu} |\Phi_{\mu}\rangle + \sum_{\mu} \sum_{ia} c_i^a(\mu) |\Phi_i^a(\mu)\rangle + \sum_{\mu} \sum_{ij,ab} c_{ij}^{ab}(\mu) |\Phi_{ij}^{ab}(\mu)\rangle + \dots \quad (2.15)$$

In the above equations redundancies may occur because a certain excited determinant is accessible from several reference determinants. Their elimination is rather straightforward, though, by simply excluding the corresponding terms. This redundancy problem will be described in more detail below, because it is not as straightforward to solve in multireference coupled-cluster methods.

Just as its single-reference sibling, truncated MRCI is neither size consistent nor size extensive.<sup>54</sup> Several schemes are routinely used to approximately correct *a posteriori* for the size-extensivity error. Among them are the so-called Pople correction and the multireference Davidson correction.<sup>55–57</sup> Other important approximately size-extensive method related to MRCI are the multireference averaged quadratic coupled-cluster (MR-AQCC) method<sup>58</sup> and the multireference averaged coupled-pair functional (MR-ACPF) method.<sup>59</sup> In these methods, a correction in the denominator is added to the usual MRCI energy functional that is made stationary with respect to the coefficients. Despite of its lack of size extensivity, MR-AQCC gives quite accurate results for a large variety of problems.<sup>25,58,60</sup>

Nevertheless there have been lots of efforts in the past 30 years to formulate a rigorously size-extensive multireference coupled-cluster (MRCC) method. Unfortunately, the generalization of the exponential wave function *ansatz* to multireference problems is quite complicated and a satisfactory solution has not been reached. The multireference coupled-cluster (MRCC) methods that have been developed so far will be discussed in the next sections.

## 2.7. Multireference coupled-cluster wave function ansätze

In principle, there are two possibilities of “marrying” Eq. 2.14 with Eq. 2.5.<sup>25</sup> First, one excitation operator acting on all reference determinants at once can be defined

$$|\Psi_{\text{MRCC}}\rangle = e^{\hat{T}} \sum_{\mu} c_{\mu} |\Phi_{\mu}\rangle, \quad (2.16)$$

which leads to the internally contracted MRCC (IC-MRCC) methods. It almost looks like the single-reference coupled-cluster *ansatz*, with the slight difference that there is no uniquely defined Fermi vacuum. As a consequence, the IC-MRCC  $\hat{T}$  operator must contain excitations into the active space and out of the active space, which makes its structure very complicated.<sup>61</sup> The derivation and implementation of IC-MRCC is thus most difficult without automatic implementation techniques.<sup>62,63</sup>

Second, one  $\hat{T}$  operator for every determinant can be defined. This possibility for the marriage is the *Jeziorski-Monkhorst ansatz* (JM *ansatz*)<sup>64</sup>

$$|\Psi_{\text{MRCC}}\rangle = \sum_{\mu} e^{\hat{T}_{\mu}} c_{\mu} |\Phi_{\mu}\rangle. \quad (2.17)$$

In this thesis, we will focus on Jeziorski-Monkhorst based methods.

It is noteworthy that multireference coupled-cluster methods can also be formulated on basis of a single-reference *ansatz* for the wave function. In these cases the multireference character is reproduced by taking selected higher excitations into account. Many different methods have been developed following this notion. The SR-MRCC method by Oliphant and Adamowicz is a prominent and numerically quite successful example.<sup>65</sup> However, these methods do not belong to the “genuine” MRCC methods since they do not treat all reference determinants  $\Phi_\mu$  on the same footing.

## 2.8. Jeziorski-Monkhorst based MRCC methods

### 2.8.1. State-universal multireference coupled-cluster theory

The Jeziorski-Monkhorst *ansatz* will now be used to define a multireference coupled-cluster method, namely state-universal multireference coupled-cluster theory (SU-MRCC). In SU-MRCC all states of a given model space are treated at the same time, hence the name of the method.

Inserting the JM *ansatz* for the wave function into the Schrödinger equation and left-projecting by  $\Phi_\nu$  leads to the following energy equation

$$\sum_{\nu}^d H_{\mu\nu}^{\text{eff}} c_{\nu} = E c_{\mu} , \quad (2.18)$$

with  $d$  as the number of determinants and the effective Hamiltonian

$$H_{\mu\nu}^{\text{eff}} = \langle \Phi_{\mu} | \hat{H} e^{\hat{T}^{\nu}} | \Phi_{\nu} \rangle . \quad (2.19)$$

Diagonalization of the effective Hamiltonian yields the energy  $E$  and the weighting coefficients  $c_{\mu}$ . For a complete model space the effective Hamiltonian matrix is a connected quantity because in that case

$$H_{\mu\nu}^{\text{eff}} = \langle \Phi_{\mu} | \hat{H} e^{\hat{T}^{\nu}} | \Phi_{\nu} \rangle \stackrel{\text{CMS}}{=} \langle \Phi_{\mu} | e^{-\hat{T}^{\nu}} \hat{H} e^{\hat{T}^{\nu}} | \Phi_{\nu} \rangle = \langle \Phi_{\mu} | \bar{H}_{\nu} | \Phi_{\nu} \rangle , \quad (2.20)$$

where the similarity transformed Hamiltonian  $\bar{H}_{\nu}$  contains connected terms only.

The amplitude equations in SU-MRCC theory can be derived using the Bloch equation,<sup>64</sup> which results in amplitude equations of the following form

$$\langle \Phi_{ij\dots}^{ab\dots}(\mu) | \bar{H}_{\mu} | \Phi_{\mu} \rangle - \sum_{\nu \neq \mu} \langle \Phi_{ij\dots}^{ab\dots}(\mu) | e^{-\hat{T}^{\mu}} e^{\hat{T}^{\nu}} | \Phi_{\nu} \rangle H_{\nu\mu}^{\text{eff}} = 0 . \quad (2.21)$$

It is obvious that the amplitude equations contain a single-reference term and a term that describes the coupling between the reference determinants. Although this coupling term does not seem very complicated, it cannot be converted into a closed expression. Note that the amplitude equations of SU-MRCC do not directly depend on the weighting coefficients. This observation is important when deriving a suitable Lagrangian for the gradient theory of SU-MRCC.<sup>66,67</sup>

Difficulties with SU-MRCC arise because of the so called *intruder-state problem*,<sup>68</sup> which leads to serious convergence issues. Intruders emerge when an excited determinant possesses a similar energy as an electronic state within the model space. The intruder-state problem significantly limits the applicability of SU-MRCC and has been tackled by carefully selecting the reference determinants for the zeroth-order wave function.<sup>68,69</sup>

## 2.8.2. State-specific multireference coupled-cluster theory

### 2.8.2.1. The redundancy problem

A natural way to avoid intruder states is to focus on one state at a time instead of considering all of them at once. This leads to state-specific coupled-cluster theories, which solve the intruder-state problem but introduce a new obstacle: The notorious redundancy problem.

To show where the redundancy problem stems from, we try to obtain amplitude equations by inserting the JM *ansatz* into the Schrödinger equation and naively left-projecting with excited state determinants  $\Phi_q$

$$\sum_{\mu} \langle \Phi_q | (\hat{H} - E) e^{\hat{T}_{\mu}} | \Phi_{\mu} \rangle c_{\mu} = 0 . \quad (2.22)$$

Eq. 2.22 does not provide enough equations for all amplitudes. The reason for this underdetermination is that the application of certain excitation operators to two different model-space determinants may yield the same excited determinant, therefore the projection spaces of the reference determinants may overlap.<sup>25,36</sup> In other words, the number of linearly independent states in  $\Phi_q$  is smaller than the number of amplitudes to be determined.

There are two strategies to solve this problem. In the first strategy the number of independent parameters is reduced, which was first done by Evangelisti<sup>70</sup> and then popularized via the MRexpT method by Hanrath.<sup>71</sup>

The second strategy is to artificially increase the number of equations by introducing sufficiency conditions. Following an argumentation by Kong,<sup>36</sup> the general strategy can be demonstrated using Eq. 2.22. Invoking sufficiency conditions means that the individual summands of Eq. 2.22 are set to zero

$$\langle \Phi_q | (\hat{H} - E) e^{\hat{T}_{\mu}} | \Phi_{\mu} \rangle c_{\mu} \stackrel{!}{=} 0 . \quad (2.23)$$

Since  $c_{\mu}$  is non-zero, one can also write

$$\langle \Phi_q | (\hat{H} - E) e^{\hat{T}_{\mu}} | \Phi_{\mu} \rangle \stackrel{!}{=} 0 . \quad (2.24)$$

Manipulating Eq. 2.25 or Eq. 2.24 leads to methods like Mukherjee's multireference coupled-cluster theory (Mk-MRCC) and Brillouin-Wigner multireference coupled-cluster theory (BW-MRCC). It is noteworthy that invoking the sufficiency conditions causes the proper residual conditions,

$$\sum_{\mu} \langle \Phi_q | (\hat{H} - E) e^{\hat{T}_{\mu}} | \Phi_{\mu} \rangle c_{\mu} = 0 . \quad (2.25)$$

not to be fulfilled anymore.

### 2.8.2.2. The MRexpT method

The MRexpT method has been proposed by Hanrath in 2005.<sup>71</sup> His idea comprises an alternative “indexing” of the amplitudes. Instead of assigning the amplitudes to the *starting* point of an excitation, the *end* point of an excitation is used as an index. In case of a linearly independent projection space  $\Phi_q$  this means that we obtain exactly the desired number of independent parameters because those amplitudes that point to the same excited determined are confined to the same value. However, since for symmetry reasons the situation  $c_\mu = -c_\nu$  might occur, a phase factor  $\chi(c_\mu)$  has to be inserted to avoid cancellation effects. The amplitudes in MRexpT are then defined as

$$\hat{T}_\mu = \chi(c_\mu) \sum_{q(\mu)} t_q \tau_q(\mu) . \quad (2.26)$$

In the above equation,  $\tau_q(\mu)$  represents a string of excitation operators. The amplitude equations in MRexpT are given by

$$\sum_{\mu} c_{\mu} \left( \langle \Phi_q | \hat{H} e^{\hat{T}_\mu} | \Phi_\mu \rangle - \langle \Phi_q | e^{\hat{T}_\mu} | \Phi_\mu \rangle \times \sum_{\nu} \frac{c_\nu}{c_\mu} \langle \Phi_\mu | \hat{H} e^{\hat{T}_\nu} | \Phi_\nu \rangle \right) = 0 . \quad (2.27)$$

Unfortunately MRexpT is not fully size extensive. To be more exact, the method possesses core extensivity but no core-valence and valence-valence extensivity.<sup>41,72,73</sup> So far, only a pilot implementation of MRexpT is available.<sup>71</sup>

Despite the simple and clever idea of reducing the number of independent parameters to face the redundancy problem, no further endeavors to develop a size-extensive method using the same premises as MRexpT have been published.

### 2.8.2.3. Brillouin-Wigner MRCC

Not much manipulation of Eq. 2.24 is necessary to derive the amplitude equations for Brillouin-Wigner multireference coupled-cluster theory<sup>36,74,75</sup>

$$\langle \Phi_q(\mu) | \hat{H} e^{\hat{T}_\mu} | \Phi_\mu \rangle - \langle \Phi_q(\mu) | e^{\hat{T}_\mu} | \Phi_\mu \rangle E = 0 . \quad (2.28)$$

As in SU-MRCC, the amplitude equations consist of a single-reference coupled-cluster part and a term which couples the reference determinants. The coupling term in BW-MRCC has straightforward, closed expressions and is rather simple in terms of implementation. However, the coupling is only mediated via the energy  $E$  and it is uncertain if this description is appropriate. It is also obvious from the above equation that BW-MRCC theory is an unconnected theory and thus lacks size extensivity.

Despite this major drawback a lot of further developments with BW-MRCC are available. For example, analytic gradients,<sup>67</sup> full and perturbative triples,<sup>76</sup> and – most recently – an F12 method have been developed.<sup>77</sup> However, because of the missing size extensivity, BW-MRCC cannot be the final answer to the MRCC problem.

### 2.8.2.4. Mukherjee's multireference coupled cluster theory

A much better solution than BW-MRCC is Mukherjee's multireference coupled-cluster (Mk-MRCC), mainly because it is manifestly size extensive.<sup>33</sup> The derivation of Mk-MRCC starts with inserting a resolution of the identity

$$\hat{H} = e^{\hat{T}_\mu} (\hat{Q} + \hat{P}) e^{-\hat{T}_\mu} \hat{H} \quad (2.29)$$

$$\hat{Q} = \sum_q |\Phi_q\rangle \langle \Phi_q| \quad (2.30)$$

$$\hat{P} = 1 - \hat{Q} = \sum_\mu |\Phi_\mu\rangle \langle \Phi_\mu| \quad (2.31)$$

into Eq. 2.22. As a consequence, a double summation over  $\mu$  and  $\nu$  appears in the equation. Interchanging the dummy indices in this double summation, substituting the projection manifold  $\langle \Phi_q|$  by  $\langle \Phi_q| e^{-\hat{T}_\mu}$  and invoking the sufficiency conditions leads to the final Mk-MRCC amplitude equation

$$\langle \Phi_q(\mu) | \bar{H}_\mu | \Phi_\mu \rangle c_\mu + \sum_{\nu \neq \mu} \langle \Phi_q(\mu) | e^{-\hat{T}_\mu} e^{\hat{T}_\nu} | \Phi_\mu \rangle H_{\mu\nu}^{\text{eff}} c_\nu = 0 . \quad (2.32)$$

In analogy to BW-MRCC, the Mk-MRCC amplitude equations consist of a single-reference term and a coupling term. Mahapatra *et al.*<sup>33</sup> succeeded in proving that the method is manifestly size extensive, which in case of the coupling term is a non-trivial task. The Mk-MRCC coupling term looks very similar to the SU-MRCC coupling term but it can be manipulated to yield closed expressions, which are rather straightforward to implement.<sup>78</sup>

A number of Mk-MRCC implementations are routinely available. Among them an implementation by Kállay and coworkers for arbitrary active spaces deserves special mention.<sup>37,79</sup> Further developments of Mk-MRCC include analytic gradients,<sup>34,80,81</sup> perturbative and full triples,<sup>35,82-84</sup> and an explicitly correlated version of Mk-MRCC.<sup>85</sup> Additionally, a spin-free version of Mk-MRCC theory has been developed.<sup>86</sup> Recently, progress has been made in formulating a response theory for Mk-MRCC in order to cope with excited states and excited-state properties. However, this response theory has proven to be problematic since certain excited states exhibit an artificial splitting due to the redundancy in the Mk-MRCC *ansatz*.<sup>38,39</sup>

## 2.9. Comparison of Jeziorski-Monkhorst based MRCC methods

In this section, the advantages and disadvantages of the different Jeziorski-Monkhorst based methods will be discussed. This discussion provides the crucial reasons why the focus of this thesis lies on the Mk-MRCC method. In Tab. 2.1, SU-MRCC, MRexpT, BW-MRCC, and Mk-MRCC are analyzed regarding a number of requirements that a "perfect" MRCC method should fulfill.

The most important criterion at present is size extensivity. If a certain MRCC method does not have this property, there is no advantage over MRCI or MR-AQCC. Of the Jeziorski-Monkhorst based methods, only Mk-MRCC and SU-MRCC strictly fulfill this requirement. SU-MRCC, however, exhibits the notorious intruder-state problem, which is a severe disadvantage. Whether or not the equations of a certain method comply with the proper residual condition,

**Table 2.1.:** Comparison of Jeziorski-Monkhorst based MRCC methods,  $d$  is the number of reference determinants

| Property            | SU-MRCC        | MRexpT | BW-MRCC        | Mk-MRCC        |
|---------------------|----------------|--------|----------------|----------------|
| Size extensivity    | Yes            | Core   | No             | Yes            |
| Intruder-state free | No             | Yes    | Yes            | Yes            |
| Proper residual     | No             | Yes    | No             | No             |
| Orbital invariance  | No             | No     | No             | No             |
| Cost                | $d \cdot$ SRCC | MRCI   | $d \cdot$ SRCC | $d \cdot$ SRCC |

is a more theoretical criterion. Especially if a method performs well in applications, it is not too problematic if this criterion is not met. It has been shown that Mk-MRCC fulfills the proper residual condition for two reference determinants if selected higher excitation are considered, which leads to the Mk-MRCCSDtq method.<sup>37,87</sup> The computational cost of Mk-MRCCSDtq, however, scales with  $d^2 \cdot$ SRCC, which makes this method less feasible, especially for large active spaces. In terms of computational scaling, MRexpT is the best available method, because it in principle scales like MRCI.

An inherent problem of the Jeziorski-Monkhorst *ansatz* is the lack of orbital invariance with respect to rotations of the active orbitals among themselves.<sup>88</sup> If higher excitations than in the Mk-MRCCSD approximation are taken into account, this dependence on the choice of orbitals is weakened. This has been shown for both, the Mk-MRCCSDtq and the Mk-MRCCSDT approximation schemes.<sup>37,82,87</sup>

In the light of this comparison, Mk-MRCC theory seems the best Jeziorski-Monkhorst method available at present. Its popularity has manifested itself in a number of prominent applications over the past years.<sup>89,90</sup> Additionally, MRexpT seems promising but not much is known about this family of methods yet.

## 2.10. Relativistic quantum chemistry

Relativistic effects are important in quantum chemistry. Viable and accurate predictions regarding chemical phenomena can often not be obtained if they are neglected. Especially for heavy elements, relativistic contributions can be larger than the electron-correlation energy.<sup>91–93</sup>

Generally, relativistic effects can be divided into two classes. The first class are spin-free (or scalar-relativistic) effects. An important example is the contraction of  $s$  and  $p$  orbitals, which – because of the better shielding of the nuclear charge – causes the  $d$  and  $f$  orbitals to expand. For heavy main-group elements this leads to the *inert-pair effect*, for transition metals it leads to a smaller energy gap between  $s$  and  $d$  shells.

The second class of relativistic effects are spin-dependent effects. In a relativistic picture,  $L$  and  $S$  are no longer good quantum numbers. Instead the quantum number  $J = L + S$  must be used because spin-angular momentum and the orbital-angular momentum are coupled. Spin-orbit coupling already appears in light elements, the splitting of the doublet line in the sodium emission spectrum is a well-known example.

According to Einstein’s theory of special relativity the speed of light is finite and it represents the maximum velocity of actions. This implies that instead of using a Galileo transformation

between inertial frames, the *Lorentz transformation*, which complies with Einstein's demand, has to be used. The momentum then does not have the usual form  $p = mv$  (with  $m$  as the mass and  $v$  as the velocity) anymore, but is given by

$$p = \frac{mv}{\sqrt{1 - \frac{v^2}{c^2}}} . \quad (2.33)$$

$c$  is the speed of light. If quantum chemistry is to be connected with special relativity, this expression must be used for the momentum in a corresponding Hamiltonian. This requirement eventually leads to the time-independent Dirac equation

$$\begin{aligned} \hat{h}^D \Psi &= W \Psi \\ \hat{h}^D &= \beta mc^2 + c\alpha \hat{\mathbf{p}} + V , \end{aligned} \quad (2.34)$$

with  $W$  as the total energy  $W = E + mc^2$  and  $V$  as the potential. The matrices  $\alpha$  and  $\beta$  have the following form

$$\alpha_i = \begin{pmatrix} \mathbf{0} & \sigma_i \\ \sigma_i & \mathbf{0} \end{pmatrix} \quad \text{and} \quad \beta = \begin{pmatrix} \mathbf{1} & \mathbf{0} \\ \mathbf{0} & -\mathbf{1} \end{pmatrix} , \quad (2.35)$$

with  $\sigma_i$  as the Pauli-spin matrices,  $\mathbf{0}$  as a  $2 \times 2$  zero matrix, and  $\mathbf{1}$  as a  $2 \times 2$  unity matrix. It can be shown that  $\hat{h}^D$  is at least four dimensional. As a consequence the wave function is a four-component spinor with the small component  $\chi$  and the large component  $\varphi$

$$\Psi = (\Psi_1, \Psi_2, \Psi_3, \Psi_4)^\top = \begin{pmatrix} \varphi \\ \chi \end{pmatrix} . \quad (2.36)$$

The Dirac equation can then be written in its two-component form as

$$\begin{pmatrix} V & c\sigma \hat{\mathbf{p}} \\ c\sigma \hat{\mathbf{p}} & V - 2mc^2 \end{pmatrix} \begin{pmatrix} \varphi \\ \chi \end{pmatrix} = E \begin{pmatrix} \varphi \\ \chi \end{pmatrix} . \quad (2.37)$$

Most chemical phenomena cannot be predicted by the Dirac equation alone because it only contains one-particle terms. The first step to include two-particle effects is achieved by considering the sum over all electrons of the Dirac Hamiltonian and augmenting it with the non-relativistic Coulomb term

$$\hat{H}^{DC} = \sum_i \hat{h}_i^D + \sum_{i < j} r_{ij}^{-1} . \quad (2.38)$$

The problem with this approach is obvious: It is not invariant in a Lorentz transformation and postulates instantaneous interactions – which according to special relativity are impossible. Making the two-particle interaction Lorentz invariant and thus accounting for the retardation in the particle-particle interaction requires the consideration of quantum electrodynamics. It

leads to the emergence of the Breit-interaction term, which consists of a magnetic term and a retardation term.

Augmenting the Dirac-Coulomb Hamiltonian with the Breit interaction results in the Coulomb-Breit Hamiltonian

$$\hat{H}^{DCB} = \sum_i \hat{h}_i^D + \sum_{i < j} \left( r_{ij}^{-1} + \frac{1}{2} \left[ \frac{\boldsymbol{\alpha}_i \boldsymbol{\alpha}_j}{r_{ij}} + \frac{(\boldsymbol{\alpha}_i \mathbf{r}_{ij})(\boldsymbol{\alpha}_j \mathbf{r}_{ij})}{r_{ij}^3} \right] \right). \quad (2.39)$$

The first correction term in the above equation is called the Gaunt interaction and arises because the electrons are moving. This produces a magnetic current and the Gaunt-interaction essentially accounts for the current-current interaction.<sup>94</sup> The second term is a retardation term, which is also sometimes called gauge term. It arises because the electromagnetic interaction is mediated by photons, which travel at a finite speed – the speed of light. Especially when calculating spin-orbit interactions, the Breit term represents an important contribution and should not be neglected.



## **Part II.**

# **Demonstrating the predictive power of quantum chemistry: Heavy-atom main-group molecules**



## 3. Introduction: Predicting properties of heavy-atom main-group molecules

*Fast is fine, but accuracy is everything.*  
– Xenophon

In this part we investigate molecules containing heavy-atom main-group elements via highly accurate quantum-chemical methods. These methods include extrapolation and additivity techniques for coupled-cluster theory and render very accurate predictions of chemical properties possible. We will show that – combined with chemical intuition – they have predictive power regarding novel chemical phenomena. Furthermore these methods allow for guiding experiments by predicting structural and spectroscopic parameters. Especially in highly accurate spectroscopic methods like rotational spectroscopy these predictions are of great value to experimentalists. Last but not least the bonding and structure of molecules with heavy main-group atoms is explained using tools of bonding analysis.

### 3.1. Heavy-atom main-group chemistry

The chemistry of heavy main-group elements often seems exotic and unfamiliar. Unusual structures and bonding situations are observed and the molecules are extremely sensitive to water and air. However, there are a lot more elements with “exotic” behavior than elements which exhibit the “usual” first-row chemistry of carbon, nitrogen, or oxygen: The elements of the second row and below show a lot of similarities while the chemistry of first-row elements vastly differs from their heavier analogues. For example, the chemical properties of the group 14 elements silicon, germanium, tin, and lead are alike while the corresponding first-row element carbon is dissimilar.

The crucial difference between elements of the first row and elements of all higher rows is the effective nuclear charge. The higher the angular momentum of an electron the smaller is its shielding effect on the positive charge of the nucleus. The nuclear charge is shielded very well in first-row elements because only  $s$  orbitals are encountered in the core regions. In these elements the maximum radial densities of  $s$  and  $p$  valence electrons are located in approximately the same region of space. Repulsion of lone pairs and hybridization are phenomena arising from this close proximity of the electrons and these effects play a big role in the chemistry of first-row elements. The tetrahedral angle that is ubiquitous to carbon chemistry is an obvious example.

Starting from the second row, however, the core orbitals include  $p$  and – starting from the fourth row – even  $d$  shells. This results in  $p$  valence orbitals that are more diffuse and stretched out in space than the corresponding  $s$  valence orbitals. The tendency to hybridize is diminished and bond angles are influenced less by repulsion effects. With growing cardinal number the bond angles rather dovetail with the angles of the atomic orbitals. For example,  $90^\circ$  angles are encountered if  $p$  orbitals form the corresponding bond.<sup>95</sup>

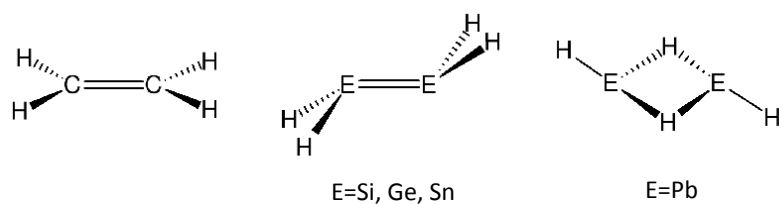


**Figure 3.1.:** Global minimum of ethene and of its heavy-atom analogues.<sup>96,97</sup>

Another consequence of the rather diffuse *p* valence orbitals is the instability of multiple bonds in heavy main-group elements. Examples are the heavy-atom analogues of ethene. Ethene itself shows a classical double bond between the carbon atoms, with  $\sigma$  bonding along the internuclear axis and  $\pi$  bonding perpendicular to it. In a thought experiment, one can imagine two triplet methylene fragments forming the ethylene molecule. The global minima of the ethene's heavy-atom analogues, however, look much different (see Fig. 3.1). For silicon, germanium, and tin, the hydrogen atoms are distorted out of the plane.<sup>96</sup> Following the same thought experiment, two interacting singlet silylene, germylene, and stannylene fragments form ethene's heavy-atom analogues, with a double donor-acceptor bond instead of  $\sigma$ - and  $\pi$ -bonding. This donor-acceptor interaction causes the distortion of the structure towards a bent geometry. In the lead analogue of ethene, this distortion is taken to the extreme and the hydrogen atoms form bridges along the Pb-Pb axis.<sup>97</sup> From the viewpoint of molecular-orbital theory, the geometrical distortion of disilene and the heavier analogues can be considered a second-order Jahn-Teller effect: As a consequence of a small HOMO-LUMO gap, the  $\sigma^*$  orbital mixes with the lone pair, which lowers the energy of the  $\pi$  bonding orbital and introduces more lone-pair character.

Experimental heavy-atom main-group chemistry is a challenge. Compounds like disilene or diplumbene are kinetically and/or thermodynamically unstable towards oxidation or other competing reactions. W. E. Dasent's infamous "non-existent molecules",<sup>98</sup> which were published in 1965, consequently contain a lot of heavy-atom analogues of ordinary first-row compounds like  $\text{SiCl}_4$ . A lot of experimental strategies like bulky ligands or stabilization via donor-acceptor interaction have been developed. Consequently, the limits that Dasent still had in mind while he declared these compounds to be non-existent could to some extent be overcome. Substituted disilenes, digermenes, distannenes and many more heavy-atom main-group molecules have thus become accessible in wet-chemical experiments.<sup>96,99–101</sup>

Additionally there are strategies to experimentally approach the unsubstituted "parent" species of these heavy-atom analogues of simple first-row molecules. Synthesis and analysis via infrared spectroscopy in a low-temperature noble-gas matrix, for example, has proven to be a very useful tool.<sup>97,102–106</sup> The strategy used in the scope of this thesis, entails a discharge experiment and a subsequent analysis by Fourier-transform rotational spectroscopy.<sup>51–53,107–109</sup> In these experiments the molecules are investigated directly in the gas phase. Because of the rather extreme conditions a lot of species are formed after applying the discharge to the reaction mixture, which makes quantum-chemical calculations particularly useful tools to find exactly the desired species.

Finally, gas-phase rotational-spectroscopy measurements of molecules containing heavy-atom main-group elements in general and second-row elements in particular give insights into

astrochemistry. In interstellar space oxidations are very unlikely, which gives rise to the formation of a lot of molecules that are highly unusual on earth. For example, the diatomic SiS has been found in the late-type star IRC+10216.<sup>110</sup>

## 3.2. Quantum chemistry and rotational spectroscopy

Quantum-chemical predictions of parameters relevant to rotational spectroscopy facilitate the characterization of molecules significantly. Predictions of rotational transitions help experimentalists to single out the species of interest in a discharge experiment and can confirm the assignment of signals. If a spectrum with a complicated fine and hyperfine structure is encountered quantum-chemical calculations can be an aid during the interpretation of the spectrum.

To understand how exactly these tasks can be achieved, we start from the rotational Hamiltonian of a rigid rotor  $\hat{H}_{rot}$ . This operator is given by

$$\hat{H}_{rot} = B_x \hat{J}_x^2 + B_y \hat{J}_y^2 + B_z \hat{J}_z^2, \quad (3.1)$$

with  $\hat{\mathbf{J}}$  as the angular momentum operator and  $B_\alpha$  ( $\alpha = x, y, z$ ) as the rotational constant,

$$B_\alpha = \frac{1}{2I_\alpha}. \quad (3.2)$$

$I_\alpha$  is the moment of inertia around the corresponding axis.<sup>111</sup> The axes  $x, y, z$  are defined by the principal axes. This means that the largest principal moment of inertia lies around the  $x$ -axis. In the following we use the  $a, b, c$  notation with  $a$  corresponding to the axis with the biggest rotational constants. Each  $a, b, c$  then corresponds to one of the axes  $x, y, z$ . In rotational spectroscopy, molecules fall into classes according to the relation of the moments of inertia around the axes  $x, y, z$ . For example, if  $I_x = I_y$  we are dealing with a so-called symmetric top or if  $I_x = I_y$  and  $I_z = 0$  the corresponding molecule is a linear top. These relations of the components of  $I$  simplify equations and spectra. In the scope of this work mostly asymmetric tops were encountered where no such simplifications can be made.

From Eq. 3.2 it is evident that a good theoretical estimate of structural parameters already gives a rough value of the rotational constants. However, this picture is incomplete because rotating molecules are, strictly speaking, not rigid. One reason for this non-rigidity is the centrifugal force that a rotating molecule experiences. The centrifugal distortion can be treated via perturbation theory

$$\hat{H}_{rot+CD} = \hat{H}_{rot}^0 + \hat{H}'_{CD}, \quad (3.3)$$

with  $\hat{H}_{rot}^0$  given by Eq. 3.1 and  $\hat{H}'_{CD}$  as the perturbation operator. For symmetric tops  $\hat{H}'_{CD}$  is given by

$$\hat{H}'_{CD} = -D_J \hat{\mathbf{J}}^4 - D_{JK} \hat{\mathbf{J}}^2 \hat{J}_z^2 - D_K \hat{J}_z^4, \quad (3.4)$$

with the  $D$ 's as the quartic centrifugal-distortion constants, indexed by quantum numbers  $J$  and/or  $K$ . For asymmetric tops a so-called reduced Hamiltonian is used, which yields a much

more complicated form of  $\hat{H}'_{CD}$  that additionally entails the centrifugal-distortion constants  $d_1$  and  $d_2$ .<sup>111</sup>

If quantum-chemical calculations are to be compared to experiment, vibrational effects have to be taken into account and the Hamiltonian given in Eq. 3.2 has to be altered accordingly. Starting from the Watson Hamiltonian, a molecular Hamiltonian in the normal-mode formalism whose spectrum gives the rotational-vibrational energy structure,<sup>112</sup> Rayleigh-Schrödinger perturbation theory can be used for an appropriate partitioning

$$\hat{H}_{rot+vib} = \hat{H}_{rot+vib}^0 + \hat{H}'_{rot+vib} . \quad (3.5)$$

$\hat{H}_{rot+vib}^0$  is given by

$$\hat{H}_{rot+vib}^0 = \hat{H}_{rot}^0 + \frac{1}{2} \sum_r \omega_r (\hat{p}_r^2 + \hat{q}_r^2) , \quad (3.6)$$

with  $p_r$  as the momentum and  $q_r$  as dimensionless normal coordinates,

$$q_r = \sqrt{\omega_r} Q_r . \quad (3.7)$$

In the above equation  $Q_r$  are the ordinary normal coordinates with the corresponding harmonic wave numbers  $\omega_r$ .  $\hat{H}'_{rot+vib}$  contains harmonic, cubic, and quartic potentials with respect to  $q_r$ .<sup>111</sup> In this way, vibrational corrections  $\Delta B_{vib}$  to the rotational constant at equilibrium geometry  $B_e$  can be calculated.

In the quantum-chemical calculations within this thesis the following procedure was used to obtain accurate predictions of spectroscopical parameters: A geometry optimization of the molecule in question was conducted at a feasible but highly accurate level of theory. For some small molecules extrapolation and additivity schemes were used to obtain a best theoretical estimate of the geometry. From this geometry the “plain” rotational constants without centrifugal-distortion and vibrational effects can directly be derived. Those constants were augmented by zero-point vibrational corrections, which were calculated at a lower level of theory. The same level of theory was used to calculate centrifugal-distortion constants. All the calculations were performed using the CFOUR quantum-chemical program package.<sup>113</sup>

### 3.3. Methods for bonding analysis

A quantum-chemical calculation gives a quantitative result on the energy or on other properties of a molecule. However, it is not trivial to build a bridge from a quantum-chemical calculation to traditional chemical concepts of bonding or reactivity. In principle, there are three possibilities for such an endeavor:

1. Analysis of the wave function and its population: In most quantum-chemical calculations a basis-set expansion of the one-electron wave functions is used. The composition of the one-electron wave functions (for example, whether  $s$ -,  $p$ -,  $d$ -, ..., basis functions contribute to a certain one-electron wave function) and their population can provide a chemical interpretation of the delocalized many-electron wave function.

2. Analysis of the electron density: Studying areas of cumulation or depletion of electron density can provide insight into the bonding situation.
3. Analysis of contributions to bonding energy: Separating the bonding energy into a carefully chosen set of energy contributions yields a better picture of the composition of a bond.

In the present work, natural bond-orbital analysis, which is an analysis of the wave function and its population, and the *atoms in molecules* analysis, an analysis of the electron density, were used to obtain more information about the bonding situation in molecules containing heavy-atom main-group elements.

### 3.3.1. Natural bond-orbital analysis

The natural bond-orbital (NBO) analysis<sup>114,115</sup> transforms an input atomic-orbital basis to orthonormal sets of natural atomic and natural bond orbitals based on the first-order reduced density matrix  $D_{(1)}$ :

$$D_{(1)}(\mathbf{x}_1, \mathbf{x}'_1) = N \int d\mathbf{x}_2 \cdots d\mathbf{x}_N \Psi(\mathbf{x}'_1, \mathbf{x}_2, \cdots, \mathbf{x}_N) \Psi^*(\mathbf{x}_1, \mathbf{x}_2, \cdots, \mathbf{x}_N) . \quad (3.8)$$

In the above equation,  $N$  is the number of electrons,  $x_N$  are electron coordinates, and  $\Psi$  represents a generic orthonormalized wave function. The diagonalization of the first-order reduced density matrix yields eigenvectors, the natural orbitals, and eigenvalues, the natural occupation numbers. Arranging the basis functions according to which atom  $A, B, C, \dots$  they are centered on, the full first-order reduced density matrix can be separated into blocks. Each block then contains contributions to certain atoms  $A, B, C, \dots$ :

$$\mathbf{D}_{(1)} = \begin{pmatrix} \mathbf{D}_{(1)}^{AA} & \mathbf{D}_{(1)}^{AB} & \mathbf{D}_{(1)}^{AC} & \vdots \\ \mathbf{D}_{(1)}^{AB} & \mathbf{D}_{(1)}^{BB} & \mathbf{D}_{(1)}^{BC} & \vdots \\ \mathbf{D}_{(1)}^{AC} & \mathbf{D}_{(1)}^{BC} & \mathbf{D}_{(1)}^{CC} & \vdots \\ \cdots & \cdots & \cdots & \cdots \end{pmatrix} \quad (3.9)$$

The eigenvectors that diagonalize the diagonal blocks  $\mathbf{D}_{(1)}^{AA}$  etc. yield the natural atomic orbitals of atom A, while the diagonalization of the off-diagonal blocks  $\mathbf{D}_{(1)}^{AB}$  etc. give the natural bond orbitals of the bond between the corresponding atoms. The occupation numbers are used as a measure to decide which natural orbitals are lone pairs, which are bonding orbitals etc.<sup>9</sup>

### 3.3.2. “Atoms in Molecules” analysis

In the *atoms in molecules* analysis the topology of the electron density is the source of information about bonding. Stationary points in the electron density allow for a rigorous separation of the density into its atomic contributions: At the nuclei a maximum in the electron density in all three directions is encountered. A nucleus is therefore called an “attractor” of the electron density. At every point in space, the gradient points into the direction of one of the

attractors, which naturally yields atomic basins separated by two-dimensional planes. Further stationary points in the electron density are the so-called bond critical points which can be taken as an indication for bonding, ring critical points, which occur in ring-shaped molecules, and cage critical points which are encountered in the center of cage-like molecules.<sup>116</sup>

## 4. Results: Structures and spectroscopic parameters of small molecules with heavy elements

*Give me insight, not numbers!*  
– Charles A. Coulson

### 4.1. HPSi and OSiS - a posteriori explanation of structure and bonding

HPSi and OSiS are heavy-atom analogues of the molecules HCN and CO<sub>2</sub>. Both species are examples of how the bonding situation can change completely when going from first- to second-row elements and how the change in bonding affects the structure of a molecule. HPSi and OSiS have been characterized to high accuracy by means of rotational spectroscopy in connection with discharge experiments.<sup>51,52,a</sup> Accurate predictions of spectroscopic parameters<sup>b</sup> were important for guiding these experiments. HPSi and OSiS are prime examples of how quantum-chemical methods can be used to explain structure and bonding *a posteriori*. The following discussion will thus focus on the third purpose of quantum chemistry: Explaining experimental results.

#### 4.1.1. Bridged HPSi

HPSi is a very simple – maybe the simplest – unsaturated compound with a silicon-phosphorus bond. The structure of HPSi has a curious feature: Numerous quantum-chemical studies established that HPSi takes on a bridged structure (see Fig. 4.1),<sup>117–120</sup> although for the isovalent compounds HCN, HNC, HSiN, and HCP the linear structure is the global minimum on the potential-energy surface.<sup>121</sup> Chesnut<sup>120</sup> predicted the energy difference between bridged HPSi and the linear HSiP to be 10.2 kcal·mol<sup>-1</sup>. However, no explanation has been given in the literature to why a bridged structure is more stable for HPSi and why the formation of HPSi is preferred over HSiP.

Indications for a valid interpretation of the bonding in bridged HPSi lie in the structural parameters because the length of a certain bond depends to some extent on the type of bonding. In Fig. 4.1 on the left hand side the semiexperimentally determined geometry<sup>c</sup> is shown. In Tab. 4.1, the parameters are compared to typical values for different types of bonding. The H-P bond length in HPSi comes very close to a typical P-H single bond (here the value for PH<sub>3</sub> is listed), while the H-Si bond length is significantly longer than in SiH<sub>4</sub>. The H-Si distance can rather be compared to a typical value for a bridging H-Si bond (1.6–1.8 Å).<sup>109</sup> The distance between P and Si bears a striking similarity to the length of a

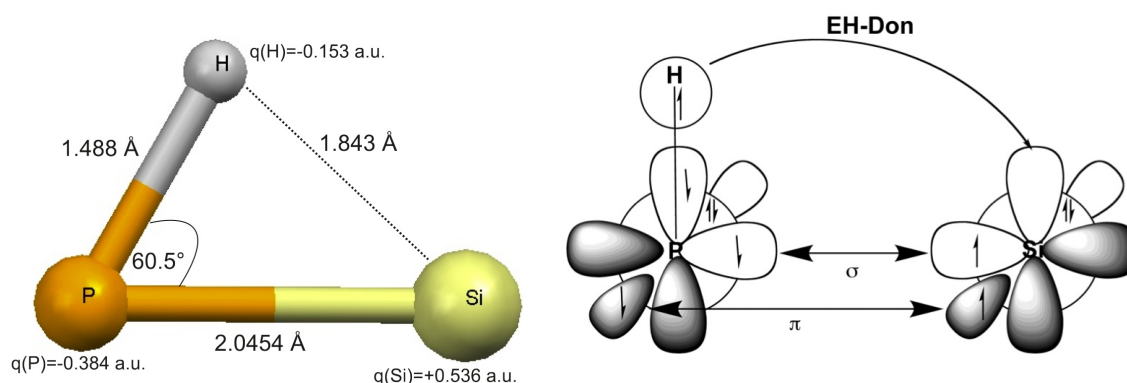
<sup>a</sup>The measurements were conducted by V. Lattanzi and M. C. McCarthy at the Smithsonian Center for Astrophysics, Harvard University.

<sup>b</sup>These calculations were carried out by J. Gauss at the Johannes Gutenberg-Universität Mainz.

<sup>c</sup>For a description of the experimental details regarding rotational-spectroscopy measurements see the appendix.

**Table 4.1.:** Comparison of semiexperimentally determined structural parameters of HPSi with typical bond lengths of different types of bonding.

|      | $R_{HPSi}^a$ | vdW <sup>122,b</sup> | single bond <sup>c</sup> | double bond <sup>c</sup> | triple bond <sup>c</sup> |
|------|--------------|----------------------|--------------------------|--------------------------|--------------------------|
| H-P  | 1.488        | 1.9                  | 1.410 <sup>123</sup>     |                          |                          |
| P-Si | 2.0454       | 3.9                  | 2.252 <sup>124</sup>     | 2.094 <sup>125</sup>     | 1.992 <sup>118</sup>     |
| H-Si | 1.843        | 3.2                  | 1.471 <sup>126</sup>     |                          |                          |

<sup>a</sup> Experimentally determined bond lengths in HPSi.<sup>b</sup> Sum of van der Waals radii.<sup>c</sup> Typical bond length for a single, double, or triple bond.**Figure 4.1.:** Left: Semiexperimental equilibrium structure of bridged HPSi, NPA charges of the atoms (CCSD/cc-pVTZ level of theory). Right: Schematic representation of orbital interactions and the resulting bonding in HPSi. Reprinted with permission from Ref. 51. Copyright 2010 Wiley-VCH Verlag GmbH & Co. KGaA, Weinheim.

typical P-Si double bond, which conveys that the P-Si bond in HPSi is indeed best described as a double bond. f

The interpretation of bonding in HPSi derived from the structural parameters is confirmed by an analysis of the natural bond orbitals (NBO).<sup>115</sup> The NBO analyses were conducted with the MOLPRO 2006.1 quantum-chemical program package<sup>127</sup> at the CCSD(T)/cc-pVTZ level of theory using experimental geometries. The analysis shows two bonding orbitals between phosphorus and silicon and one bonding orbital between phosphorus and hydrogen. On phosphorus, a lone-pair orbital is present. However, no bonding orbital between silicon and hydrogen was found, only a lone-pair orbital on silicon.

The structural parameters and the NBO analysis suggest that HPSi adopts a bent structure rather than a cyclic one. Nevertheless the data indicate significant H-Si interaction. The latter assumption is backed up by the natural population analysis (NPA) charges: The electronegativity of H and P nearly have the same value (on the Pauling scale 2.20 and 2.19, respectively) but the negative partial charge on H is substantial. This suggests that hydrogen withdraws charge from the less electronegative silicon (the electronegativity of silicon is 1.90 on the Pauling scale).

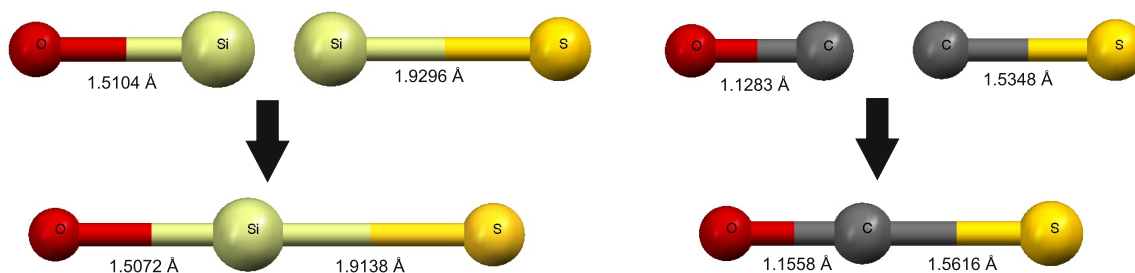


**Figure 4.2.:** Best theoretical estimate of bond lengths (calculated at the  $\text{fc-CCSD(T)/cc-pV}\infty\text{Z}+\Delta\text{T/cc-pVTZ}+\Delta\text{Q/cc-pVDZ}+\Delta\text{core/cc-pCV5Z}$  level of theory) in OSiS, OSi, and SiS and their carbon analogues.

The bonding situation is summarized in Fig. 4.1 on the right hand side: While between P and Si a classical double bond with  $\sigma$ - and  $\pi$ -bonding is formed, the H-Si interaction is non-classical and can be interpreted as a donor-acceptor interaction with the  $\sigma$  electron pair donating into the empty  $\pi$ -orbital of silicon.

The difference between bonding in HCN or HNC and HPSi can be explained by the fact that phosphorus has a much smaller tendency to form hybrid orbitals than nitrogen. Instead of adopting a Si-P triple bond in analogy to HNC, a double bond and a lone pair with mainly s-character are formed.

Giving a qualitative explanation why HPSi and not HSiP is formed is not as straightforward as explaining the emergence of a bent structure. It should be noticed, though, that linear HPSi is not a minimum on the potential-energy surface, which again emphasizes the importance of the PH-Si donor-acceptor interaction in stabilizing bridged HPSi.

HPSi is the first experimentally characterized SiP compound with a bridging hydrogen atom. It is likely that hydrogen bridging plays a role in a lot of other SiP compounds as well, which will be subject to future investigations.

#### 4.1.2. Linear OSiS

OSiS is the heavy-atom analogue of OCS. OCS has been intensively studied and its rotational and rotation-vibration spectra have rendered an accurate determination of structural parameters possible.<sup>128,129</sup> OSiS, however, has not received much attention. It was first detected by Schnöckel by means of IR spectroscopy in a low-temperature argon matrix.<sup>130</sup> Although Schnöckel already discussed the potential multiple bonding between the heavy atoms Si and S, not many further investigations of the bonding situation in OSiS have been published.

In the present work,<sup>52</sup> the equilibrium geometry of OSiS could be determined to high accuracy by means of rotational spectroscopy in connection with discharge experiments.<sup>d</sup> As during the search for HPSi, highly accurate quantum-chemical calculations were indispensable for guiding the experiments. The best theoretical estimate was calculated on a level of theory denoted as  $\text{fc-CCSD(T)/cc-pV}\infty\text{Z}+\Delta\text{T/cc-pVTZ}+\Delta\text{Q/cc-pVDZ}+\Delta\text{core/cc-pCV5Z}$ : A frozen-core (fc) CCSD(T) calculation was extrapolated to the basis-set limit and augmented with corrections for full triples (with  $\text{cc-pVTZ}$  basis set), with corrections for full quadruples (with  $\text{cc-pVDZ}$

<sup>d</sup>For a description of the experimental details regarding rotational-spectroscopy measurements see the appendix.

**Table 4.2.:** Comparison of bond lengths of OSiS, SiO, SiS, SiO<sub>2</sub>, and SiS<sub>2</sub> with those of their carbon analogues (in Å; best theoretical estimate, see text) and NPA charges (calculated with Gaussian 03<sup>133</sup> at the CCSD(T)/cc-pVTZ level, values in a.u.).<sup>52,\*</sup>

| Molecule         | $r_{SiO}$ | $r_{SiS}$ | $q_{Si}$ |
|------------------|-----------|-----------|----------|
| OSiS             | 1.5072    | 1.9138    | 1.93     |
| SiO              | 1.5104    | ...       | 1.30     |
| SiS              | ...       | 1.9236    | 0.79     |
| SiO <sub>2</sub> | 1.5066    | ...       | 2.44     |
| SiS <sub>2</sub> | ...       | 1.9161    | 1.31     |
| Molecule         | $r_{CO}$  | $r_{CS}$  | $q_C$    |
| OCS              | 1.1558    | 1.5616    | 0.62     |
| CO               | 1.1283    | ...       | 0.60     |
| CS               | ...       | 1.5348    | 0.07     |
| CO <sub>2</sub>  | 1.1599    | ...       | 1.21     |
| CS <sub>2</sub>  | ...       | 1.5525    | -0.25    |

\*Reprinted (adapted) with permission from Ref. 52. Copyright (2011) American Chemical Society.

basis set), and with a correction for core-correlation effects (with cc-pCV5Z basis set).<sup>e</sup> The values obtained as a best theoretical estimate (see Fig. 4.2) are in excellent agreement with the semiexperimentally determined values ( $r_{OSi}=1.5064$  Å,  $r_{SiS}=1.9133$  Å).

Schnöckel<sup>130,131</sup> and Bhattacharyya<sup>132</sup> considered OSiS to be a prime example for covalent multiple bonding between heavy elements. However, multiple bonding fails to explain trends in bond lengths if OSiS is compared to its diatomic “components” OSi and SiS. The best theoretical estimate of the bond lengths for all three species (see Tab. 4.2) reveals the unexpected finding that in the diatomic species the bond lengths are longer than in OSiS. This seems to contradict the assumption that the bonding situation of OSiS can best be described as a double bond while the bonds in OSi and SiS should be seen as triple bonds. In the analogous species OCS, which exhibits classical double bonds, the trend in bond lengths goes hand in hand with the change in bond order when comparing OCS to the diatomic species OC and CS (see Tab. 4.2 and Fig. 4.3).

These unexpected trends in bond lengths of OSiS thus cannot be due to a change in bond order. They can rather be rationalized by electrostatic effects. In Tab. 4.2 the charges obtained from a natural population analysis<sup>115</sup> are listed. The electronegativity of Si is 1.90 on the Pauling scale, while the electronegativity of S and O amount to 2.58 and 3.44, respectively. Consequently, silicon carries a large positive partial charge in both diatomic species, 1.30 *a.u.* in OSi and 0.79 *a.u.* in SiS. If silicon is placed between sulfur and oxygen, the partial charge becomes even larger and now amounts to 1.93 *a.u.* because electron density is withdrawn from both sides. The same trend in partial charges is visible for SiS<sub>2</sub> and SiO<sub>2</sub>. In OCS on the other hand, the charge on carbon is not much larger than in the diatomic molecule OC.

The hypothesis that electrostatic interactions are crucial for a valid explanation of the bonding situation in OSiS is supported by the Laplacian of the electron density (see Fig. 4.3). The Laplacian was calculated with Bader’s “Atoms in Molecules” program at CCSD(T)/cc-pVTZ

<sup>e</sup>These calculations were conducted by J. Gauss at the Johannes Gutenberg-Universität Mainz.

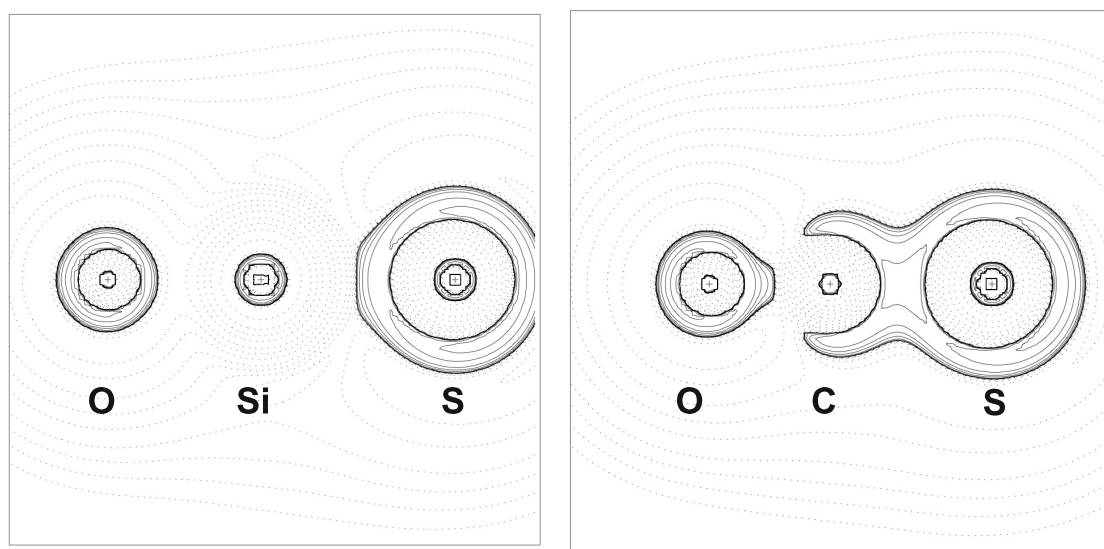


**Figure 4.3.:** Laplacian  $\nabla^2$  of the electron density  $\rho(r)$  in OSiS and OCS. Dotted lines represent areas with electron depletion ( $\nabla^2 \rho(r) > 0$ ) while continuous lines represent areas with electron concentration ( $\nabla^2 \rho(r) < 0$ ).

level of theory.<sup>134</sup> For more information about atoms-in-molecules analyses the reader is referred to Ref. 116. In OCS, the electron density is distorted in direction of the bonding and accumulates between the atoms. This conveys that bonding in OCS is highly covalent. In OSiS, the accumulation of electron density is not distorted but rather takes on a circular shape around the atoms, which is an indication for covalent bonding being less important in OSiS.

OSiS can thus be considered a second example for the major differences in bonding between first-row elements and heavier elements.

## 4.2. Cyclic SiS<sub>2</sub> – a new role of theory in chemistry

A heavy-atom analogue of OSiS with potentially interesting properties is SiS<sub>2</sub>. However, linear SiS<sub>2</sub> is not accessible via rotational spectroscopy because it does not have a permanent dipole moment. This challenge motivated the search for non-linear isomers of SiS<sub>2</sub> and led to the finding that cyclic SiS<sub>2</sub> is an energetically low-lying isomer on the potential-energy surface, which renders its characterization via rotational spectroscopy possible.

In the case of cyclic SiS<sub>2</sub>, all three purposes of theoretical chemistry were put into practice: Theoretical considerations led to the prediction of hitherto unknown chemical behavior and motivated the experimental search. The experimental search for SiS<sub>2</sub> was guided by highly accurate coupled-cluster calculations. Last but not least, a viable explanation for the chemical behavior of SiS<sub>2</sub> could be found with the help of quantum-chemical calculations.

**Table 4.3.:** Energy differences between cyclic and linear isomers of the molecules  $EE'_2$  ( $E=C, Si, Ge/E'=O, S$ ) and structural parameters of the cyclic forms.<sup>a</sup> Calculations were conducted at CCSD(T)/cc-pVQZ level of theory.\*

|                   | CO <sub>2</sub> | CS <sub>2</sub> | SiO <sub>2</sub> | SiS <sub>2</sub> | GeO <sub>2</sub> | GeS <sub>2</sub> |
|-------------------|-----------------|-----------------|------------------|------------------|------------------|------------------|
| $\Delta E$        | 143.1           | 69.4            | 59.2             | 19.3             | 33.8             | 6.5              |
| $\alpha(E'-E-E')$ | 72.6            | 75.2            | 57.7             | 61.5             | 53.4             | 59.0             |
| $r(E'-E)$         | 1.3193          | 1.7330          | 1.6541           | 2.1188           | 1.7702           | 2.2038           |
| $r(E'-E')$        | 1.5625          | 2.1265          | 1.5971           | 2.1681           | 1.5916           | 2.1712           |

<sup>a</sup> Energy difference  $\Delta E$  in kcal·mol<sup>-1</sup>, bond lengths  $r$  in Å and bond angles  $\alpha$  in °.

\*Reprinted with permission from Ref. 136. Copyright 2012 Wiley-VCH Verlag GmbH & Co. KGaA, Weinheim.

#### 4.2.1. A new perspective on the Walsh rules – predicting the accessibility of a cyclic SiS<sub>2</sub> isomer

According to the Walsh rules, the global minimum of sixteen-electron triatomics is linear.<sup>6</sup> For molecules like N<sub>2</sub>O or CO<sub>2</sub> that contain first-row elements only, the Walsh rules rigorously apply. It is less clear, though, how accurate the Walsh rules are in predicting geometries when elements of the second row or higher rows are involved. As already discussed in Sec. 3.2, classical  $\pi$ -bonds are rare between heavy elements, therefore the applicability of Walsh rules might be limited in that case. Furthermore potential-energy surfaces are often very shallow for heavy elements, which generally makes the emergence of exotic isomers more likely. Exceptions to the Walsh rules have already been found for fourteen-electron triatomics: While the highly reactive dicarbonmonoxide C<sub>2</sub>O is linear, its heavy-atom analogues Si<sub>2</sub>S exhibits a singlet ring as global minimum.<sup>108</sup> Very recently, the cyclic sixteen-electron species PSN was characterized experimentally and computationally by Zeng *et al.* as a local minimum on the potential-energy surface.<sup>135</sup>

For the heavy-atom analogues of CO<sub>2</sub> ( $EE'_2$  with  $E=C, Si, Ge/E'=O, S$ ), the Walsh rules are rigorously valid, as Tab. 4.3 shows. But the energy difference between the cyclic and the linear geometries decreases rapidly when going to heavier elements: While the cyclic isomer of CO<sub>2</sub> is 143.1 kcal·mol<sup>-1</sup> higher in energy than the linear isomer, this energy difference reduces to 19.3 kcal·mol<sup>-1</sup> in SiS<sub>2</sub> and – going down further in the periodic table – to 6.5 kcal·mol<sup>-1</sup> in GeS<sub>2</sub>. This suggests that for SiS<sub>2</sub> the cyclic isomer might be energetically accessible. Furthermore, the structural parameters of the series of molecules  $EE'_2$  demonstrates the trends that are expected when substituting first-row elements with their heavier analogues: The bond angle E'-E-E' becomes much smaller when going from E=C to E=Si. The difference in the bond angles when going from E=Si to E=Ge is much more subtle, which underlines the special status that first-row elements have.

The small energy difference between linear and cyclic SiS<sub>2</sub> was first noted by Davy and Holiday in 1995 based on a CCSD/TZ2P calculation.<sup>137,138</sup> Experimentally, however, only the linear form of SiS<sub>2</sub> is known. Schnöckel and Köppe comprehensively characterized linear SiS<sub>2</sub> by means of Raman spectroscopy in a low-temperature matrix in 1989.<sup>139,140</sup>

These considerations motivated the experimental search for SiS<sub>2</sub> by means of rotational spectroscopy in connection with a discharge experiment. A joint effort of quantum chemistry and rotational spectroscopy thus led to the first experimental characterization of cyclic SiS<sub>2</sub>.

**Table 4.4.:** Experimental transition frequencies (in MHz) of SiS<sub>2</sub> and its isotopologues <sup>29</sup>SiS<sub>2</sub> and Si<sup>34</sup>S<sup>32</sup>S.<sup>136</sup>

| Transition                             | SiS <sub>2</sub> |               | <sup>29</sup> SiS <sub>2</sub> | Si <sup>34</sup> S <sup>32</sup> S |
|--|------------------|---------------|--------------------------------|------------------------------------|
| $J''_{K''_a, K''_c} - J'_{K'_a, K'_c}$ | Frequency (MHz)  | $O - C$ (kHz) | Frequency (MHz)                | Frequency (MHz)                    |
| 2 <sub>1,1</sub> – 2 <sub>0,2</sub>    | 9682.652(3)      | –1            |                                |                                    |
| 1 <sub>1,1</sub> – 0 <sub>0,0</sub>    | 11516.526(3)     | 1             | 11286.504(3)                   | 11383.848(3)                       |
| 2 <sub>0,2</sub> – 1 <sub>1,1</sub>    | 17471.540(3)     | 1             | 17420.703(3)                   | 16965.706(3)                       |
| 3 <sub>2,2</sub> – 3 <sub>1,3</sub>    | 18598.081(3)     | 1             |                                |                                    |
| 3 <sub>1,3</sub> – 2 <sub>0,2</sub>    | 25633.786(3)     | –1            |                                |                                    |
| 2 <sub>2,0</sub> – 1 <sub>1,1</sub>    | 32715.607(3)     | –1            | 32306.914(3)                   | 32113.633(3)                       |
| 4 <sub>0,4</sub> – 3 <sub>1,3</sub>    | 32756.271(3)     | 0             |                                |                                    |
| 3 <sub>2,2</sub> – 2 <sub>1,1</sub>    | 34549.214(3)     | 0             |                                |                                    |
| 4 <sub>1,3</sub> – 3 <sub>2,2</sub>    | 39446.393(3)     | 0             |                                |                                    |

#### 4.2.2. Guidance of experiments by calculation of spectroscopic parameters

Fourier-transform microwave spectroscopy was the method of choice for the experimental search for cyclic SiS<sub>2</sub> in the discharge products of H<sub>2</sub>S and SiH<sub>4</sub>.<sup>f</sup> Highly accurate quantum-chemical calculations are of great significance for guiding the spectroscopic detection.

In the present case, the best theoretical estimate for the structural parameters was obtained on a level denoted fc-CCSD(T)/cc-pV $\infty$ Z+ $\Delta$ T/cc-pVTZ +  $\Delta$ Q/cc-pVDZ +  $\Delta$ core/cc-pCV5Z using the CFOUR quantum-chemical program package (for more information about extrapolation and additivity schemes see Sec. 2.5).<sup>113</sup> This means that a frozen-core CCSD(T) calculation was extrapolated to the basis-set limit and corrected for full triple, full quadruple, and core-correlation contributions with the given basis sets. It is assumed that bond lengths computed at this level of theory have an intrinsic accuracy of 0.001 Å.<sup>141</sup> From the best-estimate equilibrium structure the rotational constants at equilibrium  $A_e$ ,  $B_e$ , and  $C_e$ , for all plausible isotopic species of SiS<sub>2</sub> are computed. In order to access the experimentally relevant rotational constants  $A_0$ ,  $B_0$ , and  $C_0$  the zero-point vibrational corrections  $\Delta A_{vib}$ ,  $\Delta B_{vib}$ , and  $\Delta C_{vib}$  are necessary ( $A_0 = A_e + \Delta A_{vib}$ ), which were computed at CCSD(T)/cc-pCVTZ level of theory. Furthermore, centrifugal-distortion constants were calculated at the same level of theory.

Using the computed rotational constants  $A_0$ ,  $B_0$ , and  $C_0$ , the rotational transition frequency can be determined. For example, the fundamental transition  $J=1_{1,1}-0_{0,0}$  amounts to 11510 MHz. A  $\pm 0.5\%$  search in frequency around the predicted fundamental transition was undertaken and a candidate line was found at 11513 MHz. To ultimately establish that this line indeed arises from cyclic SiS<sub>2</sub>, the theoretically predicted shifts in frequency for the rare isotopic species <sup>29</sup>SiS<sub>2</sub> and Si<sup>34</sup>S were compared to experiment: The lines for the isotopologues emerged exactly at the expected shifts. In total, nine transition frequencies for the main isotopic species and three transition frequencies for the rare isotopic species could be measured (see Tab. 4.4). An example spectrum is shown in Fig. 4.4.<sup>g</sup>

<sup>f</sup>For a description of the experimental details regarding rotational-spectroscopy measurements see the appendix.

<sup>g</sup>The measurement of spectra and fit for rotational constants were conducted by V. Lattanzi and M. C. McCarthy, Smithsonian Center for Astrophysics.

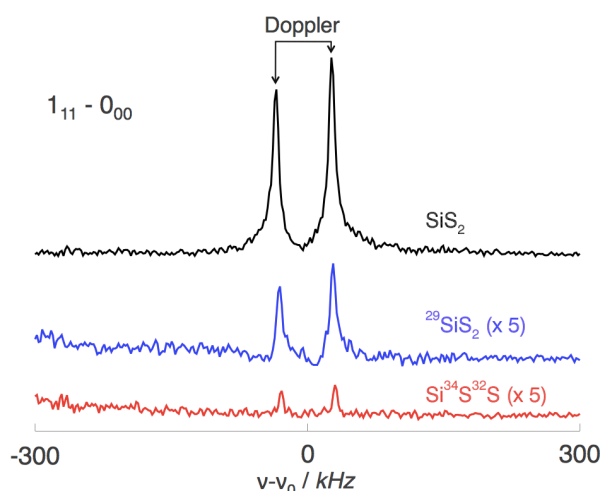


**Figure 4.4.:** Fourier-transform microwave spectra of the fundamental rotational transition for  $\text{SiS}_2$  and its isotopologues. The line shape results from Doppler splitting of the supersonic molecular beam. Reprinted with permission from Ref. 136. Copyright 2012 Wiley-VCH Verlag GmbH & Co. KGaA, Weinheim.

Experimental spectroscopic constants can be determined via a non-linear least-squares analysis of the transition frequencies with an asymmetric top Hamiltonian. For the main isotopic species a simultaneous fit of all three rotational constants,  $A$ ,  $B$ , and  $C$ , and all quartic centrifugal-distortion constants was conducted. For the minor isotopic species only the rotational constants were regarded in the fitting procedure while the centrifugal-distortion constants were fixed to the calculated value (see Tab. 4.5). In order to determine the semiexperimental structural parameters the rotational constants of all isotopic species are corrected for the calculated zero-point vibrational frequencies (see Tab. 4.6). Bond lengths and bond angles can then be determined in a least-squares minimization. These semiexperimental structural parameters are shown in Fig. 4.5 along with the theoretical best estimate. The agreement between theoretically and experimentally determined structural parameters is better than 0.2%.

#### 4.2.3. A posteriori explanation – why is cyclic $\text{SiS}_2$ energetically accessible?

The energetic accessibility of  $\text{SiS}_2$  dovetails with typical features of bonding in heavy main-group elements. Compared to  $\text{CO}_2$ , there is a lower tendency to form  $\pi$ -bonds in the linear arrangement of  $\text{SiS}_2$  because silicon as the central atom does not readily hybridize. The lack of hybridization then allows for smaller bond angles around the central atom, which makes a bent or cyclic structure more likely. However, another crucial feature for stabilizing the cyclic isomer of  $\text{SiS}_2$  is the strength of the S-S bond. From Tab. 4.3 it is already evident that comparing  $\text{CO}_2$  to  $\text{CS}_2$  the energy difference between cyclic and linear form decreases almost as much as when  $\text{CO}_2$  and  $\text{SiO}_2$  are compared.

The importance of the S-S bond is further highlighted by the Walsh diagram of  $\text{SiS}_2$ , i.e., by the plot of the orbital energies against the S-Si-S bond angle (see Fig. 4.6). Upon bending of the S-Si-S angle the degenerate  $\pi$ -orbitals split up. The decrease in bond angle goes hand in hand with an inversion of orbital occupancy, which indicates a high transition barrier and

**Table 4.5.:** Experimental and calculated spectroscopic constants (in MHz) of SiS<sub>2</sub> and its isotopologues <sup>29</sup>SiS<sub>2</sub> and Si<sup>34</sup>S<sup>32</sup>S.<sup>136</sup>

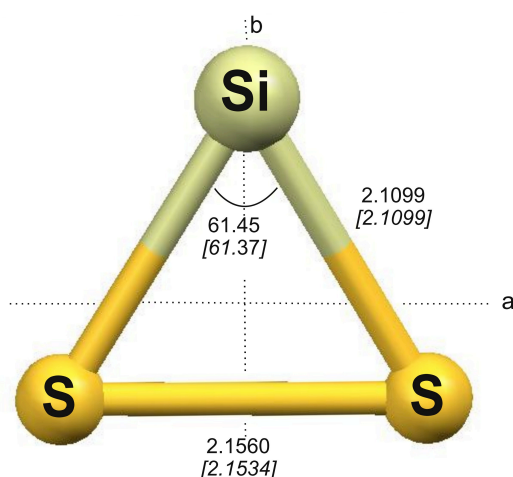
| Constant      | SiS <sub>2</sub> |                    | <sup>29</sup> SiS <sub>2</sub> |                    | Si <sup>34</sup> S <sup>32</sup> S |                    |
|---------------|------------------|--------------------|--------------------------------|--------------------|------------------------------------|--------------------|
|               | Exp.             | Calc. <sup>a</sup> | Exp.                           | Calc. <sup>a</sup> | Exp.                               | Calc. <sup>a</sup> |
| $A_0$         | 7876.6558(29)    | 7870.4             | 7687.6208(22)                  | 7681.4             | 7817.6872(20)                      | 7811.7             |
| $B_0$         | 6788.5884(13)    | 6804.5             | 6788.7144(18)                  | 6804.5             | 6577.9718(18)                      | 6593.3             |
| $C_0$         | 3639.88541(73)   | 3643.1             | 3598.8984(12)                  | 3602.2             | 3566.1760(13)                      | 3569.4             |
| $10^3 D_J$    | 2.291(76)        | 2.282              | <i>b</i>                       | 2.242              | <i>b</i>                           | 2.196              |
| $10^3 D_{JK}$ | 7.72(35)         | 7.28               | <i>b</i>                       | 7.28               | <i>b</i>                           | 6.71               |
| $10^3 D_K$    | -2.68(48)        | -2.29              | <i>b</i>                       | -2.58              | <i>b</i>                           | -1.69              |
| $10^3 d_1$    | -1.438(40)       | -1.43              | <i>b</i>                       | -1.44              | <i>b</i>                           | -1.35              |
| $10^3 d_2$    | <i>b</i>         | -0.59              | <i>b</i>                       | -0.61              | <i>b</i>                           | -0.53              |

<sup>a</sup> Rotational constants from the best-estimate structure corrected for zero-point vibrational effects (see Sec. 3.2 and text above). Centrifugal-distortion constants at the CCSD(T)/cc-pCVTZ level of theory.

<sup>b</sup> Fixed to calculated value.

**Table 4.6.:** CCSD(T)/cc-pCVTZ zero-point vibrational corrections to the rotational constants (in MHz).<sup>136</sup>

| Species                            | $\Delta A_{\text{vib}}$ | $\Delta B_{\text{vib}}$ | $\Delta C_{\text{vib}}$ |
|------------------------------------|-------------------------|-------------------------|-------------------------|
| SiS <sub>2</sub>                   | -17.42                  | -12.18                  | -13.49                  |
| <sup>29</sup> SiS <sub>2</sub>     | -16.78                  | -12.21                  | -13.07                  |
| Si <sup>34</sup> S <sup>32</sup> S | -17.23                  | -11.604                 | -13.28                  |

**Figure 4.5.:** Semiexperimental equilibrium structure of cyclic SiS<sub>2</sub>. The best theoretical estimates for the structural parameters are given in italics (bond lengths in Å, bond angles in °). Reprinted with permission from Ref. 136. Copyright 2012 Wiley-VCH Verlag GmbH & Co. KGaA, Weinheim.

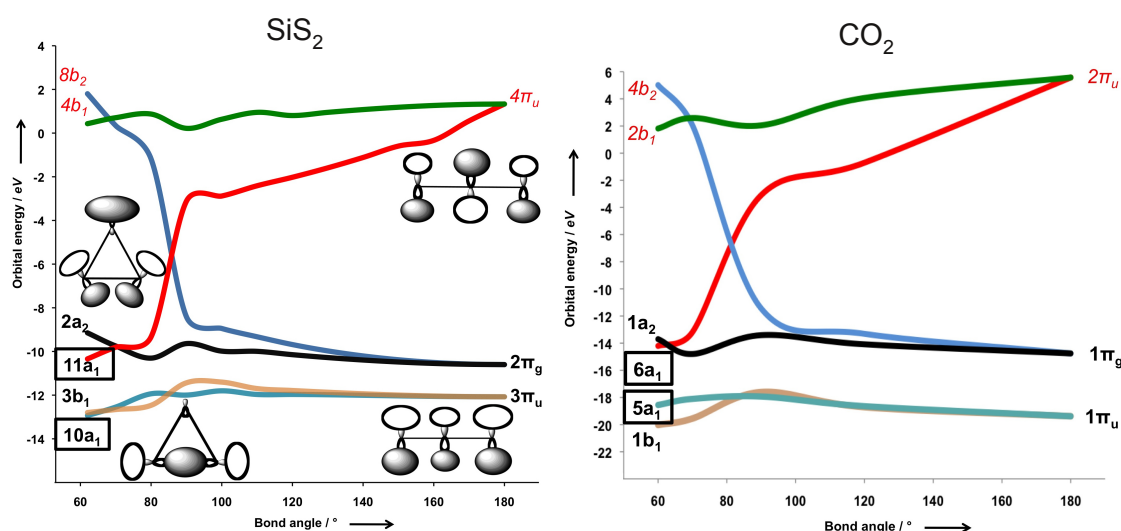


**Figure 4.6.:** Angular dependence of orbital energies (“Walsh diagrams”) of  $\text{SiS}_2$  and  $\text{CO}_2$ . Unoccupied orbitals are marked red. Reprinted (adapted) with permission from Ref. 136. Copyright 2012 Wiley-VCH Verlag GmbH & Co. KGaA, Weinheim.

thus explains the kinetic stability of  $\text{SiS}_2$ . For  $\text{SiS}_2$  this occupation inversion occurs at around  $87^\circ$ .

The Walsh diagram of  $\text{CO}_2$  looks very similar to the corresponding diagram of  $\text{SiS}_2$ . The change in orbital occupation occurs at a slightly smaller angle (approximately  $80^\circ$ ). A qualitative difference between the two diagrams can be found when looking at the energetic order of the orbitals. At the equilibrium geometry of  $\text{SiS}_2$  ( $E'-E-E'$  angle of  $62^\circ$ ) the  $10a_1$  orbital is lower in energy than the  $3b_1$  orbital and the  $11a_1$  orbital is significantly lower in energy than the  $2a_2$  orbital. The corresponding energetic order of orbitals at the equilibrium geometry of  $\text{CO}_2$  ( $E'-E-E'$  angle of  $73^\circ$ ), however, is  $1b_1 < 5a_1 < 1a_2 < 6a_1$ . Furthermore, the  $5a_1$  orbital in  $\text{CO}_2$  is destabilized with respect to the  $1\pi_u$  orbital while the corresponding  $10a_1$  orbital in  $\text{SiS}_2$  is stabilized compared to the degenerate  $3\pi_u$  orbital. The qualitative sketch of the orbitals  $10a_1$  and  $11a_1$  reveals that those orbitals include bonding interaction between the sulfur atoms.

In conclusion, the Walsh diagrams show that orbitals with a large amount of  $E'-E'$  interaction are stabilized more in the equilibrium structure of  $\text{SiS}_2$  than in the equilibrium structure of  $\text{CO}_2$ . Thus the amount of stabilization due to  $E'-E'$  bonding accounts for the energetic accessibility of  $\text{SiS}_2$ . Since the S-S bond is one of the most stable homonuclear single bonds across the periodic table with a stability of  $64 \text{ kcal}\cdot\text{mol}^{-1}$ , this does not necessarily come as a surprise. It should be noted that the S-S distance in  $\text{SiS}_2$  ( $2.156 \text{ \AA}$ ) is not much larger than in a typical S-S single bond ( $2.055 \text{ \AA}$  in  $\text{Si}_2\text{H}_2$ <sup>142</sup>).

#### 4.2.4. Cyclic $\text{SiS}_2$ and the predictive power of quantum chemistry

As a concluding remark, the case of cyclic  $\text{SiS}_2$  exemplifies an increasing significance and impact of theory in chemistry: Its purpose is not only the *a posteriori* explanation of experimental results and the guidance of experiments. Theoretical chemistry is rather able to accurately

predict chemical phenomena. During the characterization of cyclic SiS<sub>2</sub>, quantum-chemical methods were used for all three purposes of theoretical chemistry, prediction, guidance, and explanation. But it is the predictive power that really makes highly accurate coupled-cluster methods combined with chemical intuition “first-rate theory”.

### 4.3. Beyond cyclic SiS<sub>2</sub> – cyclic OSiS, OGeS, and GeS<sub>2</sub>, H<sub>2</sub>SiS<sub>2</sub>, HPS<sub>2</sub>

Cyclic SiS<sub>2</sub> opens the door to an abundance of related compounds in two respects.

First, other heavy-atom analogues of CO<sub>2</sub> probably show similar behavior as Tab. 4.3 already suggested. In GeS<sub>2</sub>, the cyclic isomer is only around 6 kcal·mol<sup>-1</sup> higher in energy than the linear isomer. For the even heavier compounds SnS<sub>2</sub> and PbS<sub>2</sub>, the lone-pair effect that is due to pronounced scalar-relativistic contributions might influence the potential-energy surface in yet another way. Furthermore, the asymmetrically substituted cyclic species OSiS, OGeS etc., whose linear forms can be characterized by rotational spectroscopy due to the permanent dipole moment, can be considered. Of this class, we will investigate the potential-energy surfaces and the parameters relevant for rotational spectroscopy of OSiS, OGeS, and GeS<sub>2</sub> more closely.

Second, cyclic SiS<sub>2</sub> is a first representative of a class of compounds that reshapes the way we think about small sulfur rings. Sulfur allotropes include a plethora of sulfur rings that are often not accessible via rotational spectroscopy because they do not have a permanent dipole moment.<sup>143,144</sup> We might be able to access these rings with more ease if we consider small sulfur rings, where one sulfur atom is substituted by another heavy main-group element: SiS<sub>2</sub> can be considered an S<sub>3</sub> ring in which one sulfur atom has been substituted by a silicon atom. However, SiS<sub>n</sub> does not emulate S<sub>n</sub> but the doubly charged species S<sub>n</sub><sup>2+</sup>, which is experimentally unknown so far. Further derivatives of SiS<sub>2</sub> that might be interesting are H<sub>2</sub>SiS<sub>2</sub> and HPS<sub>2</sub>. The singly charged S<sub>n</sub><sup>+</sup> species on the other hand have been characterized by mass spectrometry up to n=56.<sup>145,146</sup> A substituted species along the lines of SiS<sub>2</sub> that correspond to S<sub>n</sub><sup>+</sup> is PS<sub>n</sub>.<sup>147</sup> In the following we will give predictions on the chemical and spectroscopic properties of H<sub>2</sub>SiS<sub>2</sub> and HPS<sub>2</sub>.<sup>106</sup>

#### 4.3.1. Cyclic OSiS

The linear form of OSiS has recently been characterized by rotational spectroscopy (see Sec. 4.1.2).<sup>52</sup> Considering the energetic accessibility of cyclic SiS<sub>2</sub>, it is plausible that cyclic OSiS is a relatively low-lying isomer as well. The energy difference between the cyclic and linear isomer, however, is almost twice as large as the corresponding energy difference in SiS<sub>2</sub> (31.6 kcal·mol<sup>-1</sup>, see Fig. 4.7).

The reason is likely to be due to structural requirements. The equilibrium geometry of linear and cyclic OSiS was determined at fc-CCSD(T)/cc-pV<sub>∞</sub>Z+ΔT/cc-pVTZ +ΔQ/cc-pVDZ +Δcore/cc-pCV5Z level of theory (see Fig. 4.7). The resulting length of the O-S bond in cyclic OSiS (1.815 Å) is similar to that of a typical O-S single bond (1.622 Å in HSOH). The bond length of the Si-S bond is only marginally smaller than in cyclic SiS<sub>2</sub> and thus much longer than in an Si-S double bond. Compared to the typical double bond in the diatomic molecule SiO (see Fig. 4.2), the Si-O bond length in cyclic OSiS is much longer as well. These values suggest that all bonds in cyclic OSiS have mainly single-bond character.

The O-Si-S angle is considerably smaller than the S-Si-S angle in cyclic SiS<sub>2</sub>. This is a geometrical requirement if an O-S single bond is to be formed. The smaller bond angle results in a higher ring strain, which is one reason for the comparably high relative energy of the cyclic isomer in OSiS having. Another argument for the high relative energy of cyclic OSiS is the high stabilization in linear OSiS via electrostatic interactions (see Sec. 4.1).

Since the O-S single bond is quite stable (about 70 kcal·mol<sup>-1</sup> in the homolytic dissociation of

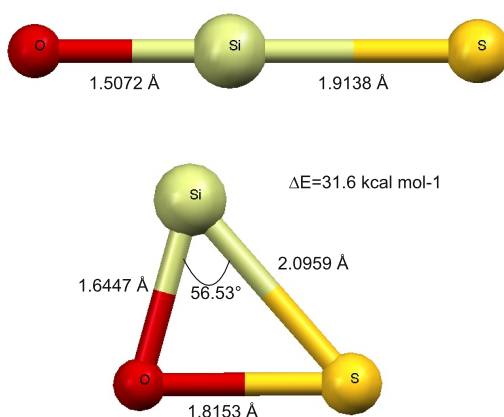


**Figure 4.7.:** Best theoretical estimates (for level of theory see text) for the structural parameters of linear and cyclic OSiS.

HOSH) when compared to the S-S or O-O single bond (about  $60 \text{ kcal}\cdot\text{mol}^{-1}$  and  $50 \text{ kcal}\cdot\text{mol}^{-1}$  in the homolytic dissociation of HSSH and HOOH, respectively),<sup>h</sup> the stabilization via the formation of the O-S single bond is quite pronounced. Therefore a lack of stabilization via the O-S single bond can be ruled out as an argument for the high relative energy of cyclic OSiS. Despite its high relative energy, cyclic OSiS was searched for experimentally by means of rotational spectroscopy. Its sizable dipole moment of 1.7 D in direction of the *a*- and 1.8 D in direction of the *b*-axis render the detection feasible. Highly accurate quantum-chemical predictions of the relevant spectroscopic parameters guided the experimental search. As for cyclic SiS<sub>2</sub>, the  $\text{fc-CCSD(T)/cc-pV}\infty\text{Z}+\Delta\text{T/cc-pVTZ}+\Delta\text{Q/cc-pVDZ}+\Delta\text{core/cc-pCV5Z}$  level of theory was used to determine a best theoretical estimate for the equilibrium structure and the rotational constants  $A_e$ ,  $B_e$ , and  $C_e$ . The zero-point vibrational corrections and centrifugal-distortion parameters were determined at  $\text{CCSD(T)/cc-pCVTZ}$  level of theory. In Tab. 4.7 and Tab. 4.8 the corresponding values are shown.

Rotational transition frequencies that are likely to be due to cyclic OSiS could be determined. At the experimental conditions already used for linear OSiS, a search for the fundamental rotational line of cyclic OSiS near 13.2 GHz was performed. A weak line was found at 13200.988 MHz, within a few MHz of the best theoretical prediction. The signal level could be significantly improved if instead of H<sub>2</sub>O, O<sub>2</sub> was used as a reactant. However, the lines of the isotopic species were too weak for the ultimate verification that this line was indeed caused by cyclic OSiS. Further experiments are necessary and will be performed in the near future.

<sup>h</sup>All these values were estimated at  $\text{CCSD(T)/cc-pCVTZ}$  level of theory without taking reorganization energies into account.

**Table 4.7.:** Calculated spectroscopic constants (in MHz) of OSiS and the isotopologues.

|               | OSiS               | $^{18}\text{O}^{28}\text{Si}^{32}\text{S}$ | $^{16}\text{O}^{29}\text{Si}^{32}\text{S}$ | $^{16}\text{O}^{28}\text{Si}^{34}\text{S}$ |
|---------------|--------------------|--|--|--|
| Constant      | Calc. <sup>a</sup> | Calc. <sup>a</sup>                         | Calc. <sup>a</sup>                         | Calc. <sup>a</sup>                         |
| $A_0$         | 21 483.0           | 19 639.5                                   | 21 356.8                                   | 21 414.5                                   |
| $B_0$         | 7 592.4            | 7 576.8                                    | 7 470.9                                    | 7 357.6                                    |
| $C_0$         | 5 598.9            | 5 456.7                                    | 5 524.1                                    | 5 465.7                                    |
| $10^3 D_J$    | 4.026              | 3.893                                      | 3.902                                      | 3.834                                      |
| $10^3 D_{JK}$ | 9.060              | 9.615                                      | 8.574                                      | 7.187                                      |
| $10^3 D_K$    | 72.202             | 57.036                                     | 72.353                                     | 85.056                                     |
| $10^3 d_1$    | -1.326             | -1.365                                     | -1.277                                     | -1.236                                     |
| $10^3 d_2$    | -0.250             | -0.279                                     | -0.238                                     | -0.227                                     |

<sup>a</sup> Rotational constants from the best-estimate structure

(fc-CCSD(T)/cc-pV $\infty$ Z+ $\Delta$ T/cc-pVTZ+ $\Delta$ Q/cc-pVDZ+ $\Delta$ core/cc-pCV5Z level of theory) corrected for zero-point vibrational effects. Centrifugal-distortion constants at the CCSD(T)/cc-pCVTZ level of theory.

**Table 4.8.:** CCSD(T)/cc-pCVTZ zero-point vibrational corrections to the rotational constants (in MHz) of OSiS and isotopologues of OSiS, CCSD(T)/cc-pCVTZ level of theory.

| Species                 | OSiS   | $^{18}\text{O}^{28}\text{Si}^{32}\text{S}$ | $^{16}\text{O}^{29}\text{Si}^{32}\text{S}$ | $^{16}\text{O}^{28}\text{Si}^{34}\text{S}$ |
|-------------------------|--------|--|--|--|
| $\Delta A_{\text{vib}}$ | -67.20 | -57.05                                     | -66.90                                     | -67.36                                     |
| $\Delta B_{\text{vib}}$ | -16.84 | -16.74                                     | -16.45                                     | -16.06                                     |
| $\Delta C_{\text{vib}}$ | -24.70 | -23.88                                     | -24.20                                     | -23.75                                     |

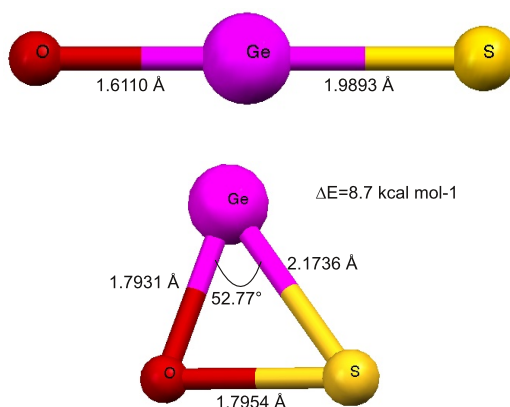


**Figure 4.8.:** Theoretical estimates (CCSD(T)/cc-pwCVQZ level of theory, with a Stuttgart-Köln ECP including 10 core electrons for germanium) for the structural parameters of linear and cyclic OGeS.

### 4.3.2. Cyclic OGeS

One strategy to weaken the ring strain in the three-membered ring OSiS and obtain an energetically accessible cyclic trimer is to consider an even heavier element as central atom. Heavier elements in general allow for smaller bond angles because the tendency to hybridize is weakened. Additionally scalar-relativistic effects start to play a bigger role in heavier elements, which also has an effect on the structure of such rings. For example, the inner s-shells contract due to scalar-relativistic effects while the outer shells expand. Consequences of this so called inert-pair effect are smaller oxidation numbers and a larger energetic gap between p- and s-shells, i.e., even less possibility for hybridization and hence to less intramolecular strain.

To examine the energetic accessibility of cyclic OGeS, the geometries of cyclic OGeS and of linear OGeS were optimized at the CCSD(T)/cc-pwCVQZ level of theory.<sup>148</sup> For germanium, a Stuttgart-Köln effective-core potential (ECP) for 10 core electrons was used. In OGeS the energy difference between linear and cyclic isomer only amounts to 8.7 kcal/mol (see Fig. 4.8). The O-Ge-S angle is slightly smaller than the O-Si-S angle in cyclic OSiS. As a consequence of the new geometrical conditions, the O-S distance in OGeS is smaller than in OSiS.

Cyclic OGeS has not been described in the literature and studies which investigate the linear isomer of OGeS are scarce as well. Hassanzadeh and Andrews characterized linear OGeS in a low-temperature argon matrix by means of vibrational spectroscopy in 1992.<sup>103</sup> Leszczynski and Kwiatkowski conducted further quantum-chemical investigation of the structure and vibrational spectra using second-order Møller-Plesset perturbation theory.<sup>105</sup>

We therefore propose an experimental search for both, linear and cyclic OGeS, by means of rotational spectroscopy. A permanent dipole moment of 1.4 D in linear OGeS and of 2.6 D in *a*- and 1.4 D in *b*-direction in cyclic OGeS renders the success of this search plausible. Reaction conditions for the discharge experiment will have to be optimized. However, the high abundance of isotopic species in germanium (the main isotope <sup>74</sup>Ge makes up about 36% of natural germanium, while the second most common isotope, <sup>72</sup>Ge, has an abundance of 28%) might facilitate the assignment of lines. Additionally, minor isotopic species with <sup>34</sup>S or <sup>18</sup>O can be considered.

Once again, guidance by quantum-chemical calculations will be important. Rotational

**Table 4.10.:** Calculated<sup>a</sup> spectroscopic constants (in MHz) of OGeS and its rare isotopic species.

|               | <sup>16</sup> O <sup>74</sup> Ge <sup>32</sup> S | <sup>18</sup> O <sup>74</sup> Ge <sup>32</sup> S | <sup>16</sup> O <sup>74</sup> Ge <sup>34</sup> S | <sup>16</sup> O <sup>72</sup> Ge <sup>32</sup> S | <sup>18</sup> O <sup>72</sup> Ge <sup>32</sup> S | <sup>16</sup> O <sup>72</sup> Ge <sup>34</sup> S |
|---------------|--|--|--|--|--|--|
| $A_0$         | 18 367.7   | 16 6723.0  | 18 223.9   | 18 384.4   | 16 688.8   | 18 241.1   |
| $B_0$         | 4 632.3  | 4 610.6  | 4 466.6  | 4 676.9  | 4 656.0  | 4 510.6  |
| $C_0$         | 3 694.8  | 3 606.3  | 3 582.1  | 3 722.8  | 3 634.8  | 3 611.1  |
| $10^3 D_J$    | 1.476  | 1.403  | 1.395  | 1.502  | 1.428  | 1.420  |
| $10^3 D_{JK}$ | 2.863  | 3.357  | 2.448  | 2.951  | 3.445  | 2.531  |
| $10^3 D_K$    | 64.246   | 51.815   | 63.578   | 64.238   | 51.795   | 63.578   |
| $10^3 d_1$    | -0.393   | -0.402   | -0.363   | -0.402   | -0.412   | -0.372   |
| $10^3 d_2$    | -0.060   | -0.068   | -0.054   | -0.062   | -0.070   | -0.056   |

<sup>a</sup> Rotational constants from the optimized structure (CCSD(T)/cc-pwCVQZ level of theory, with a Stuttgart-Köln ECP including 10 core electrons for germanium) corrected for zero-point vibrational effects (CCSD(T)/cc-pVTZ level of theory). Centrifugal-distortion constants at the CCSD(T)/cc-pVTZ level of theory.

**Table 4.11.:** CCSD(T)/cc-pVTZ zero-point vibrational corrections (in MHz) of cyclic OGeS and its rare isotopic species.

|                         | <sup>16</sup> O <sup>74</sup> Ge <sup>32</sup> | <sup>18</sup> O <sup>74</sup> Ge <sup>32</sup> S | <sup>16</sup> O <sup>74</sup> Ge <sup>34</sup> S | <sup>16</sup> O <sup>72</sup> Ge <sup>32</sup> S | <sup>18</sup> O <sup>72</sup> Ge <sup>32</sup> S | <sup>16</sup> O <sup>72</sup> Ge <sup>34</sup> S |
|-------------------------|--|--|--|--|--|--|
| $\Delta A_{\text{vib}}$ | -59.20   | -49.60   | -59.29   | -59.21   | -49.61   | -59.23   |
| $\Delta B_{\text{vib}}$ | -8.51  | -8.48  | -7.99  | -8.61  | -8.58  | -8.08  |
| $\Delta C_{\text{vib}}$ | -13.34   | -13.01   | -12.66   | -13.50   | -13.16   | -12.81   |

constants from the optimized structure of linear OGeS and minor isotopic species are listed in Tab. 4.9. The corresponding vibrational corrections and centrifugal-distortion constants were computed at CCSD(T)/cc-pVTZ level of theory and are also listed in Tab. 4.9. In Tab. 4.10 and Tab. 4.11, the corresponding numbers are shown for the cyclic isomer of OGeS.

**Table 4.9.:** Calculated<sup>a</sup> spectroscopic constants (in MHz) for linear OGeS and its rare isotopic species.

|              | <sup>16</sup> O <sup>74</sup> Ge <sup>32</sup> | <sup>18</sup> O <sup>74</sup> Ge <sup>32</sup> S | <sup>16</sup> O <sup>74</sup> Ge <sup>34</sup> S | <sup>16</sup> O <sup>72</sup> Ge <sup>32</sup> S | <sup>18</sup> O <sup>72</sup> Ge <sup>32</sup> S | <sup>16</sup> O <sup>72</sup> Ge <sup>34</sup> S |
|--------------|--|--|--|--|--|--|
| $B_0$        | 3 227.8  | 3 084.3  | 3 117.5  | 3 231.7  | 3 087.2  | 3 121.780  |
| $10^3 D$     | 4.127  | 3.671  | 3.887  | 4.130  | 3.672  | 3.891  |
| $\Delta B_0$ | -5.581   | -5.176   | -5.585   | -5.585   | -5.179   | -5.309   |

<sup>a</sup> Rotational constants from the optimized structure (CCSD(T)/cc-pwCVQZ level of theory, with a Stuttgart-Köln ECP including 10 core electrons for germanium) corrected for zero-point vibrational effects (CCSD(T)/cc-pVTZ level of theory). Centrifugal-distortion constants at the CCSD(T)/cc-pVTZ level of theory.

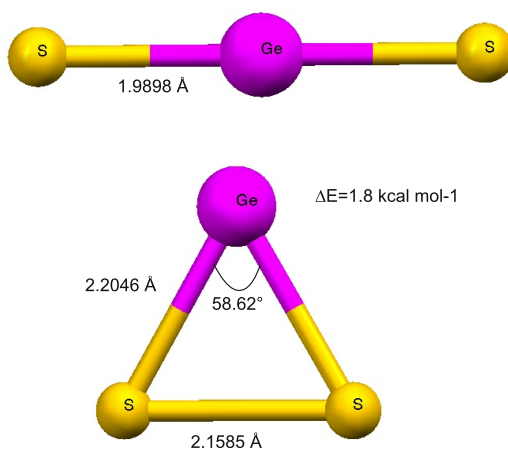


**Figure 4.9.:** Theoretical estimates (CCSD(T)/cc-pwCVQZ level of theory, with a Stuttgart-Köln ECP including 10 core electrons for germanium) for the structural parameters and relative energy of linear and cyclic GeS<sub>2</sub>.

### 4.3.3. Cyclic GeS<sub>2</sub>

Cyclic GeS<sub>2</sub> is the next heavier molecule in the series ES<sub>2</sub> (E=C,...,Pb) after SiS<sub>2</sub>. Following the differences between OSiS and OGeS and considering Tab. 4.3, we expect the potential-energy surface of GeS<sub>2</sub> to be even more shallow than for SiS<sub>2</sub>, which makes the detection of cyclic GeS<sub>2</sub> via rotational spectroscopy plausible.

Linear GeS<sub>2</sub> has been characterized by Hassanzadeh and Andrews<sup>103</sup> by means of vibrational spectroscopy and later by Friesen *et al.* by means of Raman spectroscopy.<sup>140</sup> Like linear SiS<sub>2</sub>, it is not possible to detect linear GeS<sub>2</sub> via rotational spectroscopy due to the lack of a permanent dipole moment. To our knowledge, cyclic GeS<sub>2</sub> has not been searched for yet, neither experimentally nor via theoretical methods.

We calculated an optimized structure of linear and cyclic GeS<sub>2</sub> at the CCSD(T)/cc-pwCVQZ<sup>148</sup> level of theory with a Stuttgart-Köln effective-core potential for 10 inner-shell electrons in germanium. The resulting structure is displayed in Fig. 4.9. At the given level of theory, the cyclic form is around 2 kcal·mol<sup>-1</sup> higher in energy than the linear form.

Comparing cyclic SiS<sub>2</sub> and cyclic GeS<sub>2</sub>, the stabilization via the S-S single bond is likely to be very similar. The difference between the S-S bond length in SiS<sub>2</sub> and in GeS<sub>2</sub> is marginal, which is a strong indication for the bond being of similar strength and nature. The S-Ge-S bond angle, however, is smaller than the S-Si-S angle in SiS<sub>2</sub>. As has been mentioned before, germanium in general tends to allow for smaller bond angles than silicon, therefore the ring strain is expected to be smaller in GeS<sub>2</sub> than in SiS<sub>2</sub>. It is worth mentioning that evidently the relative energy between cyclic and linear isomer of GeS<sub>2</sub> heavily depends on the method: It drops from 6.5 kcal·mol<sup>-1</sup> (CCSD(T)/cc-pVQZ level of theory, see Tab. 4.3) to 1.8 kcal·mol<sup>-1</sup> (CCSD(T)/cc-pwCQZ plus ECP 10 for Ge). It would be interesting to investigate further how important relativistic effects and core-correlation effects in this germanium compound are. Preliminary calculations with the exact two-component method (X2C)<sup>149</sup> show that the bond lengths are roughly 0.005 Å shorter in case of the X2C method and that the energy difference between linear and cyclic isomer is about 2 kcal·mol<sup>-1</sup> larger than in a non-relativistic calculation.<sup>150</sup>

**Table 4.12.:** Calculated spectroscopic constants<sup>a</sup> (in MHz) for GeS<sub>2</sub> and its isotopologues.

|               | <sup>74</sup> Ge <sup>32</sup> S <sub>2</sub> | <sup>72</sup> Ge <sup>32</sup> S <sub>2</sub> | <sup>32</sup> S <sup>74</sup> Ge <sup>34</sup> S | <sup>34</sup> S <sup>72</sup> Ge <sup>32</sup> S |
|---------------|---|---|--|--|
| $A_0$         | 6 771.6                                       | 6 771.6                                       | 6 577.5  | 6 577.6  |
| $B_0$         | 3 981.8                                       | 4 031.3                                       | 3 914.5  | 3 963.8  |
| $C_0$         | 2 503.7                                       | 2 523.2                                       | 2 450.5  | 2 469.7  |
| $10^3 D_J$    | 0.696   | 0.708   | 0.672  | 0.683  |
| $10^3 D_{JK}$ | 5.550   | 5.609   | 5.245  | 5.301  |
| $10^3 D_K$    | -1.712  | -1.783  | -1.626   | -1.693   |
| $10^3 d_1$    | -0.396  | -0.406  | -0.384   | -0.395   |
| $10^3 d_2$    | -0.185  | -0.192  | -0.180   | -0.186   |

<sup>a</sup> Rotational constants from the optimized structure (CCSD(T)/cc-pwCVQZ+ECP10(Ge) level of theory) corrected for zero-point vibrational effects. Centrifugal-distortion at the CCSD(T)/cc-pVTZ level of theory.

**Table 4.13.:** Zero-point vibrational corrections to the rotational constants (in MHz) of GeS<sub>2</sub> and its relevant isotopologues, CCSD(T)/cc-pVTZ level of theory.

|                         | <sup>74</sup> Ge <sup>32</sup> S <sub>2</sub> | <sup>72</sup> Ge <sup>32</sup> S <sub>2</sub> | <sup>32</sup> S <sup>74</sup> Ge <sup>34</sup> S | <sup>34</sup> S <sup>72</sup> Ge <sup>32</sup> S |
|-------------------------|---|---|--|--|
| $\Delta A_{\text{vib}}$ | -13.67  | -13.68  | -13.11   | -13.13   |
| $\Delta B_{\text{vib}}$ | -6.86   | -6.98   | -6.67  | -6.79  |
| $\Delta C_{\text{vib}}$ | -8.26   | -8.35   | -7.99  | -8.08  |

We propose an experimental search for cyclic GeS<sub>2</sub> by means of rotational spectroscopy. The search will be facilitated by the large dipole moment of 2.31 D around the *a*-axis. The necessary rotational constants from the optimized structure were corrected for zero-point vibrational effects at CCSD(T)/cc-pVTZ level of theory and are listed in Tab. 4.12 along with computed centrifugal-distortion constants. The zero-point vibrational corrections are listed in Tab. 4.13. The predicted parameters will be useful in guiding the experimental search for cyclic GeS<sub>2</sub>.

#### 4.3.4. H<sub>2</sub>SiS<sub>2</sub>

Since the silicon atom in SiS<sub>2</sub> carries a lone pair, it can engage in bonding with two hydrogen atoms, which results in cyclic H<sub>2</sub>SiS<sub>2</sub>. However, the addition of two hydrogen atoms makes the potential-energy surface much more complicated and allows for a plethora of other isomers. For example, the heavy-atom analogue of formic acid, S-SiH-SH, can be devised from the same composition. In analogy to formic acid a *syn*- and an *anti*-conformer can be formed by changing the Si-S-H angle. Heavy-atom analogues of carboxylic acids are highly unstable towards oxidation<sup>151</sup> and have therefore mainly been investigated by means of computational methods.<sup>152–154</sup> Only recently, in 2010, Xiong *et al.* succeeded in obtaining crystal structures of donor-acceptor stabilized O-Si-SH and O-Si-OH.<sup>99</sup> To our knowledge, the heavy-atom analogues of carboxylic acids have not been characterized in the gas phase or inert noble-gas matrices yet.

Another possible compound that can be formed from the same composition as H<sub>2</sub>SiS<sub>2</sub> is HS-Si-SH, the heavy-atom analogue of dihydroxycarbene. Dihydroxycarbene itself is a rather exotic compound that has long been proposed to play a role as an intermediate product in the decomposition of oxalic acid. In 2008, the first free dihydroxycarbene was trapped in a low-temperature argon matrix and characterized by Schreiner *et al.*<sup>155</sup> According to calculations on the coupled-cluster level that the authors report, dihydroxycarbene is around 43 kcal·mol<sup>-1</sup> higher in energy than formic acid.

These structures are by no means all possible isomers of H<sub>2</sub>SiS<sub>2</sub> but this small selection gives an impression of the complexity of the potential-energy surface of H<sub>2</sub>SiS<sub>2</sub>. In the present study, the geometry of the isomers mentioned above was optimized at CCSD(T)/cc-pCVQZ level of theory. In Fig. 4.10 the geometries and relative energies are displayed.

It is evident that the heavy-atom analogue of formic acid is the global minimum on the potential-energy surface. In analogy to formic acid, both conformers have a planar geometry. However, the *anti*-conformer is slightly lower in energy (by 1.1 kcal·mol<sup>-1</sup>) than the *syn*-conformer. In formic acid itself, the *syn*-conformer is the more stable of the conformers, additionally the energy difference between the *syn*- and *anti*-form amounts to about 4 kcal·mol<sup>-1</sup>,<sup>155</sup> a much higher value than for the silicon analogue. The structural parameters suggest that the bonding situation in S-SiH-SH is comparable to the situation in formic acid. The S-Si bond has a length comparable to diatomic SiS (about 1.93 Å, see Fig. 4.2). The Si-SH bond, on the other hand, is longer than 2 Å, which suggests that a single bond is formed.

The HS-Si-SH isomer is only 7.4 kcal·mol<sup>-1</sup> higher in energy than *anti*-S-SiH-SH, which makes it energetically better accessible than dihydroxycarbene. HS-Si-SH is planar and has C<sub>2v</sub> symmetry. It should be mentioned that even if the hydrogen atoms are deflected out of the plane initially, the geometry optimization only yields a planar structure as the local minimum. The Si-S bonds are longer than the Si-S single bonds in the S-SiH-SH isomers and in cyclic SiS<sub>2</sub>. HS-Si-SH is bent and not cyclic, i.e., it is not stabilized by an S-S bond. Instead, the sulfur atoms are saturated by hydrogen. The S-Si-S angle of 95° dovetails with the typical arrangement of atomic p-orbitals in 90° angles. Considering the small energy difference between the HS-Si-SH and S-SiH-SH isomers, HS-Si-SH also seems to be a plausible candidate for the detection via rotational spectroscopy.

The cyclic isomer H<sub>2</sub>SiS<sub>2</sub> is 13 kcal·mol<sup>-1</sup> higher in energy than *anti*-S-SiH-SH, which makes it energetically accessible for characterization via rotational spectroscopy as well. H<sub>2</sub>SiS<sub>2</sub> has C<sub>s</sub> symmetry with the hydrogen atoms perpendicular to the S-Si-S plane. The structural parameters of the three-membered S-Si-S ring are very similar to the corresponding values in cyclic SiS<sub>2</sub>. Like in cyclic SiS<sub>2</sub> the S-S bond is assumed to be crucial for stabilizing the

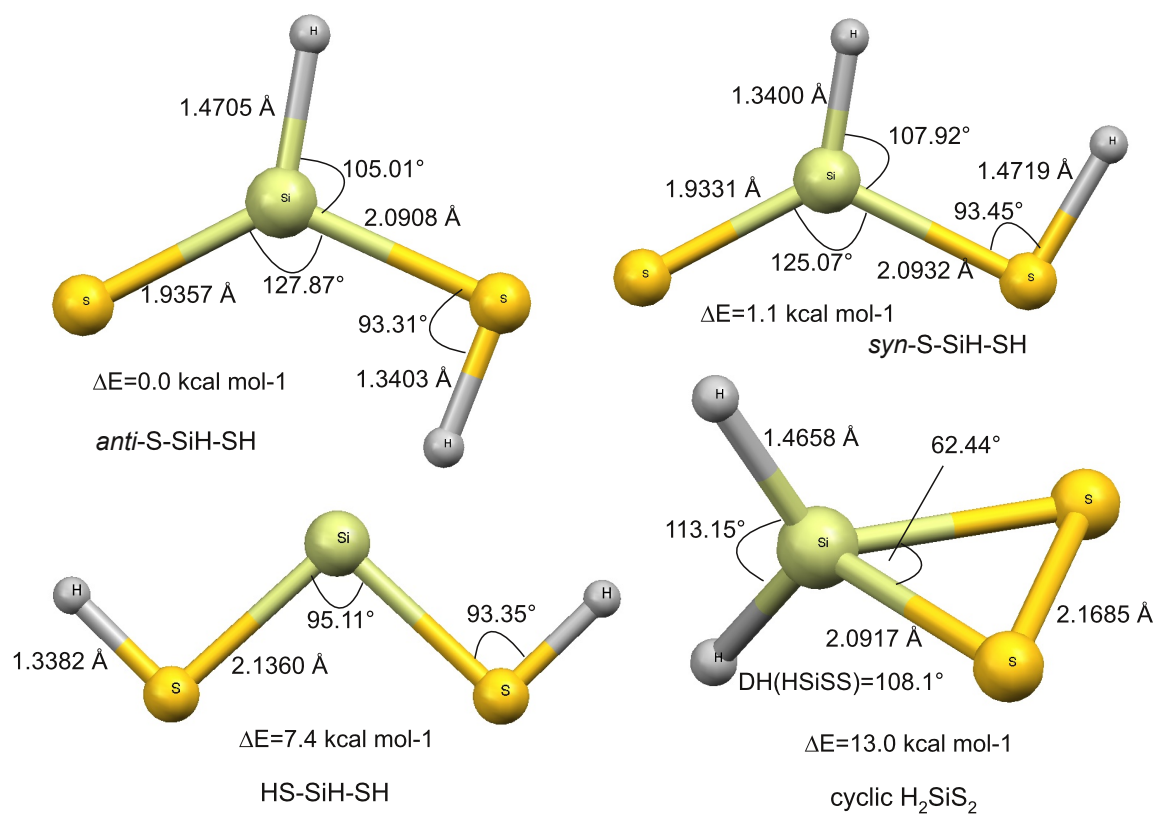


**Figure 4.10.:** Theoretical estimates (CCSD(T)/cc-pCVQZ level of theory) for the structural parameters and relative energy of *anti*-S-SiH-SH, *syn*-S-SiH-SH, HS-Si-SH, and cyclic  $\text{H}_2\text{SiS}_2$ .

**Table 4.14.:** Calculated spectroscopic constants<sup>a</sup> (in MHz) for the cyclic H<sub>2</sub>SiS<sub>2</sub> isomer and its relevant isotopologues.

|               | H <sub>2</sub> SiS <sub>2</sub> | H <sub>2</sub> <sup>29</sup> SiS <sub>2</sub> | H <sub>2</sub> Si <sup>34</sup> SS |
|---------------|---------------------------------|---|------------------------------------|
| $A_0$         | 6 839.9                         | 6 710.2                                       | 6 800.0                            |
| $B_0$         | 6 449.2                         | 6 449.2                                       | 6 246.5                            |
| $C_0$         | 3 452.8                         | 3 419.4                                       | 3 384.0                            |
| $10^3 D_J$    | 2.486                           | 2.480   | 2.248                              |
| $10^3 D_{JK}$ | 0.413                           | 0.494   | 0.345                              |
| $10^3 D_K$    | 2.338                           | 2.276   | 1.736                              |
| $10^3 d_1$    | -1.257                          | -1.261  | -1.151                             |
| $10^3 d_2$    | -0.260                          | -0.259  | -0.264                             |

<sup>a</sup> Rotational constants from the optimized structure (CCSD(T)/cc-pCVQZ level of theory) corrected for zero-point vibrational effects. Centrifugal-distortion constants at the CCSD(T)/cc-pVTZ level of theory.

**Table 4.15.:** Zero-point vibrational corrections to the rotational constants (in MHz) for the cyclic H<sub>2</sub>SiS<sub>2</sub> isomer and its isotopologues, CCSD(T)/cc-pVTZ level of theory.

|                         | H <sub>2</sub> SiS <sub>2</sub> | H <sub>2</sub> <sup>29</sup> SiS <sub>2</sub> | H <sub>2</sub> Si <sup>34</sup> SS |
|-------------------------|---------------------------------|---|------------------------------------|
| $\Delta A_{\text{vib}}$ | -27.314                         | -26.567                                       | -26.809                            |
| $\Delta B_{\text{vib}}$ | -14.420                         | -14.435                                       | -13.926                            |
| $\Delta C_{\text{vib}}$ | -14.633                         | -14.464                                       | -14.178                            |

compound. The structural parameters suggest that the addition of two hydrogen atoms does not affect the ring strain much. The verification of this hypothesis would require further investigations, though.

Our data obtained from CCSD(T)/cc-pCVQZ calculations suggests that all presented isomers can be characterized by means of rotational spectroscopy. All isomers have sizable permanent dipole moments: *anti*-S-SiH-SH carries a dipole moment of 2.24 D in direction of the *a*- and 0.51 D in direction of the *b*-axis, while the *syn*-conformer has a dipole moment of 2.88 D along the *a*- and 1.96 D along the *b*-axis. The dipole moment of HS-Si-SH amounts to 1.27 D (in direction of *b*-axis) and in H<sub>2</sub>SiS<sub>2</sub> the dipole moment has a value of 2.01 D (along the *b*-axis). Considering small sulfur rings and the close relationship to cyclic SiS<sub>2</sub>, the most interesting candidate for an experimental characterization is cyclic H<sub>2</sub>SiS<sub>2</sub>, at least in the scope of this work. In Tab. 4.14 and Tab. 4.15 the predicted rotational constants (CCSD(T)/cc-pCVQZ level of theory) as well as centrifugal-distortion constants and zero-point vibrational corrections (both at CCSD(T)/cc-pVTZ level of theory) are listed. Furthermore, the corresponding constants for minor isotopologues are given.

Considering the recent characterization of dihydroxycarbene, the experimental search for HS-Si-SH would also be particularly interesting. The rotational constants, zero-point vibrational corrections and centrifugal-distortion constants of HS-Si-SH and its minor isotopologues are listed in Tab. 4.16 and Tab. 4.17. The level of theory for the listed parameters is CCSD(T)/cc-pCVQZ for structure and rotational constants and CCSD(T)/cc-pVTZ for zero-point vibration

**Table 4.16.:** Calculated spectroscopic constants<sup>a</sup> (in MHz) for the isomer HS-Si-SH and its isotopologues.

|               | HS-Si-SH | H <sup>34</sup> S-Si-SH | HS- <sup>29</sup> Si-SH |
|---------------|----------|-------------------------|-------------------------|
| $A_0$         | 12 308.5 | 12 195.0                | 12 023.0                |
| $B_0$         | 2 929.9  | 2 849.3                 | 2 923.0                 |
| $C_0$         | 2 363.9  | 2 307.0                 | 2 353.1                 |
| $10^3 D_J$    | 1.540    | 1.471                   | 1.529                   |
| $10^3 D_{JK}$ | -13.532  | -13.130                 | -13.176                 |
| $10^3 D_K$    | 85.322   | 83.559                  | 81.935                  |
| $10^3 d_1$    | -0.444   | -0.418                  | -0.448                  |
| $10^3 d_2$    | -0.025   | -0.023                  | -0.026                  |

<sup>a</sup> Rotational constants from the optimized structure (CCSD(T)/cc-pCVQZ level of theory) corrected for zero-point vibrational effects. Centrifugal-distortion constants at the CCSD(T)/cc-pVTZ level of theory.

**Table 4.17.:** Zero-point vibrational corrections to the rotational constants (in MHz) of the isomer HS-Si-SH and its isotopologues, CCSD(T)/cc-pVTZ level of theory.

|                         | HS-Si-SH | H <sup>34</sup> S-Si-SH | HS- <sup>29</sup> Si-SH |
|-------------------------|----------|-------------------------|-------------------------|
| $\Delta A_{\text{vib}}$ | -41.467  | -41.261                 | -40.050                 |
| $\Delta B_{\text{vib}}$ | -11.282  | -10.889                 | -11.243                 |
| $\Delta C_{\text{vib}}$ | -11.633  | -11.256                 | -11.558                 |

correction and centrifugal-distortion constants.

For *anti*- and *syn*-S-SiH-SH rotational constants, zero-point vibrational corrections, and rotational constants were calculated as well. These can be found in the appendix.

Overall, we propose that a comprehensive characterization of the potential-energy surface of H<sub>2</sub>SiS<sub>2</sub> in the gas phase by means of rotational spectroscopy will be interesting and worthwhile. Since the molecules will most likely be produced in a discharge experiment from H<sub>2</sub>S and SiH<sub>4</sub>, the formation of Si-, S-, and H-containing molecules of different compositions during this process is plausible. It would therefore be interesting to also consider molecules like HSiS<sub>2</sub><sup>+</sup> or Si<sub>2</sub>SH<sub>2</sub> and their isomers in the future. Likewise, the radicals HSiS<sub>2</sub> or Si<sub>2</sub>SH are interesting open-shell system for a closer investigation.

### 4.3.5. HPS<sub>2</sub>

A further molecule related to SiS<sub>2</sub> is HPS<sub>2</sub>. Compared to SiS<sub>2</sub> the silicon has been substituted by the isovalent fragment HP. In this sense, HPS<sub>*n*</sub> can also be seen as a derivative of the doubly charged sulfur ring S<sub>*n*</sub><sup>2+</sup>. In addition to its relation to SiS<sub>2</sub>, isomers of HPS<sub>2</sub> can be considered heavy-atom analogues of nitrous acid HNO<sub>2</sub>. Nitrous acid occurs in a *cis*- and a *trans*-form, with the *trans* form as the more stable conformer. Nitrous acid is quite unstable and therefore only known in solution or in salts containing the NO<sub>2</sub><sup>-</sup> anion. However, nitrous acid plays an important role in the chemistry of the troposphere and indirectly influences the ozone concentration.<sup>156</sup> Since recently gaseous phosphorous compounds from anthropogenic sources have been identified in the atmosphere,<sup>157</sup> HPO<sub>2</sub> or even HPS<sub>2</sub> might play a role as reactants in tropospheric or stratospheric chemistry.<sup>158</sup> However, these compounds will likely be unstable towards oxidation to phosphoric acid.

Various isomers of the potential-energy surface of HPS<sub>2</sub> have been characterized before by means of infrared spectroscopy in an argon matrix<sup>106</sup> and via quantum-chemical methods.<sup>159</sup> Mielke and Andrews observe only one isomer, HPSS (for the structure see Fig. 4.11, bottom right). Following quantum-chemical calculations presented by the authors this isomer is quite high in energy compared to, for example, the branched isomer HP(S)S. The reason for its formation is probably the experimental setup, which favors the reaction of the PH radical with S<sub>2</sub> to HPSS. The isomerization of HPSS to HP(S)S is speculated to have high reaction barriers.

These hypotheses are confirmed in a computational study conducted by Yu *et al.* at MP2/6-311++G(d,p) level of theory.<sup>159</sup> The lowest lying isomer on the potential-energy surface is identified to be the heavy-atom analogue of nitrous acid, HS-PS (for structure see Fig. 4.11 at the top). The branched isomer HP(S)S follows as the second most stable isomer and is around 3.5 kcal·mol<sup>-1</sup> higher in energy than HS-PS. Yu and coworkers furthermore postulate the existence of an isomer with an P-S-S ring, which corresponds to HPS<sub>2</sub> (for the structure of HPS<sub>2</sub> see Fig. 4.11, bottom left). HP-SS is the least stable isomer, its isomerization to more stable structures is protected by a kinetic barrier of around 17 kcal·mol<sup>-1</sup>.

In the present study, the geometries of isomers HS-PS, cyclic HPS<sub>2</sub>, and HP-SS were calculated at the CCSD(T)/cc-pCVQZ level of theory. The structures and relative energies are displayed in Fig. 4.11. In analogy to nitrous acid, the *trans* isomer of HS-PS is the absolute minimum on the potential-energy surface, followed by the *cis*-isomer, which is only 1 kcal·mol<sup>-1</sup> higher in energy. The bonding in HS-PS also seems analogous to nitrous acid: The HSP-S bond has a length of around 1.92 Å, which is comparable to the length of the double bond in linear NPS (1.912 Å).<sup>135</sup> The HS-PS bond length, on the other hand is around 2.10 Å, which corresponds to the P-S bond length in cyclic NPS.<sup>135</sup> Cyclic HPS<sub>2</sub> is only around 12 kcal·mol<sup>-1</sup> higher in energy than *trans*-HS-PS. The bond lengths in the PS<sub>2</sub> ring suggest single-bond character of all bonds. The HPSS isomer is about 33 kcal·mol<sup>-1</sup> higher in energy than the *trans*-HS-PS isomer. In principle, it is possible to form a *cis*- and a *trans*-conformer of HPSS, here only the *cis*-isomer is considered, which, according to Mielke *et al.*,<sup>106</sup> is the more stable conformer. The bond lengths in HPSS indicate that the HP-SS bond is mainly of single-bond character while the HPS-S bond seems to have mainly double-bond character. However, detailed investigation of the bonding situation would be necessary to confirm this hypothesis. Viable candidates for the characterization by means of rotational spectroscopy are the HS-PS isomers and the cyclic HPS<sub>2</sub> isomer. Considering the weak signals of cyclic OSiS, which is also around 30 kcal·mol<sup>-1</sup> higher in energy than the global minimum, the HPSS isomer is probably too high in energy to be accessible. Since in the scope of this work, especially the

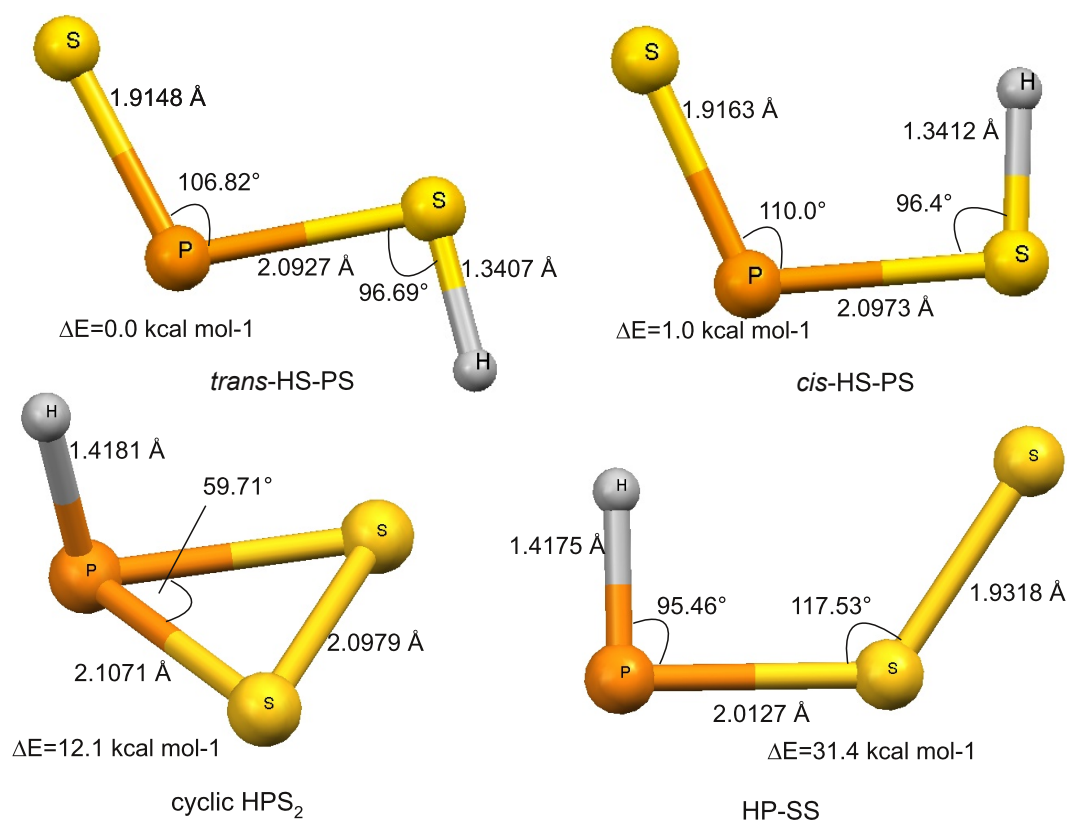


**Figure 4.11.:** Theoretical estimates (CCSD(T)/cc-pCVQZ level of theory) for the structural parameters and relative energy of *trans*-HS-PS, *cis*-HS-PS, cyclic HPS<sub>2</sub>, and HP-SS.

cyclic HPS<sub>2</sub> as a derivative of SiS<sub>2</sub> is of interest, we list its parameters relevant to rotational spectroscopy here in Tab. 4.18 and Tab. 4.19, while the corresponding parameters for the HS-PS isomers and HPSS can be found in the appendix. The only naturally occurring isotope of phosphorous is <sup>31</sup>P, therefore only data for isotopologues with <sup>34</sup>S are listed. In addition to the naturally occurring isotopic species, the deuterated molecules were considered. The rotational constants were derived from structures optimized at CCSD(T)/cc-pCVQZ level of theory. Zero point vibrational corrections and centrifugal-distortion constants were calculated at CCSD(T)/cc-pVTZ level of theory. The permanent dipole moment in cyclic HPS<sub>2</sub> amounts to 0.55 D in *c*- and -1.11 D in *a*-direction.

As a concluding remark, cyclic HPS<sub>2</sub> is a plausible candidate for detection by rotational spectroscopy to carry forward the idea of small substituted sulfur cycles. But the heavy atom analogues of nitrous acid have not been detected in the gas phase either, therefore their characterization would be very interesting as well.

**Table 4.18.:** Calculated spectroscopic constants<sup>a</sup> (in MHz) of the cyclic Isomer of HPS<sub>2</sub> and its important isotopologues.

|               | HPS <sub>2</sub> | HP <sup>34</sup> S <sup>32</sup> S | DPS <sub>2</sub> |
|---------------|------------------|------------------------------------|------------------|
| $A_0$         | 6 976.5          | 6 889.9                            | 6 810.2          |
| $B_0$         | 6 828.6          | 6 652.3                            | 6 485.8          |
| $C_0$         | 3 539.3          | 3 469.2                            | 3 486.8          |
| $10^3 D_J$    | 1.859            | 1.951                              | 1.915            |
| $10^3 D_{JK}$ | 4.894            | 3.722                              | 3.641            |
| $10^3 D_K$    | -1.179           | -0.297                             | -0.282           |
| $10^3 d_1$    | -1.143           | -1.114                             | -1.121           |
| $10^3 d_2$    | -0.483           | -0.421                             | -0.412           |

<sup>a</sup> Rotational constants from the optimized structure (CCSD(T)/cc-pCVQZ level of theory) corrected for zero-point vibrational effects. Centrifugal-distortion constants at the CCSD(T)/cc-pVTZ level of theory.

**Table 4.19.:** Zero-point vibrational corrections to the rotational constants (in MHz) of HPS<sub>2</sub> and its important isotopologues, CCSD(T)/cc-pVTZ level of theory.

|                         | HPS <sub>2</sub> | HP <sup>34</sup> S <sup>32</sup> S | DPS <sub>2</sub> |
|-------------------------|------------------|------------------------------------|------------------|
| $\Delta A_{\text{vib}}$ | -17.13           | -24.02                             | -17.55           |
| $\Delta B_{\text{vib}}$ | -28.89           | -20.86                             | -26.18           |
| $\Delta C_{\text{vib}}$ | -16.32           | -15.84                             | -15.55           |

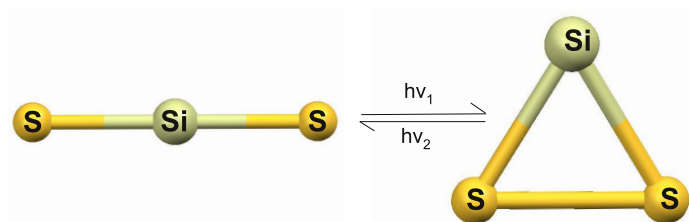


**Figure 4.12.:** Scheme of a possible photoisomerization reaction yielding cyclic SiS<sub>2</sub> via selective radiation of linear SiS<sub>2</sub> with laser light in a noble-gas matrix.

#### 4.4. Isomerization of SiS<sub>2</sub> – the need for multireference schemes.

So far we have only investigated the cyclic and linear minima on the potential-energy surface of SiS<sub>2</sub>. However, it is equally interesting to explore possible isomerization reactions that might allow for switching back and forth between the two isomers. This would open up new paths for producing cyclic SiS<sub>2</sub> in low-temperature noble-gas matrices: Since linear SiS<sub>2</sub> has been characterized in an argon matrix an isomerization reaction might produce cyclic SiS<sub>2</sub>. One important factor in isomerization reactions in general is the barrier height of the molecules since it determines the kinetic stability of the structures. In case of SiS<sub>2</sub> the quantification of the barrier height for the reaction linear SiS<sub>2</sub> → cyclic SiS<sub>2</sub> might therefore clarify why we can find cyclic SiS<sub>2</sub> in the discharge experiment despite its high relative energy: A high barrier height would explain its high kinetic stability. The first goal of this section is to determine the barrier height of the reaction linear SiS<sub>2</sub> → cyclic SiS<sub>2</sub> to the best possible accuracy.

A further interesting question to ask about the reaction of cyclic to linear SiS<sub>2</sub> is whether it is possible to induce this isomerization by selective irradiation with a laser (see. Fig. 4.12). Zeng *et al.* could recently show that such a photoisomerization is possible in the non-Walsh sixteen-electron triatomic cyclic PSN in an argon matrix. On the potential-energy surface, two more relatively low-lying isomers, linear SNP and linear SPN, are encountered and the authors could transform all three isomers into each other by mere irradiation with the correct wavelength. Such a photoisomerization in a low-temperature noble-gas matrix is plausible for SiS<sub>2</sub> as well.

Crucial for the induction of photoisomerization procedures is the structure and potential-energy surface of the molecule's electronically excited states. For a successful photoisomerization an electronically excited state, which can be reached from the ground state by an optical excitation, has to exist. This excited state has to guide the structure towards the other isomer. Furthermore, there has to be the possibility for the molecule to relax into the electronic ground state after the isomerization. Whether or not the necessary electronically excited states exist and whether they can guide the structure in a way that renders photoisomerization feasible can be studied via quantum-chemical calculations. Therefore, the second goal of this section is to predict the possibility of a photoinduced isomerization of SiS<sub>2</sub> by quantum chemistry.

However, the quantum-chemical methods required to study the reaction barrier and the excited states are of entirely different nature than in the previous chapters. So far, we have dealt with the description of minima and closed-shell molecules via extrapolation and additivity schemes comprising single-reference coupled-cluster methods. These methods give – as demonstrated earlier – very accurate results and have great predictive power in single-reference cases. Unfortunately, their predictive power breaks down for the transition state connecting cyclic

and linear SiS<sub>2</sub> because this state has multireference character. Upon decrease of the S-Si-S angle, a change in occupation occurs (see Fig. 4.6), two Slater determinants with two different closed shell occupations,  $|\cdots 11a_1^2 8b_2^0\rangle$  and  $|\cdots 11a_1^0 8b_2^2\rangle$ , are of similar importance at the transition state. For a viable description, both Slater determinants have to be treated on the same footing. This makes the transition state a multireference case and we cannot use a single-reference method to cope with it.

As a multireference method, multireference-configuration interaction (MRCI) was chosen (see also Sec. 2.6). The calculations were conducted with the Columbus quantum-chemical program package, version 7.0.<sup>160</sup> Since MRCI is not size consistent, size-consistency corrected MRCI methods like MRCI+Pople correction and multireference averaged quadratic coupled-cluster (MRAQCC), were used for comparison. Often the size-consistency errors in the absolute energy are quite large, even for small molecules. However, since the reaction of linear SiS<sub>2</sub> to cyclic SiS<sub>2</sub> is merely an isomerization reaction, the size-consistency errors for the relative energies are not expected to be large.

#### 4.4.1. Barrier height of SiS<sub>2</sub> isomerization

As discussed above, an accurate determination of the barrier height of the isomerization from linear to cyclic SiS<sub>2</sub> requires a multireference treatment. We study the electronic ground state along the reaction coordinate by means of MRCI methods with singles and doubles excitations (MRCISD). To accurately account for core-correlation effects, a cc-pCVTZ<sup>48</sup> basis set was chosen. As an active space, two electrons in two orbitals, the 11a<sub>1</sub> and 8b<sub>2</sub> orbital, were considered, i.e., a CAS(2,2) was used. As a reaction coordinate the S-Si-S angle was defined and S-Si-S angles from 180° to 60° in increments of 5° were taken into account. Close to the transition state calculations for additional angles were performed to narrow down the transition-state geometry to higher accuracy. For every angle, the Si-S distance was optimized. In Fig. 4.13 the energy profile along the reaction coordinate calculated with MRCISD, MRCISD+Pople correction, and MRAQCCSD is plotted. It is visible that the S-Si-S angle at the transition state is 105° for the MRCISD and 100° for the MRAQCCSD method. At the transition state, the coefficients for the two Slater determinants  $|\cdots 11a_1^2 8b_2^0\rangle$  and  $|\cdots 11a_1^0 8b_2^2\rangle$  are -0.67/0.67 for MRCISD and 0.66/-0.56 for MRAQCCSD, which again underlines the importance of using a multireference method for the calculation of the barrier height.

The angles at the transition state are substantially larger than suggested by the angular dependence of orbital energies in Fig. 4.6. At these angles, the Si-S bond length increases dramatically, as is evident from Fig. 4.14. It is interesting to see that the Si-S distance increases further at angles slightly smaller than the transition-state angle. The geometries of both minima and the transition state are displayed in Fig. 4.15. In general, MRCISD and MRAQCCSD methods give similar structural parameters. The bond lengths in cyclic SiS<sub>2</sub> differ from the experimental structure by around 0.01Å (see Fig. 4.5). This deviation of MRCISD from experimental values is therefore one order of magnitude larger than of extrapolated coupled-cluster methods (see Fig. 4.5), which underlines the accuracy of coupled-cluster extrapolation and additivity schemes. In terms of absolute energies, the MRCISD method gives values around 0.15 Hartree larger than MRCISD+Pople correction and around 0.2 Hartree larger than MRAQCCSD, but the energy difference between minima and transition state is very similar in both methods. These values demonstrate, though, that the size-extensivity error in terms of absolute energy is quite large.

From the calculations presented in Fig. 4.13 and 4.14 the barrier heights can be determined.

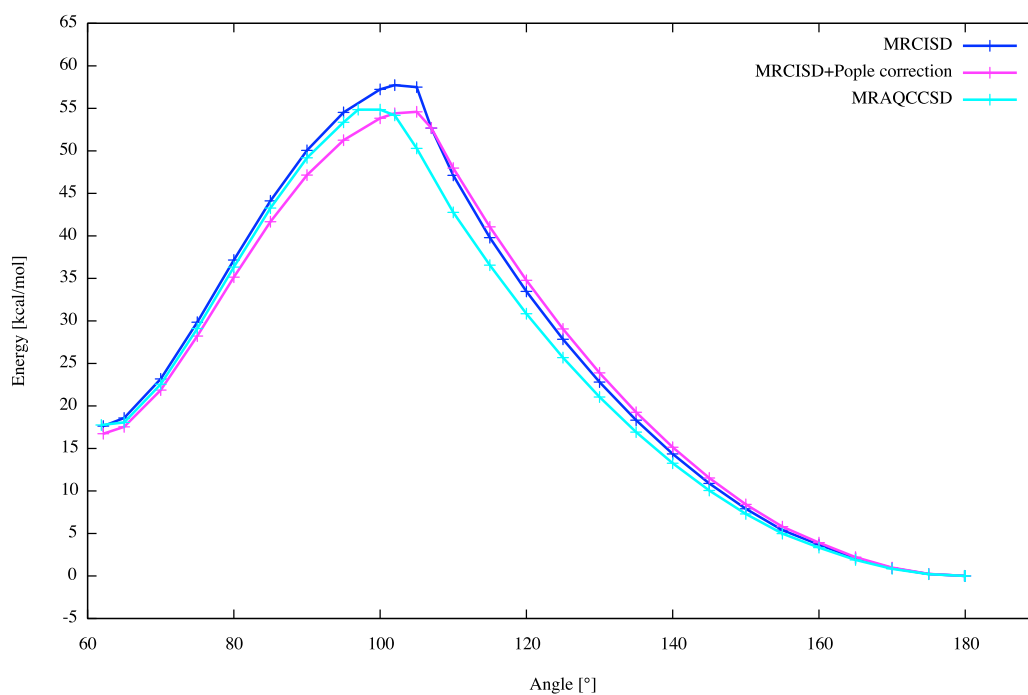


**Figure 4.13.:** Energy change along the reaction coordinate in the ring-opening reaction of cyclic  $\text{SiS}_2$ . MRCISD/cc-pCVTZ results are compared to schemes that include corrections for size extensivity. The relative energy in  $\text{kcal}\cdot\text{mol}^{-1}$  is given with respect to global minimum at  $180^\circ$ .

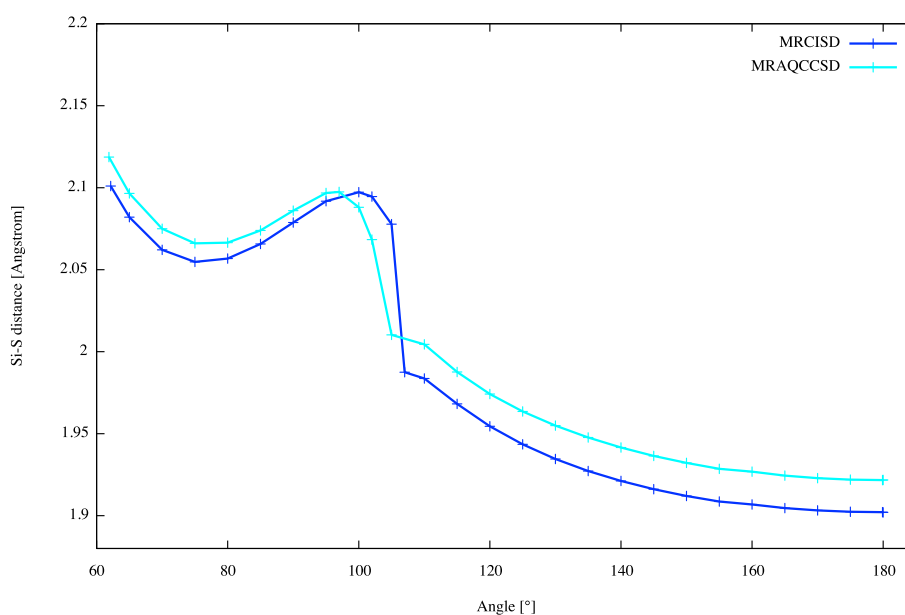


**Figure 4.14.:** Change in the Si-S distance along the reaction coordinate in the ring-opening reaction of cyclic SiS<sub>2</sub>. MRCISD/cc-pCVTZ results are compared to values from MRAQCCSD/cc-pCVTZ.

These are listed in Fig. 4.15. The difference between the values obtained from MRCISD and MRAQCCSD is only marginal. Fig. 4.15 indeed demonstrates that cyclic SiS<sub>2</sub> is protected from isomerization by a barrier of about 38 kcal·mol<sup>-1</sup>. The isomerization of linear SiS<sub>2</sub> to cyclic SiS<sub>2</sub> is thermodynamically unfavourable anyway, but additionally a barrier of around 55 kcal·mol<sup>-1</sup> would have to be overcome for this process.

To estimate how high this barrier is compared to other reactions, the isomerization of the sixteen-electron triatomic cyclic PSN serves as a good example. The reaction cyclic PSN → linear SNP has a barrier height of about 23 kcal·mol<sup>-1</sup> and the reaction of linear SPN → cyclic PSN has a barrier height of about 33 kcal·mol<sup>-1</sup>. Compared to those reactions the barrier height of SiS<sub>2</sub> is exceptionally high.

In conclusion, the hypothesis that the kinetic stability of cyclic SiS<sub>2</sub> protects it from isomerization to the energetically more stable linear SiS<sub>2</sub> could be confirmed by calculations with multireference methods. This is one reason why the search for cyclic SiS<sub>2</sub> by means of rotational spectroscopy in the discharge products of H<sub>2</sub>S and SiH<sub>4</sub> was successful.

#### 4.4.2. Excited states of SiS<sub>2</sub> – is a photoisomerization of SiS<sub>2</sub> possible?

The study of the excited states in SiS<sub>2</sub> and how they change with the S-Si-S angle might shed light on the possibility of inducing an isomerization via optical excitation in SiS<sub>2</sub>. As a method we used state-averaged (SA) MRCI calculations. A CAS(4,4) was used for the MRCI calculations, which means that the 11a<sub>1</sub>, 2a<sub>2</sub>, 4b<sub>1</sub>, and 8b<sub>2</sub> orbitals were included in the active space and four electrons are distributed into those orbitals. Only singlet states were considered. All calculations – even for the linear molecule – were performed in C<sub>2v</sub> geometry. The possibility of a photoisomerization of linear SiS<sub>2</sub> hinges on the structure of the excited

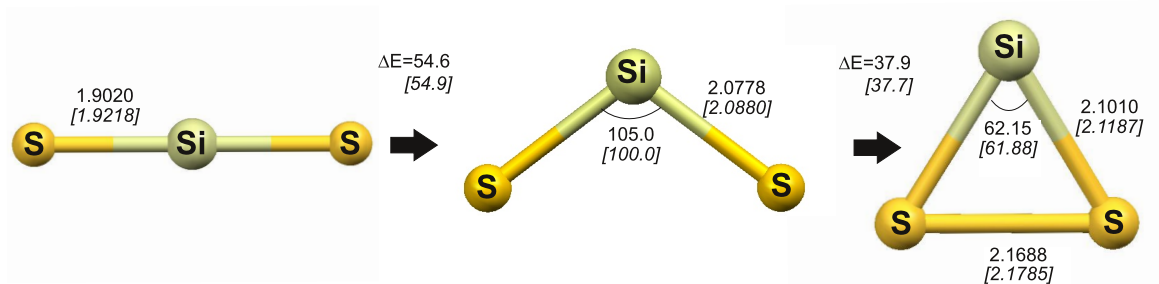


**Figure 4.15.:** Local and cyclic minima of SiS<sub>2</sub> and the connecting transition state. The energy differences are given in kcal·mol<sup>-1</sup>, angles in °, bond lengths in Å (MRCISD/cc-pCVTZ level of theory and MRAQCCSD/cc-pCVTZ values in italics).

states at the linear and cyclic minima as well as along the reaction coordinate. The structure of the excited states along the reaction coordinate is depicted in Fig. 4.16.

At linear geometry, a state for an optical excitation has to be accessible, which entails an excitation energy between 1.5 and 6 eV (wavelengths from UV light to near infrared light that can be produced with a laser) and a non-zero transition-dipole length. According to Fig. 4.16 and Tab. 4.20 the only state that fulfills these requirements at an S-Si-S angle of 180° is the 2<sup>1</sup>B<sub>2</sub> state. All other transitions are forbidden by symmetry. At structures that deviate from linear geometry, however, the transitions to all states except for the A<sub>2</sub> states are allowed in principal.

In C<sub>2v</sub> symmetry the 1<sup>1</sup>B<sub>2</sub> (together with the 1<sup>1</sup>A<sub>2</sub> state) corresponds to the degenerate 1<sup>1</sup>Π<sub>g</sub> state at 180°. The transition from X 1<sup>1</sup>Σ<sub>g</sub><sup>+</sup> → 1<sup>1</sup>Π<sub>g</sub> is forbidden by the Laporte rule but a small deviation from 180° would allow the Laporte rule to be broken. It is demonstrated in Tab. 4.20 that – in contrast to the situation at 180° – the transition moment for the excitation X 1<sup>1</sup>A<sub>1</sub> → 1<sup>1</sup>B<sub>2</sub> is non-zero for an S-Si-S angles of 170°, which implies that the bending modes of SiS<sub>2</sub> might allow for this transition.

The X 1<sup>1</sup>A<sub>1</sub> → 2<sup>1</sup>B<sub>2</sub> excitation (which corresponds to X 1<sup>1</sup>Σ<sub>g</sub><sup>+</sup> → 1<sup>1</sup>Σ<sub>u</sub><sup>+</sup> at linear geometry) has a sizable transition-dipole length at both, linear and bent geometry. However, the 2<sup>1</sup>B<sub>2</sub> state is on the very high end of accessible energies. The MRCISD value for the excitation energy is 6.58 eV at 180°, which corresponds to about 190 nm wavelength. In principle it is possible to reach this wavelength with a UV laser, for example with an ArF excimer laser.<sup>161</sup> It should be mentioned that the Pople correction reduces the predicted excitation energy slightly to 6.06 eV (which corresponds to about 205 nm wavelength).

Let us assume that either the excitation X 1<sup>1</sup>A<sub>1</sub> → 1<sup>1</sup>B<sub>2</sub> or the excitation X 1<sup>1</sup>A<sub>1</sub> → 2<sup>2</sup>B<sub>2</sub> can be achieved experimentally. Then the resulting state would have to relax to smaller S-Si-S angles in order to yield cyclic SiS<sub>2</sub> in the end. If an excitation into the 1<sup>1</sup>B<sub>2</sub> can be achieved at 180°, the transition 1<sup>1</sup>B<sub>2</sub> → X 1<sup>1</sup>A<sub>1</sub> is possible at around 100° (de-excitation energy 0.02 eV, transition moment 0.010 e · a<sub>0</sub>). This would be a feasible way to obtain the cyclic isomer of SiS<sub>2</sub> via the 1<sup>1</sup>B<sub>2</sub> state.

Starting from the 2<sup>1</sup>B<sub>2</sub> state the situation is more complicated. Since the energy of the 2<sup>1</sup>B<sub>2</sub> state increases with decreasing angles – especially at angles smaller than 100° – this relaxation would be difficult to achieve if the molecule remains in this state. However, the transition 2<sup>1</sup>B<sub>2</sub> → 2<sup>1</sup>A<sub>1</sub> might occur at 130° (the excitation energy for this transition is 0.47 eV with a

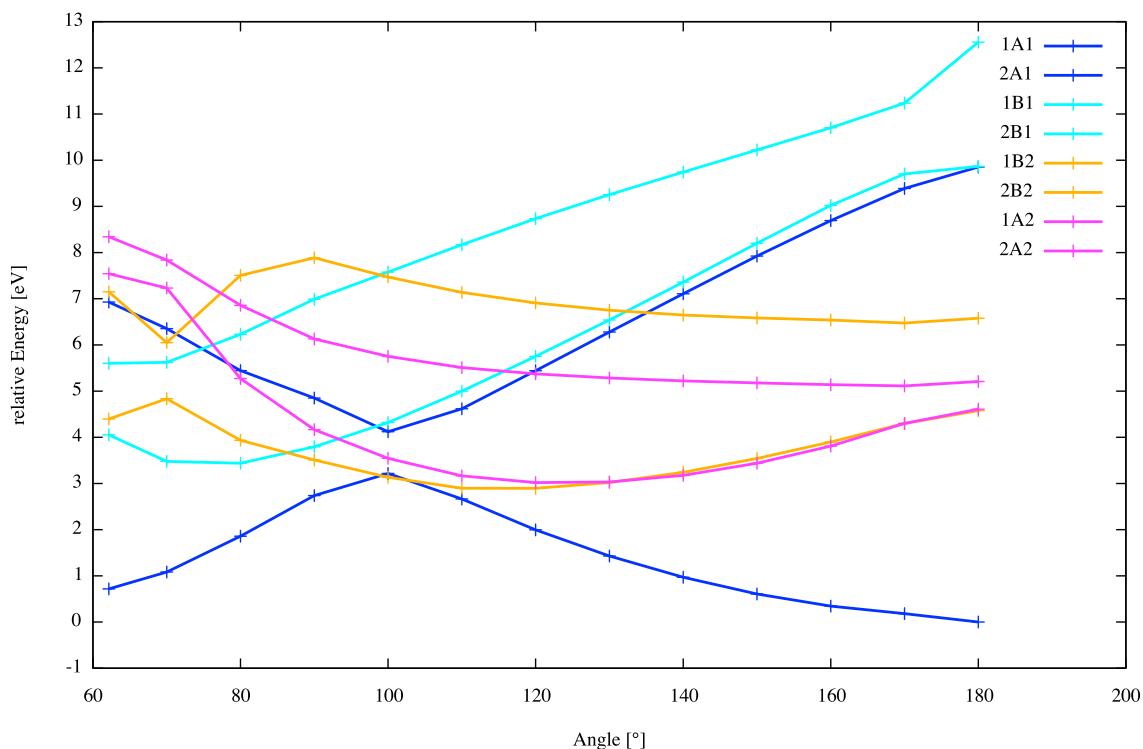


**Figure 4.16.:** Excited-state potential-energy surfaces along the reaction coordinate in the ring opening reaction of cyclic SiS<sub>2</sub>. The results were obtained on MRCISD/cc-pCVTZ level of theory. Relative energies in eV are given with the global minimum at 180° in the electronic ground state as the reference point.

transition-dipole length of  $0.006 e \cdot a_0$ ) resulting in the  $2^1A_1$  state, which could then relax into the ground state at around 100° (at 100° the excitation energy for the transition  $2^1A_1 \rightarrow 1^1A_1$  is  $-0.91$  eV with a transition-dipole length of  $1.11 e \cdot a_0$ ). The molecule must have enough initial vibrational energy, though, to counterbalance the increase in energy of the  $2^1B_2$  state and allow for S-Si-S angles of 130°.

In the light of these findings it seems easier to turn around the photoisomerization procedure: It might be feasible to start at cyclic SiS<sub>2</sub> and achieve photoisomerization to linear geometry. A possible excited state that could guide this process is the  $1^1B_2$  state. An avoided crossing seems to appear between the  $1^1B_2$  and  $2^1B_2$  states at around 70°, which goes hand in hand with an energetic increase of the  $1^1B_2$  state at increasing S-Si-S angles until 70° is reached. From 70° on, however, the  $1^1B_2$  state decreases in energy. At 100°, a transition to the X  $1^1A_1$  might be possible, which will lead to the desired linear SiS<sub>2</sub>.

As a concluding remark, it could not be definitely clarified whether a photoisomerization of linear to cyclic SiS<sub>2</sub> is experimentally feasible. All possible paths seem problematic. In terms of theory, an analysis of the excited-state dynamics, e.g., via a non-adiabatic hopping method<sup>162</sup> might shed further light on the problem. It should be mentioned that upon our proposal, P. Schreiner at Justus-Liebig-Universität, Gießen is trying to achieve a photoisomerization of linear SiS<sub>2</sub> in a noble-gas matrix experimentally but has not succeeded so far.<sup>163</sup>

**Table 4.20.:** Excitation energies (in  $eV$ ) and transition moments (in  $e \cdot a_0$ ) for transitions from the ground state in  $\text{SiS}_2$  at various S-Si-S angles. State-averaged 4-CAS(4,4)-MRCISD/cc-pCVTZ level of theory. Si-S Bond lengths were adopted from CAS(2,2)-MRCISD/cc-pCVTZ optimization (see previous Sec. 4.4.1)

| Excited state*                 | $\Delta E_{exc}$<br>MRCI | $\Delta E_{exc}$<br>MRCI+Pople | Transition-dipole length<br>MRCI |
|--------------------------------|--------------------------|--------------------------------|----------------------------------|
| 180°                           |                          |                                |                                  |
| X $1^1A_1$ ( $X^1\Sigma_g^+$ ) | 0.00                     | 0.00                           | –                                |
| $1^1B_2$ ( $1^1\Pi_g$ )        | 4.58                     | 4.42                           | 0.000                            |
| $1^1A_2$ ( $1^1\Pi_g$ )        | 4.61                     | 4.44                           | 0.000                            |
| $2^1A_2$ ( $1^1\Sigma_u^-$ )   | 5.21                     | 5.05                           | 0.000                            |
| $2^1B_2$ ( $1^1\Sigma_u^+$ )   | 6.58                     | 6.06                           | 1.991                            |
| $2^1A_1$ ( $1^1\Pi_u$ )        | 9.66                     | 9.24                           | 0.000                            |
| $1^1B_1$ ( $1^1\Pi_u$ )        | 9.87                     | 9.34                           | 0.000                            |
| 170°                           |                          |                                |                                  |
| X $1^1A_1$                     | 0.00                     | 0.00                           | –                                |
| $1^1A_2$                       | 4.12                     | 4.04                           | 0.000                            |
| $1^1B_2$                       | 4.12                     | 4.06                           | 0.382                            |
| $2^1A_2$                       | 4.93                     | 4.89                           | 0.000                            |
| $2^1B_2$                       | 6.29                     | 5.95                           | 2.058                            |
| $1^1B_1$                       | 9.52                     | 9.08                           | 0.025                            |
| 70°                            |                          |                                |                                  |
| X $1^1A_1$                     | 0.00                     | 0.00                           | –                                |
| $1^1B_1$                       | 2.40                     | 2.33                           | 0.042                            |
| $1^1B_2$                       | 3.75                     | 3.47                           | 0.370                            |
| $2^1B_1$                       | 4.54                     | 4.33                           | 0.618                            |
| $2^1B_2$                       | 4.97                     | 4.32                           | 0.109                            |
| $2^1A_1$                       | 5.27                     | 5.09                           | 0.016                            |
| 62.15°                         |                          |                                |                                  |
| X $1^1A_1$                     | 0.00                     | 0.00                           | –                                |
| $1^1B_1$                       | 3.34                     | 3.21                           | 0.031                            |
| $1^1B_2$                       | 3.68                     | 3.21                           | 0.467                            |
| $2^1B_1$                       | 4.88                     | 4.67                           | 0.887                            |
| $2^1A_1$                       | 6.12                     | 6.03                           | 0.005                            |
| $2^1B_2$                       | 6.43                     | 5.75                           | 0.402                            |

\*In parentheses the corresponding state symbol in  $D_{\infty v}$  symmetry is given.

### 4.4.3. Possible shortcomings of MRCI and alternative methods

It cannot be excluded that the ambiguous results are partially caused by shortcomings of the chosen method. MRCISD is not size consistent and may not describe dynamical correlation. In Tab. 4.20 it is evident that size-consistency corrections have a non-negligible influence on the excitation energies. The excitation energies corrected for size-consistency errors via the Pople correction are listed in the right-hand column. For some of the states the deviation between MRCISD and MRCISD+Pople correction is substantial. Especially for the  $^1B_2$  states, which are crucial for the accurate prediction of a possible photoisomerization of SiS<sub>2</sub>, the deviations are large, 0.68 eV at most. However, state-averaged MRCISD reproduces excited states well in general and it is questionable whether a “perfect” MRCC-method would give qualitatively different results.

The barrier height on the other hand is not influenced at all by the size-consistency corrections, the lack of size consistency only becomes visible in the absolute energies. The MRCISD+Pople energies are shifted by about 0.1 Hartree and the MRAQCCSD energies are shifted by about 0.15 Hartree.

The design of a rigorously size consistent (and size extensive, see Chapter 2) multireference coupled-cluster theory would solve some of the shortcomings of MRCI. Unfortunately, these methods are still not advanced enough to treat the given problem. It should be mentioned that the calculations above were repeated with a response method based on Mukherjee’s multireference coupled-cluster theory.<sup>164</sup> Due to shortcomings of the theory, the excited states could not be reproduced qualitatively, which is a decisive drawback regarding the predictive power of this method.<sup>38,39</sup>

In conclusion, MRCI methods are still the best methods at hand to describe the excited states of SiS<sub>2</sub>. However, the development of feasible and accurate multireference coupled-cluster schemes might improve the predictive power of multireference methods.



## **Part III.**

# **Improving the predictive power of quantum chemistry: Spin-orbit splittings via multireference coupled-cluster theory**



## 5. Introduction: How to calculate spin-orbit splittings with MRCC wave functions

*All theoretical chemistry is really physics and the theoretical chemists know it.*

– Richard Feynman

This thesis does not only demonstrate how much predictive power existing methods in quantum chemistry have. In this part, methods are developed that improve this predictive power. In summary, a generally applicable scheme for calculating spin-orbit splittings in  $^2\Pi$  states with multireference coupled-cluster wave functions is proposed. At present, the state-of-the-art method to tackle this problem is MRCI<sup>31,165</sup> and to our knowledge the new scheme represents a first attempt to use MRCC wave functions for the treatment of spin-orbit coupling.

In addition to being a methodological advancement, the findings also give insights into the design of multireference coupled-cluster theory, especially into the constitution of the coupling contribution in Jeziorski-Monkhorst based MRCC methods. For reasons outlined in Sec. 2.9 the focus of the developments lies on Mukherjee’s MRCC (Mk-MRCC) approach.

It should be mentioned that it is already possible to calculate spin-orbit splittings in  $^2\Pi$  states using coupled-cluster wave functions.<sup>24,166</sup> Klein and Gauss proposed a scheme, which exploits the equation-of-motion ionization-potential coupled-cluster (EOMIP-CC) scheme for this purpose. However, this approach does not comprise a genuine MRCC wave function, which is the focus of this work.

The new method for calculating spin-orbit splittings with MRCC wave functions can be embedded into coupled-cluster additivity schemes like the HEAT protocol,<sup>26</sup> (for more information on coupled-cluster extrapolation and additivity schemes see also Sec. 2.5). In the HEAT protocol, thermodynamic data of small molecules is calculated via coupled-cluster theory, typically with up to quadruple excitations. In this way the correlation energy is quantified as accurately as possible. The result is furthermore augmented by harmonic and anharmonic zero-point vibrational corrections, scalar-relativistic effects, the diagonal Born-Oppenheimer correction, and first-order spin-orbit contributions. So far, spin-orbit contributions have been calculated with multireference-configuration interaction methods since no coupled-cluster based method was available.<sup>26</sup>

Using the new scheme for calculating spin-orbit splittings via MRCC theory in coupled-cluster additivity schemes, provides a rigorous coupled-cluster treatment of all considered effects. In the following introductory chapter, the idea of how to calculate spin-orbit splittings with multireference coupled-cluster wave function is outlined.

### 5.1. Relativistic effects cause multireference character

If relativistic effects are taken into account, some simple single-reference problems turn into complicated multireference problems. This phenomenon is, for example, encountered in molecules with degenerate  $^2\Pi$  states. Calculating energy, geometry, etc., for these molecules, a

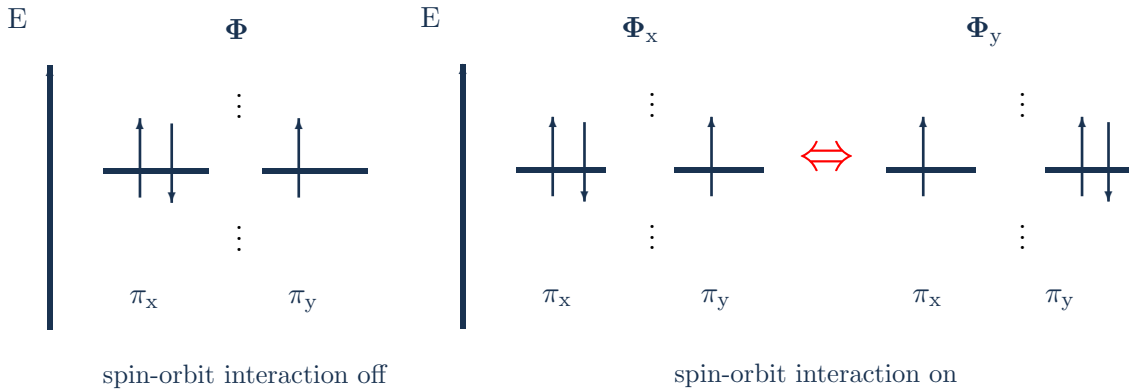


**Figure 5.1.:** As soon as spin-orbit coupling is in effect, the quantum-chemical treatment of molecules with  ${}^2\Pi$  states requires a multireference wave function

single-reference calculation suffices. The calculation of spin-orbit splittings, however, requires a multireference method. The reason for this somewhat surprising finding is that spin-orbit effects couple the two reference determinants  $\Phi_x$  and  $\Phi_y$  that differ by whether the  $\pi_x$  or the  $\pi_y$  orbital is doubly occupied (see Fig. 5.1). As a result of the coupling, the twofold  ${}^2\Pi$  state (quantum numbers  $\Lambda = 1, S = \frac{1}{2}$ ) is split into its  $J$  components, namely the  ${}^2\Pi_{1/2}$  and  ${}^2\Pi_{3/2}$  state with  $1/2$  and  $3/2$  as the corresponding  $J$  quantum numbers. A linear combination of these two components constitutes the wave functions for the  ${}^2\Pi_{1/2}$  and the  ${}^2\Pi_{3/2}$  state.

$$\Psi_{\Pi_{1/2}} = \frac{1}{\sqrt{2}}(\Phi_x - i\Phi_y), \quad \Psi_{\Pi_{3/2}} = \frac{1}{\sqrt{2}}(\Phi_x + i\Phi_y) \quad (5.1)$$

It can be easily seen that  $\Psi_{\Pi_{1/2}}$  and  $\Psi_{\Pi_{3/2}}$  are multireference wave functions since they constitute linear combinations of reference determinants  $\Phi_x$  and  $\Phi_y$ .<sup>a</sup>

## 5.2. Spin-orbit splittings in ${}^2\Pi$ states

To get a basic understanding of spin-orbit coupling in  ${}^2\Pi$  states it is worthwhile to have a closer look at their general properties. For these considerations, we use a generic (effective) one-electron spin-orbit operator  $\hat{H}^{\text{so}}$ , as for example proposed by Blume and Watson:<sup>167,168</sup>

$$\hat{H}^{\text{so}} = \text{const} \cdot \sum_{i,A} \frac{Z_A^{\text{eff}} \cdot \hat{\mathbf{s}}_i \cdot \hat{\mathbf{l}}_{iA}}{|r_i - R_A|^3}, \quad (5.2)$$

with  $Z_A^{\text{eff}}$  representing the effective nuclear charge of the  $A$ th nucleus, and  $\text{const}$  as a constant that contains the elementary charge, the mass of the electron, and the velocity of light. The key feature of the spin-orbit operator in Eq. 5.2 is the dot product of  $\hat{\mathbf{l}}_{iA}$  (the operator for the orbital-angular momentum of electron  $i$  with respect to  $R_A$  as the origin) and  $\hat{\mathbf{s}}_i$  (the spin-angular momentum of electron  $i$ ). To calculate the spin-orbit splittings, the spin-orbit

<sup>a</sup>A single-reference treatment is possible but would require the use of complex orbitals.

operator  $\hat{H}^{so}$  is spanned in the space of the degenerate states involved, which yields the matrix  $\mathbf{H}^{so}$

$$\mathbf{H}^{so} = \begin{pmatrix} 0 & \langle \Phi_x | \hat{H}^{so} | \Phi_y \rangle \\ \langle \Phi_y | \hat{H}^{so} | \Phi_x \rangle & 0 \end{pmatrix}. \quad (5.3)$$

Due to the antisymmetric properties of the matrix  $H^{so}$ , the diagonal elements are zero. The evaluation of the matrix elements is simplified when considering that only the  $z$  component of the vector operators provides non-vanishing matrix elements. This is marked by the subscript  $z$  in the following equation,

$$\langle \Phi_x | \hat{H}^{so} | \Phi_y \rangle = \langle \Phi_x | \text{const} \cdot \sum_{i,A} \frac{Z_A^{\text{eff}} \cdot [\hat{\mathbf{s}}_i \cdot \hat{\mathbf{l}}_{iA}]_z}{|r_i - R_A|^3} | \Phi_y \rangle. \quad (5.4)$$

For the eigenvalues of  $\mathbf{H}^{so}$  one obtains

$$E^{so} = \pm \sqrt{\left| \langle \Phi_x | \hat{H}^{so} | \Phi_y \rangle \right|^2}, \quad (5.5)$$

which corresponds to a spin-orbit splitting of

$$\Delta E^{so} = 2 \cdot \left| \langle \Phi_x | \hat{H}^{so} | \Phi_y \rangle \right|. \quad (5.6)$$

Considering Eq. 5.1, the above equation can also be expressed using the wave functions for the  $\Pi_{1/2}$  or the  $\Pi_{3/2}$  state

$$\Delta E^{so} = 2 \cdot \left| \langle \Psi_{\Pi_{1/2}} | \hat{H}^{so} | \Psi_{\Pi_{1/2}} \rangle \right| \quad \text{or} \quad \Delta E^{so} = 2 \cdot \left| \langle \Psi_{\Pi_{3/2}} | \hat{H}^{so} | \Psi_{\Pi_{3/2}} \rangle \right|. \quad (5.7)$$

Eq. 5.7 underlines the fact that the calculation of spin-orbit splittings in degenerate  ${}^2\Pi$  states requires a multireference wave function.

The eigenvectors to the eigenvalues in Eq. 5.5 have the following form

$$\vec{\chi}_1 = \frac{1}{\sqrt{2}} \begin{pmatrix} i \\ 1 \end{pmatrix} \quad \vec{\chi}_2 = \frac{1}{\sqrt{2}} \begin{pmatrix} -i \\ 1 \end{pmatrix}, \quad (5.8)$$

$\chi_1$  and  $\chi_2$  correspond to the  $J$  components  ${}^2\Pi_{1/2}$  and  ${}^2\Pi_{3/2}$ , respectively.

### 5.3. Calculating spin-orbit splittings in ${}^2\Pi$ states with MRCC theory

It is our goal to specifically use multireference coupled-cluster theory for the calculation of spin-orbit splittings. For this purpose the spin-orbit coupling is treated as a perturbation with the dimensionless perturbation parameter  $\gamma$  to a non-relativistic (NR) or purely scalar-relativistic (ScR) Hamiltonian  $\hat{H}$ .

$$\hat{H}^{\text{NR/ScR+SO}} = \hat{H}^{\text{NR/ScR}} + \gamma \hat{H}^{\text{so}} \quad (5.9)$$

The perturbative treatment of spin-orbit splittings is justified as long as the effects are small compared to the total energy.

Considering Eq. 5.7 it becomes obvious that the spin-orbit splittings can be calculated as a first-order property. If an MRCC wave function is desired this implies that MRCC gradient theory has to be used.

As a multireference coupled-cluster theory we choose Mk-MRCC, which – because of its size-extensivity property – is one of the most promising and the furthest developed MRCC theory at present (see Sec. 2.9 for an extensive discussion). Mk-MRCC gradient theory will be discussed in detail in Sec. 6.1.

The strategy is to calculate the coupled-cluster energy via a single-reference calculation and only treat the spin-orbit splittings via MRCC gradient theory. This implies that both determinants  $\Phi_x$  and  $\Phi_y$  must be generated within an SRCC framework. As can be easily seen in Fig. 5.1 the two determinants are related by an exchange of  $\pi_x$  and  $\pi_y$  orbitals and thus can be transformed into each other. This transformation is possible if – and only if – the  $\pi_x$  and  $\pi_y$  orbitals are equivalent. How exactly the transformation and the generation of equivalent  $\pi$  orbitals is achieved, will be described in Sec. 8.

Another reason why we can exclusively use single-reference coupled-cluster theory is that the coefficients  $c_\mu$ , which appear in the (Mk-)MRCC energy and amplitude equations (see Sec. 2.8), are fixed by symmetry. The eigenvectors of Eq. 5.8 give the corresponding expressions. In principle the outlined scheme can be performed with any spin-orbit operator. One has to observe that only the  $z$  component of this operator is necessary for the spin-orbit splittings in question (see Eq. 5.4). A plausible choice for a non-relativistic treatment is the Breit-Pauli spin-orbit operator  $\hat{H}^{\text{BPso}}$ , which is used as the perturbation operator to the non-relativistic Hamiltonian.

$$\hat{H} = \hat{H}^{\text{NR}} + \gamma \hat{H}^{\text{BPso}} . \quad (5.10)$$

However, if a full treatment of scalar-relativistic effects is desired, a good starting point for an unperturbed Hamiltonian is the spin-free Dirac-Coulomb Hamiltonian  $\hat{H}^{\text{sfDC}}$ .<sup>40</sup> It can be derived via a rigorous spin separation of the regular Dirac-Coulomb Hamiltonian into its spin-free and spin-orbit parts. In that case the resulting spin-orbit Dirac-Coulomb Hamiltonian  $H^{\text{soDC}}$  is the natural choice for the perturbation operator

$$\hat{H} = \hat{H}^{\text{sfDC}} + \gamma H^{\text{soDC}} . \quad (5.11)$$

#### 5.4. Spin-orbit splittings: A measure for the coupling contribution?

The treatment of spin-orbit coupling in  $^2\Pi$  states could shed light on theoretical problems in MRCC theory. There is the concern that in Mk-MRCC theory the reference determinants might not be sufficiently coupled.<sup>37</sup> Due to the symmetry properties of the spin-orbit operator, spin-orbit splittings can be interpreted as a direct measure for the coupling of the reference determinants. This is immediately evident if Eq. 5.3 or Eq. 5.6 are considered.

The comparison of spin-orbit splittings obtained from various Jeziorski-Monkhorst based

MRCC methods could be a further piece in the puzzle of finding the ultimate solution to MRCC theory.

In this thesis, expressions for spin-orbit splittings will therefore be derived for Brillouin-Wigner MRCC (BW-MRCC) and state-universal MRCC (SU-MRCC) as well. However, only the theory of these methods will be considered, which already gives sufficient insight into the problem.



## 6. Theoretical groundwork: From MRCC gradient theory to the spin-free Dirac-Coulomb approach

In the last chapter it became clear that the derivation of working equations for the calculation of spin-orbit splittings via (Mk-)MRCC theory requires a number of “ingredients” from previous work of other authors. All these previous developments that will be used in the next chapter for the derivation of working equations, are described here:

- (Mk-)MRCC gradient theory (see Sec. 6.1)
- A spin-orbit operator as a perturbation to the non-relativistic treatment. The choice here is the Breit-Pauli spin-orbit operator (see Sec. 6.2).
- A spin-orbit mean-field approach (SOMF) for an effective one-electron treatment. In general the spin-orbit operator has a one- and a two-electron part, which both appear in the gradient expression. However, the two-electron effects can be accounted for by cleverly defining mean-field matrix elements, which circumvents the use of the full two-electron part (see Sec. 6.3).
- A spin-free Dirac-Coulomb operator for the scalar-relativistic treatment and the corresponding spin-orbit Dirac-Coulomb operator that will be used as the perturbation (see Sec. 6.4).

Combining these “ingredients” with the special features of spin-orbit coupling (see Sec. 5 for details on these special features), working equations for the calculation of spin-orbit splittings in  ${}^2\Pi$  states via MRCC theories can be derived. Those derivations will be performed in Chapter 7).

### 6.1. Mukherjee’s multireference coupled-cluster gradient theory

For the derivation of Mk-MRCC gradient theory the Lagrangian technique is used.<sup>169</sup> The corresponding Lagrangian functional was proposed by Prochnow *et al.*<sup>34</sup>

$$\begin{aligned} \tilde{E} = & \sum_{\mu\nu} \bar{c}_\mu H_{\mu\nu}^{\text{eff}} c_\nu + \sum_{\mu} \sum_{q \in Q(\mu)} \bar{c}_\mu \lambda_q(\mu) \left[ \langle \Phi_{\mathbf{q}}(\mu) | \bar{H}_\mu | \Phi_\mu \rangle c_\mu \right. \\ & \left. + \sum_{\nu(\neq\mu)} \langle \Phi_{\mathbf{q}}(\mu) | e^{-\hat{T}^\mu} e^{\hat{T}^\nu} | \Phi_\mu \rangle H_{\mu\nu}^{\text{eff}} c_\nu \right] - \epsilon \left[ \sum_{\mu} \bar{c}_\mu c_\mu - 1 \right]. \end{aligned} \quad (6.1)$$

$\lambda$  and  $\bar{c}_\mu$  are the Lagrange multipliers that correspond to the constraints of the eigenvalue problem (Eq. 2.18) and to the amplitude equations (Eq. 2.32). The multiplier  $\epsilon$  is introduced

to ensure biorthonormality of  $c_\mu$  and  $\bar{c}_\mu$ . It should be noted that – unlike in the BW-MRCC and SU-MRCC Lagrangian – it is necessary to consider  $\bar{c}_\mu$  as a genuine Lagrange multiplier that must be determined separately. This is a consequence of the coefficients explicitly appearing in the amplitude equations of Mk-MRCC. In BW-MRCC and SU-MRCC theory, the right-hand eigenvector  $\tilde{c}_\mu$  can be used instead.

Taking the derivative with respect to the external perturbation  $\gamma$  and making a few algebraic manipulations yield the corresponding gradient expression

$$\frac{\partial \tilde{E}}{\partial \gamma} = \sum_{\mu} \bar{c}_\mu c_\mu \langle \Phi_\mu | \left( 1 + \hat{\Lambda}_\mu \right) e^{-\hat{T}^\mu} \frac{\partial \hat{H}}{\partial \gamma} e^{\hat{T}^\mu} | \Phi_\mu \rangle, \quad (6.2)$$

with the  $\Lambda_\mu$  operator defined as

$$\hat{\Lambda}_\mu = \underbrace{\sum_{q \in Q(\mu)} \hat{\tau}_q^+(\mu) \lambda_q(\mu)}_{\hat{\Lambda}_\mu^{\text{ext}}} + \sum_{\nu (\neq \mu)} \frac{\bar{c}_\nu}{c_\mu} \left[ 1 + \underbrace{\sum_{q \in Q(\nu)} \lambda_q(\nu) \langle \Phi_q(\nu) | e^{-\hat{T}^\nu} e^{\hat{T}^\mu} | \Phi_\nu \rangle}_{\hat{\Lambda}_\mu^{\text{int}}} \right] | \Phi_\mu \rangle \langle \Phi_\nu |. \quad (6.3)$$

$\hat{\Lambda}_\mu^{\text{int}}$  involves contributions due to the coupling between different reference determinants while  $\hat{\Lambda}_\mu^{\text{ext}}$  is similar to the SRCC  $\hat{\Lambda}_\mu$  operator.  $Q$  represents the excitation manifold. It is interesting that the coupling of the reference determinants, which is described by the coupling term in the amplitude equations (see Eq. 2.32), can be entirely put into the internal operator  $\hat{\Lambda}_\mu^{\text{int}}$ , thus a one-to-one correspondence between the structure of the amplitude equations and the gradient expression is established. This will be useful for the calculation of spin-orbit splittings regarding the symmetry properties of the spin-orbit operator.

The operator  $\hat{\Lambda}_\mu^{\text{int}}$  contains a term that closely resembles the Mk-MRCC coupling term, which Evangelista *et al.*<sup>78</sup> provided closed expressions for.

In the singles and doubles truncation scheme, the closed expressions for the coupling term are given by

$$\text{Singles} \quad \langle \Phi_i^a(\mu) | e^{-\hat{T}^\mu} e^{\hat{T}^\nu} | \Phi_0 \rangle = t_i^a(\nu/\mu) - t_i^a(\mu) \quad (6.4)$$

$$\begin{aligned} \text{Doubles} \quad \langle \Phi_{ij}^{ab}(\mu) | e^{-\hat{T}^\mu} e^{\hat{T}^\nu} | \Phi_0 \rangle = & -t_{ij}^{ab}(\mu) + t_{ij}^{ab}(\nu/\mu) \\ & + P(ij) t_i^a(\mu) t_j^b(\mu) \\ & - P(ij) P(ab) t_i^a(\mu) t_j^b(\nu/\mu) \\ & + P(ij) t_i^a(\nu/\mu) t_j^b(\nu/\mu). \end{aligned} \quad (6.5)$$

In the above equations,  $P(ij)$  is a permutation operator, which is defined as  $P(ij) f_{ij} = f_{ij} - f_{ji}$ . The amplitudes  $t_{ij\dots}^{ab\dots}(\nu/\mu)$  are those that the operator  $\hat{T}^\nu$  has in common with  $\hat{T}^\mu$ ,

$$t_{ij\dots}^{ab\dots}(\nu/\mu) = \begin{cases} t_{ij\dots}^{ab\dots}(\nu) & \text{if } ij\dots \in \text{occ}(\mu) \text{ and } ab\dots \in \text{vrt}(\mu) \\ 0 & \text{else} \end{cases}, \quad (6.6)$$

with  $\text{occ}(\mu)$  as the occupied and  $\text{vrt}(\mu)$  as the virtual space. Eq. 6.4 and Eq. 6.5 only have to be multiplied by the corresponding  $\lambda_q$  in order to obtain the required term in  $\hat{\Lambda}_\mu^{\text{int}}$ .

The  $\lambda$  amplitudes themselves can be determined by solving the corresponding  $\Lambda$  equations, which are obtained by invoking the stationary condition of the energy functional with respect to the amplitudes  $t$ .

$$\bar{c}_\mu \langle \Phi_\mu | (1 + \hat{\Lambda}_\mu) [\bar{H}_\mu, \hat{\tau}_q(\mu)] | \Phi_\mu \rangle c_\mu + \sum_\nu \bar{c}_\nu \langle \Phi_\nu | \frac{\partial \hat{\Lambda}_{\text{int}}(\nu)}{\partial t_q(\mu)} \bar{H}_\nu | \Phi_\nu \rangle c_\nu = 0, \quad (6.7)$$

with  $\bar{H}_\mu = e^{-\hat{T}_\mu} \hat{H} e^{\hat{T}_\mu}$  and  $\hat{\tau}_q(\mu)$  as a string of excitation operators with  $q_\mu \in Q(\mu)$ . The definition of  $\hat{\Lambda}_\mu$  is given in Eq. 6.3.

In addition to the  $\lambda$  Lagrange multipliers the  $\bar{c}_\mu$  and  $\epsilon$  multipliers have to be determined. Differentiating the energy functional  $\tilde{E}$  with respect to  $\bar{c}_\mu$ ,  $\epsilon$  can be identified as the energy  $E$ . Taking this finding into account,  $\bar{c}_\mu$  may be determined by the following equation

$$\sum_\nu \bar{c}_\nu M_{\nu\mu} = 0, \quad (6.8)$$

with the matrix elements of  $M_{\nu\mu}$  given by

$$M_{\mu\mu} = H_{\mu\mu}^{\text{eff}} - E - \sum_q \lambda_q(\mu) \sum_{\nu \neq \mu} \langle \Phi_q(\mu) | e^{-\hat{T}_\mu} e^{\hat{T}_\nu} | \Phi_\mu \rangle H_{\mu\nu}^{\text{eff}} \frac{c_\nu}{c_\mu} \quad (6.9)$$

$$M_{\nu\mu} = H_{\nu\mu}^{\text{eff}} + \sum_q \lambda_q(\nu) \langle \Phi_q(\nu) | e^{-\hat{T}_\nu} e^{\hat{T}_\mu} | \Phi_\nu \rangle H_{\nu\mu}^{\text{eff}}. \quad (6.10)$$

The matrix  $\mathbf{M}$  can be shown to have a zero eigenvalue and as a consequence Eq. 6.8 has a non-trivial solution.

An implementation of the outlined gradient theory is, for example, available in the program package CFOUR.<sup>113</sup> It has been shown that Mk-MRCCSD and Mk-MRCCSDT gradient theory give satisfactory geometries for biradicals.<sup>34,80,170</sup>

The gradient expression, Eq. 6.2 may be cast in a density-matrix formulation, which makes the evaluation of the expression more convenient and is often of computational advantage.<sup>22,171</sup> The density-matrix formulation is given by

$$\frac{\partial \tilde{E}}{\partial \gamma} = \sum_\mu \bar{c}_\mu \left[ \sum_{pq} D_{pq}(\mu) \frac{\partial f_{pq}(\mu)}{\partial \gamma} + \sum_{pqrs} \Gamma_{pqrs}(\mu) \frac{\partial \langle \Phi_p \Phi_q | \Phi_r \Phi_s \rangle}{\partial \gamma} \right] c_\mu, \quad (6.11)$$

with  $D_{pq}(\mu)$  as the one-particle density matrix of determinant  $\mu$ ,  $\frac{\partial f_{pq}(\mu)}{\partial \gamma}$  as the derivative of the Fock matrix with respect to the perturbation  $\gamma$ ,  $\Gamma_{pqrs}$  as the two-particle density matrix, and  $\frac{\partial \langle \Phi_p \Phi_q | \Phi_r \Phi_s \rangle}{\partial \gamma}$  as the derivative of the two-electron integrals. In Eq. 6.11 the two-particle density matrix is defined with respect to antisymmetrized integrals.  $\Phi_p$  denotes a spin-orbital. The one-particle density matrix  $D_{pq}(\mu)$  is given by

$$D_{pq}(\mu) = \langle \Phi_\mu | (1 + \hat{\Lambda}_\mu) e^{-\hat{T}_\mu} \{p^+ q\}_\mu e^{\hat{T}_\mu} | \Phi_\mu \rangle, \quad (6.12)$$

with the creation operator  $p^+$  and the annihilation operator  $q$  with respect to the Fermi

vacuum of determinant  $\mu$ . The two-particle density matrix  $\Gamma_{pqrs}$  reads

$$\Gamma_{pqrs}(\mu) = \frac{1}{4} \langle \Phi_\mu | (1 + \hat{\Lambda}_\mu) e^{-\hat{T}^\mu} \{p^+ q^+ sr\}_\mu e^{\hat{T}^\mu} | \Phi_\mu \rangle . \quad (6.13)$$

In analogy to single-reference theory, the density matrices and their contraction with the integral derivatives and Fock matrices can be evaluated diagrammatically. For the exact expressions and the technique of their diagrammatic evaluation, the reader is referred to Ref. 21 and Ref. 20.

## 6.2. The Breit-Pauli spin-orbit operator

A popular approximation to the Dirac Hamiltonian  $\hat{h}^D$  in Eq. 2.34 is the Pauli operator. Historically, its popularity stems from the fact that it can be partitioned into phenomenologically interpretable terms, which makes the operator particularly valuable for qualitative argumentation. Today, it is ever-present in schemes involving first-order perturbation theory. The Pauli operator can be derived via a perturbation expansion of the Dirac equation in powers of  $1/c$  (or in powers of  $\alpha = 1/c$ , respectively) after elimination of the small component.<sup>a</sup> The expansion is cut off at order  $1/c^2$ . This level actually corresponds to the lowest-order perturbation because in the relativistic expansion of the energy the powers of  $1/c$  are all even. Consequently, the Pauli operator is the lowest-order correction to a non-relativistic treatment. As is evident from Eq. 5.10 or Eq. 5.11 the spin-orbit splitting is treated as a first-order property in this work, therefore the order of perturbation in the Pauli operator suffices.

In a one-electron case, the Pauli Hamiltonian for a nuclear point charge  $Z$  in atomic units reads

$$\hat{H}^{\text{Pauli}} = \hat{T} + V - \frac{\alpha^2}{8m} \hat{\mathbf{p}}^4 + \frac{\pi\alpha^2 Z}{2} \delta(\mathbf{r}) + \frac{Z\alpha^2}{2r^3} \hat{\mathbf{s}} \cdot \hat{\mathbf{l}} . \quad (6.14)$$

In the above equation  $\hat{T}$  is the non-relativistic kinetic energy operator and  $V$  the non-relativistic potential. The first correction term to the non-relativistic part is the mass-velocity operator and contains the electronic mass  $m$  and the momentum operator  $\hat{\mathbf{p}}$ . It represents the correction to the kinetic energy because of the relativistic variations of mass with velocity. The second term is the Darwin term, which depends on the nuclear charge  $Z$  and the  $\delta$  function of  $\mathbf{r}$  (the distance between electron and nucleus). In atoms this term only affects  $s$  electrons. It accounts for the famous *Zitterbewegung*.<sup>94</sup> The third term constitutes the spin-orbit interaction and will be used as the one-electron term of the Breit-Pauli spin-orbit operator.<sup>172</sup> It features a dot product of the spin-momentum operator  $\hat{\mathbf{s}} = -\frac{1}{2}\boldsymbol{\sigma}$  and the orbital-momentum operator  $\hat{\mathbf{l}} = \hat{\mathbf{r}} \times \hat{\mathbf{p}}$ .

A drawback of the Pauli Hamiltonian is that it cannot be used in a variational calculation because it is highly singular.<sup>40</sup> In the region  $r < (Z/2mc^2)a_0$  (with  $a_0$  as the Bohr radius) the wave function is likely to collapse since the mass-velocity term dominates over the kinetic-energy term. If the Pauli Hamiltonian is used in first-order perturbation theory this does not matter. However, in such a calculation special attention has to be paid to the basis set's

<sup>a</sup>An alternative and probably more elegant route of derivation is based on the Foldy-Wouthuysen transformation.<sup>172</sup>

design of the core region.

Eq. 6.14 only contains one-electron terms. It needs to be augmented by two-electron contributions since those are indispensable to correctly account for the spin-orbit splitting and other aspects of the fine structure of spectra. To obtain the Breit-Pauli Hamiltonian, the two-electron terms must be added under the same premises (i.e., they all have to be of the order  $1/c^2$ ) as the one-electron terms. Coulomb, Gaunt, and retardation interactions are taken into account for both, spin-free and spin-orbit effects.<sup>172</sup>

Considering only the two-electron spin-orbit terms and the one-electron term in Eq. 6.14, results in the Breit-Pauli spin-orbit operator. The spin-orbit contribution from the Coulomb interaction has the following form for an atom<sup>172</sup>

$$\hat{H}^{\text{Cso}} = \sum_{i \neq j} -\frac{\alpha^2}{2r_{ij}^3} \hat{\mathbf{s}}_i \hat{\mathbf{l}}_{ij} . \quad (6.15)$$

The two-electron orbital-momentum operator in the above equation is defined as  $\hat{\mathbf{l}}_{ij} = \hat{\mathbf{r}}_{ij} \times \hat{\mathbf{p}}_i$ . The Coulomb term describes the interaction of the spin with its own orbital momentum and is therefore often called *spin-same-orbit term*.<sup>173</sup>

The spin-orbit contribution arising from the Gaunt interaction is

$$\hat{H}^{\text{Gso}} = \sum_{i \neq j} -\frac{\alpha^2}{r_{ij}^3} \hat{\mathbf{s}}_j \hat{\mathbf{l}}_{ij} . \quad (6.16)$$

In this term the spin of electron  $j$  interacts with the angular momentum of another electron and is thus called *spin-other-orbit term*.<sup>173</sup>

The retardation term of the Breit interaction only contains spin-free terms at order  $1/c^2$  and therefore does not have to be considered here.

Collecting the one- and two-electron contributions and summing over all nuclei  $A$  with nuclear charge  $Z_A$  yields the full expression for the Breit-Pauli spin-orbit operator. The expression is rewritten and the operators  $\hat{g}_{ij}$  and  $\hat{h}_i^{\text{BPso}}$  are introduced for a clear notation in subsequent derivations.

$$\hat{H}^{\text{BPso}} = \hat{H}^{\text{BPso1}} + \hat{H}^{\text{BPso2}} \quad (6.17)$$

$$\hat{H}^{\text{BPso}} = \sum_A \sum_i \hat{\mathbf{h}}_{iA}^{\text{so}} \hat{\mathbf{s}}_i + \sum_{i \neq j} \hat{\mathbf{g}}_{ij}^{\text{so}} (\hat{\mathbf{s}}_i + 2\hat{\mathbf{s}}_j) \quad (6.18)$$

$$\hat{\mathbf{h}}_{iA}^{\text{so}} = \frac{\alpha^2 Z_A}{2r_{iA}^3} \cdot \hat{\mathbf{l}}_{iA} \quad (6.19)$$

$$\hat{\mathbf{g}}_{ij}^{\text{so}} = -\frac{\alpha^2}{2r_{ij}^3} \hat{\mathbf{r}}_{ij} \times \hat{\mathbf{p}}_i \quad (6.20)$$

$$= -\frac{\alpha^2}{2r_{ij}^3} \hat{\mathbf{l}}_{ij} . \quad (6.21)$$

As was pointed out by Eq. 5.4, only the  $z$  component of the vector operators in Eq. 6.21 is necessary for calculating spin-orbit splittings in  $^2\Pi$  states. As in Eq. 5.4 this can be expressed by a subscript  $z$ . For the subsequent derivations it is nevertheless convenient to drop the

subscript, which defines short-hand notations for the corresponding operators

$$\hat{h}_{iA}^{\text{so}} = [\hat{\mathbf{h}}_{iA}^{\text{so}}]_z, \quad \hat{g}_{ij}^{\text{so}} = [\hat{\mathbf{g}}_{ij}^{\text{so}}]_z, \quad \hat{g}_{ij}^{\text{so}} \hat{s}_i = [\hat{\mathbf{g}}_{ij}^{\text{so}} \hat{\mathbf{s}}_i]_z. \quad (6.22)$$

### 6.3. Spin-orbit mean-field approximation for the Breit-Pauli spin-orbit operator

Since the expense of computing the full two-electron contribution from the Breit-Pauli spin-orbit operator is high, Hess and Marian proposed a mean-field approximation that accounts for two-electron effects without explicitly using the machinery normally required for them.<sup>174,175</sup> In other words, their proposed spin-orbit mean-field approximation (SOMF) represents an effective one-electron treatment. A helpful analogy for this approximation is the treatment of electron-electron interactions in Hartree-Fock theory:<sup>173</sup> One electron is considered to interact with the mean field of all other electrons, which is exactly how the two-electron spin-orbit interactions are treated in the SOMF interaction. The derivations presented here closely follow publications by Neese and Berning *et al.*<sup>173,176</sup>

The goal of the SOMF approximation is to express the Breit-Pauli spin-orbit operator in terms of an effective one-electron operator  $\hat{H}^{\text{SOMF}}$ , which can be written in the very general form

$$\hat{H}^{\text{BPsoMF}} = \sum_i \hat{O}_i \hat{\mathbf{s}}_i, \quad (6.23)$$

with the spatial mean-field operator  $\hat{O}_i$ .

The first step towards this goal is to define Fock-matrix like elements of the spin-orbit operator between two Slater determinants  $\Phi_1$  and  $\Phi_2$ . The Slater determinants consist of spin orbitals  $\Phi_k = \phi_k(r)\theta(s)$  with the spatial orbitals  $\phi_k$  and the spin part  $\theta(s) = \alpha(s)$  or  $\theta(s) = \beta(s)$ .  $\Phi_1$  and  $\Phi_2$  differ by a single spin-orbital excitation  $\Phi_i \rightarrow \Phi_a$ . For all subsequent derivations the Dirac notation for two-electron integrals will be used, i.e., electron 1 and electron 2 are arranged in the order  $\langle 12 || 12 \rangle$ . This implies that in the operator

$$\hat{\mathbf{g}}_{1,2}^{\text{so}} = -\frac{\alpha^2}{2r_{12}^3} \hat{\mathbf{r}}_{12} \times \hat{\mathbf{p}}_1, \quad (6.24)$$

the indices 1, 2 denote the electrons as in the Dirac notation of the integrals. It should be noted that the full operator involves the sum over all electrons, which is the reason for the occurrence of both,  $\hat{\mathbf{g}}_{1,2}^{\text{so}}$  and  $\hat{\mathbf{g}}_{2,1}^{\text{so}}$  in Eq. 6.25.

The Fock-matrix like elements then are

$$\begin{aligned} \langle \Phi_1 | \hat{H}^{\text{BPso}} | \Phi_2 \rangle &= \langle \Phi_i | \hat{H}^{\text{BPso1}} | \Phi_a \rangle + \\ &\sum_j \left( \langle \Phi_i \Phi_j | [\hat{\mathbf{g}}_{1,2}^{\text{so}} \cdot (\hat{\mathbf{s}}_1 + 2\hat{\mathbf{s}}_2) + \hat{\mathbf{g}}_{2,1}^{\text{so}} \cdot (\hat{\mathbf{s}}_2 + 2\hat{\mathbf{s}}_1)] | \Phi_a \Phi_j \rangle - \right. \\ &\left. \langle \Phi_i \Phi_j | [\hat{\mathbf{g}}_{1,2}^{\text{so}} \cdot (\hat{\mathbf{s}}_1 + 2\hat{\mathbf{s}}_2) + \hat{\mathbf{g}}_{2,1}^{\text{so}} \cdot (\hat{\mathbf{s}}_2 + 2\hat{\mathbf{s}}_1)] | \Phi_j \Phi_a \rangle \right). \end{aligned} \quad (6.25)$$

In Eq. 6.25, the first one of the two-electron terms represents the Coulomb contribution while

the second term constitutes the exchange contribution. The Coulomb contribution with the operator  $\hat{\mathbf{g}}_{1,2}^{\text{so}} \cdot (\hat{\mathbf{s}}_1 + 2\hat{\mathbf{s}}_2)$  can be rewritten in the following way:

$$\begin{aligned} & \sum_j \langle \Phi_i \Phi_j | \hat{\mathbf{g}}_{1,2}^{\text{so}} \cdot (\hat{\mathbf{s}}_1 + 2\hat{\mathbf{s}}_2) | \Phi_a \Phi_j \rangle = \\ & \sum_j [\langle \phi_i \phi_j | \hat{\mathbf{g}}_{1,2}^{\text{so}} | \phi_a \phi_j \rangle [\delta_{\theta_j \theta_i} \langle \theta_i | \hat{\mathbf{s}} | \theta_a \rangle + 2\delta_{\theta_i \theta_a} \langle \theta_j | \hat{\mathbf{s}} | \theta_j \rangle] \end{aligned} \quad (6.26)$$

The Coulomb contribution of the operator  $\hat{\mathbf{g}}_{2,1}^{\text{so}} \cdot (\hat{\mathbf{s}}_2 + 2\hat{\mathbf{s}}_1)$  becomes zero due to the permutational symmetry of the spatial integrals,

$$\langle \Phi_j \Phi_i | \hat{\mathbf{g}}_{1,2}^{\text{so}} | \Phi_j \Phi_a \rangle = 0 . \quad (6.27)$$

The spin-other-orbit contribution in Eq. 6.26 vanishes, if  $\Phi_j$  is a doubly occupied molecular orbital. However, for singly occupied molecular orbitals one has to introduce a further approximation. The approximation consists in averaging over the spin of the ‘‘spectator’’ orbitals  $\Phi_j$  in the spin-other-orbit contribution. This term then vanishes, which leads to the following full expression for the Coulomb contribution

$$\sum_j [\langle \Phi_i \Phi_j | \hat{\mathbf{g}}_{1,2}^{\text{so}} \cdot (\hat{\mathbf{s}}_1 + 2\hat{\mathbf{s}}_2) | \Phi_a \Phi_j \rangle = \sum_j [\langle \phi_i \phi_j | \hat{\mathbf{g}}_{1,2}^{\text{so}} | \phi_a \phi_j \rangle [\delta_{\theta_j \theta_i} \langle \theta_i | \hat{\mathbf{s}} | \theta_a \rangle] . \quad (6.28)$$

The exchange part can be rewritten and manipulated analogously. However, no contributions vanish.

$$\sum_j [\langle \Phi_i \Phi_j | \hat{\mathbf{g}}_{1,2}^{\text{so}} \cdot (\hat{\mathbf{s}}_1 + 2\hat{\mathbf{s}}_2) | \Phi_j \Phi_a \rangle = \sum_j [\langle \phi_i \phi_j | \hat{\mathbf{g}}_{1,2}^{\text{so}} | \phi_j \phi_a \rangle [\delta_{\theta_j \theta_a} \langle \theta_i | \hat{\mathbf{s}} | \theta_j \rangle + 2\delta_{\theta_i \theta_j} \langle \theta_j | \hat{\mathbf{s}} | \theta_a \rangle] \quad (6.29)$$

$$\sum_j [\langle \Phi_j \Phi_i | \hat{\mathbf{g}}_{1,2}^{\text{so}} \cdot (\hat{\mathbf{s}}_1 + 2\hat{\mathbf{s}}_2) | \Phi_a \Phi_j \rangle = \sum_j [\langle \phi_j \phi_i | \hat{\mathbf{g}}_{1,2}^{\text{so}} | \phi_a \phi_j \rangle [\delta_{\theta_i \theta_j} \langle \theta_j | \hat{\mathbf{s}} | \theta_a \rangle + 2\delta_{\theta_j \theta_a} \langle \theta_i | \hat{\mathbf{s}} | \theta_j \rangle] . \quad (6.30)$$

In analogy to the manipulations of the Coulomb contribution, spin averaging is performed. The contributions reduce to:

$$\sum_j [\langle \Phi_i \Phi_j | \hat{\mathbf{g}}_{1,2}^{\text{so}} \cdot (\hat{\mathbf{s}}_1 + 2\hat{\mathbf{s}}_2) | \Phi_j \Phi_a \rangle = \sum_j [\langle \phi_i \phi_j | \hat{\mathbf{g}}_{1,2}^{\text{so}} | \phi_j \phi_a \rangle \frac{3}{2} [\langle \theta_i | \hat{\mathbf{s}} | \theta_a \rangle] \quad (6.31)$$

$$\sum_j [\langle \Phi_j \Phi_i | \hat{\mathbf{g}}_{1,2}^{\text{so}} \cdot (\hat{\mathbf{s}}_1 + 2\hat{\mathbf{s}}_2) | \Phi_a \Phi_j \rangle = \sum_j [\langle \phi_j \phi_i | \hat{\mathbf{g}}_{1,2}^{\text{so}} | \phi_a \phi_j \rangle \frac{3}{2} [\langle \theta_i | \hat{\mathbf{s}} | \theta_a \rangle] \quad (6.32)$$

If the sum over spin orbitals  $j$  is transformed into a sum over spatial orbitals  $j$  with occupation numbers  $n_j$ , the final form of Eq. 6.25 is obtained and the goal formulated in Eq. 6.23 is reached:

$$\begin{aligned} \langle \Phi_1 | \hat{H}^{\text{BPso}} | \Phi_2 \rangle = & h_{ia}^{\text{BPso1}} + \sum_j n_j [\langle \phi_i \phi_j | \hat{\mathbf{g}}_{1,2}^{\text{so}} | \phi_a \phi_j \rangle \\ & - \frac{3}{2} \langle \phi_i \phi_j | \hat{\mathbf{g}}_{1,2}^{\text{so}} | \phi_j \phi_a \rangle - \frac{3}{2} \langle \phi_j \phi_i | \hat{\mathbf{g}}_{1,2}^{\text{so}} | \phi_a \phi_j \rangle] \end{aligned} \quad (6.33)$$

In order to implement Eq. 6.33, it is convenient to transform the spatial orbitals into the atomic-orbital basis by expanding them in a set of basis functions  $\{\vartheta\}$ .

$$|\phi_i\rangle = \sum_{\mu} c_{\mu i} |\vartheta_{\mu}\rangle . \quad (6.34)$$

This leads to the final working equation

$$\begin{aligned} \langle \vartheta_{\mu} | \hat{H}^{\text{BPso}} | \vartheta_{\nu} \rangle = & h_{\mu\nu}^{\text{BPso1}} + \sum_{\rho\sigma} P_{\rho\sigma} [\langle \vartheta_{\mu} \vartheta_{\rho} | \hat{\mathbf{g}}_{1,2}^{\text{so}} | \vartheta_{\nu} \vartheta_{\sigma} \rangle \\ & - \frac{3}{2} \langle \vartheta_{\mu} \vartheta_{\sigma} | \hat{\mathbf{g}}_{1,2}^{\text{so}} | \vartheta_{\rho} \vartheta_{\nu} \rangle - \frac{3}{2} \langle \vartheta_{\sigma} \vartheta_{\mu} | \hat{\mathbf{g}}_{1,2}^{\text{so}} | \vartheta_{\nu} \vartheta_{\rho} \rangle] , \end{aligned} \quad (6.35)$$

with the SCF density matrix

$$P_{\rho\sigma} = \sum_j n_j c_{\rho j} c_{\sigma j} . \quad (6.36)$$

$c_{\rho j}$  and  $c_{\sigma j}$  are the molecular-orbital expansion coefficients.

## 6.4. Exact separation of spin-free and spin-orbit terms in the Dirac-Coulomb Hamiltonian

One of our goals is the calculation of spin-orbit splittings according to Eq. 5.11. Thereby we connect the treatment of spin-orbit splittings via Mk-MRCC theory with a full four-component treatment of scalar-relativistic effects. This goal can be achieved using the spin-separated Dirac-Coulomb (DC) operator proposed by Dyall.<sup>40</sup> In general, one can rigorously separate the Dirac-Coulomb operator into spin-free and spin-orbit parts:

$$\hat{H}^{\text{DC}} = \hat{H}^{\text{sfDC}} + \hat{H}^{\text{soDC}} \quad (6.37)$$

The superscripts sfDC and soDC refer to the spin-free Dirac-Coulomb and the spin-orbit Dirac-Coulomb part. If the spin-orbit part is discarded, one obtains a spin-free four-component theory. The advantage of the spin-free theory is that (after execution of a spin-free relativistic SCF calculation) the infrastructure for correlation treatments can be used without alteration and at the same computational cost as in a non-relativistic treatment.<sup>177</sup>

The spin separation is achieved by first rewriting the small component  $\chi_i^s$  in terms of the

so-called pseudo-large component  $\Phi_i^{PL}$

$$\frac{\boldsymbol{\sigma}\hat{\mathbf{p}}}{2c}\Phi_i^{PL} = \chi_i^s. \quad (6.38)$$

The resulting equation can be manipulated using a modified form of the Dirac relation

$$(\boldsymbol{\sigma} \cdot \hat{\mathbf{p}})R(\boldsymbol{\sigma}\hat{\mathbf{p}}) = \hat{\mathbf{p}}R\hat{\mathbf{p}} + i\boldsymbol{\sigma} \cdot \hat{\mathbf{p}}R \times \hat{\mathbf{p}}, \quad (6.39)$$

with  $R$  as an arbitrary function or operator,  $\boldsymbol{\sigma}$  as the Pauli matrices, and  $\hat{\mathbf{p}}$  as the momentum operator.

#### 6.4.1. Spin-separated one-electron terms

A spin separation of the one-electron terms in the two-component Dirac operator (see Eq. 2.37) is easily achieved by observing Eq. 6.38 and Eq. 6.39. For the full Hamiltonian operator  $\hat{H}^{\text{DC1}}$  this yields

$$\begin{aligned} \hat{H}^{\text{DC1}} &= \hat{H}^{\text{sfDC1}} + \hat{H}^{\text{soDC1}} \\ &= \begin{pmatrix} V & T \\ T & \frac{\alpha^2}{4}\hat{\mathbf{p}} \cdot (V\hat{\mathbf{p}}) - T \end{pmatrix} + \begin{pmatrix} 0 & 0 \\ 0 & \frac{\alpha^2}{4}i\boldsymbol{\sigma}(\hat{\mathbf{p}}V) \times \hat{\mathbf{p}} \end{pmatrix}. \end{aligned} \quad (6.40)$$

For more information on the derivation, the reader is referred to Ref. 40 or 172. Matrix elements of this operator can be defined using the wave functions  $\Psi_i$  and  $\Psi_a$  in the two-component form, which comprises a large component denoted as  $\varphi^L$  and a pseudo-large component  $\Phi^{PL}$

$$\Psi_i = \begin{pmatrix} \varphi_i^L \\ \Phi_i^{PL} \end{pmatrix}, \Psi_a = \begin{pmatrix} \varphi_a^L \\ \Phi_a^{PL} \end{pmatrix}. \quad (6.41)$$

The matrix elements of  $\hat{H}^{\text{DC1}}$  then can be written as

$$\begin{aligned} H_{ia}^{\text{DC}} &= \begin{pmatrix} \varphi_i^L \\ \Phi_i^{PL} \end{pmatrix}^\dagger \left[ \begin{pmatrix} V & T \\ T & \frac{\alpha^2}{4}\hat{\mathbf{p}} \cdot (V\hat{\mathbf{p}}) - T \end{pmatrix} + \begin{pmatrix} 0 & 0 \\ 0 & \frac{\alpha^2}{4}i\boldsymbol{\sigma}(\hat{\mathbf{p}}V) \times \hat{\mathbf{p}} \end{pmatrix} \right] \begin{pmatrix} \varphi_a^L \\ \Phi_a^{PL} \end{pmatrix} \\ &= \langle \varphi_a^L | V | \varphi_i^L \rangle + \langle \varphi_a^L | T | \Phi_i^{PL} \rangle + \langle \Phi_a^{PL} | T | \varphi_i^L \rangle + \langle \Phi_a^{PL} | \frac{\alpha^2}{4}\hat{\mathbf{p}}(V\hat{\mathbf{p}}) - T | \Phi_i^{PL} \rangle + \\ &\quad \langle \Phi_a^{PL} | \frac{\alpha^2}{4}i\boldsymbol{\sigma}\hat{\mathbf{p}}V \times \hat{\mathbf{p}} | \Phi_i^{PL} \rangle. \end{aligned} \quad (6.42)$$

From Eq. 6.40 and 6.42 it is clear that only the small-small block contains spin-orbit interaction. All other blocks merely contribute to the scalar-relativistic treatment.

#### 6.4.2. Two-electron terms

A spin separation of the two-electron part of the Dirac-Coulomb Hartree-Fock operator  $\hat{H}^{\text{DC2}}$  can be carried out in analogy to the one-electron terms. It is difficult to show this spin

separation in a notation involving only the operators. In this case the selection of the correct components has to be ensured by using projection operators.<sup>40,172</sup> The notation becomes easier if the matrix elements  $H_{ijab}^{DC2}$  are considered directly.

The starting point for the spin separation in the matrix elements  $H_{ijab}^{DC2}$  can be written as follows

$$H_{ijab}^{DC2} = H_{ijab}^{\text{sfDC2}} + H_{ijab}^{\text{soDC2}} = \left\langle \begin{array}{l} \varphi_i^L \varphi_j^L \\ \varphi_i^L \Phi_j^{PL} \\ \Phi_i^{PL} \varphi_j^L \\ \Phi_i^{PL} \Phi_j^{PL} \end{array} \right| \left( \begin{array}{cccc} \frac{1}{r_{12}} & 0 & 0 & 0 \\ 0 & \hat{\Pi}_2 \frac{1}{r_{12}} \hat{\Pi}_2 & 0 & 0 \\ 0 & 0 & \hat{\Pi}_1 \frac{1}{r_{12}} \hat{\Pi}_1 & 0 \\ 0 & 0 & 0 & \hat{\Pi}_1 \hat{\Pi}_2 \frac{1}{r_{12}} \hat{\Pi}_2 \hat{\Pi}_1 \end{array} \right) \left| \begin{array}{l} \varphi_a^L \varphi_b^L \\ \varphi_a^L \Phi_b^{PL} \\ \Phi_a^{PL} \varphi_b^L \\ \Phi_a^{PL} \Phi_b^{PL} \end{array} \right\rangle, \quad (6.43)$$

with  $\hat{\Pi}_k = \frac{\alpha}{2} \boldsymbol{\sigma}_k \cdot \hat{\mathbf{p}}_k$  as the transformation operator causing the metric change in the small component for electron  $k = 1, 2$ . The Dirac notation is used (i.e., the electron 1 and electron 2 take on the order  $\langle 12 | | 12 \rangle$  in the two-electron integral), which clarifies which indices belong to electron 1 and which indices belong to electron 2. It should be noted that in the above equation only Coulomb interactions are taken into account. As was outlined in previous chapters, the Breit interaction is important for the proper description of spin-orbit splittings as well. In case of the Breit interaction, off-diagonal elements appear in Eq. 6.43, which can be evaluated in analogy to the Coulomb contribution. This, however, is beyond the scope of this dissertation and will be described in the thesis of Werner Schwalbach.<sup>178</sup>

In the following, the transformation of  $\frac{1}{r_{12}}$  using the operator  $\hat{\Pi}_k$  is exemplified for the term in the small-small block,  $\hat{\Pi}_1 \hat{\Pi}_2 \frac{1}{r_{12}} \hat{\Pi}_2 \hat{\Pi}_1$ ,

$$\begin{aligned} \hat{\Pi}_1 \hat{\Pi}_2 \frac{1}{r_{12}} \hat{\Pi}_2 \hat{\Pi}_1 &= \frac{\alpha^4}{16} \left( \hat{\mathbf{p}}_1 \boldsymbol{\sigma}_1 \left( \hat{\mathbf{p}}_2 \frac{1}{r_{12}} \hat{\mathbf{p}}_2 + i \boldsymbol{\sigma}_2 \hat{\mathbf{p}}_2 \frac{1}{r_{12}} \times \hat{\mathbf{p}}_2 \right) \hat{\mathbf{p}}_1 \boldsymbol{\sigma}_2 \right) \\ &= \frac{\alpha^4}{16} \left( \underbrace{\hat{\mathbf{p}}_1 \hat{\mathbf{p}}_2 \frac{1}{r_{12}} \hat{\mathbf{p}}_1 \hat{\mathbf{p}}_2}_{\text{spin-free}} + \underbrace{\hat{\mathbf{p}}_1 i \boldsymbol{\sigma}_2 \hat{\mathbf{p}}_2 \frac{1}{r_{12}} \times \hat{\mathbf{p}}_2 \hat{\mathbf{p}}_2}_{\text{spin-orbit electron 2}} + \right. \\ &\quad \left. \underbrace{i \boldsymbol{\sigma}_1 \hat{\mathbf{p}}_1 \hat{\mathbf{p}}_2 \frac{1}{r_{12}} \hat{\mathbf{p}}_2 \times \hat{\mathbf{p}}_1}_{\text{spin-orbit electron 1}} + \underbrace{i \boldsymbol{\sigma}_1 \hat{\mathbf{p}}_1 i \boldsymbol{\sigma}_2 \hat{\mathbf{p}}_2 \frac{1}{r_{12}} \times \hat{\mathbf{p}}_2 \times \hat{\mathbf{p}}_1}_{\text{spin-orbit electrons 1 \& 2}} \right). \end{aligned} \quad (6.44)$$

In the above equation it becomes clear that the different terms resulting from the application of the Dirac relation, Eq. 6.39, can be classified according to whether the spin-orbit operator acts on electron 1 or electron 2 or on both (the same is true for the scalar-relativistic operator, respectively).

Carrying out the equivalent transformation for all blocks gives the following spin-free matrix elements

$$H_{ijab}^{\text{sfDC2}} = \frac{\alpha^2}{4} \langle \varphi_i^L \varphi_j^L | \frac{1}{r_{12}} | \varphi_a^L \varphi_b^L \rangle +$$

$$\begin{aligned}
 & \frac{\alpha^2}{4} \langle \Phi_i^{PL} \varphi_j^L | \hat{\mathbf{p}}_1 \frac{1}{r_{12}} \hat{\mathbf{p}}_1 | \Phi_a^{PL} \varphi_b^L \rangle + \\
 & \frac{\alpha^2}{4} \langle \varphi_i^L \Phi_j^{PL} | \hat{\mathbf{p}}_2 \frac{1}{r_{12}} \hat{\mathbf{p}}_2 | \varphi_b^L \Phi_a^{PL} \rangle + \\
 & \frac{\alpha^4}{16} \langle \Phi_i^{PL} \Phi_j^{PL} | \hat{\mathbf{p}}_2 \hat{\mathbf{p}}_1 \frac{1}{r_{12}} \hat{\mathbf{p}}_1 \hat{\mathbf{p}}_2 | \Phi_a^{PL} \Phi_b^{PL} \rangle , \tag{6.45}
 \end{aligned}$$

and the following spin-orbit matrix elements

$$\begin{aligned}
 H_{ijab}^{soDC2} &= \frac{\alpha^2}{4} \langle \varphi_i^L \Phi_j^{PL} | i\boldsymbol{\sigma}_2 \hat{\mathbf{p}}_2 \frac{1}{r_{12}} \times \hat{\mathbf{p}}_2 | \varphi_a^L \Phi_b^{PL} \rangle + \\
 & \frac{\alpha^2}{4} \langle \Phi_i^{PL} \varphi_j^L | i\boldsymbol{\sigma}_1 \hat{\mathbf{p}}_1 \frac{1}{r_{12}} \times \hat{\mathbf{p}}_1 | \Phi_a^{PL} \varphi_b^L \rangle + \\
 & \frac{\alpha^4}{16} \langle \Phi_i^{PL} \Phi_j^{PL} | \hat{\mathbf{p}}_1 (i\boldsymbol{\sigma}_2 \hat{\mathbf{p}}_2 \frac{1}{r_{12}} \times \hat{\mathbf{p}}_2) \hat{\mathbf{p}}_1 | \Phi_a^{PL} \Phi_b^{PL} \rangle + \\
 & \frac{\alpha^4}{16} \langle \Phi_i^{PL} \Phi_j^{PL} | i\boldsymbol{\sigma}_1 \hat{\mathbf{p}}_1 (\hat{\mathbf{p}}_2 \frac{1}{r_{12}} \hat{\mathbf{p}}_2) \times \hat{\mathbf{p}}_1 | \Phi_a^{PL} \Phi_b^{PL} \rangle + \\
 & \frac{-\alpha^4}{16} \langle \Phi_i^{PL} \Phi_j^{PL} | \boldsymbol{\sigma}_1 \hat{\mathbf{p}}_1 (\boldsymbol{\sigma}_2 \hat{\mathbf{p}}_2 \frac{1}{r_{12}} \times \hat{\mathbf{p}}_2) \times \hat{\mathbf{p}}_1 | \Phi_a^{PL} \Phi_b^{PL} \rangle . \tag{6.46}
 \end{aligned}$$

The operators in Eq. 6.46 can be written in a way that resembles the Breit-Pauli two-electron spin-orbit operator more closely

$$\begin{aligned}
 H_{ijab}^{soDC2} &= \frac{-\alpha^2}{2} \langle \varphi_i^L \Phi_j^{PL} | \hat{\mathbf{s}}_2 \frac{\hat{\mathbf{r}}_{21}}{r_{12}^3} \times \hat{\mathbf{p}}_2 | \varphi_a^L \Phi_b^{PL} \rangle + \\
 & \frac{-\alpha^2}{2} \langle \Phi_i^{PL} \varphi_j^L | \hat{\mathbf{s}}_1 \frac{\hat{\mathbf{r}}_{12}}{r_{12}^3} \times \hat{\mathbf{p}}_1 | \Phi_a^{PL} \varphi_b^L \rangle + \\
 & \frac{-\alpha^4}{8} \langle \Phi_i^{PL} \Phi_j^{PL} | \hat{\mathbf{p}}_1 (\hat{\mathbf{s}}_2 \frac{\hat{\mathbf{r}}_{21}}{r_{12}^3} \times \hat{\mathbf{p}}_2) \hat{\mathbf{p}}_1 | \Phi_a^{PL} \Phi_b^{PL} \rangle + \\
 & \frac{-\alpha^4}{8} \langle \Phi_i^{PL} \Phi_j^{PL} | \hat{\mathbf{s}}_1 (\hat{\mathbf{p}}_2 \frac{\hat{\mathbf{r}}_{12}}{r_{12}^3} \hat{\mathbf{p}}_2) \times \hat{\mathbf{p}}_1 | \Phi_a^{PL} \Phi_b^{PL} \rangle + \\
 & \frac{-\alpha^4}{4} \langle \Phi_i^{PL} \Phi_j^{PL} | \hat{\mathbf{s}}_1 \hat{\mathbf{p}}_1 (\hat{\mathbf{s}}_2 \hat{\mathbf{p}}_2 \frac{1}{r_{12}} \times \hat{\mathbf{p}}_2) \times \hat{\mathbf{p}}_1 | \Phi_a^{PL} \Phi_b^{PL} \rangle . \tag{6.47}
 \end{aligned}$$

If the definition of the angular-momentum operator  $\hat{\mathbf{l}}_{ij} = \hat{\mathbf{r}}_{ij} \times \hat{\mathbf{p}}_i$  is considered, it is easy to see the connection the Breit-Pauli spin-orbit operator given in Eq. 6.21. The operator given in Eq. 6.47 can be used as a starting point for spin-orbit mean-field treatment. The corresponding derivations will be presented in the next chapter.



## 7. Theory: Derivation of working equations for the calculation of spin-orbit splittings via (Mk-)MRCC theory

*It is more important to have beauty in one's equations than to have them fit experiment*  
– Paul Dirac

Using the theoretical “ingredients” discussed in the last chapter, we are now set to derive the working equations for the calculation of spin-orbit splittings via state-specific MRCC theory. In Fig. 7.1 the derivation steps are pictured schematically for a better overview over the chapter.

Adapting gradient theory of the different Jeziorski-Monkhorst based MRCC methods to the special features of the spin-orbit interaction, general expressions for the spin-orbit splittings can be formulated for Mk-MRCC, SU-MRCC, and BW-MRCC. These give insight into the quality of coupling in Jeziorski-Monkhorst based MRCC methods. However, all further derivations and the implementation are only performed for Mk-MRCC, since it is the most promising Jeziorski-Monkhorst based MRCC method at present.

For convenience, the general expressions are reformulated in terms of density matrices. In this formulation integrals of the spin-orbit operators are contracted with coupled-cluster density matrices. In the atomic-orbital (AO) basis these expressions differ depending on whether the Breit-Pauli spin-orbit Hamiltonian or the four-component Dirac-Coulomb spin-orbit operator is used. In the latter case special attention has to be paid to which components of the wave function are involved.

Since both considered spin-orbit operators contain a one- and a two-electron term, the density-matrix formulation of the gradient is partitioned into a one-particle and a two-particle term accordingly. Discarding the two-particle terms entirely, leads to a pure one-electron treatment of the spin-orbit splittings. However, the one-electron integrals can be augmented by matrix elements of a spin-orbit mean-field (SOMF) approximation, which approximately accounts for the two-electron effects. Such a SOMF treatment has been derived by Hess and Marian for the Breit-Pauli spin-orbit operator.<sup>174</sup> In Sec. 7.4.2, the equivalent derivations will be performed for a four-component relativistic treatment using the Dirac-Coulomb spin-orbit operator. The machinery for the full two-electron treatment will only be formulated for the non-relativistic treatment with the Breit-Pauli spin-orbit operator.

### 7.1. Expression for spin-orbit splittings via state-specific MRCC theory

In this section, working equations for the calculation of spin-orbit splittings via the Mk-MRCC, SU-MRCC, and BW-MRCC methods are derived.<sup>a</sup> For all considered methods, the derivations

---

<sup>a</sup>The derivations in this section were already published in the supplementary material of Ref. 136.

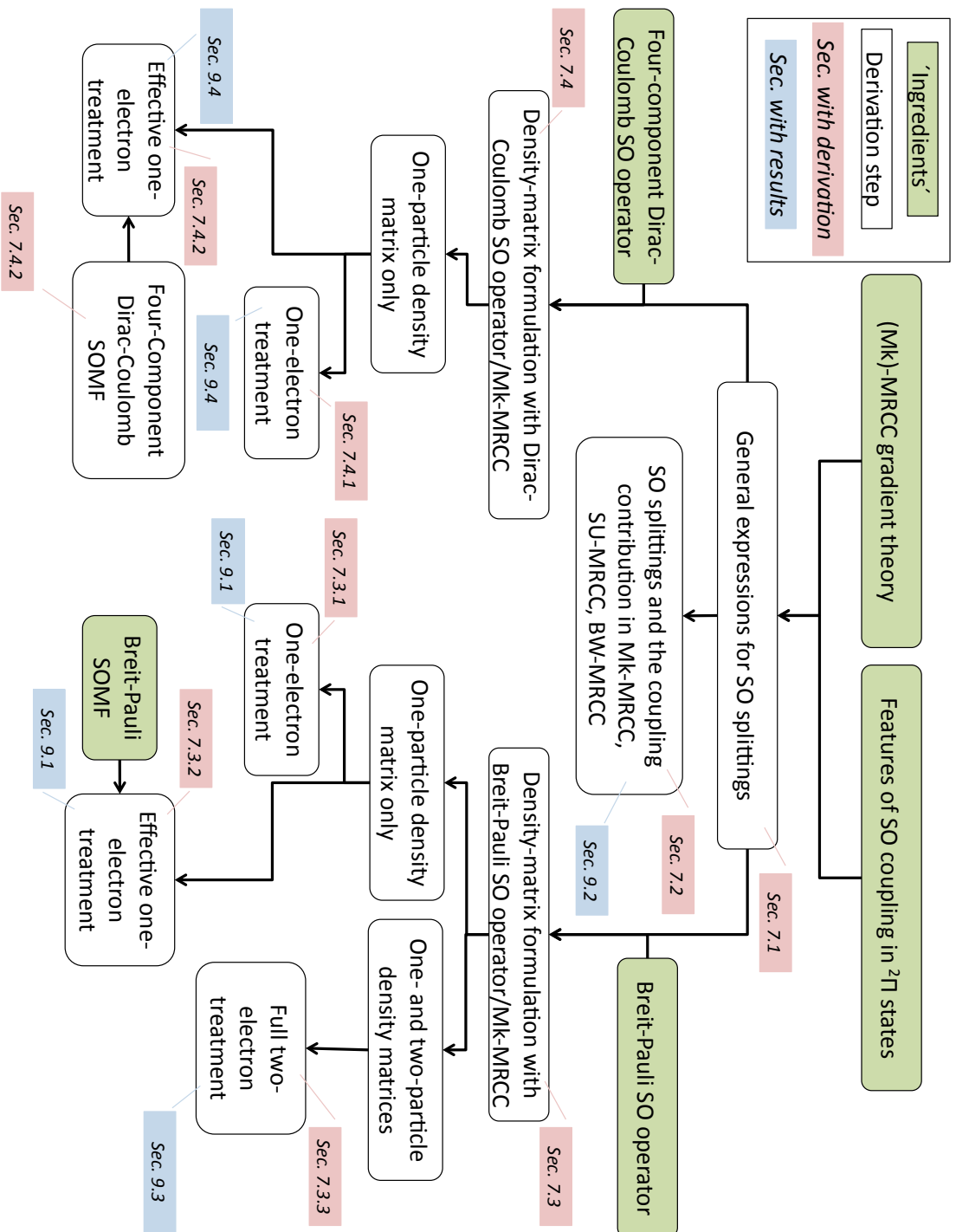


**Figure 7.1.:** Derivation scheme of working equations for the calculation of spin-orbit splittings via (Mk-)MRCC theory. All “ingredients” developed by other authors prior to this thesis are marked in green. The red legends denote in which section a certain derivation can be found, the blue legends denote in which section the corresponding results are discussed. “SO”=spin orbit, “SOMF”= spin-orbit mean-field.

follow the same procedure: After formulation of a suitable Lagrangian, a general expression for the gradient of the given MRCC theory can be obtained. If this gradient expression is used for the calculation of spin-orbit splittings in  ${}^2\Pi$  states, special symmetry restrictions can be exploited (see also Sec. 5). The equations are analyzed accordingly and can be simplified to yield a compact form. The expressions of the different methods are compared in order to obtain insight into the advantages and shortcomings of the individual theories.

### 7.1.1. Mukherjee's multireference coupled-cluster theory

Analytic gradients for Mk-MRCC have been formulated by Prochnow *et al.* (see Sec. 6.1).<sup>34</sup> The authors give an appropriate Lagrangian and the corresponding gradient expression for Mk-MRCC (see Eq. 6.1 and Eq. 6.2).

If spin-orbit splittings in  ${}^2\Pi$  states are calculated via Eq. 6.2, only non-totally symmetric terms survive due to the symmetry properties of the spin-orbit operator  $\hat{H}^{\text{so}}$ . The reference determinants of the  ${}^2\Pi$  state, which have different symmetry, are labelled with  $x$  and  $y$  as in Fig. 5.1 in the following. To emphasize the symmetry properties of the individual terms, the gradient expression is rewritten in terms of totally symmetric (“ts”) and non-totally symmetric (“nts”) contributions:

$$\frac{\partial \tilde{E}}{\partial \gamma} = \sum_x \bar{c}_x c_x \langle \Phi_x | \left( 1 + \hat{\Lambda}_x^{\text{ext,ts}} + \hat{\Lambda}_x^{\text{ext,nts}} + \hat{\Lambda}_x^{\text{int,nts}} \right) e^{-\hat{T}^x} \frac{\partial \hat{H}}{\partial \gamma} e^{\hat{T}^x} | \Phi_x \rangle. \quad (7.1)$$

Inserting an arbitrary spin-orbit operator  $\hat{H}^{\text{so}}$  instead of a generic derivative of a Hamiltonian with respect to the perturbation  $\gamma$  we obtain

$$E^{\text{so}} = \sum_x \bar{c}_x c_x \langle \Phi_x | \left( 1 + \hat{\Lambda}_x^{\text{ext,ts}} + \hat{\Lambda}_x^{\text{ext,nts}} + \hat{\Lambda}_x^{\text{int,nts}} \right) e^{-\hat{T}^x} \hat{H}^{\text{so}} e^{\hat{T}^x} | \Phi_x \rangle. \quad (7.2)$$

In the above equation, terms with a totally symmetric  $\Lambda$  operator vanish. The internal (“int”) and external (“ext”) non-totally symmetric  $\hat{\Lambda}$  operators are given by

$$\hat{\Lambda}_x^{\text{nts}} = \underbrace{\sum_{q \in Q(x)} \hat{\tau}_{q,\text{nts}}^+(x) \lambda_q^{\text{nts}}(x)}_{\hat{\Lambda}_x^{\text{ext,nts}}} + \underbrace{\sum_{y(\neq x)} \frac{\bar{c}_y}{\bar{c}_x} \left[ 1 + \sum_{q \in Q(y)} \lambda_q(y) \langle \Phi_q(y) | e^{-\hat{T}^y} e^{\hat{T}^x} | \Phi_y \rangle \right]}_{\hat{\Lambda}_x^{\text{int,nts}}} | \Phi_x \rangle \langle \Phi_y |. \quad (7.3)$$

Simplification of the term containing  $\hat{\Lambda}^{\text{int}}$  yields the following expression for the internal contribution to the spin-orbit splittings:

$$E_{\text{int}}^{\text{so}} = \sum_x \sum_{y \neq x} \bar{c}_y c_x \left( \langle \Phi_y | e^{-\hat{T}^x} \hat{H}^{\text{so}} e^{\hat{T}^x} | \Phi_x \rangle + \langle \Phi_y | e^{-\hat{T}^x} \hat{H}^{\text{so}} e^{\hat{T}^x} | \Phi_x \rangle \cdot \langle \Phi_y | \hat{\Lambda}_y e^{-\hat{T}^y} e^{\hat{T}^x} | \Phi_y \rangle \right) \quad (7.4)$$

with  $\hat{\Lambda}_y = \sum_{q \in Q(y)} \lambda_q(y) \hat{\tau}_q^+(y)$ . Inserting the factor  $\langle \Phi_y | e^{-\hat{T}^y} e^{\hat{T}^x} | \Phi_y \rangle = 1$  leads to the following equation

$$E_{\text{int}}^{\text{so}} = \sum_x \sum_{y \neq x} \bar{c}_y c_x \left( \langle \Phi_y | e^{-\hat{T}^x} \hat{H}^{\text{so}} e^{\hat{T}^x} | \Phi_x \rangle \cdot \underbrace{\langle \Phi_y | e^{-\hat{T}^y} e^{\hat{T}^x} | \Phi_y \rangle}_1 + \langle \Phi_y | e^{-\hat{T}^x} \hat{H}^{\text{so}} e^{\hat{T}^x} | \Phi_x \rangle \cdot \langle \Phi_y | \hat{\Lambda}_y e^{-\hat{T}^y} e^{\hat{T}^x} | \Phi_y \rangle \right), \quad (7.5)$$

which can be cast in a form similar to the standard gradient expression in Mk-MRCC theory:

$$E_{\text{int}}^{\text{so}} = \sum_x \sum_{y \neq x} \bar{c}_y c_x \langle \Phi_y | (1 + \hat{\Lambda}_y) e^{-\hat{T}^y} e^{\hat{T}^x} | \Phi_y \rangle \cdot \langle \Phi_y | e^{-\hat{T}^x} \hat{H}^{\text{so}} e^{\hat{T}^x} | \Phi_x \rangle. \quad (7.6)$$

The eigenvectors of the effective Hamiltonian, i.e., the weighting coefficients  $c_x$  and  $c_y$  are fixed by symmetry. To be more exact,  $c_x$  and  $c_y$  are fixed by the eigenvectors in Eq. 5.8:

$$\vec{\chi}_1 = \begin{pmatrix} c_x \\ c_y \end{pmatrix} = \frac{1}{\sqrt{2}} \begin{pmatrix} i \\ 1 \end{pmatrix} \quad \begin{pmatrix} \bar{c}_x \\ \bar{c}_y \end{pmatrix} = \frac{1}{\sqrt{2}} \begin{pmatrix} -i \\ 1 \end{pmatrix}. \quad (7.7)$$

Whether  $\vec{\chi}_1$  or  $\vec{\chi}_2$  is chosen for insertion is arbitrary since we calculate the spin-orbit splittings  $\Delta E^{\text{so}}$  as the energy difference between the  ${}^2\Pi_{1/2}$  and  ${}^2\Pi_{3/2}$  states (see Eq. 5.6).

Insertion of the coefficients in Eq. 7.6 and evaluation of the sum yields

$$E_{\text{int}}^{\text{so}} = \left| \langle \Phi_y | (1 + \hat{\Lambda}_y) e^{-\hat{T}^y} e^{\hat{T}^x} | \Phi_y \rangle \cdot \langle \Phi_y | e^{-\hat{T}^x} \hat{H}^{\text{so}} e^{\hat{T}^x} | \Phi_x \rangle \right|. \quad (7.8)$$

The non-totally symmetric external  $\hat{\Lambda}^{\text{ext},\text{nts}}$  amplitudes naturally appear in the Mk-MRCC  $\Lambda$  equations. The regular Mk-MRCC  $\Lambda$  equations

$$\bar{c}_\mu \langle \Phi_\mu | (1 + \hat{\Lambda}_{\text{ext}}(\mu) + \hat{\Lambda}_{\text{int}}(\mu)) [\bar{H}_\mu, \hat{\tau}_q(\mu)] | \Phi_\mu \rangle c_\mu + \sum_\nu \bar{c}_\nu \langle \Phi_\nu | \frac{\partial \hat{\Lambda}_{\text{int}}(\nu)}{\partial t_q(\mu)} \bar{H}_\nu | \Phi_\nu \rangle c_\nu = 0, \quad (7.9)$$

reduce to

$$\langle \Phi_x | \hat{\Lambda}_x^{\text{ext},\text{nts}} [\bar{H}_x, \hat{\tau}_q(x)] | \Phi_x \rangle + \langle \Phi_x | \hat{\Lambda}_{\text{int}} [\bar{H}_x, \hat{\tau}_q(x)] | \Phi_x \rangle = 0. \quad (7.10)$$

In the above equations,  $[\bar{H}_\mu, \hat{\tau}_q(\mu)]$  denotes the commutator of the similarity transformed Hamiltonian and the excitation operator  $\hat{\tau}_q(\mu)$ . Following the same procedure that was already applied to the internal contribution, insertion of the c coefficients and summation results in the following equation for the external contribution to  $\Delta E^{\text{so}}$

$$E_{\text{ext}}^{\text{so}} = | \langle \Phi_x | \hat{\Lambda}_{\text{ext}}^{\text{nts}}(x) e^{-\hat{T}^x} \hat{H}^{\text{so}} e^{\hat{T}^x} | \Phi_x \rangle |. \quad (7.11)$$

Adding Eq. (7.8) and Eq. (7.11) yields the final expression for the energy difference  $\Delta E^{\text{so}}$ . The spin-orbit splitting is defined as the energy difference between the two states  ${}^2\Pi_{1/2}$  and  ${}^2\Pi_{3/2}$ , which introduces a factor of two into the equation (see Eq. 5.6)

$$\begin{aligned} \Delta E^{\text{so}} = & 2 \times \left| \langle \Phi_x | \hat{\Lambda}_{\text{ext}}^{\text{nts}}(x) e^{-\hat{T}^x} \hat{H}^{\text{so}} e^{\hat{T}^x} | \Phi_x \rangle + \right. \\ & \left. \langle \Phi_y | (1 + \hat{\Lambda}_y) e^{-\hat{T}^y} e^{\hat{T}^x} | \Phi_y \rangle \cdot \langle \Phi_y | e^{-\hat{T}^x} \hat{H}^{\text{so}} e^{\hat{T}^x} | \Phi_x \rangle \right|. \end{aligned} \quad (7.12)$$

### 7.1.2. State-universal multireference coupled-cluster theory

Analytic gradients for the SU-MRCC ansatz have been derived previously (see Ref. 66 and 67) and a pilot implementation has been presented in the literature. The following derivation differs slightly from the literature in the sense that it resembles the derivation of the analytic Mk-MRCC gradient as given by Prochnow *et al.*<sup>34</sup> as closely as possible.

The energy eigenvalue equation of SU-MRCC can be rearranged to give

$$E = \sum_{\mu=1}^d \sum_{\nu=1}^d H_{\nu\mu}^{\text{eff}} c_{\mu} \tilde{c}_{\nu}, \quad (7.13)$$

where  $\tilde{c}_{\nu}$  is the left-hand eigenvector of the effective Hamiltonian and  $d$  denotes the number of determinants.

The Lagrangian can then be defined as

$$\begin{aligned} \tilde{E} = & \sum_{\mu\nu} H_{\nu\mu}^{\text{eff}} c_{\mu} \tilde{c}_{\nu} + \sum_{\mu} \sum_{q \in Q(\mu)} \lambda_q(\mu) c_{\mu} \tilde{c}_{\mu} (\langle \Phi_q(\mu) | \bar{H}_{\mu} | \Phi_{\mu} \rangle \\ & - \sum_{\nu \neq \mu} \langle \Phi_q(\mu) | e^{-\hat{T}^{\mu}} e^{\hat{T}^{\nu}} | \Phi_{\nu} \rangle H_{\nu\mu}^{\text{eff}}) + \epsilon \cdot (\sum_{\mu} \tilde{c}_{\mu} c_{\mu} - 1). \end{aligned} \quad (7.14)$$

$\lambda_q$  are the Lagrange multipliers corresponding to the amplitude equations, while  $\tilde{c}_{\mu}$  and  $c_{\mu}$  are only inserted for convenience as a prefactor in the Lagrange multipliers for the amplitude equations, since they simplify the subsequent expressions.

One difference to Mk-MRCC gradient theory is visible immediately: In SU-MRCC the coefficients of the left-hand eigenvector  $\tilde{c}$  instead of the genuine Lagrange multiplier  $\bar{c}$  are used. In other words, the Lagrange multiplier  $\bar{c}$  turns out to be the left-hand eigenvector  $\tilde{c}$ . This is possible because the amplitude equations of SU-MRCC are independent of the coefficients (see Eq. 2.21).  $\tilde{c}_{\mu}$  and  $c_{\mu}$  are defined to satisfy the biorthonormality condition

$$\sum_{\mu} \tilde{c}_{\mu} c_{\mu} = 1, \quad (7.15)$$

which is ensured by adding an additional constraint to the energy functional  $\tilde{E}$ . The gradient of the energy with respect to the perturbation  $\gamma$  becomes:

$$\frac{\partial \tilde{E}}{\partial \gamma} = \sum_{\mu} c_{\mu} \tilde{c}_{\mu} \langle \Phi_{\mu} | (1 + \hat{\Lambda}_{\mu}) e^{-\hat{T}^{\mu}} \frac{\partial \hat{H}_{\mu}}{\partial \gamma} e^{\hat{T}^{\mu}} | \Phi_{\mu} \rangle, \quad (7.16)$$

with

$$\hat{\Lambda}_\mu = \underbrace{\sum_{q \in Q(\mu)} \lambda_q(\mu) \hat{\tau}_q^+}_{\hat{\Lambda}_\mu^{\text{ext}}} + \underbrace{\sum_{\nu \neq \mu} \left( \frac{\tilde{c}_\nu}{\tilde{c}_\mu} - \sum_{q \in Q(\mu)} \lambda_q(\mu) \langle \Phi_q(\mu) | e^{-\hat{T}^\mu} e^{\hat{T}^\nu} | \Phi_\nu \rangle \right)}_{\hat{\Lambda}_\mu^{\text{int}}} | \Phi_\mu \rangle \langle \Phi_\nu | . \quad (7.17)$$

Considering spin-orbit splittings in  ${}^2\Pi$  states in analogy to Mk-MRCC theory, all totally symmetric contributions in the general SU-MRCC gradient expression

$$\frac{\partial \tilde{E}}{\partial \gamma} = \sum_x \tilde{c}_x c_x \langle \Phi_x | \left( 1 + \hat{\Lambda}_x^{\text{ext,ts}} + \hat{\Lambda}_x^{\text{ext,nts}} + \hat{\Lambda}_x^{\text{int,nts}} \right) e^{-\hat{T}^x} \frac{\partial \hat{H}}{\partial \chi} e^{\hat{T}^x} | \Phi_x \rangle , \quad (7.18)$$

vanish. The non-totally symmetric  $\hat{\Lambda}$  operators are given by

$$\hat{\Lambda}_x^{\text{nts}} = \underbrace{\sum_{q \in Q(x)} \hat{\tau}_{q,\text{nts}}^+ \lambda_q^{\text{nts}}(x)}_{\hat{\Lambda}_x^{\text{ext,nts}}} + \underbrace{\sum_{y \neq x} \left( \frac{\tilde{c}_y}{\tilde{c}_x} - \sum_{q \in Q(x)} \lambda_q(x) \langle \Phi_q(x) | e^{-\hat{T}^x} e^{\hat{T}^y} | \Phi_y \rangle \right)}_{\hat{\Lambda}_x^{\text{int,nts}}} | \Phi_x \rangle \langle \Phi_y | . \quad (7.19)$$

Simplification of the remaining  $\hat{\Lambda}^{\text{int}}$  term yields the following expression

$$E_{\text{int}}^{\text{SO}} = \sum_x \sum_{y \neq x} \left( \tilde{c}_y c_x \langle \Phi_y | e^{-\hat{T}^x} \hat{H}^{\text{so}} e^{\hat{T}^x} | \Phi_x \rangle - \tilde{c}_x c_x \langle \Phi_y | e^{-\hat{T}^x} \hat{H}^{\text{so}} e^{\hat{T}^x} | \Phi_x \rangle \cdot \langle \Phi_x | \hat{\Lambda}_x e^{-\hat{T}^x} e^{\hat{T}^y} | \Phi_y \rangle \right) . \quad (7.20)$$

As only terms with a non-totally symmetric  $\hat{\Lambda}_x$  survive, this becomes

$$E_{\text{int}}^{\text{SO}} = \sum_x \sum_{y \neq x} \left( \tilde{c}_y c_x \langle \Phi_y | e^{-\hat{T}^x} \hat{H}^{\text{so}} e^{\hat{T}^x} | \Phi_x \rangle - \tilde{c}_x c_x \langle \Phi_y | e^{-\hat{T}^x} \hat{H}^{\text{so}} e^{\hat{T}^x} | \Phi_x \rangle \cdot \langle \Phi_x | \hat{\Lambda}_x^{\text{nts}} e^{-\hat{T}^x} e^{\hat{T}^y} | \Phi_y \rangle \right) . \quad (7.21)$$

$\tilde{c}_y$  and  $c_x$  are fixed by symmetry as described above. Summation over  $x$  and  $y$  yields

$$E_{\text{int}}^{\text{SO}} = \left| \langle \Phi_y | e^{-\hat{T}^x} \hat{H}^{\text{so}} e^{\hat{T}^x} | \Phi_x \rangle + \langle \Phi_x | \hat{\Lambda}_x^{\text{nts}} e^{-\hat{T}^x} e^{\hat{T}^y} | \Phi_y \rangle \times \langle \Phi_y | e^{-\hat{T}^x} \hat{H}^{\text{so}} e^{\hat{T}^x} | \Phi_x \rangle \right| . \quad (7.22)$$

The expression above can be cast in a more elegant form,

$$E_{\text{int}}^{\text{SO}} = \left| \langle \Phi_x | (\hat{\tau}_{x \rightarrow y} - \hat{\Lambda}_x^{\text{nts}}) e^{-\hat{T}^x} e^{\hat{T}^y} | \Phi_y \rangle \times \langle \Phi_y | e^{-\hat{T}^x} \hat{H}^{\text{so}} e^{\hat{T}^x} | \Phi_x \rangle \right| , \quad (7.23)$$

with  $\hat{\tau}_{x \rightarrow y}$  representing the internal excitation, which transforms  $\Phi_x$  into  $\Phi_y$ .

The  $\hat{\Lambda}_{\text{nts}}^{\text{ext}}$  amplitudes necessary for the external contribution to the spin-orbit splittings can be

obtained via the  $\Lambda$  equations as in Mk-MRCC theory.

$$\langle \Phi_\mu | \hat{\Lambda}_x^{\text{ext}, \text{nts}}[\bar{H}_x, \hat{\tau}_q(x)] | \Phi_x \rangle + \langle \Phi_x | \hat{\Lambda}_{\text{int}}[\bar{H}_x, \hat{\tau}_q(x)] | \Phi_x \rangle = 0. \quad (7.24)$$

The only difference between Mk-MRCC and SU-MRCC theory is the expression for the internal amplitudes. Thus the contribution to the spin-orbit splitting due to the external  $\hat{\Lambda}_{\text{ext}}^{\text{nts}}$  is

$$E_{\text{ext}}^{\text{so}} = \left| \langle \Phi_x | \hat{\Lambda}_{\text{ext}}^{\text{nts}}(x) e^{-\hat{T}^x} \hat{H}^{\text{so}} e^{\hat{T}^x} | \Phi_x \rangle \right|. \quad (7.25)$$

Combining the internal and the external contribution, the energy difference  $\Delta E^{\text{so}}$  between the two electronic states  ${}^2\Pi_{1/2}$  and  ${}^2\Pi_{3/2}$  becomes

$$\begin{aligned} \Delta E^{\text{so}} = 2 \times & \left| \langle \Phi_x | \hat{\Lambda}_{\text{ext}}^{\text{nts}}(x) e^{-\hat{T}^x} \hat{H}^{\text{so}} e^{\hat{T}^x} | \Phi_x \rangle + \right. \\ & \left. \langle \Phi_x | (\hat{\tau}_{x \rightarrow y} - \hat{\Lambda}_x^{\text{nts}}) e^{-\hat{T}^x} e^{\hat{T}^y} | \Phi_y \rangle \times \langle \Phi_y | e^{-\hat{T}^x} \hat{H}^{\text{so}} e^{\hat{T}^x} | \Phi_x \rangle \right|. \end{aligned} \quad (7.26)$$

### 7.1.3. Brillouin-Wigner multireference coupled-cluster theory

Analytic BW-MRCC gradients have been derived and implemented in a pilot implementation by Pittner *et al.*<sup>67</sup> The following derivation leads to essentially the same equations, but the formulation is designed to resemble the Mk-MRCC gradient expressions given in Ref. 34 as closely as possible.

The Lagrangian of BW-MRCC theory can be written as

$$\begin{aligned} \tilde{E} = \sum_{\mu\nu} \langle \Phi_\mu | \hat{H} e^{\hat{T}^\nu} | \Phi_\nu \rangle c_\nu \bar{c}_\mu + \sum_{\mu} \sum_{q \in Q(\mu)} \bar{c}_\mu c_\mu \lambda_q(\mu) & \left( \langle \Phi_q(\mu) | \hat{H} e^{\hat{T}^\mu} | \Phi_\mu \rangle \right. \\ & \left. - \sum_{\sigma\gamma} \tilde{c}_\gamma c_\sigma \langle \Phi_q(\mu) | e^{\hat{T}^\mu} | \Phi_\mu \rangle \langle \Phi_\gamma | \hat{H} e^{\hat{T}^\sigma} | \Phi_\sigma \rangle \right) + \epsilon \left[ \sum_{\mu} \bar{c}_\mu c_\mu - 1 \right]. \end{aligned} \quad (7.27)$$

In analogy to the SU-MRCC Lagrangian, the last term ensures biorthonormality of the multipliers  $c_\mu$  and  $\bar{c}_\mu$ . The energy gradient becomes

$$\frac{\partial \tilde{E}}{\partial \gamma} = \sum_{\mu} \bar{c}_\mu c_\mu \langle \Phi_\mu | \left( 1 + \hat{\Lambda}_\mu \right) \frac{\partial \hat{H}_\mu}{\partial \gamma} e^{\hat{T}^\mu} | \Phi_\mu \rangle \quad (7.28)$$

with

$$\hat{\Lambda}_\mu = \underbrace{\sum_{q \in Q(\mu)} \lambda_q(\mu) \hat{\tau}_q^+}_{\hat{\Lambda}_\mu^{\text{ext}}} - \underbrace{\sum_{\nu \neq \mu} \frac{\bar{c}_\nu}{\bar{c}_\mu} |\Phi_\mu\rangle \langle \Phi_\nu| - \sum_{q \in Q(\mu)} \sum_{\sigma \gamma} \tilde{c}_\gamma \frac{\bar{c}_\sigma c_\sigma}{\bar{c}_\mu} \lambda_q(\sigma) \langle \Phi_q(\sigma) | e^{\hat{T}^\sigma} | \Phi_\sigma \rangle |\Phi_\mu\rangle \langle \Phi_\gamma|}_{\hat{\Lambda}_\mu^{\text{int}}} . \quad (7.29)$$

In analogy to Mk-MRCC and SU-MRCC gradient expressions, all totally symmetric terms in the BW-MRCC gradient expression,

$$\frac{\partial \tilde{E}}{\partial \gamma} = \sum_x \tilde{c}_x c_x \langle \Phi_x | \left( 1 + \hat{\Lambda}_x^{\text{ext,ts}} + \hat{\Lambda}_x^{\text{ext,nts}} + \hat{\Lambda}_x^{\text{int,nts}} \right) \frac{\partial \hat{H}}{\partial \gamma} e^{\hat{T}^x} | \Phi_x \rangle, \quad (7.30)$$

vanish if spin-orbit splittings in  ${}^2\Pi$  states are to be computed. The non-totally symmetric  $\hat{\Lambda}$  operators are given by:

$$\hat{\Lambda}_x^{\text{nts}} = \underbrace{\sum_{q \in Q(x)} \lambda_q^{\text{nts}}(x) \hat{\tau}_{q,\text{nts}}^+}_{\hat{\Lambda}_x^{\text{ext,nts}}} + \underbrace{\sum_{y \neq x} \frac{\tilde{c}_y}{\tilde{c}_x} |\Phi_x\rangle \langle \Phi_y| - \sum_{q \in Q(x)} \sum_{z, u \neq x} \tilde{c}_u \frac{\tilde{c}_z c_z}{\tilde{c}_x} \lambda_q(z) \langle \Phi_q(z) | e^{\hat{T}^z} | \Phi_z \rangle |\Phi_x\rangle \langle \Phi_u|}_{\hat{\Lambda}_x^{\text{int,nts}}} . \quad (7.31)$$

Manipulation of this equation, summation over  $x$  and  $y$  and fixing the  $c$  coefficients leads to

$$E_{\text{int}}^{\text{so}} = \left| \left( 1 - \frac{1}{2} \cdot \langle \Phi_x | \hat{\Lambda}_x e^{\hat{T}^x} | \Phi_x \rangle + \frac{1}{2} \cdot \langle \Phi_y | \hat{\Lambda}_y e^{\hat{T}^y} | \Phi_y \rangle \right) \cdot \langle \Phi_y | \hat{H}^{\text{so}} e^{\hat{T}^x} | \Phi_x \rangle \right|, \quad (7.32)$$

for the internal contribution to the spin-orbit splittings.

The  $\hat{\Lambda}_{\text{ext}}^{\text{nts}}$  amplitudes can be obtained by solving the  $\Lambda$  equations as described for SU-MRCC and Mk-MRCC theory, which leads to the following external contribution:

$$E_{\text{ext}}^{\text{so}} = \left| \langle \Phi_x | \hat{\Lambda}_{\text{ext}}^{\text{nts}}(x) \hat{H}^{\text{so}} e^{\hat{T}^x} | \Phi_x \rangle \right| \quad (7.33)$$

The energy difference  $\Delta E^{\text{so}}$  between the two electronic states  ${}^2\Pi_{1/2}$  and  ${}^2\Pi_{3/2}$  thus becomes:

$$\Delta E^{\text{so}} = 2 \times \left| \langle \Phi_x | \hat{\Lambda}_{\text{ext}}^{\text{nts}}(x) \hat{H}^{\text{so}} e^{\hat{T}^x} | \Phi_x \rangle + \left( 1 - \frac{1}{2} \langle \Phi_x | \hat{\Lambda}_x e^{\hat{T}^x} | \Phi_x \rangle + \frac{1}{2} \langle \Phi_y | \hat{\Lambda}_y e^{\hat{T}^y} | \Phi_y \rangle \right) \cdot \langle \Phi_y | \hat{H}^{\text{so}} e^{\hat{T}^x} | \Phi_x \rangle \right|. \quad (7.34)$$

## 7.2. Spin-orbit splittings – a measure for the coupling contribution

As is evident from Eq. 5.6 and generally from the considerations in Sec. 5, the spin-orbit operator directly couples the reference determinants  $\Phi_x$  and  $\Phi_y$ . Therefore, the spin-orbit

**Table 7.1.:** Comparison of expressions for spin-orbit splittings with different Jeziorski-Monkhorst based multireference coupled-cluster methods. The contribution due to the external  $\hat{\Lambda}_{\text{ext}}^{\text{nts}}$  operator is given by  $\langle \Phi_x | \hat{\Lambda}_{\text{ext}}^{\text{nts}}(x) e^{-\hat{T}^x} \hat{H}^{\text{so}} e^{\hat{T}^x} | \Phi_x \rangle$  for Mk-MRCC and SU-MRCC and  $\langle \Phi_x | \hat{\Lambda}_{\text{ext}}^{\text{nts}}(x) \hat{H}^{\text{so}} e^{\hat{T}^x} | \Phi_x \rangle$  for BW-MRCC. For the definition of  $\xi$  and  $\langle \overline{H}^{\text{so}} \rangle$  see Eq. 7.35.

| Method  | $\xi$   | $\langle \overline{H}^{\text{so}} \rangle$   |
|---------|---|--|
| SU-MRCC | $\langle \Phi_x   (\hat{\tau}_{x \rightarrow y} - \hat{\Lambda}_x^{\text{nts}}) e^{-\hat{T}^x} e^{\hat{T}^y}   \Phi_y \rangle$                                    | $\langle \Phi_y   e^{-\hat{T}^x} \hat{H}^{\text{so}} e^{\hat{T}^x}   \Phi_x \rangle$ |
| Mk-MRCC | $\langle \Phi_y   (1 + \hat{\Lambda}_y) e^{-\hat{T}^y} e^{\hat{T}^x}   \Phi_y \rangle$  | $\langle \Phi_y   e^{-\hat{T}^x} \hat{H}^{\text{so}} e^{\hat{T}^x}   \Phi_x \rangle$ |
| BW-MRCC | $(1 - \frac{1}{2} \langle \Phi_x   \hat{\Lambda}_x e^{\hat{T}^x}   \Phi_x \rangle + \frac{1}{2} \langle \Phi_y   \hat{\Lambda}_y e^{\hat{T}^y}   \Phi_y \rangle)$ | $\langle \Phi_y   \hat{H}^{\text{so}} e^{\hat{T}^x}   \Phi_x \rangle$                |

splitting can be seen as a quality measure for the coupling contribution in the different Jeziorski-Monkhorst based MRCC methods. The final expressions for the spin-orbit splittings (Eq. 7.12 for Mk-MRCC, Eq. 7.26 for SU-MRCC, and Eq. 7.34 for BW-MRCC) can be interpreted in a way that sheds light on the quality of coupling in the corresponding method.<sup>79</sup> Considering the Mk-MRCC expression for the spin-orbit splittings, for example, it becomes obvious that there are three parts of the equation that reflect different aspects of the theory,

$$\Delta E^{\text{so}} = 2 \times \left[ \underbrace{\langle \Phi_x | \hat{\Lambda}_{\text{ext}}^{\text{nts}}(x) e^{-\hat{T}^x} \hat{H}^{\text{so}} e^{\hat{T}^x} | \Phi_x \rangle}_{\text{ext.}} + 2 \times \underbrace{\langle \Phi_y | (1 + \hat{\Lambda}_y) e^{-\hat{T}^y} e^{\hat{T}^x} | \Phi_y \rangle}_{\xi_{\text{Mk-MRCC}}} \times \underbrace{\langle \Phi_y | e^{-\hat{T}^x} \hat{H}^{\text{so}} e^{\hat{T}^x} | \Phi_x \rangle}_{\langle \overline{H}^{\text{so}} \rangle} \right]. \quad (7.35)$$

The first term in Eq. 7.35 is the contribution due to the non-totally symmetric external  $\hat{\Lambda}$  operator. The second term in the equation consists of a prefactor, which is multiplied by a term corresponding to the expectation value of the similarity transformed spin-orbit operator  $\overline{H}^{\text{so}}$ . The prefactor will be referred to as  $\xi$  and the expectation value of the spin-orbit operator will be denoted  $\langle \overline{H}^{\text{so}} \rangle$  in the following.  $\langle \overline{H}^{\text{so}} \rangle$  can be considered the “unaltered” spin-orbit splittings, where the two reference determinants  $\Phi_x$  and  $\Phi_y$  are directly coupled. The prefactor  $\xi$  then represents a modulation of the expectation value  $\langle \overline{H}^{\text{so}} \rangle$ , if  $\xi < 1$  the coupling is diminished if  $\xi > 1$  it is enhanced. Therefore  $\xi$  can be interpreted as a “coupling factor” and dovetails with the quality of the coupling of the individual Jeziorski-Monkhorst based method. The coupling factor  $\xi$  can be fixed to the value one, which leaves the expectation value  $\langle \overline{H}^{\text{so}} \rangle$  unaltered. The individual Jeziorski-Monkhorst based methods differ only by the expression for  $\xi$ , which means that they only differ by the modulation of the plain expectation value  $\langle \overline{H}^{\text{so}} \rangle$ . In case of BW-MRCC there are additional differences in the equations due to the fact that the theory is disconnected. For a better overview, the different expressions for  $\xi$  are listed in Tab. 7.1.

### 7.3. Density-matrix formulation of spin-orbit splittings with Mk-MRCC

To make the evaluation of a coupled-cluster gradient expression more convenient, it may be rewritten in terms of density matrices and integral derivatives (see also Sec. 6.1).<sup>22</sup> This has been proven to be of computational advantage.<sup>171</sup> For the calculation of spin-orbit splittings with the Breit-Pauli spin-orbit operator  $\hat{H}^{\text{BPso}}$ , Eq. 7.12 is reformulated. The formulation takes on the following form

$$\Delta E^{\text{BPso}} = 2 \times \left| \sum_{pq} D_{pq}(x) f_{pq}^{\text{BPso}} + \sum_{pqrs} \Gamma_{pqrs}(x) \langle \Phi_p \Phi_q | \hat{H}^{\text{BPso}2} | \Phi_r \Phi_s \rangle \right|. \quad (7.36)$$

In  $f_{pq}^{\text{BPso}}$  are Fock-matrix elements composed with the one-electron and two-electron Breit-Pauli spin-orbit operator (for the operators see Eq. 6.21).  $\hat{H}^{\text{BPso}2}$  is the two-electron spin-orbit operator as defined by Eq. 6.21. The double vertical bars in the two-electron integral denote that antisymmetrized integrals are used.

#### 7.3.1. One-electron treatment of spin-orbit splittings

If only terms with the one-electron spin-orbit operator of Eq. 6.21 are taken into account, Eq. 7.36 reduces to

$$\Delta E^{\text{BPso}1} = 2 \times \left| \sum_{pq} D_{pq}(x) \langle \Phi_p | \hat{H}^{\text{BPso}1} | \Phi_q \rangle \right|. \quad (7.37)$$

The one-electron operator  $\hat{H}^{\text{BPso}1}$  is defined as

$$\begin{aligned} \hat{H}^{\text{BPso}1} &= \sum_i \sum_A \left[ \frac{i\alpha^2}{4} \boldsymbol{\sigma}_i \mathbf{p}_i \frac{-Z_A}{r_{iA}} \times \mathbf{p}_i \right] \\ &= \sum_i \sum_A \left[ \frac{\alpha^2 Z_A}{2r_{iA}^3} \hat{\mathbf{s}}_i \cdot \hat{\mathbf{l}}_{iA} \right]. \end{aligned} \quad (7.38)$$

For the calculation of spin-orbit splittings only the  $z$  component of  $\hat{H}^{\text{BPso}1}$  is necessary as demonstrated by Eq. 5.4. All following discussions exclusively refer to the  $z$  component of the one-electron spin-orbit operator (see Eq. 6.22). The matrix-elements  $h_{pq}^{\text{BPso}1}$  of this operator are antisymmetric with respect to an exchange of  $p$  and  $q$ .<sup>b</sup> The spatial part of the matrix elements (i.e., the matrix element of the spatial part of the operator with spatial orbitals  $\phi_p$ ) has the following permutational symmetry

$$\begin{aligned} h_{pq}^{\text{BPso}1} &= \langle \phi_p | \sum_A \frac{\alpha^2 Z_A}{2r_{iA}^3} [\hat{\mathbf{l}}_{iA}]_z | \phi_q \rangle \\ &= \langle \phi_p | \sum_A \hat{h}_{iA}^{\text{so}} | \phi_q \rangle \end{aligned}$$

<sup>b</sup>That is, if real orbitals are used.

$$\begin{aligned}
 &= - \langle \phi_q | \sum_A \hat{h}_{iA}^{\text{so}} | \phi_p \rangle \\
 &= - h_{qp}^{\text{BPso1}}
 \end{aligned} \tag{7.39}$$

It should be noted that due to the antisymmetry of the integrals, only the antisymmetric parts of the density matrix will contribute to the spin-orbit splittings.

The one-particle density matrix is given by

$$\begin{aligned}
 D_{pq} = & \left| \underbrace{\langle \Phi_x | \Lambda_x^{\text{ext,nts}} e^{-\hat{T}^x} \{p^+ q\} e^{\hat{T}^x} | \Phi_x \rangle}_{\text{external density matrix}} + \right. \\
 & \left. \underbrace{\langle \Phi_q(y) | (1 + \hat{\Lambda}_y) e^{-\hat{T}^y} e^{\hat{T}^x} | \Phi_y \rangle}_{\xi_{\text{Mk-MRCC}}} \times \underbrace{\langle \Phi_x | \hat{\tau}_{x \rightarrow y}^{\text{int}} e^{-\hat{T}^x} \{p^+ q\} e^{\hat{T}^x} | \Phi_x \rangle}_{\text{internal density matrix}} \right|,
 \end{aligned} \tag{7.40}$$

and can be evaluated diagrammatically for a given truncation scheme.<sup>22</sup> In this thesis the method of choice is Mk-MRCCSD. In Tab. 7.2 the individual diagrams and corresponding algebraic expressions are listed. The density matrix can be separated into an internal contribution (second term in Eq. 7.40) and an external contribution (first term of the same equation). The internal density matrix only contains the de-excitation operator  $\hat{\tau}_{x \rightarrow y}^{\text{int}}$  that represent a single de-excitation transforming  $\Phi_x$  into  $\Phi_y$ .  $\hat{\tau}_{x \rightarrow y}^{\text{int}}$  appears as blue arrows and bars in Tab. 7.2. The external density matrix contains operators for both, single and double de-excitation.

Furthermore, the density matrices can be grouped according to whether their indices are from the virtual or from the occupied space. The occupied-virtual density matrix  $D_{ia}$  can be combined with the virtual-occupied density matrix  $D_{ai}$  but the antisymmetry of the matrices has to be observed.

The diagrammatic evaluation provides convenient expressions for the external contribution and for the expectation value  $\langle \bar{H}^{\text{so}} \rangle$ . Additionally, however, expressions for the coupling factor  $\xi_{\text{Mk-MRCC}}$  have to be found. In that regard it is important to understand that  $\xi$  essentially consists of the usual Mk-MRCC coupling term multiplied by the correct  $\lambda_q$  multipliers. Evangelista *et al.*<sup>78</sup> provided closed expressions for the Mk-MRCC coupling term (see Eq. 6.4 and Eq. 6.5), which only have to be multiplied by the corresponding  $\lambda_q$  to serve the purpose. Further difficulties arise because of the occurrence of  $t_q(\nu/\mu)$  in the coupling term. In a single-reference coupled-cluster framework, the amplitudes  $t_q(\nu/\mu)$  have to be generated in a separate calculation step. How exactly this is achieved, will be discussed in Sec. 8.3.

According to Eq. 7.37 the density matrices have to be contracted with the integrals  $h_{pq}^{\text{BPso1}}$ . This is done in the AO basis, i.e., the density matrices are transformed into the AO basis and then are contracted with the orbitals,

$$D_{\mu\nu} = \sum_{p,q} D_{pq} \cdot c_{\mu p} c_{\nu q}. \tag{7.41}$$

The contributions from the different types of density matrices,  $D_{ab}$ ,  $D_{ij}$ , and  $D_{ia}$  are summed up. We use an unrestricted Hartree-Fock (UHF) framework for the calculations, consequently there are separate coefficients  $c_{\mu p}$  for the  $\alpha$  and for  $\beta$  spincase. Furthermore, the density

**Table 7.2.:** Diagrams and algebraic expression for the various contributions to the one-particle density matrix. Internal de-excitation operators are depicted with blue arrows and bars.

| “Internal” density matrices                     |   |  |  |  |
|---|---|--|--|--|
| $D_{ab}$  | $D_{ij}$  | $D_{ia}$   | $D_{ai}$   |  |
|   |   |  |  | $\sum_m \tau_a^{m+tb}$                           |
|   |   |  |  | $-\sum_e \tau_e^{itj}$                           |
|   |   |  |  | $\sum_m \sum_e \tau_m^{e+tae}$                   |
|   |   |  |  | $-\sum_m \sum_e \tau_e^{m+e+ta}$                 |
|   |   |  |  | $\tau_a^i$                                       |
| “External” density matrices                     |   |  |  |  |
| $D_{ab}$  | $D_{ij}$  | $D_{ia}$   | $D_{ai}$   |  |
|   |   |  |  | $\sum_m \lambda_a^{m+tb}$                        |
|   |   |  |  | $-\sum_e \lambda_e^{itj}$                        |
|   |   |  |  | $\sum_m \sum_e \lambda_e^{m+tae}$                |
|   |   |  |  | $-\sum_m \sum_e \lambda_m^{e+e+ta}$              |
|   |   |  |  | $\lambda_a^i$                                    |
| $\frac{1}{2} \sum_{m,e,f} \lambda_{ef}^{m+e+f}$ | $\frac{1}{2} \sum_{m,e,f} \lambda_{ef}^{m+e+f}$ | $-\frac{1}{2} \sum_{m,n,e} \lambda_{ae}^{m+n+e}$ | $-\frac{1}{2} \sum_{m,n,e} \lambda_{ae}^{m+n+e}$ | $\sum_{m,e,f} \sum_{m,e,f} \lambda_{ef}^{m+n+e}$ |
|   |   |  |  |  |
|   |   |  |  | $\sum_{m,e,f} \sum_{m,e,f} \lambda_{ef}^{m+n+e}$ |
|   |   |  |  | $\sum_{m,e,f} \sum_{m,e,f} \lambda_{ef}^{m+n+e}$ |

matrices  $D_{ab}$ ,  $D_{ij}$ , and  $D_{ia}$  have to be evaluated for both spin cases. Writing the equations in terms of spatial orbitals we have to take into account that there is a sign change for the  $\beta$ -spin case. After summation over the spin components the following final expression for the one-electron treatment with a Breit-Pauli spin-orbit operator is obtained

$$\Delta E^{\text{BPso1}} = 2 \times \left| \sum_{\mu\nu} (D_{\mu\nu}^{\alpha} - D_{\mu\nu}^{\beta}) \cdot h_{\mu\nu}^{\text{BPso1}} \right|. \quad (7.42)$$

### 7.3.2. Effective one-electron treatment via spin-orbit mean-field approximation

Especially for light elements, a mere one-electron treatment vastly overestimates the spin-orbit splittings. A full two-electron treatment, however, requires evaluation of the two-particle density matrix and its contraction with two-electron integrals. This might not be desirable in an efficient scheme of computation. To avoid those expensive computational steps, a spin-orbit mean-field treatment as described in Sec. 6.3 can be exploited. Then, only the one-particle density matrix is necessary, but an approximate two-electron treatment is achieved. The one-electron integrals in Eq. 7.42 are augmented with the Coulomb and exchange integrals from Eq. 6.35 to give the SOMF matrix elements

$$H_{\mu\nu}^{\text{BPso1mf}} = h_{\mu\nu}^{\text{BPso1}} + \sum_{\rho\sigma} P_{\rho\sigma} [\langle \vartheta_{\mu}\vartheta_{\rho} | \hat{g}_{1,2}^{\text{so}} | \vartheta_{\nu}\vartheta_{\sigma} \rangle - \frac{3}{2} \langle \vartheta_{\mu}\vartheta_{\sigma} | \hat{g}_{1,2}^{\text{so}} | \vartheta_{\rho}\vartheta_{\nu} \rangle - \frac{3}{2} \langle \vartheta_{\sigma}\vartheta_{\mu} | \hat{g}_{1,2}^{\text{so}} | \vartheta_{\nu}\vartheta_{\rho} \rangle]. \quad (7.43)$$

Note that again only the  $z$  component of the vector operators leads to non-vanishing matrix elements and  $\hat{g}_{1,2}^{\text{so}}$  is defined to exclusively contain this component (see Eq. 6.22). The matrix elements  $\hat{H}_{\mu\nu}^{\text{BPso1mf}}$  are inserted into Eq. 7.42

$$\Delta E^{\text{BPso1mf}} = 2 \times \left| \sum_{\mu\nu} (D_{\mu\nu}^{\alpha} - D_{\mu\nu}^{\beta}) \cdot H_{\mu\nu}^{\text{BPso1mf}} \right|. \quad (7.44)$$

As will be verified in Chapter 9, very accurate results for the spin-orbit splittings can be obtained with the SOMF approximation – despite the simplicity of the equations.

### 7.3.3. Two-electron treatment

The full two-electron treatment requires the evaluation of all terms in Eq. 7.36. The first term in this equation involves the one-particle density matrix (see Tab. 7.2), which is contracted with the Fock matrix of the spin-orbit operator. In the second term, the  $\Gamma_{pqrs}$  is contracted with the two-electron integrals.

First, we evaluate the expressions for the Fock matrix in a UHF framework. Unlike during the spin-orbit mean-field treatment, no spin averaging is carried out during the evaluation of this Fock matrix, which gives different expressions for the  $\alpha$ - and the  $\beta$ -Fock matrix.

The one-electron spin-orbit operator is given in Eq. 7.38. The two-electron operator has the form

$$\hat{H}^{\text{BPso2}} = \hat{H}^{\text{SSO}} + \hat{H}^{\text{SOO}} \quad (7.45)$$

$$= - \sum_{i,j \neq i} \frac{\alpha^2}{2r_{ij}^3} \hat{\mathbf{r}}_{ij} \times \hat{\mathbf{p}}_i \cdot (\hat{\mathbf{s}}_i + 2\hat{\mathbf{s}}_j) \quad (7.46)$$

$$\stackrel{2\Pi}{=} \sum_{i,j \neq i} [\hat{\mathbf{g}}_{ij}^{\text{so}} \cdot \hat{\mathbf{s}}_i]_z + 2[\hat{\mathbf{g}}_{ij}^{\text{so}} \cdot \hat{\mathbf{s}}_j]_z . \quad (7.47)$$

The last equality is only true for  ${}^2\Pi$  states, in which only the  $z$  component of the spin-orbit operator provides non-vanishing contributions. Using the definitions in Eq. 6.22, we can write

$$\hat{H}^{\text{BPso}2} \stackrel{2\Pi}{=} \sum_{i,j \neq i} \hat{g}_{ij}^{\text{so}} \cdot \hat{\mathbf{s}}_i + 2\hat{g}_{ij}^{\text{so}} \cdot \hat{\mathbf{s}}_j . \quad (7.48)$$

In the following, the Dirac notation is used, which means that the order of electron 1 and electron 2 is  $\langle 12 | 12 \rangle$  in the two-electron integrals. A matrix element of the full operator is antisymmetric with respect to exchange of bra and ket but symmetric with respect to exchange of electron 1 and 2:

$$\begin{aligned} \langle \phi_p \phi_q | \hat{g}_{1,2}^{\text{so}} + \hat{g}_{2,1}^{\text{so}} | \phi_r \phi_s \rangle &= \langle \phi_q \phi_p | \hat{g}_{1,2}^{\text{so}} + \hat{g}_{2,1}^{\text{so}} | \phi_s \phi_r \rangle \\ &= - \langle \phi_r \phi_s | \hat{g}_{1,2}^{\text{so}} + \hat{g}_{2,1}^{\text{so}} | \phi_p \phi_q \rangle = - \langle \phi_s \phi_r | \hat{g}_{1,2}^{\text{so}} + \hat{g}_{2,1}^{\text{so}} | \phi_q \phi_p \rangle . \end{aligned} \quad (7.49)$$

If the operator  $\hat{g}_{1,2}^{\text{so}}$  alone is considered, the corresponding matrix elements have different permutational symmetry (antisymmetric with respect to exchange of the two indices of electron 1, symmetric with respect to exchange of the indices of electron 2, no symmetry with respect to exchange of bra and ket).

Considering the full two-electron spin-orbit operator, the general expression of the Fock matrix is given by

$$\begin{aligned} f_{ia}^{\text{BPso}} &= \langle \Phi_i | \hat{H}^{\text{BPso}1} | \Phi_a \rangle + \\ &\sum_j \left( \langle \Phi_i \Phi_j | [\hat{g}_{1,2}^{\text{so}} \cdot \hat{\mathbf{s}}_1 + 2\hat{g}_{1,2}^{\text{so}} \cdot \hat{\mathbf{s}}_2 + \hat{g}_{2,1}^{\text{so}} \cdot \hat{\mathbf{s}}_2 + 2\hat{g}_{2,1}^{\text{so}} \cdot \hat{\mathbf{s}}_1] | \Phi_a \Phi_j \rangle - \right. \\ &\quad \left. \langle \Phi_i \Phi_j | [\hat{g}_{1,2}^{\text{so}} \cdot \hat{\mathbf{s}}_1 + 2\hat{g}_{1,2}^{\text{so}} \cdot \hat{\mathbf{s}}_2 + \hat{g}_{2,1}^{\text{so}} \cdot \hat{\mathbf{s}}_2 + 2\hat{g}_{2,1}^{\text{so}} \cdot \hat{\mathbf{s}}_1] | \Phi_j \Phi_a \rangle \right) . \end{aligned} \quad (7.50)$$

Since we work in a UHF framework, the  $\alpha$ - and  $\beta$ -spin case have to be considered separately. In analogy to the UHF-SCF equations, this leads to the disappearance of the exchange contribution with mixed spin. Spin-integration is carried out and Eq. 7.50 is formulated in terms of spatial orbitals  $\phi_p$  instead of spin orbitals  $\Phi_p$ . Since we perform the contraction with the density matrix in the AO basis, the spatial orbitals are expanded in a basis set

$$|\phi_j\rangle = \sum_{\mu} c_{\mu j} |\vartheta_{\mu}\rangle . \quad (7.51)$$

The SCF density matrix  $P_{\mu\nu}$  can be defined for a more compact notation

$$P_{\mu\nu}^{\alpha} = \sum_j c_{\mu j}^{\alpha} c_{\nu j}^{\alpha}, \quad P_{\mu\nu}^{\beta} = \sum_j c_{\mu j}^{\beta} c_{\nu j}^{\beta}. \quad (7.52)$$

The Fock matrices for the  $\alpha$ - and  $\beta$ -spin case can then be written as

$$\begin{aligned} f_{\mu\nu}^{\alpha, BPso} &= h_{\mu\nu}^{BPso1} + \sum_{\sigma\rho} (3P_{\sigma\rho}^{\alpha} - P_{\sigma\rho}^{\beta}) \langle \vartheta_{\mu} \vartheta_{\sigma} | \hat{g}_{1,2}^{so} | \vartheta_{\nu} \vartheta_{\rho} \rangle \\ &\quad - 3P_{\sigma\rho}^{\alpha} (\langle \vartheta_{\mu} \vartheta_{\sigma} | \hat{g}_{1,2}^{so} | \vartheta_{\rho} \vartheta_{\nu} \rangle + \langle \vartheta_{\sigma} \vartheta_{\mu} | \hat{g}_{1,2}^{so} | \vartheta_{\nu} \vartheta_{\rho} \rangle) \\ f_{\mu\nu}^{\beta, BPso} &= h_{\mu\nu}^{BPso1} + \sum_{\sigma\rho} (3P_{\sigma\rho}^{\beta} - P_{\sigma\rho}^{\alpha}) \langle \vartheta_{\mu} \vartheta_{\sigma} | \hat{g}_{1,2}^{so} | \vartheta_{\nu} \vartheta_{\rho} \rangle \\ &\quad - 3P_{\sigma\rho}^{\beta} (\langle \vartheta_{\mu} \vartheta_{\sigma} | \hat{g}_{1,2}^{so} | \vartheta_{\rho} \vartheta_{\nu} \rangle + \langle \vartheta_{\sigma} \vartheta_{\mu} | \hat{g}_{1,2}^{so} | \vartheta_{\nu} \vartheta_{\rho} \rangle). \end{aligned} \quad (7.53)$$

$$(7.54)$$

These Fock matrices now have to be contracted with the coupled-cluster density matrix  $D_{\mu\nu}$  in the AO basis (see Eq. 7.36). There is an individual  $D_{\mu\nu}$  for each spin case  $\alpha$  and  $\beta$  and naturally, each Fock matrix has to be contracted with the coupled-cluster density matrix of the same spin case. Eq. 7.36 becomes

$$\Delta E^{BPso} = 2 \times \left| \sum_{\mu\nu} (D_{\mu\nu}^{\alpha}(x) f_{\mu\nu}^{\alpha, BPso} - D_{\mu\nu}^{\beta}(x) f_{\mu\nu}^{\beta, BPso}) + \sum_{\mu\nu\sigma\rho} \Gamma_{\mu\nu\sigma\rho}(x) \langle \vartheta_{\mu} \vartheta_{\nu} | \hat{H}^{BPso2} | \vartheta_{\sigma} \vartheta_{\rho} \rangle \right|. \quad (7.55)$$

The index “(x)” in the above equation refers to the determinant  $\Phi_x$  in Fig. 5.1.

The second term in Eq. 7.55 involves the two-particle density matrix  $\Gamma_{pqrs}$ . The two-particle Mk-MRCC density matrix in Eq. 7.55

$$\begin{aligned} \Gamma_{pqrs} &= \frac{1}{4} \left| \langle \Phi_x | \Lambda_x^{\text{ext,nts}} e^{-\hat{T}^x} \{p^+ q^+ sr\} e^{\hat{T}^x} | \Phi_x \rangle + \right. \\ &\quad \left. \langle \Phi_q(y) | (1 + \hat{\Lambda}_y) e^{-\hat{T}^y} e^{\hat{T}^x} | \Phi_y \rangle \times \langle \Phi_x | \hat{\tau}_{x \rightarrow y}^{\text{int}} e^{-\hat{T}^x} \{p^+ q^+ sr\}_x e^{\hat{T}^x} | \Phi_x \rangle \right|, \end{aligned} \quad (7.56)$$

can again be evaluated diagrammatically for a given truncation scheme. Here the Mk-MRCCSD approximation is used. The corresponding expressions of the two-particle density matrix in the single-reference coupled-cluster case are well known in the literature<sup>23,179</sup> and have to be adapted to fit Eq. 7.56.

Only the antisymmetric part of the  $\Gamma_{pqrs}$  density matrices contributes to the spin-orbit splittings because of the permutational symmetry of the two-electron integrals as shown in Eq. 7.49. In analogy to the one-particle density matrix,  $\Gamma_{pqrs}$  comprises internal and external contributions with a non-totally symmetric  $\hat{\Lambda}$  operator, a non-totally symmetric internal de-excitation operator  $\hat{\tau}_{x \rightarrow y}^{\text{int}}$  and a totally symmetric  $\hat{T}$  operator. In Tab. 7.3 all diagrams and generic algebraic expressions for the internal contributions are shown. For the actual working equations, all possible spin cases must be considered and the generic expressions given in Tab. 7.3 must be altered accordingly.

**Table 7.3.:** Internal two-particle density matrices  $\Gamma_{pqrs}$ , their diagrams and generic algebraic expressions. The internal de-excitation operator is denoted with blue bars and arrows. Note that actually the density matrices multiplied by a factor of 4 are listed.

| $\Gamma_{pqrs}$ | Diagram(s) | Algebraic expression   |
|-----------------|------------|--|
| $\Gamma_{ijka}$ |            | $\sum_e \left( -t_{ij}^{ea} - \frac{1}{2}P(ij)t_i^e t_j^a \right) \tau_e^k$                |
| $\Gamma_{ciab}$ |            | $\sum_m \left( t_{mi}^{ab} + \frac{1}{2}P(ab)t_m^a t_i^b \right) \tau_c^m$                 |
| $\Gamma_{ijab}$ |            | $\sum_{e,m} t_{mi}^{ae} \tau_e^m t_j^b$  |
|                 |            | $P(ij) \sum_{e,m} t_i^e \tau_e^m t_{mj}^{ab}$  |
|                 |            | $P(ab) \sum_{e,m} t_m^a \tau_e^m \left( t_{ij}^{eb} + \frac{1}{2}P(ij)t_i^e t_j^b \right)$ |
| $\Gamma_{ajbi}$ |            | $-\tau_i^a t_b^j$  |

The contributions to the two-particle density matrices are grouped into different types according to their indices. The first two indices of  $\Gamma_{pqrs}$  always correspond to the bra indices of the integrals, while the last two indices correspond to the ket indices.

For the external two-particle density matrix, we provide example diagrams for all types of density matrices and the full algebraic expressions in Tab. 7.4.<sup>23</sup>

The density matrices where only bra and ket indices are interchanged can be combined for easier handling, which applies to  $\Gamma_{abci}/\Gamma_{ciab}$ ,  $\Gamma_{abij}/\Gamma_{ijab}$ , and  $\Gamma_{ijka}/\Gamma_{akij}$ . The antisymmetry of the density matrices has to be observed, though: Since integrals are antisymmetric with respect to interchange of bra and ket, only the corresponding parts of the density matrices contribute. These considerations reduce the nine density matrix types to the six types  $\Gamma_{abcd}$ ,  $\Gamma_{abci}$ ,  $\Gamma_{ajbi}$ ,  $\Gamma_{ijab}$ ,  $\Gamma_{ijka}$ ,  $\Gamma_{ijkl}$ .

In a UHF framework all unique spin cases have to be considered. It depends on the type of density matrix how many unique spin cases there are. For each spin case the corresponding density matrices are listed in Tab. 7.5. In this table an overlined letter denotes  $\beta$  spin, while a plain letter denotes  $\alpha$  spin.

In order to obtain the final two-particle contribution to the spin-orbit splittings, the expressions for each spin case of each type of  $\Gamma_{pqrs}$  need to be contracted with the corresponding integrals. Integrals are first evaluated in the AO basis, which means that for the contraction the density matrices have to be transformed into the AO basis. The transformation is achieved in analogy to the transformation of the one-particle density matrix, see Eq. 7.65.

For every spin case the spin operator  $\hat{s}_i$  or  $\hat{s}_j$  has to be considered. Furthermore, we have to antisymmetrize the two-electron spin-orbit integrals because of the used definition of the  $\Gamma_{pqrs}$  density matrix. Since it is computationally more convenient to use only one type of spatial integral, namely

$$g_{\mu\nu\rho\sigma} = \langle \vartheta_\mu \vartheta_\nu | \hat{g}_{1,2}^{\text{so}} | \vartheta_\rho \vartheta_\sigma \rangle , \quad (7.57)$$

this integral is used to express contributions due to  $\hat{g}_{1,2}^{\text{so}}$ , contributions due to  $\hat{g}_{2,1}^{\text{so}}$  as well as spin-same and spin-other orbit contribution. In Tab. 7.5 all antisymmetrized integrals for the full spin-orbit operator and every possible spin case expressed in terms of  $\hat{g}_{1,2}^{\text{so}}$  are listed.

The procedure of generating the expressions for the density matrices and contracting it with the correct antisymmetrized integrals is demonstrated with  $\Gamma_{abcd}$ . This is done in the molecular orbital (MO) basis, but naturally applies to the formulation in the AO basis as well. For the  $\alpha\alpha\alpha\alpha$  case (and analogously for  $\beta\beta\beta\beta$  case if the sign change is regarded) we get the following contribution  $G_{abcd}$ :

$$G_{abcd} = \sum_{a<b,c<d} \Gamma_{abcd} \times \langle \phi_a \phi_b | \hat{H}^{BPso2} | \phi_c \phi_d \rangle \quad (7.58)$$

$$= \sum_{a<b,c<d} \Gamma_{abcd} \times 3 \left( \langle \phi_a \phi_b | \hat{g}_{1,2}^{\text{so}} | \phi_c \phi_d \rangle - \langle \phi_a \phi_b | \hat{g}_{1,2}^{\text{so}} | \phi_d \phi_c \rangle \right) \quad (7.59)$$

$$+ \langle \phi_b \phi_a | \hat{g}_{1,2}^{\text{so}} | \phi_d \phi_c \rangle - \langle \phi_b \phi_a | \hat{g}_{1,2}^{\text{so}} | \phi_c \phi_d \rangle \quad (7.60)$$

$$= \frac{1}{2} \sum_{a<b,c<d} \sum_{m<n} \lambda_{ab}^{mn} \theta_{mn}^{ab} \times 3 \left( \langle \phi_a \phi_b | \hat{g}_{1,2}^{\text{so}} | \phi_c \phi_d \rangle - \langle \phi_a \phi_b | \hat{g}_{1,2}^{\text{so}} | \phi_d \phi_c \rangle \right) \quad (7.61)$$

**Table 7.4.:** External two-particle density matrices  $\Gamma_{pqrs}$ , one example diagram for each type of  $\Gamma_{pqrs}$  and algebraic expressions with  $\theta_{ij}^{ab} = t_{ij}^{ab} + \frac{1}{2}P(ij)P(ab)t_i^a t_j^b$ . Note that actually the density matrices multiplied by a factor of 4 are listed.

| $\Gamma_{pqrs}$ | Example diagram | Algebraic expression   |
|-----------------|-----------------|--|
| $\Gamma_{abcd}$ |                 | $\frac{1}{2} \sum_{mn} \lambda_{ab}^{mn} \theta_{mn}^{cd}$   |
| $\Gamma_{ciab}$ |                 | $\sum_m \theta_{mi}^{ab} \lambda_c^m - \frac{1}{2} \sum_{mn} t_i^e \lambda_{ce}^{mn} \theta_{mn}^{ab} - P(ab) \sum_{e,m} t_{in}^{ae} \lambda_{ce}^{mn} t_m^b$<br>$+ \frac{1}{2} P(ab) \sum_{e,mn} t_i^b t_{mn}^{ae} \lambda_{ce}^{mn}$   |
| $\Gamma_{abci}$ |                 | $\sum_m \lambda_{ab}^{mi} t_m^c$   |
| $\Gamma_{abij}$ |                 | $\lambda_{ab}^{ij}$  |
| $\Gamma_{ajbi}$ |                 | $-\sum_{e,m} \lambda_{ae}^{im} (t_{mj}^{eb} + t_j^e t_m^b) - \lambda_i^a t_b^j$  |
| $\Gamma_{ijab}$ |                 | $\frac{1}{4} \sum_{ef,mn} \theta_{ij}^{ef} \lambda_{ef}^{mn} \theta_{mn}^{ab} - \frac{1}{2} P(ij) \sum_{ef,mn} t_{in}^{ef} \lambda_{ef}^{mn} \theta_{mj}^{ab} - P(ij) \sum_{e,m} t_i^e \lambda_e^m \theta_{mj}^{ab}$<br>$-\frac{1}{2} P(ab) \sum_{ef,mn} t_{mn}^{af} \lambda_{ef}^{mn} \theta_{ij}^{eb} - P(ab) \sum_{e,m} t_m^a \lambda_e^m \theta_{ij}^{eb}$<br>$-\frac{1}{2} P(ab) P(ij) \sum_{ef,mn} (t_{mi}^{ae} + 2t_i^e t_m^a) \lambda_{ef}^{mn} t_{jn}^{bf}$<br>$-P(ab) P(ij) \sum_{e,m} (t_{mi}^{ae} + 2t_i^e t_m^a) \lambda_e^m t_j^b + 3P(ab) P(ij) \sum_{e,m} t_i^a t_j^e \lambda_e^m t_m^b$ |
| $\Gamma_{akij}$ |                 | $-\sum_e t_k^e \lambda_{ae}^{ij}$  |
| $\Gamma_{ijka}$ |                 | $-\sum_e \theta_{ij}^{ea} \lambda_e^k + \frac{1}{2} \sum_{ef,m} \theta_{ij}^{ef} \lambda_{ef}^{km} t_m^a + P(ij) \sum_{e,m} t_{im}^{ae} \lambda_{ef}^{mk} t_j^f$<br>$-\frac{1}{2} P(ij) \sum_{ef,m} t_{im}^{ef} \lambda_{ef}^{km} t_j^a$   |
| $\Gamma_{ijkl}$ |                 | $\frac{1}{2} \sum_{ef} \theta_{ij}^{ef} \lambda_{ef}^{kl}$   |

**Table 7.5.:** All possible spin cases of  $\Gamma_{pqrs}$  in a UHF framework, the corresponding types of  $\Gamma_{pqrs}$ , and the antisymmetrized spatial two-electron spin-orbit integrals expressed in terms of  $\hat{g}_{1,2}^{so}$  after spin-integration. Overlined indices denote the  $\beta$ -spin case.

| Spin case                  | $\Gamma_{pqrs}$   | Integral after spin-integration  |
|----------------------------|---|--|
| $\alpha\alpha\alpha\alpha$ | all   | $3 \left( \langle \phi_p \phi_q   \hat{g}_{1,2}^{so}   \phi_r \phi_s \rangle - \langle \phi_p \phi_q   \hat{g}_{1,2}^{so}   \phi_s \phi_r \rangle \right. \\ \left. + \langle \phi_q \phi_p   \hat{g}_{1,2}^{so}   \phi_s \phi_r \rangle - \langle \phi_q \phi_p   \hat{g}_{1,2}^{so}   \phi_r \phi_s \rangle \right)$   |
| $\beta\beta\beta\beta$     | all   | $3 \left( - \langle \phi_p \phi_q   \hat{g}_{1,2}^{so}   \phi_r \phi_s \rangle + \langle \phi_p \phi_q   \hat{g}_{1,2}^{so}   \phi_s \phi_r \rangle \right. \\ \left. - \langle \phi_q \phi_p   \hat{g}_{1,2}^{so}   \phi_s \phi_r \rangle + \langle \phi_q \phi_p   \hat{g}_{1,2}^{so}   \phi_r \phi_s \rangle \right)$ |
| $\alpha\beta\alpha\beta$   | $\Gamma_{\overline{a}\overline{b}\overline{c}\overline{d}}, \Gamma_{\overline{a}\overline{b}\overline{c}\overline{i}}, \Gamma_{\overline{a}\overline{j}\overline{b}\overline{i}},$<br>$\Gamma_{\overline{i}\overline{j}\overline{a}\overline{b}}, \Gamma_{\overline{i}\overline{j}\overline{k}\overline{a}}, \Gamma_{\overline{i}\overline{j}\overline{k}\overline{l}}$ | $\left( - \langle \phi_p \phi_q   \hat{g}_{1,2}^{so}   \phi_r \phi_s \rangle + \langle \phi_q \phi_p   \hat{g}_{1,2}^{so}   \phi_s \phi_r \rangle \right)$   |
| $\beta\alpha\beta\alpha$   | $\Gamma_{\overline{a}\overline{b}\overline{c}\overline{i}}, \Gamma_{\overline{a}\overline{j}\overline{b}\overline{i}}, \Gamma_{\overline{i}\overline{j}\overline{k}\overline{a}}$   | $\left( \langle \phi_p \phi_q   \hat{g}_{1,2}^{so}   \phi_r \phi_s \rangle - \langle \phi_q \phi_p   \hat{g}_{1,2}^{so}   \phi_s \phi_r \rangle \right)$   |
| $\alpha\beta\beta\alpha$   | $\Gamma_{\overline{a}\overline{j}\overline{b}\overline{i}}$   | $\left( \langle \phi_p \phi_q   \hat{g}_{1,2}^{so}   \phi_s \phi_r \rangle - \langle \phi_q \phi_p   \hat{g}_{1,2}^{so}   \phi_r \phi_s \rangle \right)$   |
| $\beta\alpha\alpha\beta$   | $\Gamma_{\overline{a}\overline{j}\overline{b}\overline{i}}$   | $\left( - \langle \phi_p \phi_q   \hat{g}_{1,2}^{so}   \phi_s \phi_r \rangle + \langle \phi_q \phi_p   \hat{g}_{1,2}^{so}   \phi_r \phi_s \rangle \right)$   |

$$+ \langle \phi_b \phi_a | \hat{g}_{1,2}^{\text{so}} | \phi_d \phi_c \rangle - \langle \phi_b \phi_a | \hat{g}_{1,2}^{\text{so}} | \phi_c \phi_d \rangle \Big). \quad (7.62)$$

For the  $\alpha\beta\alpha\beta$  spin case, the two electrons are distinguishable, which leads to unrestricted sums over the indices

$$G_{\bar{a}\bar{b}\bar{c}\bar{d}} = \frac{1}{2} \sum_{\bar{a}\bar{b},\bar{c}\bar{d}} \sum_{m\bar{n}} \lambda_{\bar{a}\bar{b}}^{m\bar{n}} \theta_{m\bar{n}}^{a\bar{b}} \times \left( - \langle \phi_a \phi_b | \hat{g}_{1,2}^{\text{so}} | \phi_c \phi_d \rangle + \langle \phi_b \phi_a | \hat{g}_{1,2}^{\text{so}} | \phi_d \phi_c \rangle \right). \quad (7.63)$$

The demonstrated procedure in principle applies to all types of  $\Gamma_{pqrs}$  and to all spin cases. In order to obtain the final two-electron contribution to the spin-orbit splittings, we have to sum over all types of  $\Gamma_{pqrs}$  and all spin cases.

## 7.4. Combination with scalar-relativistic effects

In this section, the calculation of spin-orbit splittings using multireference wave functions is connected with a rigorous four-component treatment of scalar-relativistic effects. As mentioned above and outlined in Chapter 5 (see Eq. 5.11), we use a spin-separated *ansatz*, where scalar-relativistic effects are treated via a spin-free Dirac-Coulomb approach while spin-orbit effects are accounted for as a perturbation.

Since  ${}^2\Pi$  states are open-shell cases, an unrestricted version of the spin-free Dirac-Coulomb approach is necessary. This theory has been worked out and implemented by Werner Schwabach.<sup>178</sup> Performing the unrestricted spin-free Dirac-Coulomb SCF calculation yields a set of SCF coefficients for the small and the large component, respectively. The no-pair approximation<sup>172</sup> is applied and the negative-energy states are discarded for the coupled-cluster treatment. Using the relativistic integrals and SCF coefficients, the complete machinery from the non-relativistic treatment can be exploited. The one particularity that has to be observed regards the SCF coefficients: One has to determine whether the SCF coefficients of the large (L) or of the pseudo-large (PL) component are required in a certain MO-AO transformation. In this manner the plain one-electron treatment of the spin-orbit splittings is absolutely straightforward.

For an effective one-electron treatment a modified spin-orbit mean-field approach with the spin-orbit Dirac-Coulomb operator has to be developed. The Dirac-Coulomb and the Breit-Pauli spin-orbit operators are closely related and in the non-relativistic limit both operators give the same matrix elements.

### 7.4.1. One-electron treatment

As was pointed out when discussing Eq. 6.40 and Eq. 6.42, only the small-small block in these equations contributes to the spin-orbit splittings. This means that we only have to contract the spatial matrix elements

$$H_{pq}^{\text{soDC1}} = \langle \Phi_p^{PL} | \frac{\alpha^2}{2} \hat{\mathbf{p}}V \times \hat{\mathbf{p}} | \Phi_q^{PL} \rangle \stackrel{{}^2\Pi}{=} \langle \Phi_p^{PL} | \frac{\alpha^2}{2} \left[ \hat{\mathbf{p}}V \times \hat{\mathbf{p}} \right]_z | \Phi_q^{PL} \rangle, \quad (7.64)$$

with the one-particle coupled-cluster density matrix  $D_{pq}$  in Eq. 7.37 to obtain the final result for the spin-orbit splittings. Again, it should be observed that only the  $z$  component of

the vector operator in Eq. 7.64 contributes when considering  ${}^2\Pi$  states. The corresponding integrals are given in the AO basis while  $D_{pq}$  is usually calculated in the MO basis. In the transformation of  $D_{pq}$  the SCF coefficients of the pseudo-large component have to be used,

$$D_{\mu\nu}^{PL,PL} = \sum_{p,q} D_{pq} \cdot c_{\mu p}^{PL} c_{\nu q}^{PL}. \quad (7.65)$$

Eq. 7.42 then becomes

$$\Delta E^{\text{BPso1}} = 2 \times \left| \sum_{\mu\nu} (D_{\mu\nu}^{\alpha,PL,PL} - D_{\mu\nu}^{\beta,PL,PL}) \cdot \langle \vartheta_\mu | H^{\text{soDC1}} | \vartheta_\nu \rangle \right|. \quad (7.66)$$

The evaluation of  $D_{pq}$  for spin-orbit splittings via the Mk-MRCCSD method proceeds as described in Sec. 7.3.1.

### 7.4.2. Effective one-electron treatment via a spin-orbit mean-field approach

For physically meaningful results, a spin-orbit mean-field treatment with the spin-orbit Dirac Coulomb operator is derived. The premises of the derivation are the same as for the SOMF approach with the Breit-Pauli spin-orbit operator: Fock-matrix like elements are desired that allow for an approximate treatment of two-electron effects while only requiring the use of the one-particle density matrix  $D_{pq}$ .

The following definitions (see also Sec. 7.3.3) will be used to make the notation of the following equations more compact

$$\begin{aligned} \hat{\mathbf{g}}_{1,2}^{\text{soDC2}} &= \frac{-\alpha^2}{2r_{12}^3} \hat{\mathbf{r}}_{12} \times \hat{\mathbf{p}}_1 \\ \hat{\mathbf{g}}_{2,1}^{\text{soDC2}} &= \frac{-\alpha^2}{2r_{12}^3} \hat{\mathbf{r}}_{21} \times \hat{\mathbf{p}}_2. \end{aligned} \quad (7.67)$$

If we consider spin-orbit effects as a first-order perturbation

$$\hat{\mathbf{g}}^{\text{DC2}} = \hat{\mathbf{g}}^{\text{sfDC2}} + \gamma \hat{\mathbf{g}}^{\text{soDC2}}, \quad (7.68)$$

the last term of Eq. 6.47 does not have to be considered. This term contains two spin-orbit operators acting on electron 1 and electron 2, respectively. Therefore they are of second order. The matrix elements for the two-electron spin-orbit operator defined in equation 7.68 are thus given by

$$\begin{aligned} H_{ijab}^{\text{soDC2}} &= H_{ijab}^{\text{sfDC2}} + \\ &\gamma \cdot [ \langle \varphi_i^L \Phi_j^{PL} | \hat{\mathbf{s}}_2 \cdot \hat{\mathbf{g}}_{2,1}^{\text{soDC2}} | \varphi_a^L \Phi_b^{PL} \rangle + \langle \Phi_i^{PL} \varphi_j^L | \hat{\mathbf{s}}_1 \cdot \hat{\mathbf{g}}_{1,2}^{\text{soDC2}} | \Phi_a^{PL} \varphi_b^L \rangle + \end{aligned}$$

$$\frac{\alpha^2}{4} ( \langle \Phi_i^{PL} \Phi_j^{PL} | \hat{\mathbf{p}}_1 \hat{\mathbf{s}}_2 \cdot \hat{\mathbf{g}}_{2,1}^{\text{soDC2}} \hat{\mathbf{p}}_1 | \Phi_a^{PL} \Phi_b^{PL} \rangle + \langle \Phi_i^{PL} \Phi_j^{PL} | \hat{\mathbf{s}}_1 \cdot \hat{\mathbf{p}}_2 \hat{\mathbf{g}}_{2,1}^{\text{soDC2}} \hat{\mathbf{p}}_2 | \Phi_a^{PL} \Phi_b^{PL} \rangle ) ] . \quad (7.69)$$

The derivation of the SOMF matrix elements proceeds in complete analogy to the non-relativistic spin-orbit mean-field approach: Fock-like matrix elements of the spin-orbit operator between two Slater determinants differing by a single substitution  $\Phi_i \rightarrow \Phi_a$  are defined. However, the fact that we are dealing with a four-component wave function has to be observed, which results in the following expression

$$\begin{aligned} \langle \Phi_1 | \hat{H}^{\text{somfDC}} | \Phi_2 \rangle &= \langle \Phi_i^{PL} | \hat{H}^{\text{soDC1}} | \Phi_a^{PL} \rangle + \\ \sum_j \left[ \langle \varphi_i^L \Phi_j^{PL} | \hat{\mathbf{s}}_2 \cdot \hat{\mathbf{g}}_{2,1}^{\text{soDC2}} | \varphi_a^L \Phi_j^{PL} \rangle - \langle \varphi_i^L \Phi_j^{PL} | \hat{\mathbf{s}}_2 \cdot \hat{\mathbf{g}}_{2,1}^{\text{soDC2}} | \varphi_j^L \Phi_a^{PL} \rangle + \right. \\ &\langle \Phi_i^{PL} \varphi_j^L | \hat{\mathbf{s}}_1 \cdot \hat{\mathbf{g}}_{1,2}^{\text{soDC2}} | \Phi_a^{PL} \varphi_j^L \rangle - \langle \Phi_i^{PL} \varphi_j^L | \hat{\mathbf{s}}_1 \cdot \hat{\mathbf{g}}_{1,2}^{\text{soDC2}} | \Phi_j^{PL} \varphi_a^L \rangle + \\ \frac{\alpha^2}{4} ( \langle \Phi_i^{PL} \Phi_j^{PL} | \hat{\mathbf{p}}_1 \hat{\mathbf{s}}_2 \cdot \hat{\mathbf{g}}_{2,1}^{\text{soDC2}} \hat{\mathbf{p}}_1 | \Phi_a^{PL} \Phi_j^{PL} \rangle - \langle \Phi_j^{PL} \Phi_i^{PL} | \hat{\mathbf{p}}_1 \hat{\mathbf{s}}_2 \cdot \hat{\mathbf{g}}_{2,1}^{\text{soDC2}} \hat{\mathbf{p}}_1 | \Phi_j^{PL} \Phi_a^{PL} \rangle + \\ &\left. \langle \Phi_i^{PL} \Phi_j^{PL} | \hat{\mathbf{p}}_2 \hat{\mathbf{s}}_1 \cdot \hat{\mathbf{g}}_{1,2}^{\text{soDC2}} \hat{\mathbf{p}}_2 | \Phi_a^{PL} \Phi_j^{PL} \rangle - \langle \Phi_j^{PL} \Phi_i^{PL} | \hat{\mathbf{p}}_2 \hat{\mathbf{s}}_1 \cdot \hat{\mathbf{g}}_{1,2}^{\text{soDC2}} \hat{\mathbf{p}}_2 | \Phi_j^{PL} \Phi_a^{PL} \rangle ) \right] . \quad (7.70) \end{aligned}$$

The one-electron term (first term in the above equation) is already of the desired form and does not have to be manipulated further. For the two-electron contribution more simplifications are necessary. The contributing terms can be separated into a spatial and a spin part and rewritten as follows

$$\langle \varphi_i^L \Phi_j^{PL} | \hat{\mathbf{s}}_2 \cdot \hat{\mathbf{g}}_{2,1}^{\text{soDC2}} | \varphi_a^L \Phi_j^{PL} \rangle = \langle \phi_i^L \phi_j^{PL} | \hat{\mathbf{g}}_{2,1}^{\text{soDC2}} | \phi_a^L \phi_j^{PL} \rangle \cdot \{ \delta_{\theta_i \theta_a} \langle \theta_j | \hat{\mathbf{s}} | \theta_j \rangle \} = 0 \quad (7.71)$$

$$\langle \Phi_i^{PL} \varphi_j^L | \hat{\mathbf{s}}_1 \cdot \hat{\mathbf{g}}_{1,2}^{\text{soDC2}} | \Phi_a^{PL} \varphi_j^L \rangle = \langle \phi_i^{PL} \phi_j^L | \hat{\mathbf{g}}_{1,2}^{\text{soDC2}} | \phi_a^{PL} \phi_j^L \rangle \cdot \{ \langle \theta_i | \hat{\mathbf{s}} | \theta_a \rangle \} \quad (7.72)$$

$$\langle \varphi_i^L \Phi_j^{PL} | \hat{\mathbf{s}}_2 \cdot \hat{\mathbf{g}}_{2,1}^{\text{soDC2}} | \varphi_j^L \Phi_a^{PL} \rangle = \langle \phi_i^L \phi_j^{PL} | \hat{\mathbf{g}}_{2,1}^{\text{soDC2}} | \phi_j^L \phi_a^{PL} \rangle \cdot \{ \delta_{\theta_i \theta_j} \langle \theta_j | \hat{\mathbf{s}} | \theta_a \rangle \} \quad (7.73)$$

$$\langle \Phi_i^{PL} \varphi_j^L | \hat{\mathbf{s}}_1 \cdot \hat{\mathbf{g}}_{1,2}^{\text{soDC2}} | \Phi_j^{PL} \varphi_a^L \rangle = \langle \phi_i^{PL} \phi_j^L | \hat{\mathbf{g}}_{1,2}^{\text{soDC2}} | \phi_j^{PL} \phi_a^L \rangle \cdot \{ \delta_{\theta_j \theta_a} \langle \theta_i | \hat{\mathbf{s}} | \theta_j \rangle \} \quad (7.74)$$

$$\begin{aligned} \langle \Phi_i^{PL} \Phi_j^{PL} | \hat{\mathbf{p}}_1 \hat{\mathbf{s}}_2 \cdot \hat{\mathbf{g}}_{2,1}^{\text{soDC2}} \hat{\mathbf{p}}_1 | \Phi_a^{PL} \Phi_j^{PL} \rangle &= \langle \phi_i^{PL} \phi_j^{PL} | \hat{\mathbf{p}}_1 \hat{\mathbf{g}}_{2,1}^{\text{soDC2}} \hat{\mathbf{p}}_1 | \phi_a^{PL} \phi_j^{PL} \rangle \cdot \{ \delta_{\theta_i \theta_a} \langle \theta_j | \hat{\mathbf{s}} | \theta_j \rangle \} \\ &= 0 \end{aligned} \quad (7.75)$$

$$\langle \Phi_i^{PL} \Phi_j^{PL} | \hat{\mathbf{p}}_2 \hat{\mathbf{s}}_1 \cdot \hat{\mathbf{g}}_{1,2}^{\text{soDC2}} \hat{\mathbf{p}}_2 | \Phi_a^{PL} \Phi_j^{PL} \rangle = \langle \phi_i^{PL} \phi_j^{PL} | \hat{\mathbf{p}}_2 \hat{\mathbf{g}}_{1,2}^{\text{soDC2}} \hat{\mathbf{p}}_2 | \phi_a^{PL} \phi_j^{PL} \rangle \cdot \{ \langle \theta_i | \hat{\mathbf{s}} | \theta_a \rangle \} \quad (7.76)$$

$$\langle \Phi_i^{PL} \Phi_j^{PL} | \hat{\mathbf{p}}_1 \hat{\mathbf{s}}_2 \cdot \hat{\mathbf{g}}_{2,1}^{\text{soDC2}} \hat{\mathbf{p}}_1 | \Phi_j^{PL} \Phi_a^{PL} \rangle = \langle \phi_i^{PL} \phi_j^{PL} | \hat{\mathbf{p}}_1 \hat{\mathbf{g}}_{2,1}^{\text{soDC2}} \hat{\mathbf{p}}_1 | \phi_j^{PL} \phi_a^{PL} \rangle \cdot \{ \delta_{\theta_i \theta_j} \langle \theta_j | \hat{\mathbf{s}} | \theta_a \rangle \} \quad (7.77)$$

$$\langle \Phi_i^{PL} \Phi_j^{PL} | \hat{\mathbf{p}}_2 \hat{\mathbf{s}}_1 \cdot \hat{\mathbf{g}}_{1,2}^{\text{soDC2}} \hat{\mathbf{p}}_2 | \Phi_j^{PL} \Phi_a^{PL} \rangle = \langle \phi_i^{PL} \phi_j^{PL} | \hat{\mathbf{p}}_2 \hat{\mathbf{g}}_{1,2}^{\text{soDC2}} \hat{\mathbf{p}}_2 | \phi_j^{PL} \phi_a^{PL} \rangle \cdot \{ \delta_{\theta_j \theta_a} \langle \theta_i | \hat{\mathbf{s}} | \theta_j \rangle \} . \quad (7.78)$$

In Eq. 7.71 and Eq. 7.75 the left-hand side becomes zero because of permutational symmetry.

To simplify things further, we now average over the spin of the spectator orbitals  $\varphi_j^L$  or  $\Phi_j^{PL}$ . This leads to the final form of the effective one-electron operator. The average occupation number  $n_j$  is introduced and the sum over spin orbitals is turned into a sum over spatial orbitals. The resulting expression for the matrix elements  $\langle \Psi_1 | \hat{H}^{\text{sofDC}} | \Psi_2 \rangle$  has the following form

$$\begin{aligned}
\langle \Phi_1 | \hat{H}^{\text{sofDC}} | \Phi_2 \rangle &= \langle \Phi_i^{PL} | \hat{H}^{\text{soDC1}} | \Phi_a^{PL} \rangle + \\
\sum_j n_j &\left[ \langle \phi_i^{PL} \phi_j^L | \hat{\mathbf{g}}_{1,2}^{\text{soDC2}} | \phi_a^{PL} \phi_j^L \rangle - \right. \\
&\frac{1}{2} \langle \phi_i^L \phi_j^{PL} | \hat{\mathbf{g}}_{2,1}^{\text{soDC2}} | \phi_j^L \phi_a^{PL} \rangle - \frac{1}{2} \langle \phi_i^{PL} \phi_j^L | \hat{\mathbf{g}}_{1,2}^{\text{soDC2}} | \phi_j^{PL} \phi_a^L \rangle + \\
&\frac{\alpha^2}{4} \langle \phi_i^{PL} \phi_j^{PL} | \hat{\mathbf{p}}_2 \hat{\mathbf{g}}_{1,2}^{\text{soDC2}} \hat{\mathbf{p}}_2 | \phi_a^{PL} \phi_j^{PL} \rangle - \\
&\left. \frac{1}{2} \cdot \frac{\alpha^2}{4} \langle \phi_i^{PL} \phi_j^{PL} | \hat{\mathbf{p}}_2 \hat{\mathbf{g}}_{1,2}^{\text{soDC2}} \hat{\mathbf{p}}_2 | \phi_j^{PL} \phi_a^{PL} \rangle - \frac{1}{2} \cdot \frac{\alpha^2}{4} \langle \phi_i^{PL} \phi_j^{PL} | \hat{\mathbf{p}}_1 \hat{\mathbf{g}}_{2,1}^{\text{soDC2}} \hat{\mathbf{p}}_1 | \phi_j^{PL} \phi_a^{PL} \rangle \right]. \tag{7.79}
\end{aligned}$$

The spatial orbitals can now be expanded in a basis set

$$|\phi_i^{PL}\rangle = \sum_{\mu} c_{\mu i}^{PL} |\vartheta_{\mu}\rangle, \quad |\phi_i^L\rangle = \sum_{\mu} c_{\mu i}^L |\vartheta_{\mu}\rangle \tag{7.80}$$

which results in the following expression for the spin-orbit matrix elements in atomic orbitals

$$\begin{aligned}
\langle \vartheta_{\mu} | \hat{H}^{\text{sofDC}} | \vartheta_{\nu} \rangle &= \langle \vartheta_{\mu}^{PL} | \hat{H}^{\text{soDC1}} | \vartheta_{\nu}^{PL} \rangle + \\
\sum_{\rho\sigma} n_j &\left[ c_{\rho}^L c_{\sigma}^L \langle \vartheta_{\mu}^{PL} \vartheta_{\rho}^L | \hat{\mathbf{g}}_{1,2}^{\text{soDC2}} | \vartheta_{\nu}^{PL} \vartheta_{\sigma}^L \rangle - \right. \\
&\frac{1}{2} \cdot c_{\rho}^{PL} c_{\sigma}^L \langle \vartheta_{\mu}^L \vartheta_{\rho}^{PL} | \hat{\mathbf{g}}_{2,1}^{\text{soDC2}} | \vartheta_{\sigma}^L \vartheta_{\nu}^{PL} \rangle - \frac{1}{2} \cdot c_{\rho}^L c_{\sigma}^{PL} \langle \vartheta_{\mu}^{PL} \vartheta_{\rho}^L | \hat{\mathbf{g}}_{1,2}^{\text{soDC2}} | \vartheta_{\sigma}^{PL} \vartheta_{\nu}^L \rangle + \\
&c_{\rho}^{PL} c_{\sigma}^{PL} \frac{\alpha^2}{4} \langle \vartheta_{\mu}^{PL} \vartheta_{\rho}^{PL} | \hat{\mathbf{p}}_2 \hat{\mathbf{g}}_{1,2}^{\text{soDC2}} \hat{\mathbf{p}}_2 | \vartheta_{\nu}^{PL} \vartheta_{\sigma}^{PL} \rangle - \\
&\frac{1}{2} \cdot c_{\rho}^{PL} c_{\sigma}^{PL} \frac{\alpha^2}{4} \langle \vartheta_{\mu}^{PL} \vartheta_{\rho}^{PL} | \hat{\mathbf{p}}_2 \hat{\mathbf{g}}_{1,2}^{\text{soDC2}} \hat{\mathbf{p}}_2 | \vartheta_{\sigma}^{PL} \vartheta_{\nu}^{PL} \rangle - \\
&\left. \frac{1}{2} \cdot c_{\rho}^{PL} c_{\sigma}^{PL} \frac{\alpha^2}{4} \langle \vartheta_{\mu}^{PL} \vartheta_{\rho}^{PL} | \hat{\mathbf{p}}_1 \hat{\mathbf{g}}_{2,1}^{\text{soDC2}} \hat{\mathbf{p}}_1 | \vartheta_{\sigma}^{PL} \vartheta_{\nu}^{PL} \rangle \right]. \tag{7.81}
\end{aligned}$$

Eq. 7.81 can directly be compared to the expression of the spin-orbit mean-field treatment of the Breit-Pauli spin-orbit operator, Eq. 6.35. The equation falls into two parts, the first comprising matrix elements of the spin-orbit operator  $\hat{g}_{i,j}^{\text{soDC2}}$  (first three terms) and the second comprising the “mixed” spin-orbit and scalar-relativistic operator  $\hat{\mathbf{p}}_i \cdot \hat{g}_{i,j}^{\text{soDC2}} \hat{\mathbf{p}}_i$ . Except for the prefactor, which is 1/2 in the relativistic case and 3/2 in the non-relativistic case (see Eq.

6.35), the structure of the first three terms and of the fourth, fifth, and sixth term dovetails exactly with the structure of Eq. 6.35, respectively: There is one Coulomb contribution and there are two exchange contributions that are related to each other by swapping electron 1 with electron 2.

The difference between the relativistic and non-relativistic prefactors arises because in the relativistic treatment there is no equivalent to the so-called spin-other orbit contribution in the Breit-Pauli treatment. The spin-other orbit contribution corresponds to the contribution from the Gaunt interaction and is responsible for the prefactor of 3/2 in Eq. 6.35. In the relativistic treatment only the Coulomb interaction is regarded so far and all other possible interactions were discarded. If the Gaunt interaction were taken into account the prefactor of 3/2 would arise in the non-relativistic limit of Eq. 7.81.

The terms in Eq. 7.81 can be combined according to whether they carry indices of the PL or L component. In other words, the terms of the equations are situated on different “blocks” when writing the equation in matrix form. If we use a compact notation and combine all terms belonging to a certain block we can write

$$\langle \vartheta_\mu | \hat{H}^{\text{somfDC}} | \vartheta_\nu \rangle = H_{\mu\nu}^{\text{soDC1,PL,PL}} + \left[ H_{\mu\nu(\text{so})}^{\text{soDC2,PL,PL}} + H_{\mu\nu(\text{so})}^{\text{soDC2,L,PL}} + H_{\mu\nu(\text{so})}^{\text{soDC2,PL,L}} + H_{\mu\nu(\text{mixed})}^{\text{soDC2,PL,PL}} \right]. \quad (7.82)$$

In Eq. 7.82 the two-electron terms are labelled with “(so)” if they involve matrix elements of a pure spin-orbit operator and they are labelled with “(mixed)” if the corresponding operator is a mixed spin-orbit and scalar-relativistic operator. The above notation is convenient for the formulation of the final expression for the spin-orbit splittings.

In order to finally calculate the spin-orbit splittings in  $^2\Pi$  states with a full relativistic spin-orbit mean-field treatment, the equivalent of Eq. 7.44 has to be formulated. Note that in case of  $^2\Pi$  states only the  $z$  component of the vector operators in Eq. 7.81 leads to non-vanishing matrix elements. Furthermore it is crucial to transform the one-particle coupled-cluster density matrices  $D_{pq}$  with the SCF coefficients from the correct block (pseudo large or large block). Using the notation of Eq. 7.82, the expression for the effective one-electron spin-orbit splitting becomes

$$\begin{aligned} \Delta E^{\text{somfDC}} = 2 \times \sum_{\mu\nu} & \left[ \sum_{pq} \left( D_{pq} c_{\mu p}^{\alpha,L} c_{\nu q}^{\alpha,PL} - D_{pq} c_{\mu p}^{\beta,L} c_{\nu q}^{\beta,PL} \right) H_{\mu\nu(\text{so})}^{\text{soDC2,L,PL}} \right. \\ & + \sum_{pq} \left( D_{pq} c_{\mu p}^{\alpha,PL} c_{\nu q}^{\alpha,L} - D_{pq} c_{\mu p}^{\beta,PL} c_{\nu q}^{\beta,L} \right) H_{\mu\nu(\text{so})}^{\text{soDC2,PL,L}} \\ & \left. + \sum_{pq} \left( D_{pq} c_{\mu p}^{\alpha,PL} c_{\nu q}^{\alpha,PL} - D_{pq} c_{\mu p}^{\beta,PL} c_{\nu q}^{\beta,PL} \right) \left( H_{\mu\nu}^{\text{soDC1,PL,PL}} + H_{\mu\nu(\text{so})}^{\text{soDC2,PL,PL}} + H_{\mu\nu(\text{mixed})}^{\text{soDC2,PL,PL}} \right) \right]. \end{aligned} \quad (7.83)$$

Eq. 7.83 is the final working equation and can be implemented using the machinery developed for the Breit-Pauli spin-orbit mean-field treatment.

## 8. Implementation

### 8.1. General implementation scheme

The various schemes for calculating spin-orbit splittings via Mk-MRCC theory were implemented in the quantum-chemical program package CFOUR.<sup>113</sup> For the time being we restrict ourselves to Mk-MRCCSD, i.e., to Mk-MRCC theory with single and double excitations. We consider molecules with open-shell  $^2\Pi$  states and the electronic structure shown in Fig. 5.1. Our implementation requires the molecules to be calculated in  $C_{2v}$  symmetry and it requires the use of an unrestricted Hartree-Fock (UHF) calculation for the reference function. As described in Sec. 5 the computation of spin-orbit splittings under these premises can be achieved using a single-reference coupled-cluster framework, which implies that we never have to perform a genuine multireference coupled-cluster calculation.

The implementation scheme sketched in Fig. 8.1 is valid for all variants of calculating spin-orbit splittings considered in this thesis (one-electron, effective one-electron and full two-electron treatment and spin-free Dirac Coulomb based scalar-relativistic treatment).

The first step in the calculation of spin-orbit splittings is the solution of the corresponding SCF equations (box 1 in Fig. 8.1). We have already mentioned in Sec. 5 that a reference determinant with equivalent  $\pi_x$  and  $\pi_y$  orbitals is required. In the present implementation this is achieved by an averaged UHF-SCF procedure, which will be described below. In case of a four-component calculation the corresponding spin-free UHF-SCF program has to be called instead to obtain SCF coefficients for large and pseudo-large component. The next step is the computation of all necessary spin-orbit integrals in the AO basis (box 2). For the two-electron spin-orbit integrals, the implementation by Stopkowicz and Gauss<sup>180</sup> in CFOUR was exploited. Using the SCF coefficients and occupation numbers, special spin-orbit matrix elements can be evaluated (box 3, see Eq. 6.35 for the spin-orbit mean-field matrix elements of the Breit-Pauli spin-orbit operator, Eq. 7.54 for the Fock matrix elements required for a full two-electron treatment, and Eq. 7.81 for the spin-orbit mean-field matrix elements with a spin-separated Dirac-Coulomb operator).

Subsequently, a single-reference coupled-cluster calculation (box 4) is performed to obtain the  $t$  amplitudes. The evaluation of the gradient also demands the computation of the totally-symmetric  $\lambda$  amplitudes, which can be conducted using the regular implementation of the  $\Lambda$  equations in CFOUR (box 5). For the computation of the coupling factor  $\xi_{\text{Mk-MRCC}}$  (box 7)  $t$  amplitudes of both determinants and  $\lambda$  amplitudes of one determinant are required (for the general equation of the coupling factor see Tab. 7.1, the exact closed expressions can be found in Ref. 78 and in Eq. 6.5). The  $t$  amplitudes of the second determinant are generated from the first determinant by a symmetry operation (box 6), the exact procedure is described below in Sec. 8.3. Examining the expression for  $\xi_{\text{Mk-MRCC}}$  reveals that we must furthermore provide the amplitudes  $t_{ij\dots}^{ab\dots}(\nu/\mu)$  (see Sec. 6.1, Eq. 6.5 for the exact definition),<sup>78</sup> which we evaluate after the generation of the second determinant. Finally, the non-totally symmetric  $\Lambda$  equations (box 8, see Eq. 7.9) have to be solved in order to obtain the complete set of  $\lambda$  amplitudes for the gradient calculation. Note that in a framework with  $C_{2v}$  symmetry the

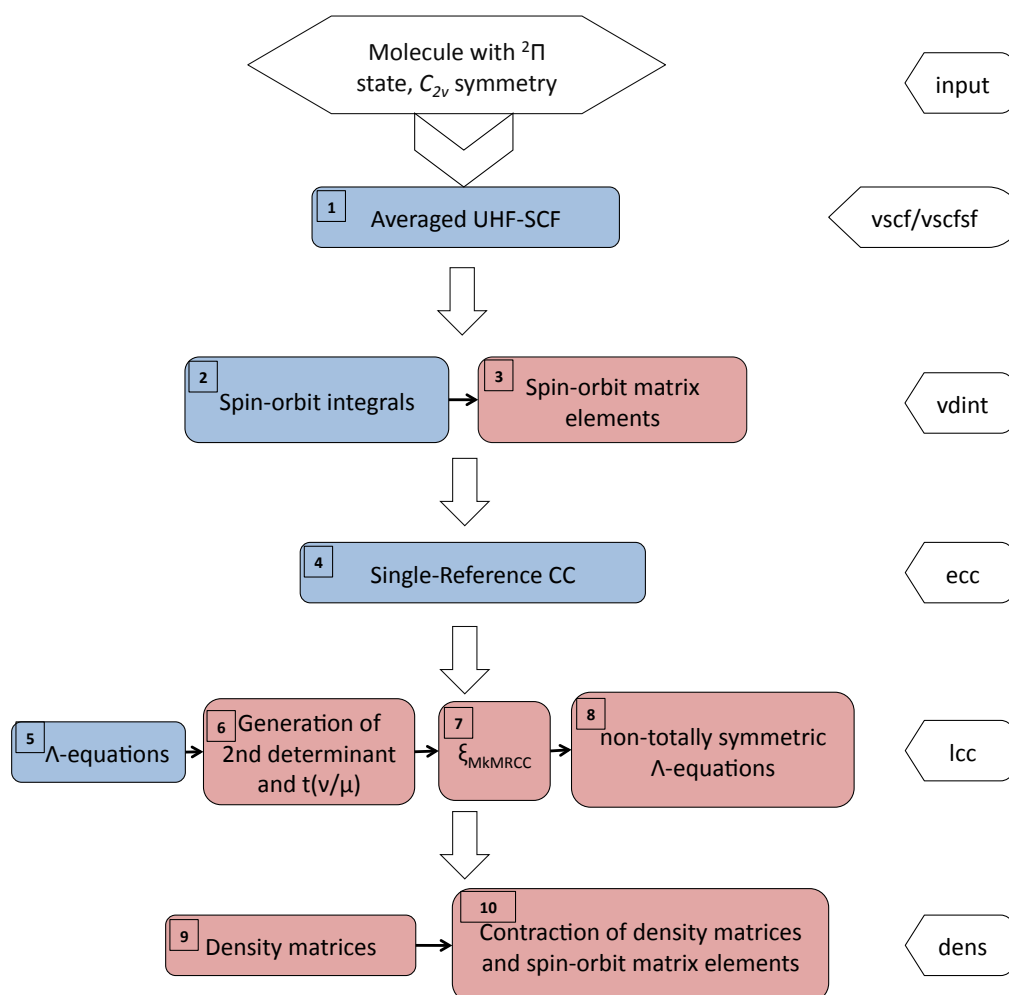


**Figure 8.1.:** Implementation scheme: The steps in red boxes were programmed in the scope of this thesis, while for the steps in blue boxes the existing implementation could be used without (much) alteration. On the right hand side the modules in CFOUR of the corresponding calculation steps are named.

non-totally symmetric  $\lambda$  amplitudes are of  $A_2$  symmetry.

The one- and/or two-particle density matrices can then be evaluated using the  $\lambda$  and the  $t$  amplitudes (box 9). The expressions for those density matrices are given in Tab. 7.2 for the one-particle density matrices and in Tab. 7.3 and Tab. 7.4 for the two-particle density matrices. Contracting the density matrices with the spin-orbit integrals or spin-orbit-matrix elements (box 10, see Eq. 7.42 for a one-electron treatment, Eq. 7.44 for the spin-orbit mean-field treatment, Eq. 7.36 for the full two-electron treatment, and Eq. 7.83 for a relativistic spin-orbit mean-field treatment) provides the final result for the spin-orbit splittings.

## 8.2. Reference function: Averaged UHF

For the calculation of the spin-orbit splittings, two reference determinants  $\Phi_x$  and  $\Phi_y$  with equivalent  $\pi$  orbitals have to be provided. This becomes particularly obvious when looking at the  $\pi_x$  and  $\pi_y$  orbitals in Fig. 8.2: In the two reference determinants these two orbitals differ by occupation. If one reference determinant is to be constructed from the other reference determinant by exchange of  $\pi_x$  and  $\pi_y$ , these two  $\pi$  orbitals must be equivalent. This is achieved by averaging over the two reference determinants when solving the unrestricted Hartree-Fock equations (see Fig. 8.2). During the UHF-SCF calculation orbitals corresponding to two different occupations ( $\pi_x^2\pi_y^1$  for determinant  $\Phi_x$  and  $\pi_x^1\pi_y^2$  for determinant  $\Phi_y$ ) are generated. We average over the SCF coefficients of these two occupations to obtain orbitals that are averaged over  $\Phi_x$  and  $\Phi_y$ .

Using this wave function allows for the generation of both determinants  $\Phi_x$  and  $\Phi_y$  from merely one reference determinant by a symmetry operation.

## 8.3. Generation of two determinants in an SRCC framework

Our idea for the calculation of spin-orbit splittings via Mk-MRCC theory (see Sec. 5) implies the use of a single-reference coupled-cluster framework. For the evaluation of the coupling term  $\xi_{\text{Mk-MRCC}}$ , however, the  $t$  amplitudes of both determinants are necessary. We therefore have to generate the  $t$  amplitudes of the second determinant in a distinct calculation step, which is possible because the two reference determinants are symmetry related in a well-defined way. The  $t$  amplitudes of the second reference determinant  $\Phi_y$  can be generated from the

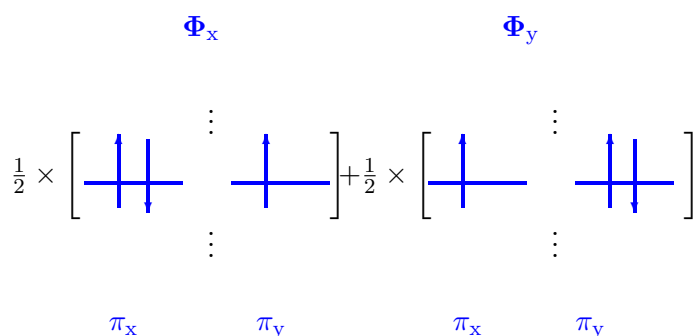


**Figure 8.2.:** Averaged UHF-SCF procedure to obtain a reference determinant with equivalent  $\pi_x$  and  $\pi_y$  orbitals.

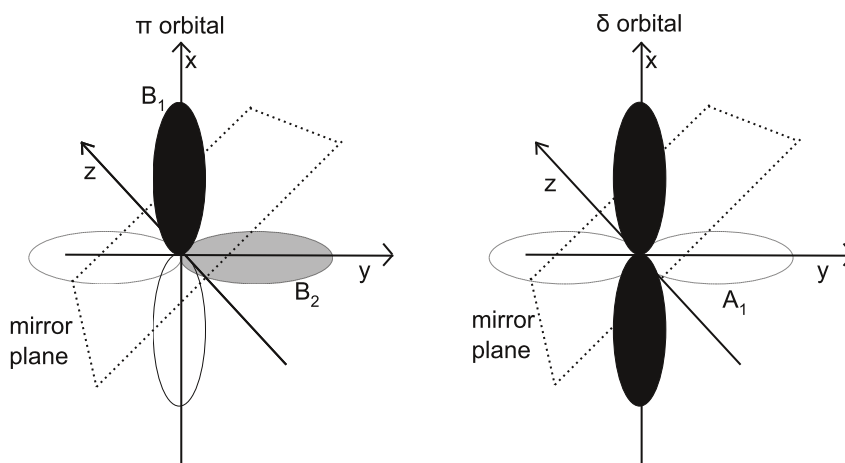


**Figure 8.3.:** Generation of  $\Phi_y$  from  $\Phi_x$  via a symmetry operation: Reflection of  $\pi$  orbitals through a mirror plane transforms orbitals of  $B_1$  symmetry into orbitals of  $B_2$  symmetry and vice versa. Reflection of  $\delta$  orbitals through the same mirror plane results in a sign change.

amplitudes of the first reference determinant  $\Phi_x$  by reflection across a mirror plane (see Fig. 8.3). In the present implementation we restrict ourselves to  $C_{2v}$  point group. This means that the active orbitals,  $\pi_x$  and  $\pi_y$ , belong to irreducible representations  $B_1$  or  $B_2$ , respectively. All amplitudes with  $B_1$  symmetry have to be exchanged with all amplitudes of  $B_2$  symmetry in order to transform the amplitudes of determinant  $\Phi_x$  into the amplitudes of reference determinant  $\Phi_y$ . This is feasible in CFOUR because symmetry is exploited for entities like coefficients and amplitudes, which allows for saving them in a symmetry-blocked structure according to the irreducible representations of their indices (see Fig. 8.4).<sup>181</sup> Furthermore all orbitals of  $\delta$  symmetry belonging to irreducible representations  $A_1$  and all  $\phi$  orbitals belonging to irreducible representations  $B_1$  and  $B_2$  change sign during the symmetry operation (see Fig. 8.3). Strictly speaking, also the  $\gamma$  and  $\eta$  orbitals should change sign, but these do not appear if g- and h-functions are omitted in the calculations.

Furthermore, we have to generate the amplitudes  $t_{ij\dots}^{ab\dots}(\nu/\mu)$  (see Eq. 6.6), which in our case with the two determinants  $\Phi_x$  and  $\Phi_y$  may be called  $t_{ij\dots}^{ab\dots}(y/x)$ . These have to be evaluated since they appear in the closed expression of the Mk-MRCC coupling term.

In our case this implies that the individual amplitudes have to be set to zero according to Eq. 6.6 in a separate calculation step. Looking more closely at the structure of the two determinants it becomes obvious that this only concerns the amplitudes of the  $\beta$ -spin case that carry the indices of the highest occupied  $\pi_y$  and the lowest unoccupied  $\pi_x$  orbital.

## 8.4. Verification

A good strategy for the verification is indispensable to test a newly written program. Therefore we will spend a few words on the verification of our implementation, since this is in our case by no means a trivial task.

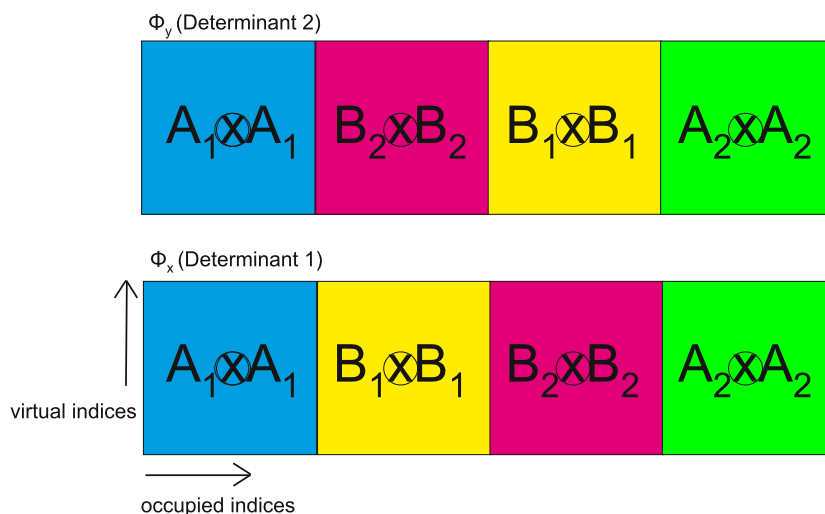


**Figure 8.4.:** Symmetry-blocked structure of amplitudes in CFOUR. Strategy to generate amplitudes of  $\Phi_y$  (Determinant 2, top panel) from amplitudes of  $\Phi_x$  (Determinant 1, bottom panel) for the singles amplitudes. For the doubles amplitudes the same strategy is used but the symmetry-blocked structure is more complicated.

The averaging procedure (box 1 in Fig. 8.1) could be tested by comparing the orbitals: The orbitals of  $B_1$  and  $B_2$  symmetry always have to be equivalent after the UHF-SCF calculation. The evaluation of spin-orbit matrix elements from spin-orbit integrals and SCF coefficients (box 3) was verified via an independently written program, that was kept as simple and straightforward as possible.<sup>a</sup> Furthermore, the sign of the relativistic spin-orbit mean-field matrix elements (see Eq. 7.81) was verified by taking the non-relativistic limit and comparing the result to the non-relativistic spin-orbit mean-field matrix elements, Eq. 6.35. Testing examples were  $F_2$  with several basis sets (the largest one was a double-zeta basis), OH with several basis sets (up to triple-zeta basis), and SeH with a 3-21G basis set.

The generation of the second determinant (box 6) could be checked by doing two calculations with the two different occupations,  $\pi_x^2\pi_y^1$  and  $\pi_x^1\pi_y^2$ . The amplitudes of the second determinant for one occupation are then equal to the amplitudes of the first determinant of the other occupation. As testing examples OH, SH, and ClO were considered up to a triple-zeta basis, additionally SeH with a 3-21G basis set was verified. The calculation of the coupling factor  $\xi_{Mk-MRCC}$  (box 7), of the non-totally symmetric  $\lambda$  amplitudes (box 8), and of the one- and two-particle densities (box 9) were verified by adapting the existing CFOUR Mk-MRCC implementation<sup>34</sup> to perform a Mk-MRCC gradient calculation under the same premises that are required for the calculation of spin-orbit splittings but without exploitation of symmetry. The resulting one- and two-particle density matrices were contracted with the spin-orbit integrals in a simple *incore* program, which verified the contraction (box 10) and the final result. To check whether the result of the relativistic spin-orbit mean-field treatment was correct after contraction of density matrices and integrals, the non-relativistic limit of the four-component calculation was compared to a non-relativistic calculation. Testing examples

<sup>a</sup>This program was written by the author. These types of programs for verification are sometimes paraphrased as *incore programs* in lab slang, another name for them is *kiss programs* (“keep it simple and stupid”).

were OH up to triple-zeta basis and SeH/3-21G. For the (effective) one-electron treatment ClO up to triple-zeta basis and SH up to double-zeta basis were checked as well.

## 9. Applications: Spin-orbit splitting in di- and triatomic molecules

*Tolle numerum omnibus rebus et omnia pereunt.*  
– St. Isidore of Seville

Although Dirac’s advice to make beautiful theories (see headline of Chapter 7) certainly is a good guideline when deriving a new *ab initio* method in quantum chemistry, it is not quite enough for these methods to consist of beautiful equations. Only the final numbers and their comparison to experiment can tell whether it is reasonable to use a new method for the calculation of spin-orbit splittings in applications. In this section, we present the actual results for the spin-orbit splittings in molecules with  $^2\Pi$  states computed with the various variants of our theory for exactly this purpose.

### 9.1. One-electron and effective one-electron treatment of spin-orbit interaction

In this section, the results from the non-relativistic one-electron treatment (1-el) and effective one-electron treatment via the spin-orbit mean-field method (SOMF) are presented. The details of the (effective) one-electron treatment are described in Sec. 7.3.

In Tab. 9.1 the spin-orbit splittings for diatomic molecules with a  $^2\Pi$  ground state computed at Mk-MRCCSD/cc-pCVQZ level of theory are listed. Basis sets of the cc-pCVXZ family<sup>182</sup> were chosen for the calculations because a comprehensive description of the core region is essential to obtain reliable spin-orbit splittings. At quadruple-zeta level the basis-set convergence is reached as Tab. 9.2 shows, which justifies the use of the cc-pCVQZ basis-set for subsequent calculations. It should be mentioned that g, h, and i functions were omitted in the calculation, which might have an influence on the basis-set convergence.

In Tab. 9.1 the computed spin-orbit splittings are compared to experimental values. The experimental spin-orbit splittings are typically obtained by measuring electronic transitions by means of ultraviolet or visible spectroscopy. For example, if the transitions  $^2\Sigma \rightarrow ^2\Pi_{1/2}$  and  $^2\Sigma \rightarrow ^2\Pi_{3/2}$  can be identified, the spin-orbit splitting is the difference in energy between those two transitions.<sup>183</sup> It should be mentioned that it is important to have rotationally resolved spectra at hand in order to ultimately identify the transitions.

The results obtained from a one-electron treatment are always too large but become more accurate for heavy elements than for light elements. For example, for OH, the one-electron result is around 50% larger than the experimental value, while for SeH the difference between the one-electron result and experiment amounts to roughly 7%. These deviations are well in line with previous studies.<sup>166,184</sup>

The SOMF treatment, on the other hand, provides values that are slightly too small compared to experiment. Two aspects of the method might be the limiting factor: First, the SOMF approximation is known to cause spin-orbit splittings to be too small. Second, the Mk-MRCCSD description might limit the accuracy. Whether the SOMF or the Mk-MRCCSD

approximation is the crucial limitation can be checked by considering results from methods with different *ansätze* for the wave function while always using the SOMF approximation for the two-electron effects. In Tab. 9.1 the values obtained from MRCISD and from EOMIP-CCSD calculations with SOMF are listed. These values also tend to be smaller than experiment. MRCISD+SOMF results for OH and SH provided by Berning *et al.* in Ref. 176 are slightly larger than Mk-MRCCSD values but the difference is within such a small range that it might be caused by basis-set effects. For ClO, however, the MRCISD method differs greatly from experimental data. It should be mentioned that the ClO result improves if the 1s and 2s orbital remain uncorrelated.<sup>176</sup> The comparison of Mk-MRCCSD to EOMIP-CCSD results gives a mixed picture. EOMIP-CCSD values for OH, BrO, and ClO are closer to the experimental result than Mk-MRCCSD. For SH and SeH, however, Mk-MRCCSD gives the better values. One possible effect causing the difference between EOMIP-CCSD and Mk-MRCCSD is the use of different orbitals. As described in Sec. 5, the EOMIP-CC *ansatz* uses orbitals of OH<sup>-</sup>, while Mk-MRCCSD uses averaged UHF-SCF orbitals as discussed in Sec. 8.

It should be mentioned that the use of the singles and doubles truncation might also be an important limitation of the Mk-MRCCSD accuracy. The use of (selected) higher excitations, realized for example in the Mk-MRCCSDT or the Mk-MRCCSDtq methods, is known to improve the Mk-MRCC method substantially.<sup>37,82</sup> Therefore the use of these schemes would probably also improve the results.

In addition to the spin-orbit splittings for diatomics with a <sup>2</sup>Π ground state, we provide values for selected triatomics in Tab. 9.3. Unfortunately, experimental values are available only for NCS and N<sub>2</sub>O<sup>+</sup>, for all other species we provide MRCI or internally contracted (IC) MRCI values as a comparison. As for the diatomic species a mere one-electron treatment of the spin-orbit effects vastly overestimates the spin-orbit splittings but gives more accurate values if heavier elements are involved. The SOMF treatment gives a surprisingly good agreement with experiment for N<sub>2</sub>O<sup>+</sup>, in case of NCS it even overestimates the spin-orbit splittings. This might be due to the lack of vibrational averaging. In experiment the bending mode of the triatomic molecules is always activated, which breaks the <sup>2</sup>Π symmetry. This might decrease the spin-orbit coupling. However, this can only be verified by calculating the corresponding numbers. For the MRCI values provided for CCl, CCF, and CCO<sup>-</sup> vibrational effects were not taken into account, either.

In conclusion, the Mk-MRCCSD method in connection with the SOMF approximation gives satisfactory results for the spin-orbit splittings. Especially for light elements, a mere one-electron treatment, however, is not a valid description.

## 9.2. Spin-orbit splittings as a quality measure for the coupling contribution

Spin-orbit splittings can be interpreted as a direct measure for the coupling contribution in Jeziorski-Monkhorst based MRCC methods (see Sec. 5.4), therefore the quality of coupling in a certain method can be evaluated via this property.

For a more complete picture of how the coupling is reflected in the expressions for the spin-orbit splittings, we defined and discussed the coupling factor  $\xi$  (see Sec. 7.2), furthermore we defined the  $\langle \hat{H}^{so} \rangle$  values, where the  $\xi$  is fixed to the value one.  $\langle \hat{H}^{so} \rangle$  therefore represents the unaltered value for the expectation value of a similarity transformed spin-orbit operator. The values of  $\xi$  can provide insights into the quality of coupling in a specific Jeziorski-Monkhorst based MRCC theory.

**Table 9.1.:** Computed spin-orbit splittings for diatomic species with a  $^2\Pi$  ground state using Mk-MRCCSD.<sup>a</sup> Values were obtained either with a one-electron spin-orbit operator (1-el) or within the spin-orbit mean-field approximation (SOMF) and are compared to experimental data, MRCISD,<sup>b</sup> and EOMIP-CCSD<sup>a</sup> results. All values are given in  $\text{cm}^{-1}$ .

| Species | $R^c$  | exp.                     | Mk-MRCC |        | MRCISD <sup>176</sup> | EOMIP-CCSD |        |
|---------|--------|--------------------------|---------|--------|-----------------------|------------|--------|
|         |        |                          | 1-el    | SOMF   | SOMF                  | 1-el       | SOMF   |
| OH      | 0.9697 | 139.2 <sup>28</sup>      | 211.6   | 135.1  | 136.98                | 211.6      | 137.30 |
| SH      | 1.3409 | 377.0 <sup>28</sup>      | 463.8   | 374.7  | 377.58                | 457.4      | 370.2  |
| SeH     | 1.5811 | 1764.4 <sup>183</sup>    | 1890.6  | 1707.6 | ...                   | 1857.3     | 1679.0 |
| ClO     | 1.5696 | 320.3 <sup>28</sup>      | 416.6   | 312.1  | 279.33                | 418.1      | 315.0  |
| BrO     | 1.7172 | 975.4 <sup>185,186</sup> | 1064.5  | 918.5  | ...                   | 1093.4     | 947.5  |

<sup>a</sup> cc-pCVQZ basis set, g functions have been omitted<sup>b</sup> uncontracted cc-pV5Z basis, g and f functions have been omitted, see Ref. 176<sup>c</sup> Bond length  $R$  given in Å**Table 9.2.:** Basis-set convergence of computed spin-orbit splittings for OH, SH, and ClO using Mk-MRCCSD and the cc-pCVXZ basis sets (with g-, h-, and i-functions omitted). Values from a one-electron treatment (1-el) and from a SOMF treatment are listed. All values are in  $\text{cm}^{-1}$ .

| Basis    | OH    |       | SH    |       | ClO   |       |
|----------|-------|-------|-------|-------|-------|-------|
|          | 1-el  | SOMF  | 1-el  | SOMF  | 1-el  | SOMF  |
| cc-pCVDZ | 201.2 | 126.2 | 458.2 | 369.8 | 385.2 | 284.4 |
| cc-pCVTZ | 210.5 | 133.7 | 462.6 | 373.6 | 409.3 | 305.3 |
| cc-pCVQZ | 211.6 | 135.1 | 463.8 | 374.7 | 416.6 | 312.1 |
| cc-pCV5Z | 211.6 | 135.3 | 464.2 | 375.2 | 418.2 | 313.7 |

**Table 9.3.:** Computed spin-orbit splittings for triatomic species with a  $^2\Pi$  ground state<sup>a</sup> using Mk-MRCCSD and a one-electron treatment (1-el) or the SOMF approximation. The results are compared to experimental or MRCI data. All values are given in  $\text{cm}^{-1}$ 

| Species                       | $R1^b$ | $R2^b$ | exp.                 | MRCI                | 1-el  | SOMF  |
|-------------------------------|--------|--------|----------------------|---------------------|-------|-------|
| CCO <sup>-</sup>              | 1.308  | 1.221  | ...                  | 57.8 <sup>c</sup>   | 104.3 | 61.0  |
| CCF                           | 1.271  | 1.276  | ...                  | 53.776 <sup>d</sup> | 99.4  | 57.2  |
| CCCl                          | 1.2964 | 1.6224 | ...                  | 101.02 <sup>e</sup> | 170.2 | 122.2 |
| NCS                           | 1.159  | 1.631  | 325.3 <sup>187</sup> | ...                 | 450.3 | 360.4 |
| N <sub>2</sub> O <sup>+</sup> | 1.154  | 1.182  | 132.4 <sup>188</sup> | ...                 | 209.0 | 130.9 |

<sup>a</sup> cc-pCVQZ basis set without g functions<sup>b</sup> Bond length  $R1$  between first and second atom,  $R2$  between second and third atom, in Å<sup>c</sup> MRCI/aug-cc-pVTZ level of theory, see Ref. 189<sup>d</sup> IC-MRCI/cc-pCVTZ level of theory, see Ref. 190<sup>e</sup> IC-MRCI/cc-pCVQZ level of theory, see Ref. 191

**Table 9.4.:** Comparison of spin-orbit splittings computed with Mk-MRCCSD to  $\langle \bar{H}^{\text{so}} \rangle$  values.<sup>a</sup> Results for the dimensionless coupling factor  $\xi$  for Mk-MRCCSD (see Tab. 7.1) are provided. All values are given in  $\text{cm}^{-1}$ .

| Species | $R^b$  | exp.                     | Mk-MRCC |        |        | $\langle \bar{H}^{\text{so}} \rangle$ |        |
|---------|--------|--------------------------|---------|--------|--------|---------------------------------------|--------|
|         |        |                          | 1-el    | SOMF   | $\xi$  | 1-el                                  | SOMF   |
| OH      | 0.9697 | 139.2 <sup>28</sup>      | 211.6   | 135.1  | 0.9595 | 220.6                                 | 140.8  |
| SH      | 1.3409 | 377.0 <sup>28</sup>      | 463.8   | 374.7  | 0.9454 | 490.6                                 | 396.4  |
| SeH     | 1.5811 | 1764.4 <sup>183</sup>    | 1890.6  | 1707.6 | 0.9501 | 1989.9                                | 1797.3 |
| ClO     | 1.5696 | 320.3 <sup>28</sup>      | 416.6   | 312.1  | 0.9416 | 442.4                                 | 331.6  |
| BrO     | 1.7172 | 975.4 <sup>185,186</sup> | 1064.5  | 918.5  | 0.9356 | 1137.7                                | 981.7  |

<sup>a</sup> cc-pCVQZ basis set, g functions have been omitted<sup>b</sup> Bond length  $R$  given in Å**Table 9.5.:** Basis-set convergence of  $\langle \bar{H}^{\text{so}} \rangle$  values and of the dimensionless Mk-MRCCSD coupling factor  $\xi$  for OH, SH, and ClO. The SOMF approximation was used to account for two-electron effects. All values are given in  $\text{cm}^{-1}$ .

| Basis    | OH                                    |        | SH                                    |        | ClO                                   |        |
|----------|---------------------------------------|--------|---------------------------------------|--------|---------------------------------------|--------|
|          | $\langle \bar{H}^{\text{so}} \rangle$ | $\xi$  | $\langle \bar{H}^{\text{so}} \rangle$ | $\xi$  | $\langle \bar{H}^{\text{so}} \rangle$ | $\xi$  |
| cc-pCVDZ | 129.3                                 | 0.9756 | 383.4                                 | 0.9646 | 298.5                                 | 0.9532 |
| cc-pCVTZ | 138.4                                 | 0.9655 | 393.4                                 | 0.9497 | 323.6                                 | 0.9442 |
| cc-pCVQZ | 140.8                                 | 0.9595 | 396.4                                 | 0.9454 | 331.6                                 | 0.9416 |
| cc-pCV5Z | 142.2                                 | 0.9515 | 397.6                                 | 0.9435 | 334.1                                 | 0.9398 |

Here, in Tab. 9.4-9.6 we provide the numeric values for the coupling factor of Mk-MRCC,  $\xi_{\text{Mk-MRCC}}$ , and for  $\langle \hat{H}^{\text{so}} \rangle$ . It is evident that  $\xi_{\text{Mk-MRCC}}$  is always slightly smaller than one, which means that it “decouples” the  $\langle \hat{H}^{\text{so}} \rangle$  values by 4-8%. Considering that the  $\langle \hat{H}^{\text{so}} \rangle$  values are much larger than experimental values without exception, a viable  $\xi$  seems to be required to be smaller than one.  $\xi$  and  $\langle \hat{H}^{\text{so}} \rangle$  show a similar basis-set convergence as can be seen in Tab. 9.5. It is interesting that with increasing basis set  $\xi$  decreases.

Considering the satisfactory agreement of Mk-MRCCSD spin-orbit splittings with experimental values, the coupling in Mk-MRCCSD seems to be acceptable. But since Mk-MRCCSD neither gives considerably better values than MRCISD nor than EOMIP-CCSD it is debatable, whether  $\xi_{\text{Mk-MRCC}}$  has the optimal value. These observations are valid for diatomics (Tab. 9.4) and triatomics (Tab. 9.6) alike.

### 9.3. Comprehensive one- and two-electron treatment of spin-orbit splittings

The spin-orbit mean-field approximation provides results that compare well to experiment, therefore the SOMF description of two-electron spin-orbit effects seems to be satisfactory. However, it is desirable to quantify the errors made in order to correctly attribute the remaining deviations from experiment. This can be achieved by comparing the SOMF values to results

**Table 9.6.:**  $\langle \bar{H}^{so} \rangle$  values and results for the dimensionless Mk-MRCCSD coupling factor  $\xi$  for triatomic species with a  $^2\Pi$  ground state<sup>a</sup> using the SOMF approximation. MRCI or experimental results are given as a comparison. All values are given in  $\text{cm}^{-1}$ 

| Species                       | R1 <sup>b</sup> | R2 <sup>b</sup> | exp.                 | MRCI                | Mk-MRCC | $\langle \bar{H}^{so} \rangle$ | $\xi$  |
|-------------------------------|-----------------|-----------------|----------------------|---------------------|---------|--------------------------------|--------|
| CCO <sup>-</sup>              | 1.308           | 1.221           | ...                  | 57.8 <sup>d</sup>   | 61.0    | 65.8                           | 0.9263 |
| CCF                           | 1.271           | 1.276           | ...                  | 53.776 <sup>e</sup> | 57.2    | 61.3                           | 0.9342 |
| CCCl                          | 1.2964          | 1.6224          | ...                  | 101.02 <sup>f</sup> | 122.2   | 131.3                          | 0.9311 |
| NCS                           | 1.159           | 1.631           | 325.3 <sup>187</sup> | ...                 | 360.4   | 384.8                          | 0.9366 |
| N <sub>2</sub> O <sup>+</sup> | 1.154           | 1.182           | 132.4 <sup>188</sup> | ...                 | 130.9   | 141.3                          | 0.9264 |

<sup>a</sup>cc-pCVQZ basis set without g functions<sup>b</sup> Bond length R1 between first and second atom, R2 between second and third atom, in Å<sup>d</sup>MRCI/aug-cc-pVTZ level of theory, see Ref. 189<sup>e</sup>IC-MRCI/cc-pCVQZ level of theory, see Ref. 191<sup>f</sup>IC-MRCI/cc-pCVTZ level of theory, see Ref. 190**Table 9.7.:** Spin-orbit splittings computed with Mk-MRCCSD.<sup>a</sup> Comparison of one-electron contribution (1-el), spin-orbit mean-field approximation (SOMF), and one- and two-electron contribution (1-el+2-el). All values are given in  $\text{cm}^{-1}$ .

| Species | R <sup>b</sup> | exp.                  | 1-el   | SOMF   | 1-el+2-el |
|---------|----------------|-----------------------|--------|--------|-----------|
| OH      | 0.9697         | 139.2 <sup>28</sup>   | 211.6  | 135.1  | 136.1     |
| SH      | 1.3409         | 377.0 <sup>28</sup>   | 463.8  | 374.7  | 374.9     |
| SeH     | 1.5811         | 1764.4 <sup>183</sup> | 1890.6 | 1707.6 | 1708.2    |
| ClO     | 1.5696         | 320.3 <sup>28</sup>   | 409.3  | 305.3  | 306.6     |

<sup>a</sup> cc-pCVQZ basis set, for ClO cc-pCVTZ basis set, g functions have been omitted<sup>b</sup> Bond length R given in Å**Table 9.8.:** Basis-set convergence of computed spin-orbit splittings for OH, SH, and ClO using Mk-MRCCSD and the cc-pCVXZ basis sets (with g functions omitted). Values from a spin-orbit mean-field treatment (SOMF) and from a comprehensive treatment of one- and two-electron contribution (1-el+2-el) are listed. All values are in  $\text{cm}^{-1}$ .

| Basis    | OH    |           | SH    |           | SeH    |           |
|----------|-------|-----------|-------|-----------|--------|-----------|
|          | SOMF  | 1-el+2-el | SOMF  | 1-el+2-el | SOMF   | 1-el+2-el |
| cc-pCVDZ | 126.2 | 128.4     | 369.8 | 370.5     | 1666.6 | 1667.0    |
| cc-pCVTZ | 133.7 | 134.9     | 373.6 | 374.1     | 1691.4 | 1692.0    |
| cc-pCVQZ | 135.1 | 136.1     | 374.7 | 374.9     | 1707.6 | 1708.2    |

obtained in a comprehensive treatment of one- and two-electron effects as described in Sec. 7.3.3.

In Tab. 9.7 the corresponding values are given for various species. The full one- and two-electron treatment deviates only marginally from the SOMF treatment. For OH the two values differ by  $1.0 \text{ cm}^{-1}$  (using a cc-pCVQZ basis set), for SeH the difference only amounts to  $0.6 \text{ cm}^{-1}$  at the same level of theory. The fact that the SOMF approximation becomes better for heavier elements<sup>175,176,184</sup> is thus confirmed in Tab. 9.7. In general, two-electron effects are less important in molecules with heavy elements than in molecules with light elements, which dovetails with the accuracy trends of the SOMF approximation.

Considering the basis-set convergence shown in Tab. 9.8, the behavior of SOMF and the comprehensive one- and two-electron treatment show similar characteristics. If basis sets of double-zeta quality are used, basis-set convergence is definitely not reached. Starting from triple-zeta quality, the convergence is almost reached, but the use of a quadruple-zeta basis set still makes the result a few wave numbers larger. The difference between SOMF and the comprehensive treatment seems to become smaller with growing basis set. For example, in OH the cc-pCVDZ values differ by  $2.2 \text{ cm}^{-1}$ , the cc-pCVTZ values differ by  $1.2 \text{ cm}^{-1}$ , and the cc-pCVQZ values differ by  $1.0 \text{ cm}^{-1}$ .

In summary, the rigorous treatment of two-electron effects is necessary if an accuracy of  $1.0 \text{ cm}^{-1}$  or better is to be achieved. However, the SOMF treatment is an excellent approximation, especially if a computationally efficient treatment is desired. The results convey that particularly for heavy elements the deviations from experimental spin-orbit splittings in Tab. 9.1 cannot be attributed to the SOMF approximation. Rather they are probably due to shortcomings of Mk-MRCCSD theory or due to the missing scalar-relativistic effects.

## 9.4. Scalar-relativistic contribution to the spin-orbit splittings

Using the derivations and implementation presented in this work to combine the treatment of scalar-relativistic effects via a spin-free Dirac Coulomb SCF treatment with the calculation of spin-orbit splittings via Mk-MRCCSD, we investigate how large the scalar-relativistic contribution to spin-orbit splittings is. It is particularly interesting, how the scalar-relativistic contribution changes as the cardinal number of the element increases. We naturally expect that the scalar-relativistic contribution becomes more important for heavy elements.

To verify this hypothesis, the series OH, SH, SeH, and TeH has been studied. Especially in TeH the scalar-relativistic effects are expected to play a major role. Calculations on the relativistic effects in this series have previously been conducted, for example by Pisani *et al.*<sup>192</sup> at Dirac-Coulomb Hartree-Fock level and by Hirata *et al.*,<sup>193</sup> who used third-order Douglas-Kroll-Hess coupled-cluster theory. Their results confirm the growing importance of scalar-relativistic effect for heavier elements. In an earlier work, Balasubramanian and co-workers focussed on relativistic calculations of the electronic states of TeH.<sup>194</sup> In contrast to the abundance of computational data on TeH, experimental data is rare and only a somewhat rough estimate of the spin-orbit splittings of TeH in the  $^2\Pi$  state has been provided by Donovan *et al.*<sup>29</sup>

In the present work, a one-electron treatment and a spin-orbit mean-field (SOMF) treatment are considered. As described in Sec. 7.4 contributions due to the Breit interaction are neglected for the time being. An uncontracted ANO-RCC basis set<sup>195</sup> was used for all four-component calculations. It is not advisable to use basis sets that were contracted with schemes designed for non-relativistic calculations because these basis sets are known to provide unreliable results

in spin-free Dirac Coulomb calculations.<sup>196</sup> Analyzing both, values from a mere one-electron treatment and values from a SOMF treatment (excluding Breit-interaction) given in Tab. 9.9, reveals that the contribution due to scalar-relativistic effects is almost negligible in case of OH and SH. Considering the numbers provided in Tab. 9.9 it is evident that scalar-relativistic effects are indispensable in reproducing experimental results for SeH and TeH. Going from SH to SeH the scalar-relativistic contribution increases by several orders of magnitude. It is even bigger in TeH, but looking at the increase relative to the total spin-orbit splittings the jump from SeH to TeH is not quite as big as from SH to SeH. This is depicted graphically in Fig. 9.1. It would be interesting to investigate how the filling of the d-shells is connected with the big increase in scalar-relativistic effects for SeH compared to SH, but this is beyond the scope of this work.

While the scalar-relativistic effects become more important when going to heavier elements, the two-electron effects due to the Coulomb interaction become less important. This is illustrated in Fig. 9.2. For SeH the two-electron Coulomb contribution and the scalar-relativistic contribution are of the same order of magnitude, for TeH the scalar-relativistic contribution is considerably larger than the two-electron Coulomb contribution.

As further examples, we investigate the series SiN, SiP, and SiAs. These molecules and their spectroscopic properties are of special interest because SiN has been found in space, to be more specific in the outerstellar region of the star IRC+10216.<sup>197,198</sup> Since it has been verified that phosphorous and arsenic are present in these types of stars,<sup>51,199</sup> it is likely that SiP and SiAs are of interstellar significance as well. It should be mentioned, though, that all nuclei heavier than iron are much less likely to occur in space than lighter nuclei, which makes SiAs the less probable species.

In SiN, the  $^2\Pi$  state is not the ground state but a low-lying excited state, which various quantum-chemical and experimental analyses show.<sup>200,201</sup> SiP and SiAs, however, have a  $^2\Pi$  ground state. These two species have hardly been investigated yet, neither via quantum-chemical nor via experimental methods. Ornellas *et al.* predicted the spin-orbit splittings in SiP to amount to  $175.72\text{ cm}^{-1}$  in the vibrational ground state. This value was computed via IC-MRCISD/cc-pVQZ calculations and includes vibrational averaging. Batista *et al.* estimate the spin-orbit splittings for SiAs to amount to about  $568\text{ cm}^{-1}$  at the CASSCF/MRCI/aV5Z level of theory considering both one- and two-electron contributions.<sup>202,203</sup>

The Mk-MRCCSD method (see Tab. 9.9) gives similar results. However, even if two-electron effects are taken into account our estimate for the spin-orbit splittings in SiAs is considerably larger than the estimate by Batista *et al.* In terms of relativistic effects, the scalar-relativistic contribution in SiN and SiP is minuscule while scalar-relativistic effects become more important in SiAs. This is in line with our findings regarding the series OH to TeH. It would be furthermore interesting to consider the even heavier analogues SiSb and SiBi.

In conclusion, scalar-relativistic contributions to spin-orbit splittings are negligible if elements of the first and second row are involved. However, starting from the third row scalar-relativistic effects play a major role and it is not possible to reproduce experimental results correctly when these effects are neglected.

**Table 9.9.:** Spin-orbit splittings using Mk-MRCCSD and a Dirac-Coulomb (DC) treatment of scalar-relativistic effects. An uncontracted ANO-RCC basis set was used, g functions were excluded. All values are given in  $\text{cm}^{-1}$ , bond lengths are given in  $\text{\AA}$ . The difference between the non-relativistic (nr) and the scalar-relativistic treatment is given by  $\Delta$ .

|                              | OH                  | SH                  | SeH                 | TeH               | SiN                 | SiP                | SiAs               |
|------------------------------|---------------------|---------------------|---------------------|-------------------|---------------------|--------------------|--------------------|
| <i>R</i>                     |                     |                     |                     |                   |                     |                    |                    |
|                              | 0.9697 <sup>a</sup> | 1.3409 <sup>c</sup> | 1.5811 <sup>b</sup> | 1.74 <sup>c</sup> | 1.6419 <sup>d</sup> | 2.089 <sup>e</sup> | 2.191 <sup>f</sup> |
| One-electron contribution    |                     |                     |                     |                   |                     |                    |                    |
| nr                           | 210.3               | 461.8               | 1855.9              | 3615.4            | 137.8               | 229.2              | 741.7              |
| DC                           | 210.4               | 463.7               | 1903.8              | 3884.1            | 138.1               | 229.8              | 763.7              |
| $\Delta$                     | 0.1                 | 1.9                 | 47.9                | 268.7             | 0.3                 | 0.6                | 22.0               |
| SOMF, no Breit-interaction   |                     |                     |                     |                   |                     |                    |                    |
| nr                           | 152.35              | 390.7               | 1707.5              | 3421.7            | 103.7               | 189.0              | 674.6              |
| DC                           | 152.41              | 392.1               | 1751.4              | 3687.4            | 103.8               | 189.6              | 689.8              |
| $\Delta$                     | 0.06                | 1.4                 | 43.9                | 265.7             | 0.1                 | 0.6                | 15.2               |
| SOMF, with Breit-interaction |                     |                     |                     |                   |                     |                    |                    |
| nr                           | 134.34              | 372.9               | 1675.6              | 3382.0            | 94.0                | 179.3              | 655.5              |
| DC <sup>g</sup>              | 134.40              | 374.3               | 1719.5              | 3647.7            | 94.1                | 179.9              | 670.7              |
| $\Delta$                     | 0.06                | 1.4                 | 43.9                | 265.7             | 0.1                 | 0.6                | 15.2               |
| exp.                         | 139.2 <sup>a</sup>  | 377.0 <sup>a</sup>  | 1764.4 <sup>b</sup> | 3840 <sup>c</sup> | ...                 | ...                | ...                |

<sup>a</sup>See Ref. 28, <sup>b</sup>see Ref. 183, <sup>c</sup>see Ref. 29

<sup>d</sup>See Ref. 201, <sup>e</sup>see Ref. 204, <sup>f</sup>see Ref. 202

<sup>g</sup> The Breit contribution from the Dirac-Coulomb-Breit treatment was estimated by a spin-orbit mean-field calculation using the Breit-Pauli Hamiltonian as a perturbation to a non-relativistic Hamiltonian.

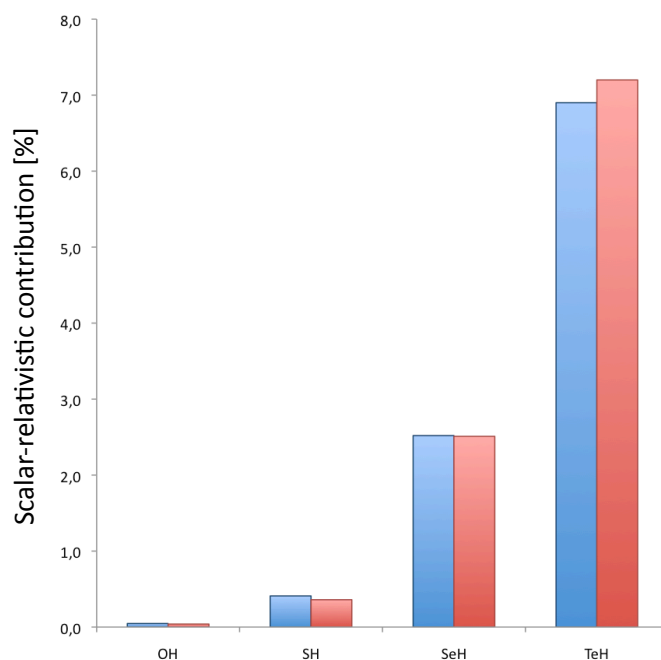


**Figure 9.1.:** Scalar-relativistic contribution (in %) to the spin-orbit splittings in OH, SH, SeH, and TeH (see also Tab. 9.9). Blue columns represent the scalar-relativistic contribution to the one-electron treatment of spin-orbit splittings, red columns for the SOMF treatment (without Breit-interaction).

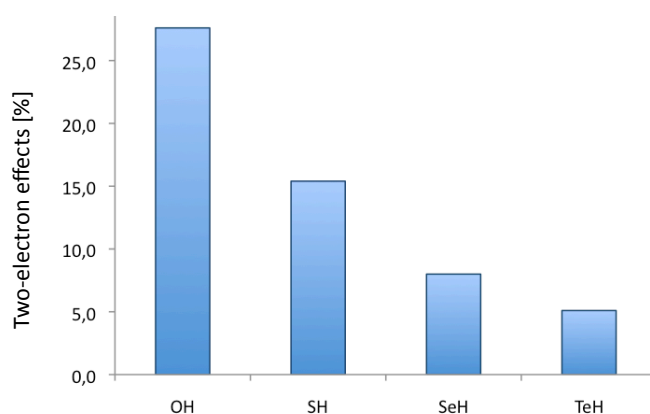


**Figure 9.2.:** Contribution of two-electron effects (in %) to the spin-orbit splittings (calculated with a spin-free Dirac-Coulomb treatment of scalar-relativistic effects, only two-electron Coulomb interaction and no Breit interaction considered) in OH, SH, SeH, and TeH (see also Tab. 9.9).

**Table 9.10.:** Comparison of “best-estimate spin-orbit splittings” (see Eq. 9.2) in this dissertation and experimental value in  $\text{cm}^{-1}$ .

|                                     | OH    | SH    | SeH    | TeH    |
|-------------------------------------|-------|-------|--------|--------|
| best-estimate spin-orbit splittings | 136.4 | 376.8 | 1752.3 | 3647.0 |
| experimental value                  | 139.2 | 377.0 | 1764.4 | 3840   |
| deviation                           | -2.8  | -0.2  | -12.1  | -193.0 |

## 9.5. Accuracy in calculations of spin-orbit splittings with Mk-MRCC

The goal of this dissertation is to provide a method for the calculation of spin-orbit splittings that is sufficient for sub-chemical accuracy. This implies that the spin-orbit splittings should not deviate by more than  $10 \text{ cm}^{-1}$  or  $0.1 \text{ kJ}\cdot\text{mol}^{-1}$  from reliable experimental values. This section discusses whether this goal is achieved by the presented method.

For this purpose the full spin-orbit splittings are partitioned into various contributions, namely the one-electron contribution  $\Delta E_{1\text{-el}}^{\text{so}}$ , the two-electron contribution  $\Delta E_{2\text{-el}}^{\text{so}}$ , which can be approximated in a SOMF treatment, and the contribution due to scalar-relativistic effects  $\Delta E_{\text{DC}}^{\text{so}}$

$$\Delta E^{\text{so}} = \underbrace{\Delta E_{1\text{-el}}^{\text{so}} + \Delta E_{2\text{-el}}^{\text{so}}}_{\text{approx. by } \Delta E_{\text{SOMF}}^{\text{so}}} + \Delta E_{\text{DC}}^{\text{so}}, \quad (9.1)$$

which can also be written in the following way

$$\Delta E^{\text{so}} = \underbrace{\Delta E_{\text{SOMF}}^{\text{so}} + (\Delta E_{1\text{-el}}^{\text{so}} + \Delta E_{2\text{-el}}^{\text{so}} - \Delta E_{\text{SOMF}}^{\text{so}})}_{\Delta E_{1\text{-el}+2\text{-el}}^{\text{so}}} + \Delta E_{\text{DC}}^{\text{so}}. \quad (9.2)$$

All the contributions in Eq. 9.2 are evaluated for the best available basis set and method. For example, the difference between a relativistic and a non-relativistic calculation of the SOMF value including the Breit interaction constitutes the scalar-relativistic contribution. The sum of all these contributions will in the following be referred to as “best-estimate spin-orbit splittings”. On which levels exactly the contributions were calculated is listed in Appendix 10.4. In Tab. 9.10 these best estimates are compared to experimentally determined spin-orbit splittings. As examples, a series of analogous molecules was chosen to compare the accuracy across the periodic table. It is evident that if first- and second-row elements are involved, an accuracy of  $10 \text{ cm}^{-1}$  can easily be achieved. For heavier elements this seems to be harder.

In Tab. 9.11 deviations from experiment are listed if only individual contributions in Eq. 9.2 are considered. In this way it is easier to see, which contributions are crucial for achieving the desired accuracy. It is obvious that for third- and fourth-row elements the consideration of scalar-relativistic effects is an absolute requirement if an accuracy of  $10 \text{ cm}^{-1}$  is to be achieved. Furthermore it once again becomes visible that the two-electron effects are the larger the lighter the involved elements. The values in Tab. 9.11 are depicted graphically in Fig. 9.3, only this time the relative deviation from experiment is shown. This deviation of

**Table 9.11.:** Deviations of calculated spin-orbit splittings from experimental values in  $\text{cm}^{-1}$ . Results with a mere one-electron treatment (1-el), a SOMF treatment (SOMF), a full treatment of one- and two-electron effects (1-el+2-el) and the same value augmented by scalar-relativistic effects (1-el+2-el+DC) are considered. For all contributions the best available value was chosen, for the definition of the contributions see Eq. 9.2.

| Contributions             | OH   | SH   | SeH   | TeH    |
|---------------------------|------|------|-------|--------|
| 1-el                      | 72.4 | 87.2 | 126.2 | -224.6 |
| SOMF                      | -3.9 | -1.8 | -56.8 | -468.0 |
| 1-el+2-el                 | -2.9 | -1.6 | -56.2 | ...    |
| 1-el+2-el+DC <sup>a</sup> | -2.8 | -0.2 | -12.1 | -193.0 |

<sup>a</sup> In case of TeH SOMF+DC

the best-estimate spin-orbit splittings is similar across the periodic table and amounts to less than 2% in case of OH, SH and SeH and to 5% in case of TeH. The latter large deviation is probably due to basis-set errors.

It is worthwhile to briefly discuss the influence of basis sets to accuracy. As is evident in Tab. 9.2 and Tab. 9.8 the errors made by using basis sets smaller than cc-pCVQZ are larger than the error made by the SOMF approximation (compared to a comprehensive treatment of the two-electron effects). For light elements the basis-set error limits the accuracy much more than scalar-relativistic effects. It can therefore not be stressed enough how important it is to use a sufficiently large basis set in the calculation of spin-orbit splittings. In case of the non-relativistic calculation with the Breit-Pauli spin-orbit operator (see also Sec. 6.2) it is furthermore important to use basis sets that are especially designed to describe core-core and core-valence correlation well. For heavy elements like Te often the required basis sets are not available, which is a major limitation to accuracy. The large errors made in case of TeH (see Tab. 9.11) can probably be attributed to the use of an uncontracted ANO-RCC basis set, which is certainly too small (see Tab. 9.9) to provide converged results.

In conclusion, an accuracy of  $10 \text{ cm}^{-1}$  can be reached for molecules with first- and second-row elements by

- using the SOMF approximation,
- using basis sets that accurately describe core-core and core-valence correlation of at least quadruple-zeta quality.

For molecules with third- and fourth-row elements the required accuracy is not necessarily achieved. The recommendations for getting as close to this accuracy as possible are

- using of the SOMF approximation,
- using that accurately describe core-core and core-valence correlation of at least quadruple-zeta quality,
- accounting for the scalar-relativistic contribution.

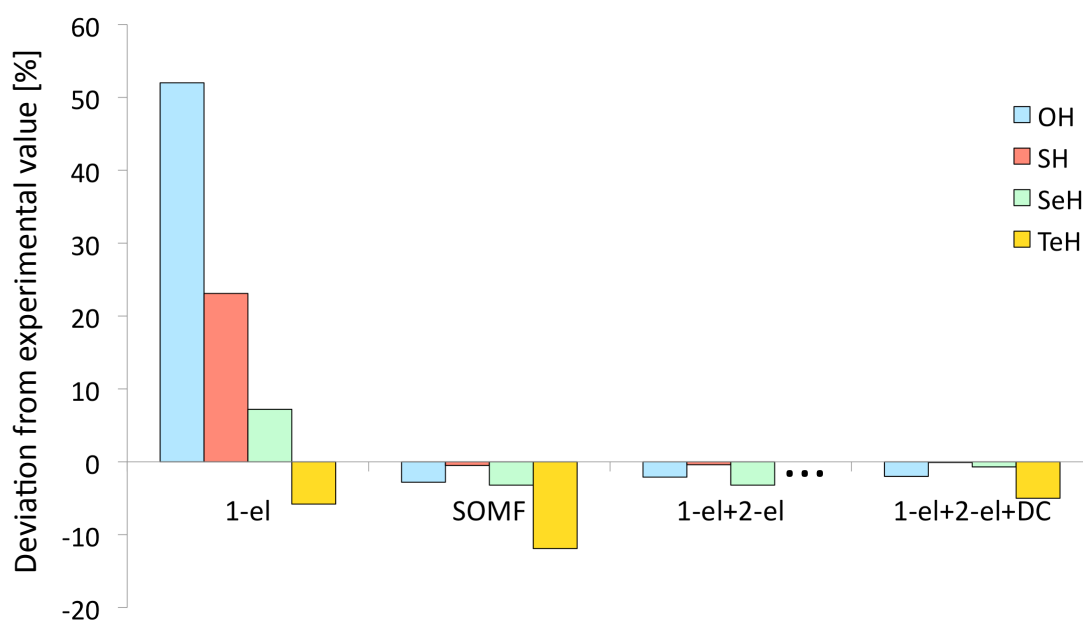


**Figure 9.3.:** Deviation of calculated spin-orbit splittings from experiments in % when only calculating one-electron effects (1-el), when using the SOMF approximation (SOMF), when fully accounting for one-electron and two-electron contributions (1-el+2-el) and when augmenting the latter with relativistic contributions from a spin-free Dirac-Coulomb treatment (1-el+2-el+DC), see also Tab. 9.11. The dots in the 1-el+2-el for TeH mean that this calculation was not performed for TeH.

**Part IV.**

**Epilogue**



## 10. Conclusion

*Wer am Ende ist, kann von vorne anfangen, denn  
das Ende ist der Anfang von der anderen Seite.*

*– Karl Valentin*

### 10.1. The endeavor for predictive power via coupled-cluster theory

Predictive power is the crucial criterion for distinguishing “first-rate theories” in quantum chemistry. In this regard, great advances have been achieved in the past decades due to methodological progress and growing computer power. This dissertation contributes to this development by *demonstrating* and *improving* the predictive power of quantum chemistry. In the quest for predictive power, we follow a quantitative paradigm. This signifies that calculations are supposed to match highly accurate experiments regarding the accuracy, which is for example important when verifying the interpretation of spectra in difficult cases. Among the many possible quantum-chemical methods in this context, coupled-cluster theory is the method of choice. It possesses theoretical rigor, the description of electron correlation can be systematically improved, the errors made during the calculations are controllable, and – last but not least – the method is size extensive.

### 10.2. Demonstration of coupled-cluster theory’s predictive power: New heavy-atom main group molecules

The demonstration of coupled-cluster theory’s predictive power is undertaken using the example of hitherto unknown small heavy-atom main group molecules (see Part II). The search for new molecules is performed as a joint venture with experimentalists, who measured and interpreted their rotational spectra. Since the species are produced in a discharge experiment, it is not trivial to assign the correct lines to the molecule in question. Consequently, it is extremely important to provide reliable quantum-chemical predictions for the rotational constants with an accuracy of 0.1% or better, which typically corresponds to 5-10 MHz. We show that this accuracy can be reached using single-reference coupled-cluster extrapolation and additivity schemes. Additionally it is crucial to account for zero-point vibrational and centrifugal-distortion effects.

Nevertheless, the role of quantum chemistry in the search for the molecules HPSi and linear OSiS focusses on the guidance and verification of experiments by highly accurate predictions and on the explanation of experimental results. We provide chemically comprehensible explanations for the bonding situations of these two molecules using tools of bonding analysis. The bridged structure of HPSi is explained via a non-classical donor-acceptor interaction, while the surprising trends in bond length of OSiS can be attributed to electrostatic interactions. In this way it is shown how nowadays the development of simple, chemical rules for bonding and structure can be derived from first-principle quantum chemistry.

The predictive power of coupled-cluster methods, which is so pivotal in making them “first-rate chemical theories”, is demonstrated in case of cyclic SiS<sub>2</sub>. SiS<sub>2</sub> is a 16-electron triatomic,

which is predicted to be linear by the Walsh rules. However, cyclic  $\text{SiS}_2$  exemplifies that these qualitative rules must be interpreted with caution in case of molecules with heavy atoms because the cyclic isomer is only  $18 \text{ kcal}\cdot\text{mol}^{-1}$  higher in energy than the linear isomer. Connecting chemical intuition and highly accurate coupled-cluster calculations eventually led to the verification that – although linear  $\text{SiS}_2$  is the global minimum on the potential-energy surface – cyclic  $\text{SiS}_2$  is experimentally accessible via rotational spectroscopy in connection with a discharge experiment.

In contrast to  $\text{HPSi}$  and  $\text{OSiS}$ , quantum-chemical calculations for  $\text{SiS}_2$  were not only essential for guiding experiments and making them chemically comprehensible: Theoretical predictions on the stability of the compound preceded and initiated the experimental search. Referring to Charles A. Coulson (see quote of Chapter 4), quantum chemistry provides insight *and* numbers in case of cyclic  $\text{SiS}_2$ .

Cyclic  $\text{SiS}_2$  opens the door to a lot of related compounds. First, the structure and spectroscopic parameters for other cyclic 16-electron triatomic molecules composed of carbon and oxygen analogues were calculated. Cyclic  $\text{OSiS}$  is about  $30 \text{ kcal}\cdot\text{mol}^{-1}$  higher in energy than its linear form. In this case the energetic accessibility is questionable and so far the experimental search has been inconclusive. More promising are cyclic  $\text{OGeS}$  and  $\text{GeS}_2$ , which are predicted to be only 9 and  $2 \text{ kcal}\cdot\text{mol}^{-1}$  higher in energy than the linear isomers. Second,  $\text{SiS}_2$  can be seen as a derivative of a small sulfur ring, where one sulfur atom is substituted by another heavy main-group element. This leads to the consideration of cyclic  $\text{H}_2\text{SiS}_2$  and cyclic  $\text{HPS}_2$ , where the sulfur atom in an  $\text{S}_3$  ring is substituted by the fragments  $\text{H}_2\text{Si}$ - or  $\text{HP}$ -. These two compounds have rather complicated potential-energy surfaces and in this dissertation predictions have been made for various isomers.

A further interesting aspect of cyclic  $\text{SiS}_2$  is, whether there is the possibility to synthesize it by photoisomerization (i.e., irradiation with a distinct wave length) of linear  $\text{SiS}_2$  in a noble-gas matrix. Single-reference coupled-cluster methods fail in the treatment of this problem because the transition state of the reaction  $\text{linear SiS}_2 \rightarrow \text{cyclic SiS}_2$  is a multireference case. Using multireference configuration-interaction calculations, we investigated the excited states' potential-energy surface and could demonstrate two possibilities how a photoisomerization might be achieved. Our predictions await experimental realization.

### **10.3. Improvement of coupled-cluster theory's predictive power: Spin-orbit splittings in $^2\Pi$ states with multireference coupled-cluster wave functions**

Part III of this dissertation contributes to improving the predictive power of quantum chemistry by developing new methods within multireference coupled-cluster theory. To be more precise, the goal is to calculate spin-orbit splittings in  $^2\Pi$  states. If spin-orbit interaction in these states is switched on, they need to be treated using a multireference wave-function *ansatz*. Looking at the successes of coupled-cluster theory it seems highly appealing to use a multireference coupled-cluster wave function for this purpose. The reason why this was difficult in the past is that it is extremely difficult to generalize coupled-cluster theory to multireference cases. Among the many variants of coupled-cluster theory, we choose Mukherjee's multireference coupled-cluster theory because it possesses the important property of size extensivity.

In terms of accuracy the goal of this dissertation is two-fold: First, we consider thermochemical applications, in which case it is desirable to calculate spin-orbit splittings that deviate no more

than  $10\text{ cm}^{-1}$  ( $0.1\text{ kJ}\cdot\text{mol}^{-1}$ ) from accurate experimental measurements. For molecules with first- and second-row elements this goal could be achieved, for heavy elements some of the deviations are slightly larger. Second, the goal is to approach an accuracy of  $1\text{ cm}^{-1}$  or better in order to achieve "spectroscopic accuracy" and match UV/Vis measurements regarding the determination of spin-orbit splittings. This is not achieved, but the presented method can be seen as a stepping stone towards an accuracy of  $1\text{ cm}^{-1}$ .

Based on the findings of this dissertation, different effects that limit the accuracy can be identified and quantified. Considering only the one-electron contribution, the resulting spin-orbit splittings are much too large. For example, in OH the one-electron value amounts to  $211.6\text{ cm}^{-1}$  (cc-pCVQZ basis set) while the experimental value is  $139.2\text{ cm}^{-1}$ . Approximating the two-electron effects by a spin-orbit mean-field method, the values come much closer to the experiment. The calculation with the spin-orbit mean-field approximation and a cc-pCVQZ basis set yields  $135.1\text{ cm}^{-1}$ . If the two-electron contribution is fully considered without any approximation the resulting value is  $136.1\text{ cm}^{-1}$ . Compared to the spin-orbit mean-field approximation, the full two-electron calculation therefore does not make a large difference. But if a very high accuracy is desired, the spin-orbit mean-field treatment must be taken with caution. It should be noted that the choice of the basis set also plays a major role in achieving a satisfactory accuracy. Basis-set convergence is definitely not reached when using basis sets of less than quadruple-zeta quality.

The fact that the results of spin-orbit splittings are in general slightly too small can probably be attributed to shortcomings in Mukherjee's multireference coupled-cluster theory with single and double excitations. To be more precise, the insufficient description of coupling between reference determinants might be the crucial limitation of accuracy. By defining a "coupling factor" in the expressions for the spin-orbit splittings, this possible limitation can be made visible in the equations. By introducing this coupling factor we propose a general quality measure for coupling of reference determinants in MRCC methods. Possibly the spin-orbit splittings would give an even better agreement with experiments, if triple excitations were taken into account, since higher excitations have been shown to improve Mk-MRCC results for a number of other properties.<sup>35,37,81,82</sup>

Compared to other state-of-the-art methods for the calculation of spin-orbit splittings in degenerate  $\Pi$  states with a Breit-Pauli spin-orbit operator, Mk-MRCC performs well. In multireference configuration-interaction theory with single and double excitations, for example, the quality of results compared to experiment varies greatly with the species. For OH, the MRCISD results deviate slightly less from experiment than Mk-MRCCSD but for ClO, the results show a very large deviation.

Scalar-relativistic effects are quite unimportant for the spin-orbit splittings of OH. When considering its heavy-atom analogues they play a major role, though. The calculation of spin-orbit splittings was combined with the calculation of scalar-relativistic effects by the spin-free Dirac-Coulomb approach to quantify how large the scalar-relativistic contributions to the spin-orbit splittings are. Beginning at the third row in the periodic table they are certainly non-negligible. In TeH, for example, scalar-relativistic effects increase the spin-orbit splittings by about 7%. This is larger than the two-electron Coulomb effects, which amount to about 5% of the full spin-orbit splittings!

In conclusion, the calculation of spin-orbit splittings in  ${}^2\Pi$  states with Mukherjee's multireference coupled-cluster method gives satisfactory results. In connection with the HEAT protocol,<sup>26</sup> the method will be useful to account for the spin-orbit contribution in computational thermochemistry. The method's accuracy is high enough to make it an appropriate

replacement of the multireference configuration-interaction scheme that is presently used. In this way the HEAT protocol will become methodologically more consistent because all considered effects will be computable via coupled-cluster theory.

Last but not least it should be mentioned that even if a better solution to the multireference coupled-cluster problem will be formulated in the next few years, the ideas of how to calculate first-order spin-orbit splittings with MRCC wave functions presented in this thesis – the calculation of the spin-orbit matrix elements as a first-order property via gradient theory – still holds and is universally applicable. Once the “holy grail” has been found, our proposal can thus be implemented in the framework of the perfect MRCC method without delay.

### 10.4. Outlook

This dissertation consolidates the role of quantum chemistry as a fundamental chemical discipline by demonstrating and improving its predictive power. Compared to the age of chemistry as an independent scientific discipline, quantum chemistry has only just begun playing this role – and there is a lot of room for boosting it by allowing for calculations with even higher accuracy for bigger, more realistic systems that can be performed in a shorter amount of computer time. If the developments will continue with the same rapidity as today, the role of quantum chemistry as an inspirational source and a pathfinder for experiments will be even more natural in a few years. Today, theoretical and experimental chemistry go hand in hand and inspire each other on equal terms. It is desirable for chemistry as a whole to strengthen this relationship in the future.

## Bibliography

- [1] Kitaigorosky, A. I., *Quote from lecture, International Union of Crystallography, Amsterdam*, August 1975.
- [2] Born, M. and Jordan, P., *Z. Phys.*, 1925, **34**, 858.
- [3] Graulich, N.; Hopf, H. and Schreiner, P. R., *Chem. Soc. Rev.*, 2010, **39**, 1503.
- [4] Lewis, G. N., *J. Am. Chem. Soc.*, 1916, **38**, 762.
- [5] Heitler, W. and London, F., *Z. Phys.*, 1927, **44**, 455.
- [6] Walsh, A. D., *J. Chem. Soc.*, 1953, page 2266.
- [7] Lennard-Jones, J. E., *Trans. Faraday Soc.*, 1929, **25**, 668.
- [8] Moore, G., *Electronics*, 1965, **38**, 4–6.
- [9] Jensen, F., *Introduction to Computational Chemistry*, John Wiley & Sons, Weinheim, 2nd ed., 2006.
- [10] Dyker, C. A.; Lavallo, V.; Donnadiou, B. and Bertrand, G., *Angew. Chem. Int. Ed.*, 2008, **47**, 3206.
- [11] Tonner, R. and Frenking, G., *Chem. Eur. J.*, 2008, **14**, 3260.
- [12] Tonner, R. and Frenking, G., *Chem. Eur. J.*, 2008, **14**, 3273.
- [13] Reiher, M. and Netz, P., *Chem. unserer Zeit*, 1999, **33**, 177.
- [14] Perdew, J. P.; Ruzsinszky, A.; Tao, J.; Staroverov, V. N.; Scuseria, G. E. and Csonka, G. I., *J. Chem. Phys.*, 2005, **123**, 62201.
- [15] Ruscic, B.; Pinzon, R. E.; Morton, M. L.; von Laszewski, G.; Bittner, S. J.; Nijssure, S. G.; Amin, K. A.; Minkoff, M. and Wagner, A. F., *J. Phys. Chem. A*, 2004, **108**, 9979.
- [16] Ventura, O. N. and Kieninger, M., *Pure Appl. Chem*, 1998, **70**, 2301.
- [17] McCarthy, M. C.; Gottlieb, C. A.; Gupta, H. and Thaddeus, P., *Astrophys. J.*, 2006, **652**, L141.
- [18] Szabo, A. and Ostlund, N., *Modern Quantum Chemistry*, Dover Publications, Mineola, New York, 1996.
- [19] Löwdin, P.-O., *Int. J. Quantum Chem.*, 1995, **55**, 77.
- [20] Shavitt, I. and Bartlett, R. J., *Many-Body Methods in Chemistry and Physics: MBPT and Coupled-Cluster Theory*, Cambridge University Press, Cambridge, UK, 2009.

- [21] Crawford, T. D. and Schaefer III, H. F. In *Reviews in Computational Chemistry, Volume 14*; Wiley VCH, 2000; page 33.
- [22] Gauss, J. In *Modern Methods and Algorithms of Quantum Chemistry*, Grotendorst, J., Ed., Vol. 1; John von Neumann Institute for Computing, Jülich, 2000; pages 509–560.
- [23] Gauss, J. and Stanton, J. F., *J. Chem. Phys.*, 1995, **103**, 3561.
- [24] Stanton, J. F. and Gauss, J., *J. Chem. Phys.*, 1994, **101**, 8938.
- [25] Köhn, A.; Hanauer, M.; Mück, L. A.; Jagau, T.-C. and Gauss, J., *WIREs Comput Mol Sci.*, 2012, **in print**, doi: 10.1080/00268976.2012.697585.
- [26] Tajti, A.; Szalay, P. G.; Császár, A. G.; Kállay, M.; Gauss, J.; Valeev, E. F.; Flowers, B. A.; Vázquez, J. and Stanton, J. F., *J. Chem. Phys.*, 2004, **121**, 11599.
- [27] Heckert, M.; Kállay, M.; Tew, D. P.; Klopper, W. and Gauss, J., *J. Chem. Phys.*, 2006, **125**, 044108.
- [28] Huber, K. P. and Herzberg, G., *Constants of Diatomic Molecules*, Vol. 980, Van Nostrand Reinhold, New York, 1979.
- [29] Donovan, R. J.; Little, D. J. and Konstantatos, J., *J. Chem. Soc. Faraday Trans. 2*, 1972, **68**, 223.
- [30] Harding, M. E.; Vázquez, J.; Ruscic, B.; Wilson, A. K.; Gauss, J. and Stanton, J. F., *J. Chem. Phys.*, 2008, **128**, 114111.
- [31] Lischka, H.; Shepard, R.; Pitzer, R. M.; Shavitt, I.; Dallos, M.; Müller, T.; Szalay, P. G.; Seth, M.; Kedziora, G. S.; Yabushita, S. and Y., Z. Z., *Phys. Chem. Chem. Phys.*, 2001, **3**, 664.
- [32] Hess, B.; Buenker, R. J.; Marian, C. M. and Peyerimhoff, S. D., *Chem. Phys.*, 1982, **71**, 79.
- [33] Mahapatra, U. S.; Datta, B. and Mukherjee, D., *J. Chem. Phys.*, 1999, **110**, 6171.
- [34] Prochnow, E.; Evangelista, F. A.; Schaefer III, H. F.; Allen, W. D. and Gauss, J., *J. Chem. Phys.*, 2009, **131**, 064109.
- [35] Evangelista, F. A.; Prochnow, E.; Gauss, J. and Schaefer III, H. F., *J. Chem. Phys.*, 2010, **132**, 074107.
- [36] Kong, L., *Int. J. Quantum Chem.*, 2009, **109**, 441.
- [37] Das, S.; Kállay, M. and Mukherjee, D., *J. Chem. Phys.*, 2010, **133**, 234110.
- [38] Jagau, T.-C. and Gauss, J., *J. Chem. Phys.*, 2011, **137**, 044115.
- [39] Jagau, T.-C. and Gauss, J., *J. Chem. Phys.*, 2011, **137**, 044116.
- [40] Dyal, K. G., *J. Chem. Phys.*, 1994, **100**, 2118.
- [41] Hanrath, M., *Chem. Phys.*, 2009, **356**, 31.

- [42] Čiček, J., *J. Chem. Phys.*, 1966, **45**, 4256.
- [43] Gauss, J. In *Encyclopedia of Computational Chemistry*, Schleyer, P.; Allinger, N. L.; Clark, T.; Gasteiger, J.; Kollmann, P. A.; Schaefer III, and Schreiner, P. R., Eds.; Wiley, Chichester, 1998; pages 615–636.
- [44] Thomas, J. R.; DeLeeuw, B. J.; Vacek, G. and Schaefer, H. F., *J. Chem. Phys.*, 1993, **98**, 1336.
- [45] Raghavachari, K.; Trucks, G. W.; Pople, J. A. and Head-Gordon, M., *Chem. Phys. Lett.*, 1989, **157**, 479.
- [46] Bartlett, R. J.; Watts, J. D.; Kucharski, S. A. and Noga, J., *Chem. Phys. Lett.*, 1990, **165**, 513.
- [47] Lee, Y. S.; Kucharski, S. A. and Bartlett, R. J., *Chem. Phys. Lett.*, 1984, **81**, 5906.
- [48] Dunning, Jr., T. H., *J. Chem. Phys.*, 1989, **90**, 1007.
- [49] Feller, D., *J. Chem. Phys.*, 1993, **98**, 7059.
- [50] Helgaker, T.; Klopper, W.; Koch, H. and Noga, J., *J. Chem. Phys.*, 1997, **106**, 9639.
- [51] Lattanzi, V.; Thorwirth, S.; Halfen, D. T.; Mück, L. A.; Ziurys, L. M.; Thaddeus, P.; Gauss, J. and McCarthy, M. C., *Angew. Chem. Int. Ed.*, 2010, **49**, 5661.
- [52] Thorwirth, S.; Mück, L. A.; Gauss, J.; Tamassia, F.; Lattanzi, V. and McCarthy, M. C., *J. Chem. Phys. Lett.*, 2011, **2**, 1228.
- [53] Mück, L. A.; Lattanzi, V.; Thorwirth, S.; McCarthy, M. C. and Gauss, J., *Angew. Chem. Int. Ed.*, 2012, **51**, 3695.
- [54] Szalay, P. G.; Müller, T.; Gidofalvi, G.; Lischka, H. and Shepard, R., *Chem. Rev.*, 2012, **112**, 108.
- [55] Langhoff, S. R. and Davidson, E. R., *Int. J. Quant. Chem.*, 1974, **8**, 61.
- [56] Pople, J. A.; Seeger, R. and Krishnan, R., *Int. J. Quant. Chem.*, 1977, **10**, 149.
- [57] Hubač, I.; Mach, P. and Wilson, S., *Int. J. Quantum Chem.*, 2002, **89**, 198.
- [58] Szalay, P. G. and Bartlett, R. J., *Chem. Phys. Lett.*, 1993, **214**, 481.
- [59] Gdanitz, R. J. and Ahlrichs, R., *Chem. Phys. Lett.*, 1988, **143**, 413.
- [60] Szalay, P. G.; Müller, T. and Lischka, H., *Phys. Chem. Chem. Phys.*, 2000, **2**, 2067.
- [61] Mahapatra, U. S.; Datta, B.; Bandyopadhyay, B. and Mukherjee, D., *Adv. Quantum Chem.*, 1998, **30**, 163.
- [62] Evangelista, F. A. and Gauss, J., *J. Chem. Phys.*, 2011, **134**, 114102.
- [63] Hanauer, M. and Köhn, A., *J. Chem. Phys.*, 2011, **134**, 204111.
- [64] Jeziorski, B. and Monkhorst, H. J., *Phys. Rev. A*, 1981, **24**, 1668.

- [65] Oliphant, N. and Adamowicz, L., *Chem. Phys.*, 1991, **94**, 1229–1236.
- [66] Szalay, P. G. and Bartlett, R. J., *J. Chem. Phys.*, 1994, **101**, 4936.
- [67] Pittner, J. and Smydke, J., *J. Chem. Phys.*, 2007, **127**, 114103.
- [68] Piechuc, P. and Kowalski, K., *Int. J. Mol. Sci.*, 2002, **3**, 676.
- [69] Li, X. and Paldus, J., *J. Chem. Phys.*, 2003, **119**, 5320.
- [70] Evangelisti, S., *Eur. Phys. J. D*, 2002, **20**, 61.
- [71] Hanrath, M., *J. Chem. Phys.*, 2005, **123**, 084102.
- [72] Hanrath, M., *J. Chem. Phys.*, 2008, **128**, 154118.
- [73] Hanrath, M. and Engels-Putzka, A., *Theor. Chem. Acc.*, 2008, **122**, 197.
- [74] Hubač, I. and Neogrády, P., *Phys. Rev. A*, 1994, **50**, 4558.
- [75] Pittner, J.; Nachtigall, P.; Čársky, P.; Mášik, J. and Hubač, I., *J. Chem. Phys.*, 1999, **110**, 10275.
- [76] Demel, O. and Pittner, J., *J. Chem. Phys.*, 2008, **128**, 104108.
- [77] Kežuch, S.; Demel, O.; Pittner, J.; Ten-no, S. and Noga, J., *Chem. Phys. Lett.*, 2011, **511**, 418–423.
- [78] Evangelista, F. A.; Allen, W. D. and Schaefer III, H. F., *J. Chem. Phys.*, 2007, **127**, 024102.
- [79] Das, S.; Mukherjee, D. and Kállay, M., *J. Chem. Phys.*, 2010, **132**, 074103.
- [80] Jagau, T.-C.; Prochnow, E.; Evangelista, F. A. and Gauss, J., *J. Chem. Phys.*, 2010, **132**, 144110.
- [81] Prochnow, E. *New Developments in State-Specific Multireference Coupled-Cluster Theory* Dissertation, Johannes Gutenberg-Universität, Mainz, 2010.
- [82] Evangelista, F. A.; Simmonett, A. C.; Allen, W. D.; Schaefer, H. F. and Gauss, J., *J. Chem. Phys.*, 2008, **128**, 124104.
- [83] Bhaskaran-Nair, K.; Demel, O.; Šmydke, J. and Pittner, J., *J. Chem. Phys.*, 2011, **134**, 154106.
- [84] Prochnow, E.; Harding, M. E. and Gauss, J., *J. Chem. Theory Comput.*, 2010, **6**, 2339.
- [85] Demel, O.; Kežuch, S.; Švaňa, M.; Ten-no, S. and Pittner, J., *Phys. Chem. Chem. Phys.*, 2012, **14**, 4753–4762.
- [86] Datta, D. and Mukherjee, D., *J. Chem. Phys.*, 2009, **131**, 044124.
- [87] Evangelista, F. A. and Gauss, J., *J. Chem. Phys.*, 2010, **133**, 044101.
- [88] Kong, L., *Int. J. Quantum Chem.*, 2010, **110**, 2603.

- [89] Schreiner, P. R.; Reisenauer, H. P.; Pickard IV, F. C.; Simmonett, A. C.; Allen, W. D.; Mátyus, E. and Czászár, A. G., *Nature*, 2008, **453**, 906.
- [90] Schreiner, P. R.; Reisenauer, H. P.; Ley, D.; Gerbig, D.; Wu, C.-H. and Allen, W. D., *Science*, 2011, **332**, 1300.
- [91] Pyykkö, P., *Chem. Rev.*, 1988, **88**, 563.
- [92] Pyykkö, P., *Ann. Rev. Phys. Chem.*, 2012, **63**, 45.
- [93] Ahuja, R.; Blomqvist, A.; Larsson, P.; Pyykkö, P. and Zaleski-Ejgierd, P., *Phys. Rev. Lett.*, 2011, **106**, 018301.
- [94] Strange, P., *Relativistic Quantum Mechanics*, Cambridge University Press, Cambridge, UK, 1st ed., 1998.
- [95] Kutzelnigg, W., *Angew. Chem. Int. Ed.*, 1984, **23**, 272.
- [96] Power, P. P., *Chem. Rev.*, 1999, **99**, 3463.
- [97] Wang, X. and Andrews, L., *J. Am. Chem. Soc.*, 2003, **125**, 6581.
- [98] Dasent, W. E., *Nonexistent Compounds: Compounds of Low Stability*, Dekker, New York, 1st ed., 1965.
- [99] Xiong, Y.; Yao, S. and Driess, M., *Angew. Chem. Int. Ed.*, 2010, **49**, 6642.
- [100] Driess, M.; Block, S.; Brym, M. and Gamer, M. T., *Angew. Chem. Int. Ed.*, 2006, **45**, 2293.
- [101] Fischer, R. C. and Power, P. P., *Chem. Rev.*, 2010, **110**, 3877.
- [102] Wang, X. and Andrews, L., *J. Phys. Chem. A*, 2003, **107**, 11371.
- [103] Hassanzadeh, P. and Andrews, L., *J. Phys. Chem.*, 1992, **96**, 6181.
- [104] Schnöckel, H. and Köppe, R. In *Organosilicon Chemistry I: From Molecules to Materials*, Auner, N. and Weis, J., Eds.; Wiley-VCH, Weinheim, 2008; chapter 35, page 147.
- [105] Leszczynski, J. and Kwiatkowski, J. S., *J. Phys. Chem.*, 1993, **97**, 12189.
- [106] Mielke, Z. and Andrews, L., *J. Phys. Chem.*, 1993, **97**, 4313.
- [107] McCarthy, M. C.; Yu, Z.; Sari, L.; Schaefer, H. F. and Thaddeus, P., *J. Chem. Phys.*, 2006, **124**, 74303.
- [108] McCarthy, M. C.; Gottlieb, C. A.; Thaddeus, P.; Thorwirth, S. and Gauss, J., *J. Chem. Phys.*, 2011, **134**, 034306.
- [109] Sari, L.; McCarthy, M. C.; Schaefer, H. F. and Thaddeus, P., *J. Am. Chem. Soc.*, 2003, **125**, 11409.
- [110] Mauersberger, R.; Ott, U.; Henkel, C.; Cernicharo, J. and Gallino, R., *Astron. Astrophys.*, 2004, **426**, 219–227.

- [111] Puzzarini, C.; Stanton, J. F. and Gauss, J., *Int. Rev. in Phys. Chem.*, 2010, **29**, 273.
- [112] Meyer, H., *Annu. Rev. Phys. Chem.*, 2002, **53**, 141.
- [113] see <http://www.cfour.de>.
- [114] Weinhold, F., *J. Comp. Chem.*, 2012, **33**, 2363.
- [115] Reed, A. E.; Curtiss, L. A. and Weinhold, F., *Chem. Rev.*, 1988, **88**, 899.
- [116] Bader, R. F., *Atoms in Molecules - A Quantum Theory*, Clarendon Press, Oxford, 1990.
- [117] Baboul, A. G. and Schlegel, H. B., *J. Am. Chem. Soc.*, 1996, **118**, 8444.
- [118] Lai, C.-H.; Su, M.-D. and Chu, S.-Y., *Inorg. Chem.*, 2002, **41**, 1320.
- [119] Dykema, K. J.; Truong, T. N. and Gordon, M. S., *J. Am. Chem. Soc.*, 1985, **107**, 4535.
- [120] Chesnut, D., *Chem. Phys.*, 2005, **315**, 59.
- [121] Devarajan, D. and Frenking, G., *Chem. Asian J.*, 2012, **7**, 1296.
- [122] Bondi, A., *J. Phys. Chem.*, 1964, **68**, 441.
- [123] Loomis, C. C. and Strandberg, M. W. P., *Phys. Rev.*, 1951, **81**, 798–807.
- [124] Driess, M.; Reisgys, M. and Pritzkow, H., *Angew. Chem. Int. Ed.*, 1992, **31**, 1510.
- [125] Allen, F. H.; Davies, J. E.; Galloy, J. J.; Johnson, O.; Kennard, O.; Macrae, C. F.; Mitchell, E. M.; Mitchell, G. F.; Smith, J. M. and Watson, D. G., *J. Chem. Inf. Comput. Sci.*, 1991, **31**, 187–204.
- [126] Keiichi, O.; Matsuura, H.; Endo, Y. and Hirota, E., *J. Mol. Spectr.*, 1986, **118**, 1 – 17.
- [127] *MOLPRO version 2006.1*, see <http://www.molpro.net>.
- [128] Toth, R. A.; Sung, K.; Brown, L. R. and Crawford, T. J., *J. Quant. Spectrosc. Radiat. Transfer*, 2010, **111**, 1193.
- [129] Golubiatnikov, G. Y.; Lapinov, A. V.; Guarnieri, A. and Knöchel, R., *J. Mol. Spectrosc.*, 2005, **234**, 190.
- [130] Schnöckel, H., *Angew. Chem. Int. Ed.*, 1980, **19**, 323.
- [131] Schnöckel, H.; Göcke, H. J. and Köppe, R., *Z. Anorg. All. Chem.*, 1989, **578**, 159.
- [132] Bhattacharyya, A. A.; Bhattacharyya, A.; Oleksik, J. and Turner, A., *Inorg. Chim. Act.*, 1981, **53**, L163.
- [133] *Gaussian 03, revision C.02 by M. Frisch et al. in connection with the NBO 3.0 program by Weinhold.*
- [134] *AIMPAC program package*, see <http://www.chemistry.mcmaster.ca/aimpac>.
- [135] Zeng, X.; Beckers, H.; Willner, M. and Francisco, J. S., *Angew. Chem. Int. Ed.*, 2012, **51**, 3334.

- [136] Mück, L. A. and Gauss, J., *J. Chem. Phys.*, 2012, **136**, 111103.
- [137] Davy, R. and Holiday, S., *Chem. Phys. Lett.*, 1995, **232**, 313.
- [138] Wang, S.-F.; Feng, J.-K.; Sun, C.-C.; Liu, P.; Gao, Z. and Kong, F.-A., *Theor. Chem. Acc.*, 2001, **106**, 163.
- [139] Schnöckel, H. and Köppe, R., *J. Am. Chem. Soc.*, 1989, **111**, 4583.
- [140] Friesen, M.; Junker, M. and Schnöckel, H., *Heteroat. Chem.*, 1999, **10**, 658.
- [141] Thorwirth, S.; Gauss, J.; McCarthy, M. C.; Shindo, F. and Thaddeus, P., *Chem. Comm.*, 2008, page 5292.
- [142] Behrend, J.; Mittler, P.; Winnewisser, G. and Yamada, K., *J. Mol. Spectrosc.*, 1991, **150**, 99.
- [143] Thorwirth, S.; McCarthy, M. C.; Gottlieb, C. A.; Thaddeus, P.; Gupta, H. and Stanton, J. F., *J. Chem. Phys.*, 2005, **123**, 054326.
- [144] Isobe, K.; Yoshiki, O.; Vázquez de Miguel, A.; Zhu, T.-W.; Nishioka, T.; Ogura, T. and Kitagawa, T., *Angew. Chem. Int. Ed.*, 1994, **33**, 1882.
- [145] Martin, T. P., *J. Chem. Phys.*, 1984, **81**, 4426.
- [146] Hearley, A. K.; Johnson, B. F.; McIndoe, J. and Tuck, D. G., *Inorg. Chim. Acta*, 2002, **334**, 105.
- [147] Mielke, Z.; Brabson, G. D. and Andrews, L., *J. Phys. Chem.*, 1991, **95**, 75.
- [148] Dunning, Jr, T. H. and Yousaf, K. E., *J. Chem. Phys.*, 2010, **133**, 174116.
- [149] Dyal, K., *J. Chem. Phys.*, 1997, **106**, 9618.
- [150] Gauss, J., *Personal Communication*, 2012.
- [151] Damrauer, R. and Hankin, J. A., *Chem. Rev.*, 1995, **95**, 1137.
- [152] Remko, M., *THEOCHEM*, 1999, **492**, 203.
- [153] Remko, M. and Van Duijnen, P. T., *Chem. Phys. Lett.*, 1999, **308**, 242.
- [154] Remko, M.; Liedl, K. R. and Rode, B. M., *Chem. Phys. Lett.*, 1996, **263**, 379.
- [155] Schreiner, P. R. and Reisenauer, H. P., *Angew. Chem. Int. Ed.*, 2008, **47**, 7071.
- [156] Lammel, G. and Cape, J. N., *Chem. Soc. Rev.*, 1996, **25**, 361.
- [157] Glindemann, D.; Edwards, M. and Kusch, P., *Atmos. Env.*, 2003, **37**, 2429.
- [158] Yekutieli, M.; Lane, J. R.; Gupta, P. and Kjaergaard, H. G., *J. Phys. Chem. A*, 2010, **114**, 7544.
- [159] Yu, H.; Chi, Y. J.; Fu, H. G.; Huang, X. R.; Li, Z. S. and Sun, J. Z., *Sci. China, Ser. B*, 2002, **45**, 282.

- [160] <http://www.univie.ac.at/columbus/>.
- [161] Waynant, R. W. and Elton, R. C., *Proceedings of the IEEE*, 1976, **64**, 1059.
- [162] Barbatti, M., *WIREs Comput Mol Sci.*, 2011, **1**, 620.
- [163] Schreiner, P., *Personal Communication*, 2012.
- [164] Jagau, T.-C., *Dissertation, Johannes Gutenberg-Universität Mainz*, 2012.
- [165] Werner, H.-J., *Adv. Chem. Phys.*, 1987, **69**, 1.
- [166] Klein, K. and Gauss, J., *J. Chem. Phys.*, 2008, **129**, 194106.
- [167] Blume, M. and Watson, R. E., *Proc. Roy. Soc. A*, 1962, **270**, 127.
- [168] Blume, M. and Watson, R. E., *Proc. Roy. Soc. A*, 1963, **271**, 565.
- [169] Helgaker, T. and Jørgensen, P., *Adv. Quantum Chem.*, 1988, **19**, 183.
- [170] Evangelista, F. A.; Prochnow, E.; Gauss, J. and Schaefer, H. F., *J. Chem. Phys.*, 2010, **132**, 074107.
- [171] Rice, J. and Amos, R., *Chem. Phys. Lett.*, 1985, **122**, 585.
- [172] Dyall, K. G. and Fægri, K., *Relativistic Quantum Chemistry*, Oxford University Press, New York, 2007.
- [173] Neese, F., *J. Chem. Phys.*, 2005, **122**, 34107.
- [174] Heß, B.; Marian, C. M.; Wahlgren, U. and Gropen, O., *Chem. Phys. Lett.*, 1996, **251**, 365.
- [175] Marian, C. M., *WIREs Comput. Mol. Sci.*, 2012, **2**, 187.
- [176] Berning, A.; Schweizer, M.; Werner, H.-J.; Knowles, P. and Palmieri, P., *Mol. Phys.*, 2000, **98**, 1823.
- [177] Cheng, L. and Gauss, J., *J. Chem. Phys.*, 2011, **134**, 244112.
- [178] Schwalbach, W. and Gauss, J., *Personal Communication*, 2012.
- [179] Gauss, J. and Stanton, J. F., *J. Chem. Phys.*, 1996, **104**, 2574.
- [180] Stopkowicz, S. and Gauss, J., *J. Chem. Phys.*, 2011, **134**, 064114.
- [181] Stanton, J. F.; Gauss, J.; Watts, J. D. and Bartlett, R. J., *J. Chem. Phys.*, 1991, **94**, 4334.
- [182] Woon, D. E. and Dunning, Jr., T. H., *J. Chem. Phys.*, 1995, **103**, 4572.
- [183] Bollmark, P.; Lindgren, B.; Rydh, B. and Sassenberg, U., *Phys. Scr.*, 1978, **17**, 561.
- [184] Marian, C. M. and Wahlgren, U., *Chem. Phys.*, 1996, **251**, 357.
- [185] Drouin, B. J.; Miller, C. E.; Müller, H. S. P. and Cohen, E. A., *J. Mol. Spectrosc.*, 2001, **205**, 128.

- 
- [186] Cohen, E. A.; Pickett, H. M. and Gellar, M., *J. Mol. Spectrosc.*, 1981, **87**, 459.
- [187] Ouazbir, M.; Chambaud, G.; Rosmus, P. and Knowles, P. J., *Phys. Chem. Chem. Phys.*, 1999, **1**, 2649.
- [188] Gritli, H.; Lakhdar, Z. B.; Chambaud, G. and Rosmus, P., *Chem. Phys.*, 1993, **178**, 223.
- [189] Panten, D., *Chem. Phys. Lett.*, 1999, **311**, 390.
- [190] Tarroni, R., *Chem. Phys. Lett.*, 2003, **380**, 624.
- [191] Tarroni, R. and Carter, S., *J. Chem. Phys.*, 2005, **123**, 014320.
- [192] Pisani, L. and Clementi, E., *J. Chem. Phys.*, 1995, **103**, 9321.
- [193] Hirata, S.; Yanai, T.; de Jong, W. A.; Nakajima, T. and Hirao, K., *J. Chem. Phys.*, 2004, **120**, 3297.
- [194] Balasubramanian, K.; Han, M. and Liao, M. Z., *J. Chem. Phys.*, 1987, **86**, 4979.
- [195] Roos, B. O.; Veryazov, V. and Widmark, P., *Theor. Chem. Acc.*, 2004, **111**, 345.
- [196] Mastalerz, R.; G, B.; Lindh, R. and Reiher, M., *J. Chem. Phys.*, 2007, **127**, 074105.
- [197] Ziurys, L. M.; Clemens, D. P.; Saykally, R. J.; Colvin, M. and Schaefer, H. F., *Astrophys. J.*, 1984, **281**, 219.
- [198] Turner, B. E., *Astrophys. J.*, 1992, **388**, L35.
- [199] Cardelli, J. A.; Federman, S. R.; Lambert, D. L. and Theodosiou, C. E., *Astrophys. J.*, 1993, **416**, L41.
- [200] Cai, Z.-L.; Martin, J. M. L. and François, J. P., *J. Mol. Spectrosc.*, 1998, **188**, 27.
- [201] Yamada, C.; Hirota, E.; Yamamoto, S. and Saito, S., *J. Chem. Phys.*, 1988, **88**, 46.
- [202] Batista, A. P. L. and Ornellas, F. R., *Personal Communication*, 2012.
- [203] Batista, A. P. L. and Ornellas, F. R., *Mol. Phys.*, 2012, **in print**, doi: 10.1080/00268976.2012.697585.
- [204] Ornellas, F. R.; Andrazza, C. M. and De Almeida, A. A., *Astrophys. J.*, 2000, **538**, 675.
- [205] McCarthy, M. C.; Chen, W.; Travers, M. J. and Thaddeus, P., *Astrophys. J. Suppl. Ser.*, 2000, **129**, 611–623.



# Appendix

## Experimental methods used for rotational-spectroscopy measurements

All experiments regarding rotational spectroscopy described in this thesis were conducted by Valerio Lattanzi and Michael McCarthy, Smithsonian Center for Astrophysics, Harvard University, Cambridge. Specifically, the performed experiments involved Fourier-transform microwave spectroscopy of a molecular beam. The spectrometer is describe in Ref. 205 and operates from 5 to 43 GHz. The molecules HPSi, cyclic and linear OSiS, and SiS<sub>2</sub> were produced by application of a low-current discharge to the reactants. For HPSi the reactants were PH<sub>3</sub> and SiH<sub>4</sub>, for linear OSiS, SiH<sub>4</sub>, H<sub>2</sub>S, and H<sub>2</sub>O were used. Cyclic OSiS was produces using SiH<sub>4</sub>, H<sub>2</sub>S, and O<sub>2</sub> and for SiS<sub>2</sub> the reactants were SiH<sub>4</sub> and H<sub>2</sub>S. All reactants were heavily diluted in neon, their concentration amounted to about 0.2%. The discharge was applied to a short gas pulse created by a mechanical valve in a throat of a nozzle. The flow rate and the discharge potential were optimized until the strongest lines were obtained. To be more accurate, the discharge potential was 1.0-1.2 kV, the flow rate ranged from 20 to 25 cm<sup>3</sup>min<sup>-1</sup> and the pulse rate of the nozzle amounted to 6 Hz with a stagnation pressure of 2.5 kTorr behind the valve. The spectroscopic search for the rotational transitions was guided by highly accurate quantum-chemical predictions for the rotational constants.<sup>51-53</sup>

## Spectroscopic parameters of S-SiH-SH, HS-PS, and HP-SS

### S-SiH-SH

The relevant spectroscopic parameters of the two species *anti*-S-SiH-SH and *syn*-S-SiH-SH that were discussed in Sec. 4.3.4 are listed below in Tab. 1, Tab. 2, Tab. 3, and Tab. 4. Naturally occurring minor isotopic species were also considered.

**Table 1.:** Calculated spectroscopic constants<sup>a</sup> (in MHz) of *anti*-S-SiH-SH and its isotopologues

|               | S-SiH-SH | <sup>34</sup> S-SiH-SH | S-SiH- <sup>34</sup> SH | S- <sup>29</sup> SiH-SH |
|---------------|----------|------------------------|-------------------------|-------------------------|
| $A_0$         | 23 247.0 | 23 060.6               | 23 127.2                | 22 864.3                |
| $B_0$         | 2 386.3  | 2 317.3                | 2 315.1                 | 2 386.3                 |
| $C_0$         | 2 161.9  | 2 103.5                | 2 102.3                 | 2 158.5                 |
| $10^3 D_J$    | 0.629    | 0.597                  | 0.595                   | 0.626                   |
| $10^3 D_{JK}$ | -27.685  | -26.954                | -26.865                 | -27.214                 |
| $10^3 D_K$    | 710.746  | 701.938                | 705.855                 | 605.039                 |
| $10^3 d_1$    | -0.124   | -0.116                 | -0.115                  | -0.126                  |
| $10^3 d_2$    | -0.004   | -0.003                 | -0.003                  | -0.004                  |

<sup>a</sup> Rotational constants from the best-estimate structure (CCSD(T)/cc-pCVQZ level of theory) corrected for zero-point vibrational effects. Centrifugal-distortion constants at the CCSD(T)/cc-pVTZ level of theory.

**Table 2.:** Zero-point vibrational corrections (in MHz) of *anti*-S-SiH-SH and its important isotopologues, CCSD(T)/cc-pVTZ level of theory

|              | S-SiH-SH | <sup>34</sup> S-SiH-SH | S-SiH- <sup>34</sup> SH | S- <sup>29</sup> SiH-SH |
|--------------|----------|------------------------|-------------------------|-------------------------|
| $\Delta A_0$ | -15.170  | -15.488                | -14.614                 | -13.844                 |
| $\Delta B_0$ | -6.364   | -6.131                 | -6.178                  | -6.323                  |
| $\Delta C_0$ | -7.619   | -7.338                 | -7.365                  | -7.586                  |

**Table 3.:** Calculated spectroscopic constants<sup>a</sup> (in MHz) of *syn*-S-SiH-SH and its isotopologues

|               | S-SiH-SH | <sup>34</sup> S-SiH-SH | S-SiH- <sup>34</sup> SH | S- <sup>29</sup> SiH-SH |
|---------------|----------|------------------------|-------------------------|-------------------------|
| $A_0$         | 23 342.9 | 23 154.9               | 23 129.5                | 22 946.7                |
| $B_0$         | 2 395.2  | 2 326.1                | 2 326.5                 | 2 395.1                 |
| $C_0$         | 2 170.1  | 2 111.7                | 2 111.8                 | 2 166.6                 |
| $10^3 D_J$    | 0.655    | 0.621                  | 0.624                   | 0.652                   |
| $10^3 D_{JK}$ | -28.471  | -27.679                | -27.620                 | -27.981                 |
| $10^3 D_K$    | 704.749  | 695.977                | 691.687                 | 688.786                 |
| $10^3 d_1$    | -0.129   | -0.121                 | -0.121                  | -0.131                  |
| $10^3 d_2$    | -0.004   | -0.003                 | -0.003                  | -0.004                  |

<sup>a</sup> Rotational constants from the best-estimate structure (CCSD(T)/cc-pCVQZ level of theory) corrected for zero-point vibrational effects. Centrifugal-distortion constants at the CCSD(T)/cc-pVTZ level of theory.

**Table 4.:** Zero-point vibrational corrections (in MHz) of *syn*-S-SiH-SH and its important isotopologues, CCSD(T)/cc-pVTZ level of theory

|              | S-SiH-SH | <sup>34</sup> S-SiH-SH | S-SiH- <sup>34</sup> SH | S- <sup>29</sup> SiH-SH |
|--------------|----------|------------------------|-------------------------|-------------------------|
| $\Delta A_0$ | -130.161 | -129.681               | -128.587                | -127.489                |
| $\Delta B_0$ | -2.959   | -2.822                 | -2.871                  | -2.919                  |
| $\Delta C_0$ | -5.717   | -5.465                 | -5.496                  | -5.713                  |

## HS-PS and HP-SS

The relevant spectroscopic parameters of *trans*-HS-PS, *cis*-HS-PS, and HP-SS that were discussed in Sec. 4.3.5 are listed below in Tab. 5-10. In addition to the naturally occurring minor isotopic species, the spectroscopic constants for the deuterated molecules are listed as well.

**Table 5.:** Calculated spectroscopic constants<sup>a</sup> (in MHz) of the isomer *trans*-HS-PS and its isotopologues

|               | HSPS     | H <sup>34</sup> SPS | HSP <sup>34</sup> S | DSPS     |
|---------------|----------|---------------------|---------------------|----------|
| $A_0$         | 16 790.4 | 16 637.2            | 16 615.5            | 16 559.3 |
| $B_0$         | 2 927.3  | 2 842.1             | 2 844.9             | 2 829.22 |
| $C_0$         | 2 489.6  | 2 424.5             | 2 425.8             | 2 413.70 |
| $10^3 D_J$    | 1.165    | 1.110               | 1.111               | 1.016    |
| $10^3 D_{JK}$ | -17.034  | -16.493             | -16.543             | -14.524  |
| $10^3 D_K$    | 186.03   | 181.790             | 182.677             | 166.307  |
| $10^3 d_1$    | -0.289   | -0.271              | -0.271              | -0.246   |
| $10^3 d_2$    | -0.014   | -0.014              | -0.013              | -0.012   |

<sup>a</sup> Rotational constants from the best-estimate structure (CCSD(T)/cc-pCVQZ level of theory) corrected for zero-point vibrational effects. Centrifugal-distortion constants at the CCSD(T)/cc-pVTZ level of theory.

**Table 6.:** Zero-point vibrational corrections (in MHz) of the isomer *trans*-HS-PS and its isotopologues, CCSD(T)/cc-pVTZ level of theory

|              | HSPS   | H <sup>34</sup> SPS | HSP <sup>34</sup> S | DSPS   |
|--------------|--------|---------------------|---------------------|--------|
| $\Delta A_0$ | -30.74 | -30.40              | -31.18              | -21.99 |
| $\Delta B_0$ | -9.53  | -9.23               | -9.12               | -8.93  |
| $\Delta C_0$ | -10.63 | -10.29              | -10.41              | -9.66  |

**Table 7.:** Calculated spectroscopic constants<sup>a</sup> (in MHz) of the isomer *cis*-HS-PS and its isotopologues

|               | HSPS     | H <sup>34</sup> SPS | HSP <sup>34</sup> S | DSPS     |
|---------------|----------|---------------------|---------------------|----------|
| $A_0$         | 17 006.0 | 16 905.1            | 16 829.4            | 15 767.0 |
| $B_0$         | 2 876.3  | 2 790.1             | 2 797.2             | 2 860.5  |
| $C_0$         | 2 458.9  | 2 392.2             | 2 395.9             | 2 418.6  |
| $10^3 D_J$    | 0.981    | 0.927               | 0.930               | 0.990    |
| $10^3 D_{JK}$ | -13.241  | -12.809             | -12.880             | -11.441  |
| $10^3 D_K$    | 167.105  | 165.061             | 164.149             | 124.445  |
| $10^3 d_1$    | -0.235   | -0.218              | -0.220              | -0.243   |
| $10^3 d_2$    | -0.012   | -0.011              | -0.011              | -0.013   |

<sup>a</sup> Rotational constants from the best-estimate structure (CCSD(T)/cc-pCVQZ level of theory) corrected for zero-point vibrational effects. Centrifugal-distortion constants at the CCSD(T)/cc-pVTZ level of theory.

**Table 8.:** Zero-point vibrational corrections (in MHz) of the isomer *cis*-HSHP and its isotopologues, CCSD(T)/cc-pVTZ level of theory

|              | HSPS   | H <sup>34</sup> SPS | HSP <sup>34</sup> S | DSPS   |
|--------------|--------|---------------------|---------------------|--------|
| $\Delta A_0$ | +73.44 | +73.25              | +72.07              | +40.38 |
| $\Delta B_0$ | -18.16 | -17.49              | -17.49              | -15.42 |
| $\Delta C_0$ | -14.46 | -14.04              | -14.03              | -12.70 |

**Table 9.:** Calculated spectroscopic constants<sup>a</sup> (in MHz) of the isomer HP-SS and its isotopologues

|               | HP-SS    | HP- <sup>34</sup> SS | HP-SS <sup>34</sup> | DP-SS    |
|---------------|----------|----------------------|---------------------|----------|
| $A_0$         | 25 004.7 | 24 099.1             | 24 773.3            | 22 412.2 |
| $B_0$         | 2 587.9  | 2 588.0              | 2 513.0             | 2 571.7  |
| $C_0$         | 2 343.1  | 2 334.9              | 2 278.5             | 2 304.0  |
| $10^3 D_J$    | 0.811    | 0.803                | 0.769               | 0.820    |
| $10^3 D_{JK}$ | -17.637  | -16.786              | -17.116             | -14.520  |
| $10^3 D_K$    | 334.092  | 312.386              | 328.339             | 229.648  |
| $10^3 d_1$    | -0.180   | -0.184               | -0.168              | -0.188   |
| $10^3 d_2$    | -0.008   | -0.008               | -0.007              | -0.009   |

<sup>a</sup> Rotational constants from the best-estimate structure (CCSD(T)/cc-pCVQZ level of theory) corrected for zero-point vibrational effects. Centrifugal-distortion constants at the CCSD(T)/cc-pVTZ level of theory.

**Table 10.:** Zero-point vibrational corrections (in MHz) of the isomer HP-SS and its isotopologues, CCSD(T)/cc-pVTZ level of theory

|              | HP-SS  | HP- <sup>34</sup> SS | HP-S <sup>34</sup> S | DP-SS  |
|--------------|--------|----------------------|----------------------|--------|
| $\Delta A_0$ | +34.92 | +35.18               | +34.08               | +1.38  |
| $\Delta B_0$ | -12.79 | -12.69               | -12.33               | -11.06 |
| $\Delta C_0$ | -12.29 | -12.12               | -11.87               | -11.86 |

## Calculation of “best-estimate” spin-orbit splittings

The calculation of best-estimate spin-orbit splittings presented in Sec. 9.5 (Tab. 9.10, Tab. 9.11, and Fig. 9.3) followed Eq. 9.2. In order to evaluate the scalar-relativistic contribution, the difference between a relativistic and a non-relativistic spin-orbit mean-field treatment was computed. In the relativistic treatment the two-electron Breit interaction was approximated by the non-relativistic value (see also Tab. 9.9). The following basis sets were used for the calculation of the best-estimate spin-orbit splittings:

| Species | 1-el        | SOMF        | 1-el+2el | DC          |
|---------|-------------|-------------|----------|-------------|
| OH      | cc-pCV5Z    | cc-pCV5Z    | cc-pCVQZ | unc-ANO-RCC |
| SH      | cc-pCV5Z    | cc-pCV5Z    | cc-pCVQZ | unc-ANO-RCC |
| SeH     | cc-pCVQZ    | cc-pCVQZ    | cc-pCVQZ | unc-ANO-RCC |
| TeH     | unc-ANO-RCC | unc-ANO-RCC | ...      | unc-ANO-RCC |

## List of the author's publications

### Publications relevant for this work

- Lattanzi, V.; Thorwirth, S.; Halfen, D. T.; Mück, L. A.; Ziurys, L. M.; Thaddeus, P.; Gauss, J. and McCarthy, M. C., "Bonding in the Heavy Analogue of Hydrogen Cyanide: The Curious Case of Bridged HPSi", *Angew. Chem. Int. Ed.*, 2010, **49**, 5661.// "Die Bindungsverhältnisse in schweren Analoga des Cyanwasserstoffs: Der merkwürdige Fall des HPSi", *Angew. Chem.*, 2010, **122**, 5795.
- Thorwirth, S.; Mück, L. A.; Gauss, J.; Tamassia, F.; Lattanzi, V. and McCarthy, M. C., "Silicon Oxysulfide, OSiS: Rotational Spectrum, Quantum-Chemical Calculations, and Equilibrium Structure", *J. Phys. Chem. Lett.*, 2011, **2**, 1228.
- Mück, L. A.; Lattanzi, V.; Thorwirth, S.; McCarthy, M. C. and Gauss, J., "Cyclic SiS<sub>2</sub>: A New Perspective on the Walsh Rules", *Angew. Chem. Int. Ed.*, 2012, **51**, 3695.// "Cyclisches SiS<sub>2</sub>: Die Walsh-Regeln in neuem Licht", *Angew. Chem.*, 2012, **124**, 3755.
- Mück, L. A. and Gauss, J., "Calculation of Spin-Orbit Splittings in Degenerate Open-Shell States via Mukherjee's Multireference Coupled-Cluster Theory: A Measure for the Coupling Contribution", *J. Chem. Phys.*, 2012, **136**, 111103.
- Köhn, A.; Hanauer, M.; Mück, L. A.; Jagau, T.-C. and Gauss, J., "State-Specific Multireference Coupled-Cluster Theory", *WIREs Comput. Mol. Sci.*, 2012, doi: 10.1002/wcms.1120.

### Further publications

- Mück, L. A.; Timoshkin, A. Yu.; von Hopffgarten, M. and Frenking, G., "Donor-Acceptor Complexes of Noble Gases", *J. Am. Chem. Soc.*, 2009, **131**, 3942.
- Mück, L. A.; Timoshkin, A. Yu. and Frenking, G., "Design of Neutral Lewis Superacids of Group 13 Elements", *Inorg. Chem.*, 2012, **51**, 640.